SMARTBIOCONTROL
BioProd
Avec le soutien du Fonds européen
de développement régional
Met steun van het Europees Fonds
voor Regionale Ontwikkeling

UNIVERSITÉ DE LILLE – SCIENCES ET TECHNOLOGIES
ÉCOLE DOCTORALE SCIENCE DE LA MATIÈRE, DU RAYONNEMENT ET DE L'ENVIRONNEMENT
Et
UNIVERSITÉ DE LIÈGE – GEMBLOUX AGRO-BIO TECH

Thèse

Présentée par Hannah Luise BRÜCK

Pour l'obtention du titre de :

Docteur de l'Université de Lille en Ingénierie des fonctions biologiques et
Docteur de l'Université de Liège – Gembloux Agro-Bio Tech en Sciences agronomiques et Ingénierie biologique

Strain engineering and process design for continuous surfactin production in biofilm bioreactors with *Bacillus subtilis* 168

Génie génétique et conception d'un procédé continu pour la production de surfactine dans des bioréacteurs à biofilm avec *Bacillus subtilis* 168

Préparée à l'Institut Charles Viollette et au TERRA Teaching and Research Centre

Soutenue publiquement le 28 septembre 2020

Jury :

Philippe JACQUES, Professeur	Université de Liège, Belgique	Directeur
François COUTTE, Professeur associé	Université de Lille, France	Directeur
Frank DELVIGNE, Professeur	Université de Liège, Belgique	Co-directeur
Ines MANDIC-MULEC, Professeur	University of Ljubljana, Slovénie	Rapportrice
Ralf TAKORS, Professeur	University of Stuttgart, Allemagne	Rapporteur
Valérie LECLERE, Professeur	Université de Lille, France	Présidente
Aurore RICHEL, Professeur	Université de Liège, Belgique	Examinatrice
Dominique TOYE, Professeur	Université de Liège, Belgique	Examinatrice

Strain engineering and process design for continuous surfactin production in biofilm bioreactors with *Bacillus subtilis* 168

Hannah Luise BRÜCK

Dissertation originale présentée en vue de l'obtention du grade de docteur en Sciences agronomiques et Ingénierie biologique de l'Université de Liège – Gembloux Agro-Bio Tech, et en Ingénierie des fonctions biologiques de l'Université de Lille

Promoteurs :
Université de Liège – Gembloux Agro-Bio Tech :
Philippe JACQUES, Frank DELVIGNE
Université de Lille :
François COUTTE

Année académique : 2019 – 2020

COMMUNAUTÉ FRANÇAISE DE BELGIQUE

UNIVERSITÉ DE LIÈGE – GEMBLOUX AGRO-BIO TECH

Et

UNIVERSITÉ DE LILLE (FRANCE) – SCIENCES ET TECHNOLOGIES

Strain engineering and process design for continuous surfactin production in biofilm bioreactors with *Bacillus subtilis* 168

Hannah Luise BRÜCK

Dissertation originale présentée en vue de l'obtention du grade de docteur en Sciences agronomiques et Ingénierie biologique de l'Université de Liège – Gembloux Agro-Bio Tech, et en Ingénierie des fonctions biologiques de l'Université de Lille

Promoteurs :
Université de Liège – Gembloux Agro-Bio Tech :
Philippe JACQUES, Frank DELVIGNE
Université de Lille :
François COUTTE

Année académique : 2019 – 2020

© BRÜCK Hannah Luise, 14-09-2020.

Abstract

Biofilm bioreactors show promise for continuous microbial biosurfactant production due to the natural robustness of self-immobilized cells and the possible design of processes avoiding foam formation. The widely used bacterial strain *B. subtilis* 168 has the potential to produce surfactin, a powerful biosurfactant with exceptional biological activities and various industrial applications. However, *B. subtilis* 168 exhibits only poor biofilm formation capacities and thus entails limited cell adhesion capacities.

In order to improve the natural cell immobilization of *B. subtilis* 168 to adapt this strain better to biofilm cultivation, filamentous mutant strains with restored exopolysaccharide (EPS) production were generated. The impacts of the genetic modifications were evaluated through colonization assays and by measuring the biofilm formation capacity under low shear stress in a drip-flow reactor (DFR). Subsequently, the most performant strains were selected and cultivated in a newly designed continuous trickle-bed biofilm bioreactor containing highly structured metal packing elements for biofilm formation. Moreover, a bacterial growth model was built able to describe the growth dynamics of the planktonic cells and the biofilm in the system.

The colony development was strongly affected by filamentous cell growth and EPS production which was manifested through an enhanced surface spreading and colonization capacity. In the DFR and trickle-bed biofilm bioreactor, the EPS^+ mutants showed significantly increased performances regarding the biofilm formation and surfactin production capacities. Whereas cell filamentation had a minor impact on the processes, but contributed to a better cell cohesion in the biofilm and led to reduced cell detachment during the cultivation. Thus, EPS production and filamentous cell growth contributed considerably to an improved process performance in the system. In addition, continuous fermentation has shown to be favorable for a high surfactin productivity. The experimental data from the trickle-bed biofilm bioreactor were in good accordance with those obtained by simulations with the developed growth model. Hence, the growth model has been successfully validated and could be used for further process optimization.

Résumé

Les bioréacteurs à biofilm représentent une technologie prometteuse pour la production continue de biosurfactants microbiens grâce à la robustesse naturelle des cellules immobilisées et à la conception possible de procédés évitant la formation de mousse. La souche bactérienne *B. subtilis* 168 a le potentiel de produire de la surfactine, un biosurfactant puissant qui possède des activités biologiques exceptionnelles ayant des applications industrielles diverses. Cependant, *B. subtilis* 168 ne présente que de faibles capacités de formation de biofilms et donc entraîne des capacités d'adhésion cellulaire limitées.

Afin d'améliorer l'immobilisation cellulaire naturelle de *B. subtilis* 168 et pour mieux adapter cette souche à la culture de biofilms, des mutants filamenteux avec une production d'exopolysaccharides (EPS) restaurée ont été générés. Les impacts des modifications génétiques ont été évalués par des tests de colonisation et en mesurant la capacité de formation de biofilm sous faible contrainte de cisaillement dans un réacteur à écoulement goutte à goutte (DFR). Par la suite, les souches les plus performantes ont été sélectionnées et cultivées dans un bioréacteur à biofilm à film tombant continu contenant des éléments de garnissage métallique structurés pour la formation de biofilm. De plus, un modèle de croissance bactérienne a été développé pour décrire la dynamique de croissance des cellules planctoniques et du biofilm dans le système.

Le développement des colonies a été fortement affecté par la croissance des cellules filamenteuses et la production d'EPS ce qui s'est manifesté par une capacité accrue d'étalement de surface et de colonisation. Dans le DFR et le bioréacteur à biofilm à film tombant, les mutants EPS^+ ont montré des performances significativement augmentées concernant la formation de biofilm et les capacités de production de surfactine. La filamentation cellulaire a eu un impact mineur sur le procédé mais a contribué à une meilleure cohésion cellulaire dans le biofilm et a également conduit à un détachement cellulaire réduit pendant la culture. Ainsi, la production d'EPS et la croissance des cellules filamenteuses ont considérablement contribué à l'amélioration des performances du procédé dans le système. De plus, la culture en mode continu s'est révélée favorable à une production élevée en surfactine. Les données expérimentales du bioréacteur à biofilm à film tombant sont concordantes avec celles obtenues par des simulations avec le modèle de croissance développé. Par conséquent, le modèle de croissance a été validé avec succès et pourrait être utilisé pour une optimisation ultérieure de procédés à biofilm.

Acknowledgements

The accomplishment of this PhD was a long and sometimes tricky journey accompanied by ups and downs. Nevertheless, the time passed very fast and I have experienced a lot within this time. This was certainly due to the particularity of this PhD thesis which was performed in joint supervision between two countries, Belgium and France.

First of all, I would like to thank my supervisors Philippe Jacques, Frank Delvigne and François Coutte that have accompanied me during the four years of my PhD thesis and contributed considerably to the successful completion of this work. The insightful discussions and your encouragements throughout my PhD Thesis kept inspiring me and motivated me to go further. I am especially thankful to Philippe Jacques for giving me the possibility to extend my PhD thesis to finish my research work.

I am thankful to Pascal Dhulster for his advices and giving me the opportunity to work in his laboratory to perform the experiments. Many thanks to Debarun who introduced me to the "*Bacillus*" community and prepared me for this PhD thesis. Your advices in genetic engineering help me a lot during the start of my thesis. Nuria, Carolina, Gabi, Hamza, Awa, Yanath, Mahammed and Ludivine, I greatly enjoyed the nice and pleasant time and lunch breaks we passed together in Lille.

I want to thank the whole MiPI team and the team in Lille for their effort, cooperativeness and for all their advices they gave me during my PhD thesis which made me advancing continuously. I am very thankful that I could take profit from the expertise and equipment of both laboratories. This permitted me to get to know a multitude of new things and to continuously improve my skills. The alternating stays in Lille and Gembloux gave me the possibility to share many special moments of conviviality with lovely people from both sides.

Special thanks to Cathy for her help with the assembling and disassembling of the reactor for the numerous experiments I have performed. I am thankful to Sam and Andrew for their additional help in the pilot hall for the organization and autoclaving of the reactors and the pleasant working atmosphere. Many thanks also to Andrew for the design of some very nice technical figures.

I am also thankful to Sébastien Gofflot for the prosperous collaboration for the culture samples analysis from the trickle-bed biofilm reactor. Thank you for the fruitful discussions and your advices and encouragements during the last part of my work. Many thanks to Neil Moustier who conducted the sample analysis. I am grateful to Kaija and Patricio for their friendly welcome and for letting me stay overnight in Gembloux during the laborious and endless reactor experiences.

I would like to gratefully thank the European INTERREG V SmartBioControl / BioProd project, the University of Liège and the Hauts-de-France Region for their financial support during my whole work.

I would like to express my sincere gratitude to my family who supported me my whole life and enabled me to pursue my sports as well as academic career. It gives me strength to know that I can always count on you although we do not live nearby.

This journey would not have been the same without the support of my wonderful husband Joachim. Thanks to you, I discovered Belgium, a small but very colorful and vivacious country at the heart of Western Europe offering many lovely places to enjoy food and drinks and to meet nice people in order to simply enjoy life. I am very grateful for your presence and having supporting me during the four years of work for my PhD. You helped me to survive the stress and recharge my batteries when it was necessary to accomplish successfully this work.

Scientific valorization

Scientific articles

- ARTICLE 1 (included in Chapter 3, supplementary data are partly included in Chapter 2, section 3.2):
  Hannah L. Brück, F. Delvigne, P. Dhulster, P. Jacques, F. Coutte, “Molecular strategies for adapting *Bacillus subtilis* 168 biosurfactant production to biofilm cultivation mode,” *Bioresour. Technol.*, vol. 293, no. 122090, pp. 1–8, 2019.

- ARTICLE 2 (included in Chapter 4):
  Hannah L. Brück, F. Coutte, P. Dhulster, S. Gofflot, P. Jacques, F. Delvigne, “Growth Dynamics of Bacterial Populations in a Two-Compartment Biofilm Bioreactor Designed for Continuous Surfactin Biosynthesis,” *Microorganisms*, vol. 8, no. 679, pp. 1–19, 2020.

Scientific conferences

- KEYNOTE ORAL COMMUNICATION:
  Hannah Brück, François Coutte, Didier Lecouturier, Krasimir Dimitrov, Jean-Sébastien Guez, Frank Delvigne, Pascal Dhulster, Philippe Jacques: “Bioprocédés innovants pour la production de biosurfactants microbiens de nature lipopeptidique.” (Congress SFGP, 15-17/10/2019, Nantes, France)

- ORAL COMMUNICATION:
  Hannah Brück, François Coutte, Frank Delvigne, Pascal Dhulster, Philippe Jacques: “Surfactin production optimization in biofilm bioreactors using genetically modified *Bacillus subtilis* 168 strains with improved adhesion capacities.” (European Congress of Applied Biotechnology (ECAB5), 15/09 - 19/09/2019, Florence, Italy)

- ORAL COMMUNICATION:
  Hannah Brück, François Coutte, Frank Delvigne, Pascal Dhulster, Philippe Jacques: “Biofilm-based bioprocess optimization by morphology engineering of *Bacillus subtilis*.” (12th European Symposium On

Biochemical Engineering Sciences (ESBES), 09/09 – 12/09/2018, Lisbon, Portugal)

- POSTER:
  Hannah Brück, François Coutte, Frank Delvigne, Pascal Dhulster, Philippe Jacques: "Optimization of biosurfactant production in a trickle-bed biofilm reactor with genetically improved bacteria." (25th National Symposium for Applied Biological Science (NSABS), 31/01/2020, Gembloux, Belgium)

- POSTER:
  Hannah Brück, François Coutte, Frank Delvigne, Pascal Dhulster, Philippe Jacques: "Optimisation de la production de biosurfactants dans des bioréacteurs à biofilm en utilisant des bactéries génétiquement modifiées ayant des capacités d'adhérence améliorées." (Congress SFGP, 15-17/10/2019, Nantes, France)

- POSTER:
  François Coutte, **Hannah Brück**, Debarun Dhali, Joachim Niehren, Cristian Versari, Valérie Leclere, Pascal Dhulster, Frank Delvigne, Philippe Jacques: "MOLECULAR STRATEGIES FOR ADAPTING *BACILLUS* CELL TO OVERPRODUCE SURFACTIN IN BIOFILM BASED PROCESSES." (20th International Conference on Bacilli and Gram-Positive Bacteria, 23 – 26/07/2019, Washington, D.C., USA)

- POSTER:
  Hannah Brück, François Coutte, Frank Delvigne, Pascal Dhulster, Philippe Jacques: "Optimization of scalable biofilm bioreactors with genetically improved bacteria for microbial biosurfactant production." (Congress (Bio-)Polymers and Ecocircularity: From Challenges to Opportunities, 08 – 09/05/2019, Gosselies, Belgium)

- POSTER:
  Hannah Brück, Romain Bouchat, Andrew Zicler, Frank Delvigne: "Morphology engineering of *Bacillus* sp.: single cell analysis based on microfluidic cultivation devices." (1st international EUROMBR Training Course – Applications of microbioreactors in bioprocess development, 24 – 28/09/2018, University of Braunschweig, Germany)

- POSTER:

Hannah Brück, François Coutte, Frank Delvigne, Pascal Dhulster, Philippe Jacques: "Generation of hyperfilamentous *B. subtilis* mutants to optimize the lipopeptide production in biofilm bioreactors part II." (Interreg SMARTBIOCONTROL Symposium, 24/01/2018, Gent, Belgium)

- POSTER:
  Hannah Brück, François Coutte, Frank Delvigne, Pascal Dhulster, Philippe Jacques : "Génération de mutants hyperfilamenteux de *Bacillus subtilis* pour la production de lipopeptides en bioréacteur à biofilm." (Journées Condorcet 2017, 08 – 09/06/2017, Villeneuve d'Ascq, France)

- POSTER:
  Hannah Brück, François Coutte, Frank Delvigne, Pascal Dhulster, Philippe Jacques: "Generation of hyperfilamentous *B. subtilis* mutants to optimize the surfactin production in biofilm bioreactors." (French Federation of Biotechnology - Bioreactors Symposium 2017, 15 – 16/05/2017, Villeneuve d'Ascq, France)

Scientific events

- ORAL COMMUNICATION:
  "Generation of *Bacillus subtilis* 168 mutants with increased adhesion capacities for the production of lipopeptides in biofilm bioreactors." (SMARTBIOCONTROL Symposium, 04/06/2019, Kruishoutem, Belgium)

- ORAL COMMUNICATION:
  "Biofilm-based bioprocess optimization by morphology engineering of *Bacillus subtilis* to improve surfactin production." (Webinar SMARTBIOCONTROL BioProd, 02/04/2019, Gembloux Agro-Bio Tech – Liège University)

- ORAL COMMUNICATION:
  "Generation of hyperfilamentous *Bacillus subtilis* mutants to optimize the lipopeptide production in biofilm bioreactors." (TERRA Seminar, 15/12/2017, Gembloux Agro-Bio Tech – Liège University)

Table of Contents

Abstract .... **i**

Résumé .... **iii**

Acknowledgements .... **v**

List of Figures .... **xvii**

List of Tables .... **xxii**

List of Abbreviations .... **xxiv**

Preface **1**

Chapter 1: State of the art

1. *Bacillus subtilis* 7
  1.1 Origin of *Bacillus subtilis* 7
  1.2 Genomic features 7
  1.3 Swarming motility and biofilm formation 8
  1.4 Commercial interest 10
2. Lipopeptides produced by *Bacillus* species 10
  2.1 Structure of surfactin and fengycin 11
  2.2 Nonribosomal peptide synthesis of surfactin 12
  2.3 Regulation of surfactin biosynthesis 13
  2.4 Properties and applications of surfactin 14
3. Biotechnological surfactin production processes 16
  3.1 Impact of medium composition 16
  3.2 Effect of process parameter 17
  3.3 Strain Engineering 17
  3.4 Bioprocess design 18
    3.4.1 Foaming processes 19
    3.4.2 Processes with cell immobilization 19
    3.4.3 Processes without foam formation 21
  3.5 Downstream process operations 24
  3.6 Industrial relevance of biosurfactant processes 24
4. Biofilm bioreactors – a promising and challenging alternative for continuous bioprocesses 26

4.1 Biofilms: a lifestyle of microorganisms in nature 26

4.2 Assembly and development of *B. subtilis* biofilms 26

4.3 Biofilm regulatory pathways in *B. subtilis* 27

4.4 Biofilm-based bioprocesses 29

4.5 Trickle-bed biofilm reactor for enhanced lipopeptide production 31

5. Metabolic or morphology engineering for the design of more efficient microbial cell factories? 33

5.1 Yield optimization through metabolic engineering 33

5.2 The approach of synthetic morphology 33

5.3 Modulating the bacterial cell shape 34

5.4 Morphology engineering as new concept for process optimization . 35

Chapter 2: Genetic engineering and screening of *B. subtilis* 168 strains with improved colonization capacities 39

1. Introduction 41

2. Materials and methods 42

2.1 Strains 42

2.2 Media compositions 44

2.3 Construction of the mutant strains 44

2.3.1 Plasmid, gDNA extraction and PCR fragment purification 44

2.3.2 Introduction of the *sfp* gene 44

2.3.3 Markerless gene deletion strategy “Pop in – pop out” 46

2.4 Analysis of microcolony formation on agarose pads 50

2.5 LB agar plates colonization assay 50

2.6 Analysis of the biofilm formation capacity 51

2.7 Bacterial growth analysis in a micro-bioreactor fermentation system 51

2.8 Lipopeptide analysis 52

2.9 Cell dry weight analysis of cells adhered to the DFR coupon 53

2.10 Biofilm composition analysis 53

3. Results and discussion 53

3.1 Robust biofilm formation in *B. subtilis* 168 strains modifies the lipopeptide biosynthesis 53

3.2 Cell filamentation showed a strong impact on microcolony formation 57

3.3 EPS production and cell filamentation improved the spreading and colonization capacity 60

3.4 The specific maximum cell growth rates were not strongly affected by the genetic modifications 62

3.5 Neither EPS production nor cell filamentation affected negatively the surfactin production in suspended cultures 63

3.6 Biofilm formation capacities on DFR coupons under low shear stress 64

3.6.1 EPS^+ mutants exhibited strong colonization capacities 64

3.6.2 Strains with improved adhesion capacities produced higher amounts of surfactin 67

3.7 The task of exopolysaccharides in *B. subtilis* biofilms....................68

4. Conclusions 70

Chapter 3: Molecular strategies for adapting *B. subtilis* 168 biosurfactant production to biofilm cultivation mode 73

1. Introduction 76

2. Materials and methods....................77

2.1 Strains and strain construction....................77

2.2 Time-lapse microscopy analysis of single *B. subtilis* cells....................80

2.3 Drip-flow reactor composition and growth conditions....................80

2.4 Cell counting after initial adhesion on the drip-flow reactor support 80

2.5 Cell dry weight analysis of the adhered cells after 48 h 81

2.6 Real-time observation of biofilm formation dynamics in the drip-flow reactor 81

2.7 Surfactin production analysis 81

2.8 Statistical analysis 83

3. Results and discussion....................83

3.1 Single cell phenotypic characterization of filamentous *B. subtilis* strains 83

3.2 Evaluation of colonization and biofilm formation capacity in a continuous drip-flow reactor 84

3.2.1 Initial cell adhesion capacity 84

3.2.2 Biofilm formation capacity 85

3.2.3 Cell colonization and biofilm development mode in the drip-flow reactor 89

3.2.4 Enhanced biofilm formation leads to higher surfactin production 91

4. Conclusions 91

Chapter 4: Growth dynamics of bacterial populations in a two-compartment bioreactor designed for continuous surfactin biosynthesis 95

1. Introduction 98

2. Materials and methods 99

2.1 Strains 99

2.2 Biofilm growth visualization on drip-flow reactor coupons 100

2.3 Design of the lab-scale trickle-bed biofilm reactor and culture conditions 100

2.4 Determination of the mean residence time in the packing tower.... 102

2.5 Biomass dry weight determination 102

2.6 Glucose Analysis 103

2.7 Surfactin analysis 103

2.8 Total organic carbon analysis and establishment of the mass balance 103

2.9 Biofilm reactor compartment model 104

2.10 Determination of the volumetric oxygen mass-transfer coefficient K_La in the stirred tank reactor by dynamic gassing-in/gassing-out method.... 105

2.11 Mathematical development of a growth model to describe the microbial population dynamics 106

2.11.1 Batch fermentation 107

2.11.2 Continuous fermentation 108

3. Results 108

3.1 Design of a two-compartment biofilm reactor to promote the biofilm proliferation 108

3.2 The EPS^+ strain exhibited enhanced performance in the biofilm reactor 109

3.2.1 Planktonic cell growth and biofilm development 110

3.2.2 Both strains displayed similar glucose consumption profiles..... 111

3.2.3 Increased biofilm development enhanced the surfactin productivity 112

3.2.4 Carbon utilization pointed out a totally different biofilm formation rate between the two *B. subtilis* strains......112

3.3 Modeling of microbial population dynamics......113

4. Discussion......117

Chapter 5: Impact of filamentous *B. subtilis* 168 mutants on the process performance and stability of a continuous trickle-bed biofilm reactor......123

1. Introduction......125

2. Materials and methods......126

2.1 Strains......126

2.2 Set-up of the lab-scale trickle biofilm reactor and culture conditions 126

2.3 Cell morphology analysis by microscopy......126

2.4 Biomass dry weight determination......126

2.5 Metabolite analysis......126

2.6 Surfactin analysis......127

3. Results and discussion......127

3.1 Impact of filamentous growth and/or EPS production on the process performance......127

3.1.1 Cell adhesion and detachment......128

3.1.2 Biofilm distribution on the packing elements......129

3.1.3 Filamentous growth resulted in stronger cell cohesion and aggregate formation in the developed biofilm......130

3.1.4 Main carbon source consumption......132

3.1.5 Surfactin productivity......132

3.1.6 Primary metabolite production......134

3.2 Impact of nutritional stress on the behavior of the bacterial populations......136

3.2.1 The filamentous EPS^+ strain BBG512 exhibited increased adhesion capacities under limited nutritional growth conditions......136

3.2.2 Reduced glucose availability increased the biofilm yield......138

3.3 Nutritional stress simulation......139

4. Conclusions......141

Chapter 6: General conclusions and perspectives 145
1. General conclusions.. 147
2. Perspectives 149

Appendix 153
I. Primers 155
II. Landy MOPS medium recipe... 157
III. Videos of microcolony formation.. 158
IV. Python 3.7 code of the growth model.. 159
V. Statistical analysis: Chi-square goodnes of fit test 164
VI. Impact of prophage elements on the biofilm formation of *B. subtilis* 168 167

List of Figures

Figure 1. Overview of the strategy pursued in this work. 2

Figure 2. (A) Swarming motility on 0.7% LB agar plates of NCIB3610 and *B. subtilis* 168. Bacterial growth appears in white and uncolonized agar is black (adapted from [17]). (B) Colony biofilm of the wild-type strain NCIB3610 (left side) and *B. subtilis* 168 (right side). The scale bar corresponds to 1 cm [11]....................8

Figure 3. Colony and pellicle phenotypes of *B. subtilis* 168 and *B. subtilis* 168 with five corrected mutations compared to the ones of the parent strain NCIB3610 (adapted from [6]). 10

Figure 4. Detailed structure of (A) surfactin nC14 and (B) fengycin nC15 isomers (adapted from [24]). 11

Figure 5. Schematic illustration of the surfactin assembly line via the nonribosomal peptide synthesis pathway. 12

Figure 6. Overview of the regulation cascade involved in surfactin expression (adapted from [24]). 13

Figure 7. Overview of the various industrial applications of biosurfactants [52]. 15

Figure 8. Bioreactor set-up with integrated foam overflow collector for lipopeptide production [70]. 19

Figure 9. Carrier-assisted lipopeptide production in a stirred tank reactor with foam collector and cell recycle system [76]. 20

Figure 10. Three phase inverse fluidized bed bioreactor with an integrated liquid recycle system **(**adapted from [78]**).** 21

Figure 11. Set-up of the rotating discs reactor used for lipopeptide production. ..22

Figure 12. Basic set-up of the bubbleless bioreactor with aeration through an external air/liquid membrane contactor [74]. 23

Figure 13. A typical life cycle of a *B. subtilis* biofilm with its different development stages [120]. 27

Figure 14. Co-existing cell differentiation programs in *B. subtilis* biofilms and the spatiotemporal distribution patterns of the different cell subpopulations [49]. 28

Figure 15. Different factors that affect biofilm formation and structure in biofilm-based processes [122]. 30

Figure 16. (a) Metal structured packing element for the trickle-bed biofilm reactor. The packing element is assembled with corrugated, structured, gauze stainless steel sheets. (b) Schematic representation of the enhanced gas-liquid mass transfer in the packing elements with developed biofilm on the packing surface [141]. 31

Figure 17. Experimental set-up of the 20 L trickle-bed biofilm reactor designed by Zune et al. [92]. The reactor vessel contains a structured metal packing element where the biofilm is developing. The nutrient delivery for the cells on the packing element is guaranteed through the continuous recirculating of the medium. Air is injected under the packing element to avoid foam formation. 32

Figure 18. (A) Schematic representation of the septum formation in *B. subtilis* 168. The bundling of the FtsZ filaments (in yellow) is organized through protein rings formed by SepF (in red) that are anchored to the cell membrane [160]; (B) Septum formation in a unmodified *B. subtilis* 168 strain (left side) and in a *ΔsepF* mutant strain (right side), adapted from [161]. 34

Figure 19. Atypical cell morphologies of *B. subtilis* CU1065 strains that have been observed after the alteration of the cytoplasmic membrane composition due to the deletion of several enzymes involved in the synthesis of membrane lipids (adapted from [162]). Cells from the exponential growth phase were strained with the fluorescent membrane dye FM 4-64. (A) Triple mutant (*ΔmprF, ΔpssA, ΔywnE*) exhibiting strongly filamentous cell growth. (B) Quadruple mutant (*ΔmprF, ΔpssA, ΔywnE, ΔugtP*) showing aggregates of curled cells. 35

Figure 20. Genetic map of the plasmid pBG129 containing a functional *sfp* gene to restore the surfactin production in *B. subtilis* 168. 45

Figure 21. Principle of the markerless gene deletion strategy "Pop in – pop out". The technique consists of three principal steps: (I) Construction of the master strain, (II) replacement of the target gene by the gene deletion cassette and (III) the cassette excision through the direct repeat sequences. 46

Figure 22. Genetic map of the plasmid pBG402 used to construct the master strain. 47

Figure 23. Primer design to extract the up- and downstream element of the gene of interest to be deleted for the gene deletion cassette synthesis. 49

Figure 24. Set-up of the drip flow reactor device composed of six parallel flow chambers containing each a silicone coupon for biofilm development. 51

Figure 25. (A) Growth curves of the three *B. subtilis* 168 mutants with robust biofilm forming capacities recorded with a Biolector® micro-biorector fermentation system. (B) Surfactin concentration measured in the Biolector® cultures after 48 h. (C) Fengycin concentration present in the Biolector® cultures after 48 h. 54

Figure 26. (A) DFR silicone coupons colonized by the control strain BBG111 and the *B. subtilis* mutants with restored biofilm formation after 48 h of incubation. (B) Measured cell dry weight of the adhered cells on the silicone coupons. (C) Measured surfactin concentration in mg L^{-1} of the *B. subtilis* mutants at the end of incubation (48 h) in the DFR. 56

Figure 27. Single cell growth behavior of the genetically modified *B. subtilis* strains with less efficient cell division. Cultivations have been made on agarose pads and pictures have been taken after 0, 4 and 8 hours. 58

Figure 28. Single cell growth behavior of the genetically modified B. subtilis strains with changed membrane composition. Cultivations have been made on agarose pads and pictures have been taken after 0, 4 and 8 hours. 59

Figure 29. Spreading capacity of the *B. subtilis* 168 mutants with (A) less efficient cell division and (B) perturbed membrane composition on 0.7% agar LB plates. The colony development has been followed during 8 days by measuring the colony diameter. The standard deviation is indicated by error bars. 61

Figure 30. Growth curves of the different strains recorded with a Biolector® micro-bioreactor fermentation system. ...62

Figure 31. Surfactin concentration measured in suspended cell cultures of the engineered strains after 48h of incubation in a Biolector® system. ...64

Figure 32. DFR coupons colonized by the different *B. subtilis* mutant strains. Microscope images of Gram stained biofilm samples taken from the coupons are presented on the left or right side of the corresponding strain. ...65

Figure 33. Determined cell dry weight of the cells adhered to the DFR coupons. (A) EPS$^-$ and (B) EPS$^+$ *B. subtilis* strains. ...65

Figure 34. Amount of produced surfactin present in the total volume of liquid culture medium that passed the reactor and in the biofilm after 48 h of incubation in the DFR. (A) EPS$^-$ and (B) EPS$^+$ *B. subtilis* strains. ...67

Figure 35. RL5260 biofilm developed on a DFR coupon with colored water droplets deposited on the biofilm surface to demonstrate the hydrophobicity. ...68

Figure 36. Molecular strategies to obtain a lipopeptide producing *B. subtilis* 168 strain adapted to biofilm cultivation mode: (I) insertion of a functional *sfp* gene [86], (II) restoration of the *epsC* gene [6], (III) provoking of filamentous growth through the gene deletion of *sepF* [159]. ...79

Figure 37. UPLC-MS analysis of a culture sample of *B. subtilis* RL5260. (I) Elution profile of the surfactin isomers. Small letters (a-e) indicate the corresponding recorded mass spectrum presented in (II); (II) Mass spectrum showing the $[M+H]^+$ and $[M+Na]^+$ m/z peaks of the surfactin isomers C-12 to C-16, respectively. ...82

Figure 38. Colony development of the *B. subtilis* mutants on 0.7% agar LB plates. The agar LB plates were inoculated with 2.5 µL of diluted pre-cultures (OD = 1), allowed to dry and incubated at 30°C for 48h. Four replicates were performed per strain. ...84

Figure 39. Initial cell adhesion capacity of the *B. subtilis* strains on the DFR coupons. Samples were taken after an incubation time of 6 h (batch phase) followed by 1 h of continuous flow (~13 mL h^{-1}) to flush gently away non-adhering cells in the DFR. The counted numbers of colony forming units are presented with the corresponding standard deviation. Significant differences ($p < 0.05$) between groups are indicated by small letters (a, b or c). ...85

Figure 40. (A) Schematic view of the drip-flow cultivation device with six parallel growth chambers. Each chamber contains a coupon for evaluating biofilm development; An integrated glass window allows real-time analysis of the biofilm development. (B) Cell adhesion and biofilm formation capacities of the engineered *B. subtilis* strains on a silicone coupon in the DFR. A colored water droplet was placed on the top of the biofilm formed by RL5260 as an indicator for hydrophobicity. (C) Measured amount of cell dry weight in g per m^2 of coupon area. The values are represented with the corresponding standard deviation. Significant differences ($p < 0.05$) between groups are indicated by small letters (a, b or c). (D)

Structure of the uncolonized silicone coupon surface recorded with a 3D high resolution digital microscope.. 86

Figure 41. Scheme displaying cell colonization and biofilm development over time on the silicone coupons in the DFR. The arrows in dark blue indicate which biofilm development stage was reached by the different engineered *B. subtilis* strains. A video showing the biofilm growth dynamics of RL5260 can be found online (https://pod.univ-lille.fr/video/9995-biofilm-formation-dynamics-in-a-drip-flow-reactor/) with the password "DFR".. 89

Figure 42. (A) Experimental set-up of the lab-scale trickle-bed biofilm reactor. (B) Packing tower (side view). (C) Top view image of one stainless steel structured packing element colonized by a biofilm.. 100

Figure 43. Schematic description of the growth model developed for the two-compartment trickle-bed biofilm reactor. The transition of the cells between the two compartments from the sessile (1) and planktonic (2) state and vice versa takes place in the packing tower (see **Figure 42** for a scheme of the cultivation set-up). The scheme shows an enlarged view of a support element inserted in the packing tower and describes the parameters that were used to build the growth model (see **Table 8**, page 106 for a detailed description)... 105

Figure 44. Demonstration of the biofilm development of a strain producing exopolysaccharides (RL5260, left side) or not (BBG111, right side). The images show sections of colonized silicone coupons incubated under identical growth conditions in a drip-flow reactor for 48 h... 110

Figure 45. A) Growth curves of planktonic cells and (B) amount of adhered dry biomass on the packing tower at the end of the continuous culture measured for each strain in the trickle-bed biofilm reactor. The standard deviation is indicated by error bars. 110

Figure 46. Glucose concentrations present in the bulk medium for the two *B. subtilis* 168 strains during the cultivation. The standard deviation of the measurements is indicated by error bars.. 111

Figure 47. (A) Cumulative total organic carbon (TOC) consumption by the cells during the cultivation of the two *B. subtilis* 168 strains. (B) Cumulative biofilm development on the packing elements estimated via the TOC mass balance and obtained biomass-TOC conversion yields. Error bars indicate the standard deviation of the measurements.. 112

Figure 48. Glucose consumption, planktonic cells and biofilm development predicted by the model for the two-compartment system for BBG111 (A) and RL5260 (B). The model results are drawn with a continuous line and the experimental results are added as point references for comparison. 116

Figure 49. Development of the planktonic cells in the medium for the different mutant strains. The non-filamentous strains are presented with a continuous line and their filamentous counterparts with a dashed line in the same color. 128

Figure 50. Biofilm distribution on the different packing elements; number 1 to 5 correspond to the packing order from the top to the bottom of the packing tower. 129

Figure 51. Microscope images of biofilm samples taken from the packing elements. 131
Figure 52. Glucose concentration measured in the culture medium for each strain during the batch and continuous (D = 0.5 h^{-1}) cultivation phase. 132
Figure 53. (A) Lactic acid and (B) acetic acid concentration measured in the culture medium for all strains cultivated in the trickle-bed biofilm bioreactor. 135
Figure 54. (A) Measured glucose concentration in the medium; (B) development of the planktonic cells in the medium and (C) final amount of adhered biofilm for RL5260 and BBG512 cultivated under limited glucose conditions during the continuous cultivation phase (feeding rate 1 g L^{-1} h^{-1}) in the trickle-bed biofilm reactor. 137
Figure 55. Glucose consumption, planktonic cells and biofilm development under glucose limited conditions predicted by the model for BBG512 (A) and RL5260 (B). Simulations results are drawn with a continuous line and the experimental results are shown as point references for comparison. 140
Figure 56. Biofilm development of the strain TF8A lacking three prophages (*ΔSPß*, *Δskin* and *ΔPBSX*) on the DFR coupons in comparison to *B. subtilis* 168 and RL5260 (*sfp*$^{+}$, *epsC*$^{+}$) (A) and mutant strains lacking one of the prophages (B) after 48 h of incubation in the DFR with Landy medium. 167

List of Tables

Table 1. Overview of different existing lipopeptide production processes and their corresponding advantages and disadvantages **[25]**. 24

Table 2. Strains and plasmids used in this work with their corresponding genotype or plasmid composition. 43

Table 3. Maximum specific growth rates of the *B. subtilis* 168 mutants in the Biolector® cultures (determined between 2 to 6 h) with the corresponding standard deviation. 63

Table 4. Biofilm dry weight and the relative amounts of EPS and cells present in the biofilm formed by EPS producing strains in the DFR. 69

Table 5. Bacterial strains and plasmids used in this study. 78

Table 6. Surfactin production and productivity of the engineered strains grown in continuous DFR biofilm cultures after 48h of cultivation with the corresponding standard deviation. 91

Table 7. Strains used in this study. 100

Table 8. List of parameters used for the model construction. 106

Table 9. Surfactin productivity of the two *B. subtilis* 168 strains measured in the bulk medium during batch and continuous cultivation. 112

Table 10. General model parameters and their corresponding values used for *B. subtilis* BBG111 (*sfp*$^+$, *epsC*^{0}) and RL5260 (*sfp*$^+$, *epsC*$^+$). 114

Table 11. Parameters related to cell adhesion and detachment that were introduced into the model. 115

Table 12. *B. subtilis* 168 derivative strains used in this study. 126

Table 13. Biomass ratio (g biofilm dry weight / g planktonic cell dry weight) determined for each strain. 130

Table 14. Determined glucose-to-biofilm conversion yields $Y_{Biofilm/S}$ for the different strains. 132

Table 15. Surfactin mean productivities and production yields during the cultivation. 133

Table 16. Strain comparison of RL5260 and BBG512 under limited glucose feeding conditions. 138

Table 17. Introduced model parameters for the simulation of nutritional stress in the trickle-bed biofilm bioreactor. 139

Table 18. List of primers that were used to construct the master strain and the gene deletion cassette. The name, sequence and number of nucleotides (Nt) is mentioned in the list. 155

Table 19. Components of the Landy MOPS medium. 157

Table 20. List of the direct links to the video files showing the microcolony development of the different strains and the corresponding password to get access. 158

Table 21. Results of the Chi-square goodness of fit test for the model and experimental data obtained with BBG111 (chapter 4). 164

Table 22. Results of the Chi-square goodness of fit test for the model and experimental data obtained with RL5260 (chapter 4). 165

Table 23. Results of the Chi-square goodness of fit test for the model and experimental data obtained with BBG512 under limited glucose feeding conditions (chapter 5)...165

Table 24. Results of the Chi-square goodness of fit test for the model and experimental data obtained with RL5260 under limited glucose feeding conditions (chapter 5)...166

List of Abbreviations

µL	Microliter
µm	Micrometer
Ala	Alanine
Asp	Aspartic acid
B. amyloliquefaciens	*Bacillus amyloliquefaciens*
B. subtilis	*Bacillus subtilis*
cm	Centimeter
Cm	Chloramphenicol
DFR	Drip-flow reactor
E. coli	*Escherichia Coli*
EPS	Exopolysaccharide(s)
Erm	Erythromycin
FA	Fatty acid
g	Gram
Glu	Glutamic acid
h	Hour
HPLC	High-performance liquid chromatography
Ile	Isoleucine
L	Liter
LB	Lysogeny broth
Leu	Leucine
M	Moles per liter
mg	Milligram
min	Minute
mL	Milliliter
mM	Millimole per liter
MOPS	3-Morpholinopropane-1-sulfonic acid
MS	Mass spectrometry
Neo	Neomycin
NRPS	Nonribosomal peptide synthetase

Nt	Nucleotides
OD$_{600\ nm}$	Optical density at 600 nm
ODE	Ordinary differential equation
Opp	Oligopeptide permease
ORF	Open reading frame
Orn	Ornithine
PBS	Phosphate buffered saline
PCR	Polymerase chain reaction
PHA	Polyhydroxyalkanoates
PP	Polypropylene
PPT	Phosphopantetheinyl transferase
Pro	Proline
Rap	Response regulator aspartyl-phosphate
RP	Reverse phase
Spc	Spectinomycin
SSF	Solid-state fermentation
TEI	Type I thioesterase
TEII	Type II thioesterase
TFA	Trifluoroacetic acid
Thr	Threonine
TOC	Total organic carbon
Tyr	Tyrosine
UPLC	Ultra-performance liquid chromatography
Val	Valine

Preface

In today's world, sustainable and economical processes are becoming increasingly important since it is an urgent need to reduce the carbon emissions and environmental pollution in order to protect our planet. A new era is emerging in which people with increasing demand prefer biological over chemically synthesized products due to their biodegradability and sustainability. Microbial biosurfactants are multifunctional molecules that could be exploited in many industrial sectors to replace the environmentally harmful chemical counterparts. Consequently, they are considered as key technology for sustainable development nowadays. The use of microorganism as industrial workhorses is a strongly developing industry providing huge possibilities for the production of defined biological products through strain engineering that are environmentally sustainable. Metabolic engineering and synthetic biology permit to increase the production yield making industrial production processes feasible. The existing biotechnological processes are mostly based on suspension cultures in stirred tank reactors. In the last years, biofilms are gaining increasing attention to exploit them for the production of value-added products in immobilized cell cultures, a promising alternative technique for the design of new bioprocesses. Biofilms, microbial communities attached to a surface embedded into a self-produced matrix, are already successfully used for waste-water treatment and bioremediation. Natural characteristics like high cell densities in biofilms are beneficial for high production rates and the biofilm matrix synthesis protects the cell from external influences. Biofilms have a high potential in economically efficient continuous fermentation processes. For microbial biosurfactant production, biofilm cultivations are especially beneficial since they permit to design processes avoiding foam formation. However, the understanding and control of the cellular development in biofilm-based bioprocesses is still limited and needs further research to achieve more stable processes through a better growth control of the biofilm in the system. *B. subtilis* 168 is widely used in the academic and industrial sectors for the production of value-added products due to its high secretion capacity. As special feature, this bacterial strain is able to produce lipopeptide-type biosurfactants with exceptional biological activities. However, the cell adhesion capacities of this strain are limited due to a deficiency in biofilm formation.

The overall objective of this thesis was to increase the biofilm formation capacities of *B. subtilis* 168 by genetic engineering in order to adapt this strain better to the biofilm cultivation mode and to develop an appropriate biofilm-based continuous surfactin production process allowing a simplified downstream processing of the target biomolecule. **Figure 1** describes the different steps of the strategy pursued in this work.

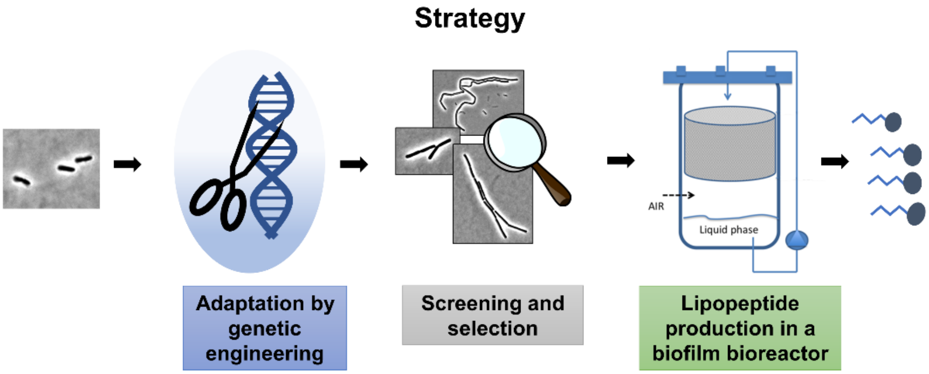
Strategy
AIR
Liquid phase
Adaptation by genetic engineering
Screening and selection
Lipopeptide production in a biofilm bioreactor

Figure 1. Overview of the strategy pursued in this work.

In the beginning, different genetic engineering strategies affecting the cell morphology and exopolysaccharide expression were applied in order to increase the colonization capacities of *B. subtilis* 168 to adapt the strain better for biofilm-based cultivation systems. After a screening study under low shear stress conditions in a drip-flow biofilm reactor, the most performant strains were cultivated in a newly designed lab-scale trickle-bed biofilm bioreactor for lipopeptide production. The process parameters were adapted in order to promote biofilm formation and reduce the presence of planktonic cells. A growth model able to describe the development of the planktonic cells and biofilm in the system has been developed and validated and can be used for further process optimization in the future.

The work has been divided into several chapters that are briefly described in the following.

Chapter 1: State of the art

The first chapter starts with a literature review giving the necessary background information and describing the current development in the research field.

Chapter 2: Genetic engineering and screening for *B. subtilis* 168 strains with increased colonization capacities

The second chapter describes the genetic engineering strategies used to generate different *B. subtilis* 168 mutants with improved colonization capacities. Furthermore, it provides a detailed overview of the applied methods and results of the screening techniques showing the impact of exopolysaccharide production and/or cell filamentation on the colonization capacities of the engineered *B. subtilis* 168 mutants. Parts of the supplementary data of article I (chapter 3) are included in this chapter (section 3.2).

Chapter 3: Molecular strategies for adapting *B. subtilis* 168 biosurfactant production to biofilm cultivation mode (Article I)

The third chapter is in dependence on the second chapter. The most performant strains have been selected to take a deeper look for their capacity to be cultivated in a continuous biofilm-based bioreactor. The focus is on the drip-flow biofilm cultivation device to further characterize the strains in terms of initial adhesion capacity and the impact of surfactin production on the biofilm formation. Moreover, a growth model has been developed that permits to describe the colonization and biofilm formation on the drip-flow reactor coupons.

Chapter 4: Growth dynamics of bacterial populations in a two-compartment biofilm bioreactor reactor designed for continuous surfactin biosynthesis (Article II)

In the fourth chapter, a lab-scale two-compartment trickle-bed biofilm bioreactor has been designed on the basis of previous works in the laboratory. The system was characterized and poor and strong biofilm forming *B. subtilis* 168 strains were cultivated using a combined batch and continuous process mode. A growth model was established able to describe the development of the planktonic and biofilm population in the system. Process operations were adapted in order to enhance biofilm formation on the packing element and reduce the development of planktonic cells.

Chapter 5: Impact of filamentous *B. subtilis* 168 mutants on the process performance and stability of a continuous trickle-bed biofilm reactor

The fifth chapter deals with the cultivation of *B. subtilis* 168 strains with improved adhesion capacities to further increase the stability of the biofilm population in the previously designed trickle-bed biofilm bioreactor. The impact of filamentous growth and EPS production on biofilm development and detachment was examined. Besides, the growth behavior under limited carbon conditions has been investigated. Simulations with the model under nutritional limitations has been performed and compared with the experimental values to further validate the model.

The work ends with **Chapter 6** giving general conclusions relying on the entire obtained results and possible perspectives and the **Appendix** providing some additional information of the performed work.

CHAPTER 1

State of the art

1. *Bacillus subtilis*

1.1 Origin of *Bacillus subtilis*

B. subtilis is a facultative aerobic growing, flagellated, endospore-forming, rod-shaped Gram-positive bacterium that can be found in soil, water sources and in association with plants [1–3]. *B. subtilis* is the best-characterized Gram-positive bacterium and has been intensively studied for more than a half-century [1]. The bacterium is the focus of a variety of research interests in the academic and industrial sectors [4].

The ancestor (ATCC6051 equal to NCIB3610) of the commonly used *B. subtilis* laboratory strains was isolated around 1900 by Meyer and Gottheil at the Marburg University [4–6]. In 1947, Burkholder and Giles isolated *B. subtilis* 168, an L-tryptophan auxotrophic mutant strain, after having treated the *B. subtilis* Marburg strain with ultraviolet and x-radiation [4, 7]. A few years later, Spizizen described the high transformation efficiency of *B. subtilis* 168 with wild-type DNA [4, 8]. As a result of this work, *B. subtilis* 168 was subsequently disseminated and became an extensively studied research object worldwide [4, 6]. The domesticated *B. subtilis* strain 168 is the most well-known and widely used laboratory strain [9]. *B. subtilis* 168 represents an ideal research model organism due to its ease of genetic manipulation and efficient growth under laboratory conditions [9]. However, introduced plasmids are instable in *B. subtilis* [10] and thus it is necessary to use genetic manipulation techniques that affect directly the genome.

1.2 Genomic features

The revelation of the complete genome sequence of *B. subtilis* 168 in 1997 [1] has provided more insights into the lifestyle and characteristics of the organism [11]. The genome has been updated and reannotated in 2009 [12].

In the genome, numerous genes coding for degradative enzymes, secretion pathways, transporters, quorum sensing regulators and two-component signal-transduction pathways have been identified [1]. *B. subtilis* is highly adaptable to diverse environments within the biosphere [11]. Given that *B. subtilis* secretes numerous enzymes, the organism is able to degrade and use diverse substrates and thus survives in a continuously changing environment [10]. As a response to environmental stress or nutrient depletion, *B. subtilis* forms highly resistant dormant endospores [11]. Nearly 4% of the genome code for large multifunctional enzymes involved in secondary metabolite production of antimicrobial compounds such as the lipopeptides surfactin and fengycin [1]. Lipopeptides are produced by the nonribosomal peptide synthetase (NRPS) pathway. It represents an alternative biosynthesis pathway to the ribosomal machinery where mRNA templates are translated to proteins in cells [13]. Nonribosomal peptides are assembled via large multifunctional enzymes (NRPS) that are able to generate peptides with a strong structural diversity and various biological activities [13, 14].

No virulence genes were found which is in accordance with the fact that *B. subtilis* is considered as non-pathogenic [11]. In the evolution of this strain through horizontal gene transfer, bacteriophage infection has played an important role since the genome contains at least ten prophages or prophage-like elements (among them the most known are PBSX, SPß and skin element) or remnants of prophages [1].

1.3 Swarming motility and biofilm formation

B. subtilis 168 is a laboratory strain that is generally used for molecular genetic studies due to the increased genetic natural competence and the simplicity to introduce genetic modifications [11]. However, the improved fitness of *B. subtilis* 168 in the laboratory as a result of its domestication comes along with some deficiencies in the traits that are characteristic for wild-type strains [11]. The laboratory strain *B. subtilis* 168 lost the capacity of swarming and the formation of architecturally complex biofilm or pellicle structures; all behaviors that are observed for wild-type strains of *B. subtilis* (**Figure 2**) [15, 16].

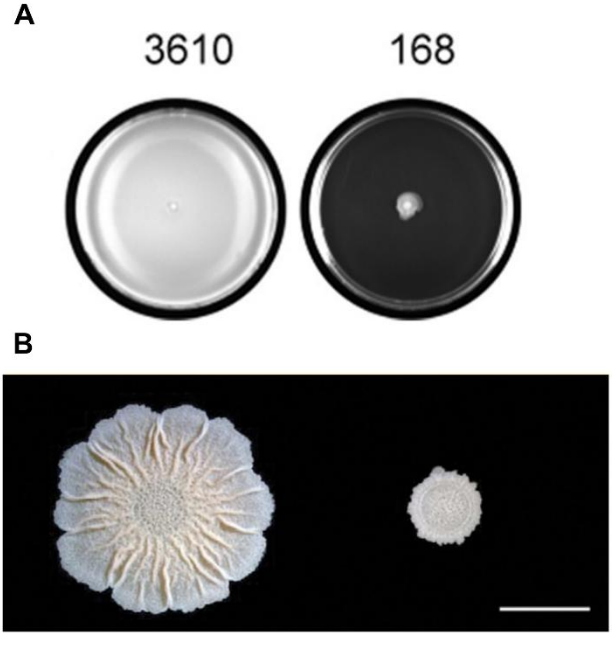

Figure 2. (A) Swarming motility on 0.7% LB agar plates of NCIB3610 and *B. subtilis* 168. Bacterial growth appears in white and uncolonized agar is black (adapted from [17]). (B) Colony biofilm of the wild-type strain NCIB3610 (left side) and *B. subtilis* 168 (right side). The scale bar corresponds to 1 cm [11].

Swarming motility describes the bacterial cell movement on surfaces and requires functional flagella as well as the production of a surfactant to reduce the surface tension [18]. The loss of swarming capacity in *B. subtilis* 168 is due to frameshift mutations in the *sfp* and *swrA* coding sequences [18, 19]. The *sfp* gene codes for an enzyme that performs posttranslational modifications of the NRPS required for surfactin synthesis [20]. The protein SwrA is necessary to activate the gene expression for flagellar biosynthesis [17]. Beside the impact on swarming motility, surfactin reacts also as trigger molecule for biofilm formation through the activation of a quorum sensing signaling pathway that induces the expression of genes involved in the extracellular matrix synthesis [21]. However, the mutation in the *sfp* gene is not the only one responsible for the attenuated biofilm formation capacity of *B. subtilis* 168 compared to the wild-type strain NCIB3610.

McLoon et al. [6] identified three additional mutations that have accumulated during the domestication process of *B. subtilis* 168 and cause the inability to form robust biofilm structures. First, a point mutation in the exopolysaccharide production gene *epsC*, located in the *epsA-O* operon, is responsible for the defective exopolysaccharide production and thus the reduced biofilm matrix synthesis [6]. Secondly, a mutation in the *swrA* gene contributes to impaired biofilm formation [6]. SwrA stimulates the *fla/operon* in wild-type strains needed for swarming motility and poly-γ-polyglutamic acid production and thus has potentially as well an impact on biofilm formation [6]. The third biofilm-attenuating mutation that has been identified is located in the promoter of the regulatory gene *degQ* which is involved in the signaling pathway leading to the secretion of degradative enzymes [6]. Additionally, McLoon et al. [6] have shown that a plasmid, notably the plasmid-borne gene *rapP*, present in NCIB3610 but lost in *B. subtilis* 168, strongly influenced the biofilm architecture. After introducing *rapP* and the correction of the *sfp, epsC, swrA* and *degQ* gene in *B. subtilis* 168, the biofilm robustness was completely restored and comparable to that of the wild parent strain NCIB3610 as **Figure 3** demonstrates [6].

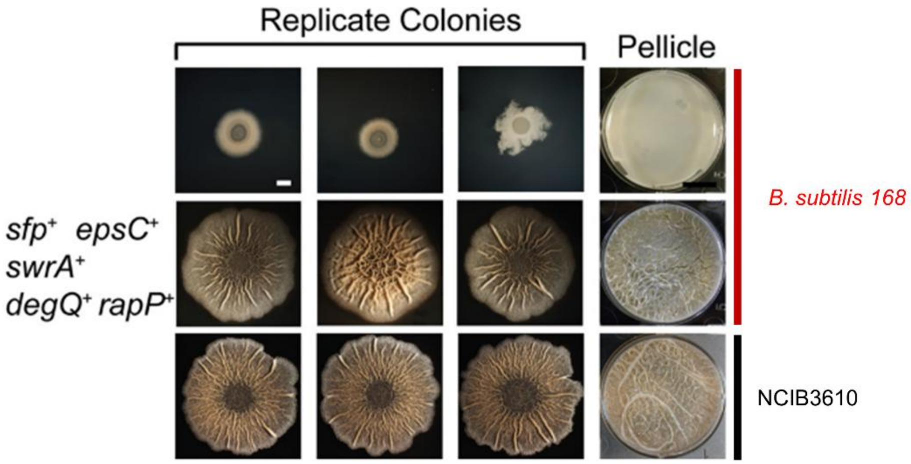

Figure 3. Colony and pellicle phenotypes of *B. subtilis* 168 and *B. subtilis* 168 with five corrected mutations compared to the ones of the parent strain NCIB3610 (adapted from [6]).

1.4 Commercial interest

Bacillus species are dominant bacterial workhorses in many microbial industrial fermentation processes [22]. The enzymes produced by *Bacillus* species represent about 60% of the industrial enzyme market [10]. They are very attractive industrial organisms due to their high growth rates combined with high production yields (20 to 25 gram per liter) [23]. In addition, *B. subtilis* is able to secrete proteins directly into the fermentation broth which offers major advantages for the downstream processing of the products [10, 23]. Moreover, *B. subtilis* possesses a generally regarded as safe (GRAS) status recognized by the Food and Drug Administration due to the absence of toxic by-products [22, 23].

2. Lipopeptides produced by *Bacillus* species

The lipopeptides from *Bacillus* species were discovered and first isolated during the 1950s and 1960s [24]. Lipopeptides are amphiphilic molecules that are composed of a peptide cycle which is linked to a fatty acid chain of different lengths and isomeries [24]. Nowadays, the demand of these bioactive compounds is exponentially growing due to their remarkable physiochemical properties and biological activities [25].

The lipopeptides produced by *Bacillus* species were first classified into three main families named as surfactin, fengycin, and iturin [24]. Later, kurstakin [26] and locillomycin [27], two new lipopeptide families, have been discovered. The laboratory strain *B. subtilis* 168 contains the genetic loci that code for the large multifunctional nonribosomal peptide synthetases *srf* and *pps* and thus is a potential producer of surfactin and fengycin [1, 28].

2.1 Structure of surfactin and fengycin

Surfactin is a cyclic lipopeptide composed of a heptapeptide with the amino acid sequence L-Glu – L-Leu – D-Leu – L-Val – L-Asp – D-Leu – L-Leu that is closed by a lactone ring with the ß-OH group of the fatty acid chain [24, 29]. The chemical structure is presented in **Figure 4A**.

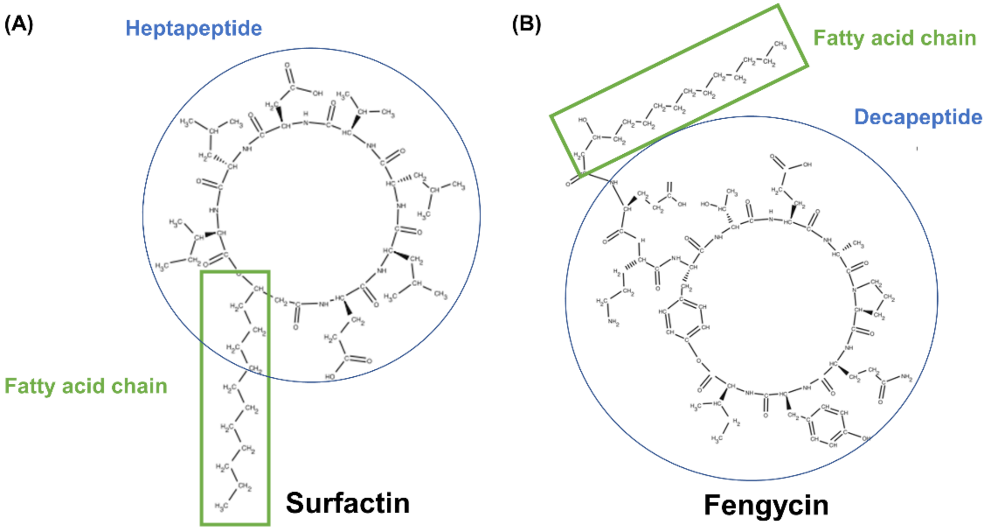

Figure 4. Detailed structure of (A) surfactin nC14 and (B) fengycin nC15 isomers (adapted from [24]).

Depending on the surfactin isomers, the ß-hydroxy fatty acid chain can contain 12 to 16 carbon atoms with *normal*, *iso* or *anteiso* configurations [24, 29, 30]. The most abundant surfactin isomers are usually composed of C14 and C15 fatty acid chains [24]. Various surfactin isomers have already been described with either amino acid substitutions or different fatty acid residues [31, 32]. These variations occur depending on the *B. subtilis* strain, the nutritional and environmental conditions [33, 34]. Fengycin (**Figure 4B**), also called plipastatin, is composed of a ß-hydroxy fatty acid that is linked to the N terminus of a decapeptide consisting of the amino acid sequence L-Glu – D-Orn – (D or L)-Tyr – D-*allo*-Thr – L-Glu – D-(Ala or Val) – L-Pro – L-Glu – (L or D)-Tyr – L-Ile [24, 35–38]. 8 of the 10 amnio acids are organized in a cyclic structure closed by a lactone ring [24, 35]. The fatty acid chain contains 14 to 18 carbon atoms, but C15 to C17 fatty acid chains are the mainly present variants [24].

Surfactin and fengycin have both very interesting biological activities [24]. While surfactin is prominent for its extraordinary surfactant power, fengycin is known to display strong antifungal activities [39, 40]. However, the main focus in this work will be on surfactin whose synthesis with the involved regulation mechanisms and properties will be more detailed in the following.

2.2 Nonribosomal peptide synthesis of surfactin

The NRPS involved in surfactin synthesis is encoded by the *srfA* operon composed of four open reading frames (ORF) [32]. The first three ORF are designated *srfAA* (402 kDa), *srfAB* (401 kDa) and *srfAC* (144kDa) and represent the NRPS subunits that permit to elongate the oligopeptide chain [32]. The subunits are composed of either three modules (SrfAA and SrfAB) or one (SrfA-C) [41]. Each of the seven module is responsible for the incorporation of one amino acid [41, 42], as shown in **Figure 5**.

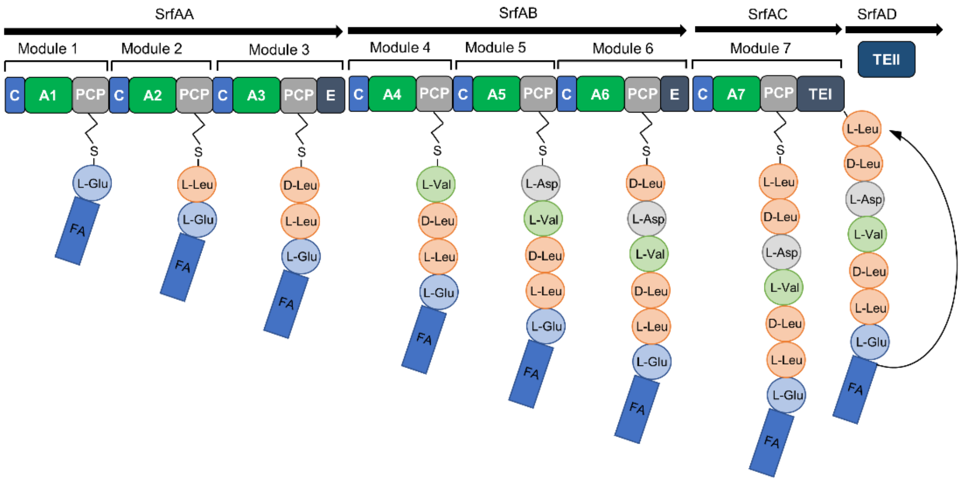

Figure 5. Schematic illustration of the surfactin assembly line via the nonribosomal peptide synthesis pathway.

The modules are composed of a condensation (C), adenylation (A) and peptidyl carrier (PCP) domain [32]. The last modules of SrfAA and SrfAB contain an additional epimerization domain for the conversion of L-Leu into D-Leu [32]. The SrfAC module consist additionally of a type I thioesterase (TEI) domain which catalyzes the lactone bond formation between the carboxylate group of Leu-7 and the hydroxyl group of the ß-hydroxy fatty acid just before the release of the mature surfactin molecule [24, 41]. The last OFR *srfAD* (40 kDa) is not directly involved in the elongation process of the heptapeptide, but codes for an external type II thioesterase (TEII) whose function is to recycle defective PCP domains [32, 41].

For a functional surfactin synthesis, posttranslational modifications of the PCP domains are necessary which are executed by a phosphopantetheinyl transferase (PPT) encoded by the *sfp* gene [20, 32]. The PPTase Sfp catalyzes the conversion of the surfactin synthetase from the apoform to the holoform to activate the enzyme complex for the subsequent surfactin synthesis [20]. Sfp transfers the phosphopantethein group from CoA to the PCP domains and thus introduces a reactive thiol terminus to these domains to enable the load of amino acids and peptide bond formation [20, 32]. The surfactin synthesis is initiated through the presence of an CoA-activated ß-hydroxylated fatty acid recognized by the first condensation domain in SrfAA [43]. This C domain starts with the catalyzation of the fatty acid acylation with the amino group of the first amino acid L-Glu [43].

2.3 *Regulation of surfactin biosynthesis*

The expression of the surfactin synthetase, encoded by the *srfA* operon, is linked to a complex regulatory cascade which can be stimulated through external and growth-dependent factors [32]. The induction of surfactin biosynthesis depends on quorum-sensing molecules and pleiotropic regulators [24]. The regulation mechanisms are linked to cell differentiation pathways for competence, sporulation and biofilm formation [24]. **Figure 6** gives an overview of the different regulation mechanisms and the genes involved in surfactin production.

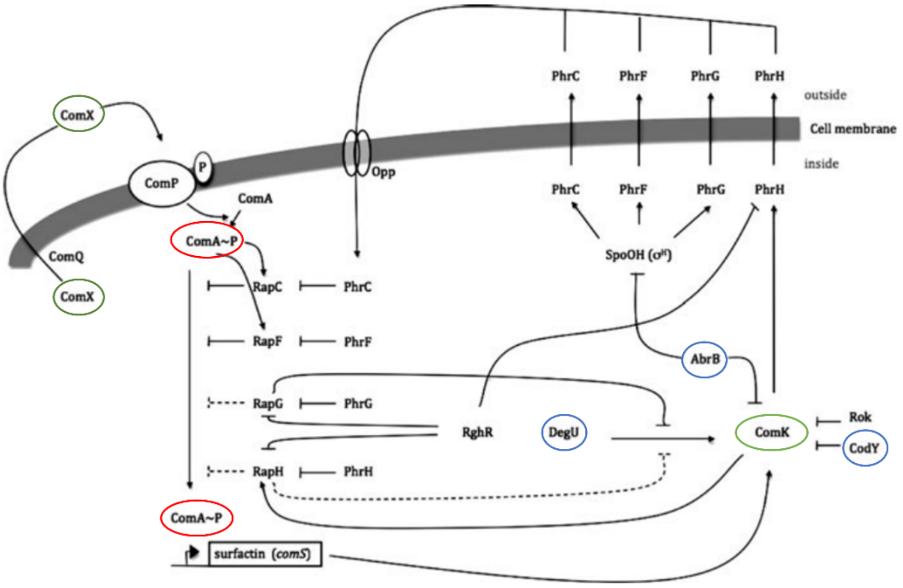
PhrC
PhrF
PhrG
PhrH
outside
Cell membrane
inside
ComX
ComP
P
Opp
ComA
ComA~P
ComQ
ComX
PhrC
PhrF
PhrG
PhrH
SpoOH (σH)
RapC
PhrC
RapF
PhrF
AbrB
RapG
PhrG
RghR
DegU
ComK
Rok
CodY
RapH
PhrH
ComA~P
surfactin (comS)

Figure 6. Overview of the regulation cascade involved in surfactin expression (adapted from [24]).

In the transitional growth phase, *B. subtilis* cells are able to acquire natural competence due to the induction of several gene regulation mechanisms [44]. This enables the cell the uptake of exogenous DNA [44]. Competence in *B. subtilis* is initiated through the expression of ComK which starts at the end of the exponential growth phase [45]. For an optimal competence development a sufficiently high cell density is required [45]. Upon competence initiation, the pheromone ComX is secreted and accumulates in the medium [24]. ComP is stimulated through the extracellular ComX and activates ComA in the cell through phosphorylation [24]. Subsequently, ComA-P induces the expression of the surfactin operon *srfA* [24]. The expression of the surfactin synthetase, encoded by the *srfA* operon, is thus directly linked to the cell growth and cell density of *B. subtilis* [32]. The ComX-dependent regulation pathway is additionally affected by Phr peptides and response regulator aspartyl-phosphate (Rap) phosphatases which modulate the phosphorylation state of ComA [24]. The Phr peptides are synthesized as small proteins and secreted to be processed in pentapeptides which are then reimported into the cell through an oligopeptide permease (Opp) [24]. The expressions of *rapG*, *rapH* and *phrH* are known to be repressed by RghR [24].

Besides the ComX-dependent pathway, the surfactin operon expression is affected by global regulators including AbrB, DegU, and CodY [24]. These regulators are involved in different cell differentiation pathways and thus are associated to a specific physiological state of *B. subtilis* [32]. AbrB is a key regulator that inhibits the expression of surfactin in *B. subtilis* as well as various genes during the exponential growth phase including the biofilm matrix genes [46, 47]. During the transitional growth phase, the gene expression is reorganized after repression of AbrB by the master regulator for sporulation Spo0A [46]. DegU is part of the DegS-DegU two-component signal transduction system that coordinates multicellular behavior [48]. The system is involved in the activation of genetic competence and responsible for the activation of gene expression for degradative enzymes as well as the formation of the hydrophobic BslA layer in sessile cells [32, 48, 49]. CodY is a global regulator that controls more than a hundred genes which are repressed during exponential growth and induced when cells encounter nutrient limitations [50]. The transcription of the competence gene *comK* and the surfactin operon *srfA* are inhibited by CodY during the exponential growth phase [44].

2.4 Properties and applications of surfactin

Microbial biosurfactants have a great structural diversity which leads to multifunctional useful properties [51]. **Figure 7** gives a general overview of the broad potential application fields of biosurfactants in industry.

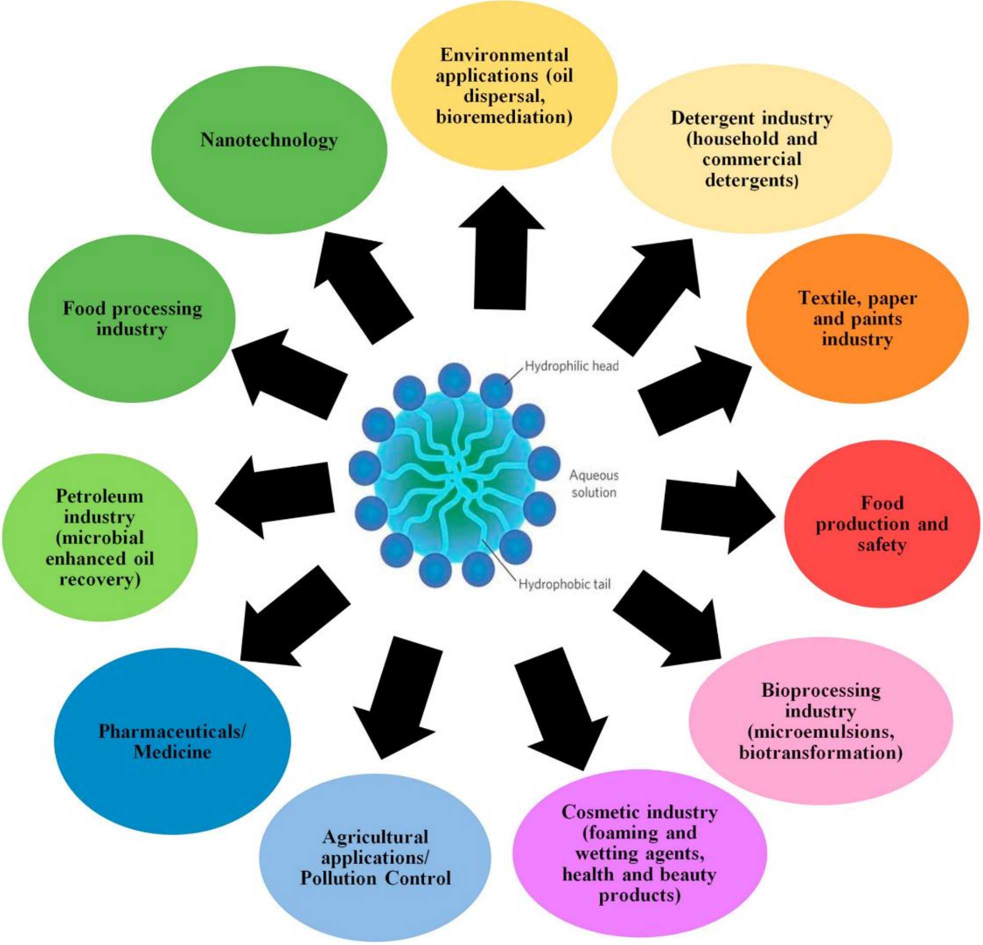
Environmental applications (oil dispersal, bioremediation)
Detergent industry (household and commercial detergents)
Textile, paper and paints industry
Food production and safety
Bioprocessing industry (microemulsions, biotransformation)
Cosmetic industry (foaming and wetting agents, health and beauty products)
Agricultural applications/ Pollution Control
Pharmaceuticals/ Medicine
Petroleum industry (microbial enhanced oil recovery)
Food processing industry
Nanotechnology
Hydrophilic head
Aqueous solution
Hydrophobic tail

Figure 7. Overview of the various industrial applications of biosurfactants [52].

The biosurfactant surfactin has exceptional foaming and emulsifying properties as well as interesting biological activities which can be exploited in various fields including agriculture, pharmaceuticals and medical products, as well as in the cosmetic, food, environmental and petroleum industry [24]. Surfactin is one of the most powerful biosurfactant able to reduce the surface tension of water from 72 to 27 mN/m with a minimum load of 0.005% [53] and represents an interesting alternative to the commercial chemical surfactants [54]. The biomolecule provides several advantages over chemical compounds regarding their lower toxicity, biodegradability and specificity [55]. Moreover, several potential therapeutic applications of surfactin exist due to its antimycoplasma, antiviral and anti-inflammatory properties [24, 53, 56–58].

Lipopeptide-type biosurfactants like surfactin gain especially increasing interest in the phytosanitary field, where they can be used as biocontrol agents to replace chemical pesticides for a more sustainable agriculture [59]. Surfactin displays specific biological activities reacting directly against various pathogens as well as has strong elicitor capacities [40, 60, 61]. Thereby, surfactin has the potential to stimulate inducible defense mechanisms in plants a phenomenon referred to as "induced systemic resistance" [62]. This kind of induction enhances the defensive capacity of plants and contributed to the resistance of plants against invasive phytopathogens [62].

3. *Biotechnological surfactin production processes*

Biosurfactant production is considered as a key technology for sustainable development in the 21st century [63]. There is an increasing awareness to replace chemical surfactants by the more eco-friendly microbial surfactants in various industrial sectors [55]. However, for industrial implementation it is necessary to reduce the cost price of biosurfactants to make them competitive with the synthetic counterparts [25, 55].

In the following, the effects of medium composition and process parameters on surfactin production are presented. Furthermore, optimizing strategies based on strain engineering and process design that have been applied to increase the surfactin yield are described as well as existing downstream processes are briefly mentioned.

3.1 *Impact of medium composition*

In contrast to the production of other secondary metabolites whose production is induced upon nutrient depletion, surfactin production is induced by actively growing cells and thus probably enters in competition with cellular growth [30, 64]. The biosynthesis of surfactin starts during the exponential growth phase and continues over a broad range of the cell cycle when the availability of nutrients is guaranteed [64]. The highest surfactin production occurs at the end of the exponential growth phase [64]. Given that the regulation and induction of surfactin is growth-dependent, the medium composition has a strong impact on the surfactin production. Landy medium with glutamic acid as nitrogen and 2% glucose as carbon source [65] and the medium of Cooper with NH_4NO_3 as nitrogen and 4% glucose as carbon source [66] are two chemically defined culture media widely established for enhanced surfactin production with *B. subtilis* [24, 67]. Landy medium has a molar C:N ratio of 27:1, whereas the medium of Cooper has a ratio of 13:1 [65–67]. High C/N ratios limit bacterial growth and favor instead the cell metabolism and production of metabolites [63]. The addition of trace metals to the medium has shown to have a significant impact on lipopeptide production [67]. The addition of iron or manganese salts increased significantly the surfactin production [66]. Wei et al. [68] showed, that beside iron and manganese, potassium and magnesium ions have a positive impact on surfactin production.

3.2 Effect of process parameter

Different cultivation conditions like pH, temperature, dissolved oxygen and the aeration rate that have an impact on cellular growth affect as well the surfactin production in *B. subtilis* [69]. The pH regulation is important for surfactin production and should be maintained around 7 since too low pH values reduce surfactin production as well as cause the precipitation of surfactin under a pH of 6.0 [24, 53]. Wild-type *B. subtilis* strains are mostly cultivated at 30°C in surfactin production processes [66, 70–81]. Whereas derivatives of the laboratory strain *B. subtilis* 168 are mainly incubated at 37°C, as a higher temperature favors the growth rate as well as the surfactin production [82–84].

Sufficient oxygen supply and efficient mass transfer have shown to play a major role in the surfactin production kinetics [53]. Yeh et al. [76] reported an enhanced surfactin production with *B. subtilis* ATCC 21332 by using a high aeration rate to guarantee sufficient oxygen supply and a good mass transfer efficiency in a carrier-assisted bioreactor. In flask cultures, low filling volumes and high shaking frequencies resulted in an improved surfactin production with *B. subtilis* BBG21 [77]. The surfactin concentration increased strongly with an increased volumetric oxygen transfer coefficient K_La within the range from 0.003 to 0.015 s^{-1} [77]. Under limited oxygen supply, the anerobic growth of a *B. subtilis* wild-type strain results in the production of primary metabolites such as acetate, lactate, acetoin and 2,3-butandiol [85].

3.3 Strain Engineering

Coutte et al. [86] replaced the native *srfA* promoter by a constitutive one to bypass the natural complex regulation of the *srfA* operon in *B. subtilis* 168 (cf. **Figure 6**, page 13). In this case, surfactin production occurred earlier in the growth phase and was 5-fold higher after 6 h of culture. However, although surfactin production was naturally induced only at the end of the exponential growth phase (6 to 8 h), the overall surfactin productivity in a long-term fermentation was higher with the native *srfA* promoter [86]. This is linked to the fact that the native promoter of *srfA* in *B. subtilis* 168 is very efficient and much stronger than the one present in wild-type strains like *B. subtilis* ATCC6633, as proved by Duitman et al. [87]. The disruption of the plipastatin (fengycin) operon led to a significantly enhanced surfactin production as well as an improved spreading behavior [86]. Coutte et al. [86] supposed that the deletion of the plipastatin operon results in an increase availability of precursors like β-hydroxy fatty acids and branched chain amino acids necessary for the lipopeptide biosynthesis.

By means of metabolic engineering, a strain that overproduces leucine, an important precursor for surfactin synthesis, was constructed by Coutte et al. [83]. Gene deletion were performed on the basis of an established reaction network model that predicted potential gene knockouts for an increased leucine production in *B. subtilis* [83]. An engineered strain with *codY* deletion exhibited a 21-fold increased surfactin production [83]. Another work [82] examined the impact of *lpdV* and *codY* deletion in *B. subtilis* BSB1 on quantitative and qualitative surfactin production. The specific surfactin production was enhanced about 5.8-fold for the *codY* mutant and 1.4-fold for the *lpdV* mutant. Interestingly, the *lpdV* mutant produced mainly the surfactin C_{14} isoform which possess enhanced foaming capacities compared to the other surfactin isoforms [82, 88].

Hu et al. [89] constructed a strain by combining several genetic engineering strategies. The genetic modifications affected the upstream precursor supplement, the *srfA* operon transcription module, the downstream surfactin efflux and the cell resistance [89]. First, they inserted a functional *sfp* in *B. subtilis* 168 to restore surfactin production [89]. Subsequently, several competitive pathways were knocked out to reduce the energy expense of the strain [89]. Gene clusters responsible for the expression of the synthetases involved in fengycin, siderophore and polyketides production were deleted [89]. Furthermore, biofilm formation-related genes (*epsA-O* and *tasA-sipW-yqxM*) were knocked out to limit the transcriptional activity of these genes [89]. The cellular tolerance to surfactin as well as the efflux was improved by overexpressing self-resistance associated proteins and transporters through the insertion of strong constitutive promoters [89]. Moreover, the branched-chain fatty acid biosynthesis was strengthened for an increased supply of precursor through the overexpression of enzymes involved in this pathway [89]. Performed genetic modifications that affected the glycolytic pathway increased the cell growth but did not have a positive effect on surfactin production [89]. The transcription level of the *srfA* operon was improved by increasing the expression of the positive regulators ComQXPA and knocking out negative regulators like Rap, CodY and SinI [89]. As a result of the performed genetic modifications, a final surfactin production of 12.8 g L^{-1} could be reached [89]. This corresponds to a 32-fold increase compared to the initial strain [89]. However, the initial surfactin production of the control strain (*sfp*$^{+}$) was mentioned as 0.4 g L^{-1} although *B. subtilis* 168 *sfp*$^{+}$ strains have already been reported to produce more than 1 g L^{-1} in Landy MOPS medium [86]. Moreover, Hu et al. do not specify the surfactin yield (produced surfactin per dry weight). Regarding the presented growth curves, the cultures seemed to reach high cell dry weights. This would mean an average surfactin yield of ~1 g g^{-1} was reached which is comparable to the one obtained by Coutte et al. [83].

3.4 Bioprocess design

In general, the existing surfactin production strategies are either based on foaming processes (suspended cultures), reduced foaming processes with immobilized cells or processes without foam formation [25].

3.4.1 Foaming processes

Foaming processes take the advantage of the high foaming capacity of lipopeptides [25]. **Figure 8** shows an example of a bioreactor set-up with foam overflow.

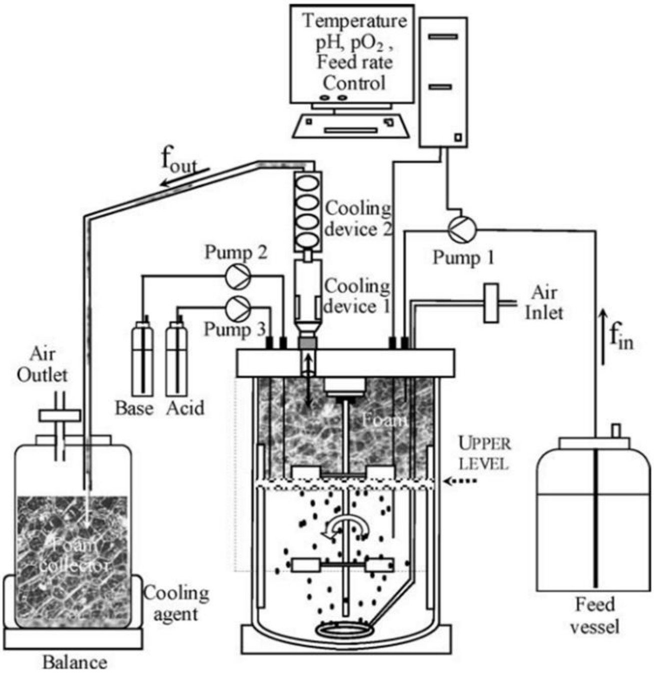
Temperature
pH, pO_2,
Feed rate
Control
f_{out}
Cooling device 2
Pump 2
Pump 1
Cooling device 1
Air Inlet
Pump 3
f_{in}
Air Outlet
Base
Acid
Foam
UPPER LEVEL
Foam collector
Cooling agent
Feed vessel
Balance

Figure 8. Bioreactor set-up with integrated foam overflow collector for lipopeptide production [70].

The lipopeptide are separated from the bulk medium through a foam fractionation strategy [25]. A foam column is coupled with the fermenter and collects the produced foam with the concentrated lipopeptides into a vessel [25, 70]. Foam fractionation was exploited in several bioprocesses to extract lipopeptides [66, 70–73, 75, 81, 90]. The continuous removal of surfactin through foam fractionation during fermentation improved significantly the yield [66]. The problem is that excessive foam formation is also coupled to a high loss of culture volume [73]. The cells often remained trapped in the foam which results in a cell loss and affects negatively the production yield [25, 73, 76]. Moreover, it is challenging to control exactly the foaming rate in the process [25].

3.4.2 Processes with cell immobilization

Cell immobilization has been shown to be beneficial for surfactin production in several cases. Yeh et al. [75] have shown that the addition of solid activated carbon carriers enhanced the surfactin production of *B. subtilis* ATCC 21332 (wild-type strain) up to 36-fold compared to conventional suspended cultures. The carrier seemed to act as growth stimulant for the suspended cells and served as support for biofilm development which both promoted an increased surfactin production [75]. Overflowing foam was collected in a device that permitted to recycle the cells and to introduce the foam in an acidic tank for surfactin precipitation (cf. **Figure 9**) [76].

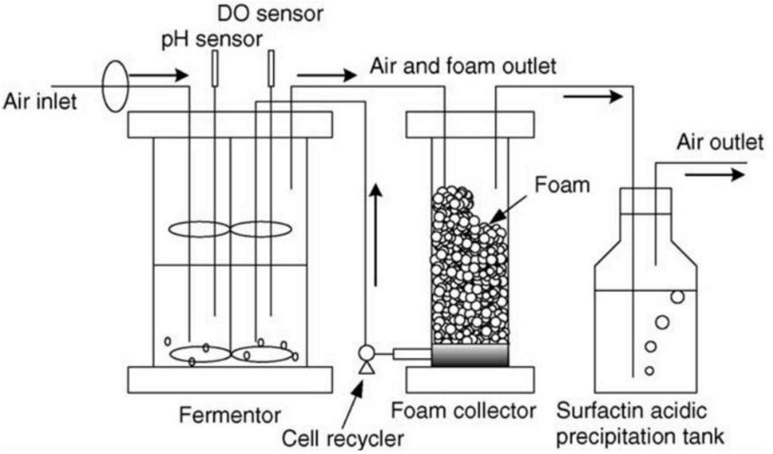

Figure 9. Carrier-assisted lipopeptide production in a stirred tank reactor with foam collector and cell recycle system [76].

Iron coated polypropylene (PP) particles that were added in batch stirred tank reactors promoted biomass development of *B. subtilis* ATCC 21332 through biofilm formation and led to enhanced lipopeptide production [91]. The cultures with cell immobilization on the PP pellets produced two to four times more lipopeptides than simple suspended cell cultures [91]. Chtioui et al. [79] performed batch cultures in flasks with added carbon activated PP particles that were colonized by *B. subtilis* ATCC 21332. The attached cells produced two to four times more lipopeptides than freely suspended cells [79]. The same carbon activated PP particles were used by Fahim et al. [78] in a three phase inverse fluidized bed bioreactor with liquid recycle providing an enhanced air-liquid mass transfer (**Figure 10**).

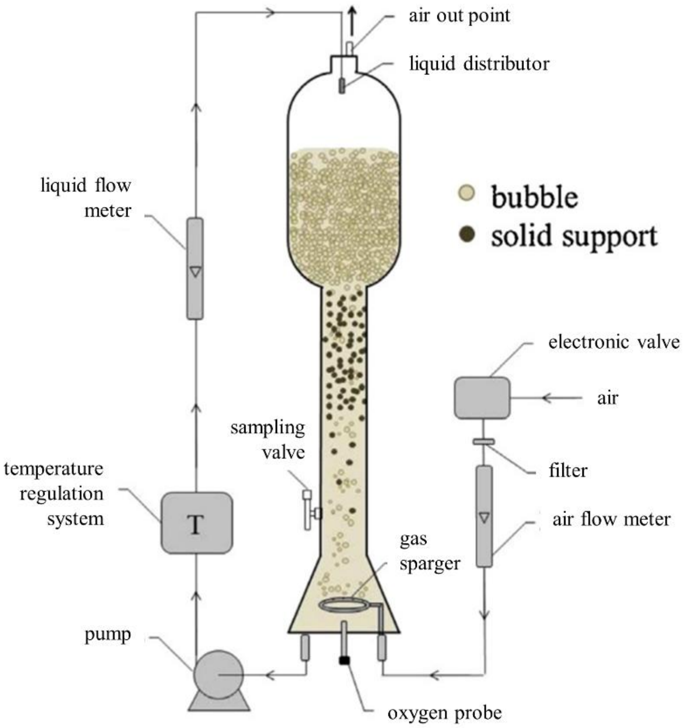
air out point
liquid distributor
liquid flow meter
bubble
solid support
electronic valve
air
sampling valve
temperature regulation system
T
filter
air flow meter
gas sparger
pump
oxygen probe

Figure 10. Three phase inverse fluidized bed bioreactor with an integrated liquid recycle system (adapted from [78]**).**

After a pre-colonization step with *B. subtilis* ATCC 21332, the particles were used to generate a fluidized bed in the reactor for lipopeptide production [78]. The cell immobilization had likewise a positive effect on the lipopeptide production [78].

3.4.3 Processes without foam formation

For an efficient surfactin production a sufficient oxygen mass transfer is required [76]. The surfactin productivity increases with an increasing aeration rate, however, too high agitation results in excessive foam formation [76]. Mechanical foam breaker or the addition of a high concentration of antifoam agents affect negatively the physiology of cells [92]. A smart bioreactor design is necessary to optimize the agitation and aeration strategies in order to minimize excessive foam formation and technical damage on the system [76]. Different types of lipopeptide production bioprocesses that avoid foam formation have been proposed based on a rotating discs bioreactor, solid-state fermentation (SSF), an air/liquid membrane contactor and biofilm bioreactors [25].

The rotating discs bioreactor developed by Chtioui et al. [93] is surface aerated and thus prevents foam formation during lipopeptide production. **Figure 11** shows the set-up of this bioreactor.

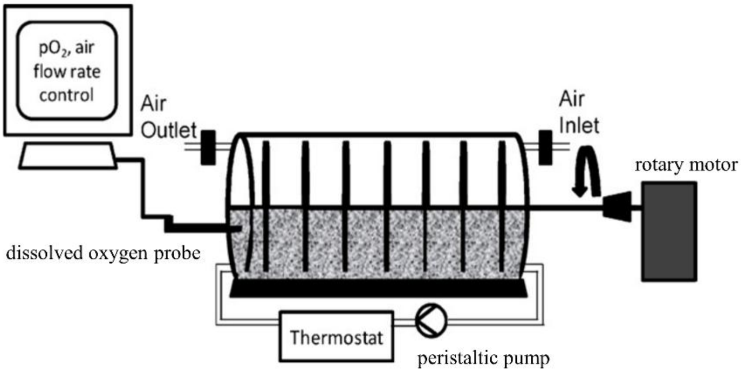

Figure 11. Set-up of the rotating discs reactor used for lipopeptide production.

The rotating discs are partially immersed in the medium. During fermentation, the planktonic cells were developing as well as the discs became colonized through biofilm formation of *B. subtilis* ATCC 21332. However, the air-liquid surface contact and the agitation of the culture medium were not sufficient to provide an appropriate oxygenation for surfactin production. In this set-up, surfactin production was relatively low, whereas the conditions of oxygen limitation and cell immobilization seem to increase significantly the fengycin production.

SSF is an interesting alternative biosurfactant production strategy since it allows to use cheap substrates and avoids foam formation [94]. However, the downstream processes for the biosurfactants extraction still need to be optimized [94]. Another challenge is the monitoring and control of process parameter since the packed-bed systems are not homogenous and thus process intensification approaches are limited [67]. Surfactin has been produced by SSF using industrial waste like bean curd residue (okara) as medium or wheat bran [95]. Ohno et al. [95] were able to produce about 10 g surfactin per kg dry solid using the recombinant *B. subtilis* MI113 strain. Slivinski et al. [96] reached 3.3 g per kg dry solids equivalent to a surfactin concentration of 809 mg L^{-1} with a non-recombinant *B. pumilus* strain using okara with sugarcarne gabasse as substrate. The optimal surfactin production temperature was in both cases 37°C [95–97].

Air/liquid membrane contactor were initially used in wastewater treatment [25, 98]. However, they are also convenient for aerobic biosurfactant production since this technology prevents foam formation by providing in the same time an high air-liquid mass transfer [25, 74, 84]. For the bioreactor aeration, oxygen is transferred into the culture medium via an organic membrane with a high specific surface area [25]. The air is injected in one of the membrane compartment and the other part is alimented with the culture medium [25]. Depending on the membrane surface and pore size, a K_La of up to 39 h^{-1} can be achieved (cf. [74]). Using this technology, Coutte et al. developed a bubbleless membrane bioreactor (**Figure 12**) for lipopeptide production that can be operated in a batch [74] or continuous fermentation mode [84].

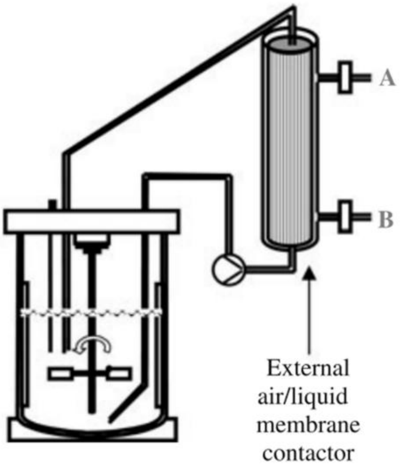

Figure 12. Basic set-up of the bubbleless bioreactor with aeration through an external air/liquid membrane contactor [74].

Surfactin production in the batch bubbleless membrane bioreactor with *B. subtilis* ATCC 21332 was comparable with to one obtained using the foaming bioreactor (~250 mg L^{-1}) [25, 74]. The continuous process mode was coupled to a continuous surfactin extraction and cell recycling system [84]. A combination of microfiltration and ultrafiltration permitted to continuously separate the biomass from the culture medium for cell recycling and to extract the lipopeptides from the broth [84]. The surfactin productivity was enhanced by applying an increased dilution rate [84]. A mean productivity of 110 mg L^{-1} h^{-1} was reached at a dilution rate of $D = 0.2\ h^{-1}$ [84]. An issue of this technology is that the membrane is exposed to fouling through cell adhesion and surfactin adsorption which reduces the oxygen transfer and thus affects negatively the surfactin production [25]. However, the thin biofilm which was growing on the aerated membrane seemed to be the main consumer of the supplied oxygen and thus probably contributed also essentially to the overall surfactin production [84]. In contrast to the biofilm, planktonic cells had a minor impact on the productivity due to the reduced oxygen respiration [84]. For a stable continuous process, an optimal biofilm thickness on the membrane has to be ensured in order to reduce oxygen limitation for maintaining the productivity over time [84]. **Table 1** summarizes the existing lipopeptide production processes that were presented and gives an overview of the process advantages and disadvantages.

Table 1. Overview of different existing lipopeptide production processes and their corresponding advantages and disadvantages **[25]**.

Bioprocess	Advantages	Disadvantages
Foaming bioreactor	Complete extraction of the lipopeptide Could be easily developed from stirred tank bioreactors	Foam volume Process limited by foam formation kinetic Loss of cells and culture medium
Three phase inversed fluidized bed	High oxygen transfer rate	Foaming control
Rotating discs bioreactors	Simple process	Low oxygen transfer rate
Biofilm Bioreactors	Continuous lipopeptide production and purification Reduced loss of biomass	Biofilm control
Air/liquid membrane contactors	Continuous lipopeptide production and purification	Membrane fouling Size and price of the membrane
Solid state fermentation	Simple process	Limited control

Biofilm bioreactors are promising interesting alternative systems for the continuous production of lipopeptide and will be presented more into detail in the following chapter as they are the focus of this work.

3.5 Downstream process operations

The most widely applied technique for initial surfactin recovery from the culture supernatant is acid precipitation with HCl [24, 99]. Subsequently, downstream purifications operations like solvent extraction, membrane ultrafiltration, adsorption and size exclusion chromatography are applied to further purify the lipopeptides [24, 99]. To get lipopeptides of high purity or individual lipopeptide isoforms for therapeutic applications, reversed-phase chromatography is the most appropriate purification technique [32, 99].

3.6 Industrial relevance of biosurfactant processes

The current process approaches do not yet allow an economically competitive production of lipopeptides at industrial scale for large-scale field applications, but they are already commercially available [100]. The Japanese company KANEKA started the first mass production of sodium surfactin by cultivating a surfactin overproducing strain in an optimized medium in order to reach high product titers [101]. In 2009, KANEKA started to commercialize sodium surfactin, still linked to a high cost price, as additive for personal care and cosmetic products [102]. Different lipopeptides, among them surfactin, are produced at pilot scale with *Bacillus* species by the start-up company Lipofabrik SARL (France). Lipofabrik has the ambition to make a further up-scale and to operate the first industrial lipopeptide production plant in Europe [103].

The most studied biosurfactants beside lipopeptides are glycolipids which are composed of carbohydrates linked to a long-chain hydroxyl fatty acid [104]. The best-known glycolipids are sophorolipids and rhamnolipids [104]. For sophorolipids, industrial processes have already been successfully implemented since they are synthesized by non-pathogenic yeast strains in high concentrations (over 400 g/L) in batch or fed-batch fermentations by using renewable resources or waste streams as feedstocks [100, 105, 106]. Currently, sophorolipids hold the largest global biosurfactant market share in the detergent industries applying biosurfactants [55]. They can be produced in sufficient quantities and qualities for the use in cosmetic and consumer products [100, 105]. For example, the Belgium company Ecover, which has emerged as one of the top biosurfactant producer on the market, produces laundry and dishwasher cleaning agents containing sophorolipids as detergents [55, 107, 108]. According to a press release, Evonik Industries AG (Germany) started the commercialization of sophorolipids in 2016 for household and personal care products after installing a production line at industrial scale in Slovakia [109].

As for lipopeptides, sufficient oxygen supply during the fermentation process is a key factor for sophoro- and rhamnolipid production [105, 110]. However, sophorolipids are low foaming surfactants and insoluble in the bulk medium in their dominant lactonic form which avoids excessive foam formation and facilitates the downstream processing of the molecules [100, 106, 111]. Yet, this is not the case for rhamnolipids which have excellent foaming capacities [110]. Rhamnolipids are primarily produced by *Pseudomonas* species [100]. They have also a broad application field as additives in consumer goods like cosmetics, household detergents and medical products as well as can serve as biocontrol agents [112]. Current processes for rhamnolipid production are mainly based on batch and fed-batch processes with foam fractionation [55, 113]. Although foam control presents a huge obstacle for the scale-up of rhamnolipid production which is necessary for a successful commercialization [110]. Many efforts have been made for the development of economical production processes through the use of low-cost feedstocks, culture medium optimization and efficient fermentation processes [110]. Some research groups described the successful implementation of SSF for rhamnolipid production [114–116]. However, alternative production processes avoiding foam formation like air-liquid membrane contactors or biofilm-based processes, which are used for lipopeptide production, are less considered in literature. Nevertheless, in the last years industrial production processes have been developed. In 2016, Evonik announced the construction of a pilot plant for rhamnolipid production through bacterial fermentation on their site in Slovakia [109]. Three years later, Evonik commercialized together with Unilever a new hand dishwashing liquid containing rhamnolipids produced by bacteria and disclosed a strong ambition of future growth in the biosurfactant market [117].

4. Biofilm bioreactors – a promising and challenging alternative for continuous bioprocesses

4.1 Biofilms: a lifestyle of microorganisms in nature

Primarily, microorganisms have been characterized as planktonic, freely suspended cells [118]. However, microorganisms naturally tend to adhere to surfaces and to develop structural communities surrounded by a self-produced matrix of extracellular polymeric substances [119]. Van Leeuwenhoek was the first one to describe microorganisms that attach to and grow on tooth surfaces [118]. His observations can be attributed to the discovery of microbial biofilms [118]. A biofilm is a tightly surface-associated community of microorganisms that are sticking together by a self-produced organic extrapolymer matrix [120]. The key components of the matrix are extracellular polysaccharides and proteins [121]. However, extracellular DNA and dead cells are also part of the extracellular matrix [121].

In natural environments, communities of surface-associated bacteria or biofilms are the predominant mode of microbial life [49]. Biofilm formation can be found on almost all natural and artificial surfaces [120]. The organization of the microbial community in a biofilm structure offers several benefits including easy access to substrates and nutrients, as well as increased resistance against external menaces like antibiotics and disinfectants [119].

On the one hand, microbial biofilms can cause many detrimental effects on human health for example as infections on implants or in patients with cystic fibrosis [122]. Moreover, they often cause biofouling in industrial systems [122]. However, the beneficial aspects of biofilms can be also exploited in industrial settings [120]. Microbial biofilms play an important role in wastewater treatment, bioremediation and the production of various value-added products [98, 122, 123].

4.2 Assembly and development of B. subtilis biofilms

B. subtilis biofilms are predominantly studied using the wild-type strain NCIB3610 [124]. The wild-type strains of *B. subtilis* are able to form robust and highly structured biofilms on solid surfaces and at liquid/air interfaces [125]. Many commonly used laboratory strains are deficient or produce only faint biofilms compared to their ancestral wild type strains [126], like the widely used laboratory strain *B. subtilis* 168 as described above [127].

The biofilm formation generally includes four development stages: initial attachment by planktonic cells, irreversible attachment by the production of EPS, maturation and detachment [119]. **Figure 13** represents a typical life cycle of a *B. subtilis* biofilm.

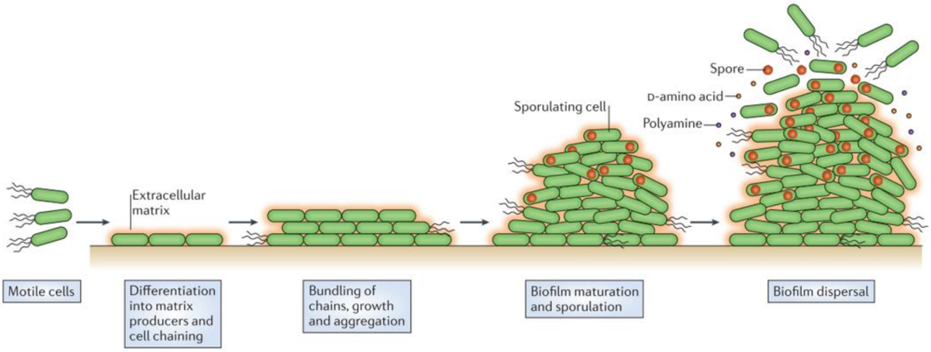
Spore
D-amino acid
Polyamine
Sporulating cell
Extracellular matrix
Motile cells
Differentiation into matrix producers and cell chaining
Bundling of chains, growth and aggregation
Biofilm maturation and sporulation
Biofilm dispersal

Figure 13. A typical life cycle of a *B. subtilis* biofilm with its different development stages [120].

In the first stage, the surface is conditioned by the macromolecules present in the bulk medium [128]. The planktonic cells in the medium are transported by diffusion or convection to the surface or reaching it by self-motility [128]. The initial attachment of the microorganisms depends on the physicochemical properties of the cells and the surface and on the attractive or repulsive forces generated between the surfaces such as electrostatic, hydrophobic interactions and van der Waals attractions [119].

After the attachment, the microorganisms start to multiply and form microcolonies [119]. Further development and cell differentiation lead to matrix producer cells and the formation of macrocolonies embedded into an extracellular matrix [119]. The produced exopolymer compounds provide benefits like an improved adhesion to the support, resistance against antimicrobial compounds and an enhanced surface spreading capacity [129–131]. The extracellular matrix is comparable to a sponge that enables both structural integrity of the biofilm and the flow of small molecules into and out of the biofilm [119]. The biofilm matrix is highly hydrated and represents the main part of the biofilm volume, whereas cells occupy only between 10% and 50% of the total biofilm volume [119]. In the following, the biofilm maturation starts which is observable through an increasing complexity of the biofilm architecture [119]. With increased aged of the biofilm, cell detachment can occur due to strong fluid dynamics and shear effects of the bulk medium or as a result of quorum-sensing regulation [119, 122].

4.3 Biofilm regulatory pathways in B. subtilis

In the beginning of biofilm formation, the attachment of a single cell to a surface is followed by a two-dimensional microcolony growth and pursued by a three-dimensional development of the biofilm colony and biofilm maturation [132]. Within the biofilm, functionally distinct subpopulations of cells are emerging due to differential gene expression in response to external signals [120]. In the biofilm, cell-to-cell communication, cell growth, nutrient consumption and waste production are omnipresent and consequently local microenvironments or molecular gradients are formed [133]. As a result of these gradients, phenotypic differentiation occurs by differential gene expression in response to the local environments that are sensed by the bacteria [133]. **Figure 14** summarizes the different cell differentiation programs executes by *B. subtilis*.

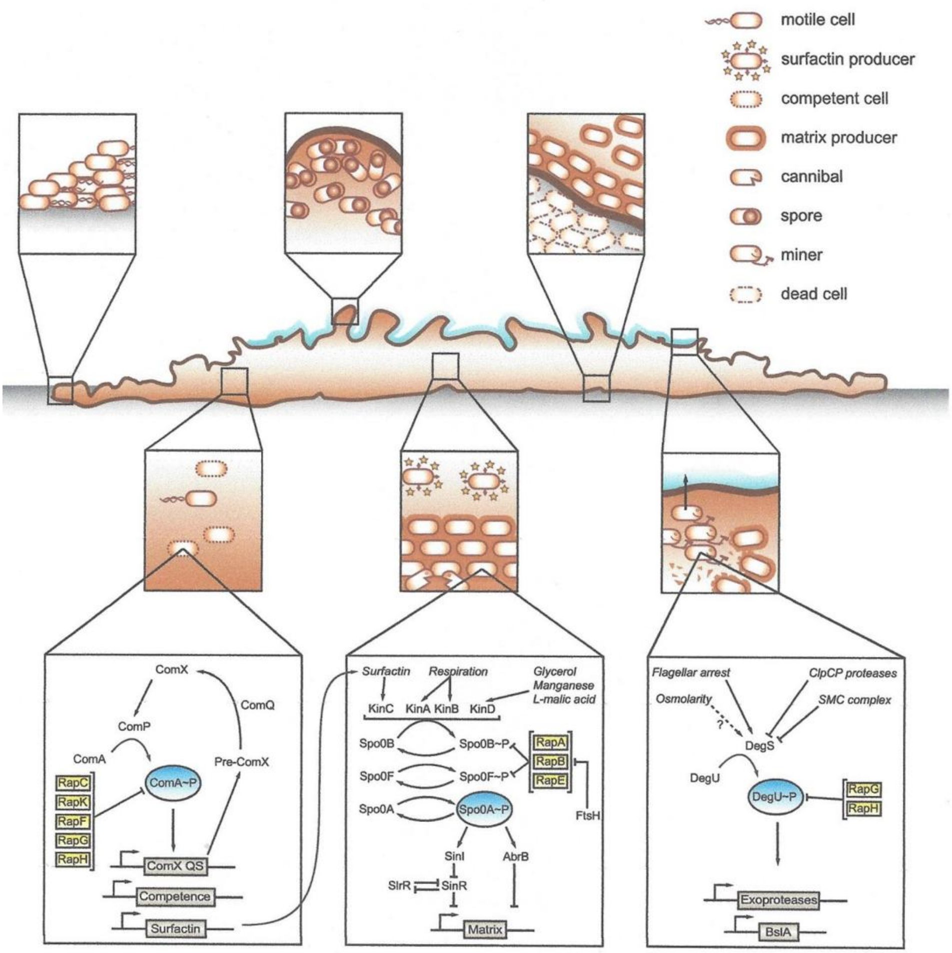
motile cell
surfactin producer
competent cell
matrix producer
cannibal
spore
miner
dead cell
ComX
ComQ
ComP
ComA
Pre-ComX
ComA~P
RapC
RapK
RapF
RapG
RapH
ComX QS
Competence
Surfactin
Surfactin
Respiration
Glycerol
Manganese
L-malic acid
KinC
KinA
KinB
KinD
Spo0B
Spo0B~P
Spo0F
Spo0F~P
Spo0A
Spo0A~P
RapA
RapB
RapE
FtsH
SinI
AbrB
SlrR
SinR
Matrix
Flagellar arrest
ClpCP proteases
Osmolarity
SMC complex
?
DegS
DegU
DegU~P
RapG
RapH
Exoproteases
BslA

Figure 14. Co-existing cell differentiation programs in *B. subtilis* biofilms and the spatiotemporal distribution patterns of the different cell subpopulations [49].

During the biofilm formation, the cells evolve from initially short motile rods into long chains of non-motile cells that adhere to each other and to the surface via the self-produced extracellular matrix [120]. The cells are able to switch from a planktonic to a sessile state by downregulating the expression of flagellar genes and by inducing simultaneously the expression of genes involved in the extracellular matrix production [49]. The sessile cells then start forming chains via the repression of cell-wall hydrolases that became embedded into the self-produced extracellular matrix [49]. The extracellular matrix of *B. subtilis* biofilms contain mainly EPS and proteins [49]. The 15-gene-operon *epsA-O (eps)* is responsible for the EPS production [49]. *Eps*-defective mutants are deficient in robust biofilm formation [6, 49, 134]. The main protein component of the biofilm matrix is TasA. This protein is encoded by the three gene-operon *tapA-sipW-tasA* [124]. During the final stages of biofilm maturation, *B. subtilis* produces as particular feature a highly-ordered and stable hydrophobic layer as coating of the biofilm, which is composed of the surface-active protein BslA [49, 135]. BslA is essential for the architecturally complex structure and hydrophobicity of the mature biofilm [124]. The hydrophobic layer formed by BslA serves as water-repellent barrier for the protection of the bacterial community in natural habitats [49].

The differentiation in distinct subpopulations of cell types is required for the formation of architecturally complex structured biofilms [49]. The genetic mechanisms that regulate the cell differentiation are activated through exogenous and endogenous signals [49]. The three master regulators ComA, Spo0A and DegU are activated through phosphorylation when the cells become sessile and induce the cell differentiation program [49]. Initially, ComA-P induces natural competence and activates the pathway for surfactin production [49]. Spo0A is indirectly activated by surfactin molecules through KinC and triggers in the following spore formation and matrix production depending on the concentration level in the cell [49]. DegU-P favors the formation of the hydrophobic BslA layer [49].

4.4 Biofilm-based bioprocesses

Biofilm reactors have been widely used in waste water treatment and bioremediation as well as for production of value-added products like ethanol, acetic acid and lactic acid [122, 123, 136–138]. They are either operated as packed-bed or fluidized-bed reactors using active or passive cell immobilization [122]. Cell immobilization improves the genetic stability of the cells and permits to reach high cell concentrations and thus guarantees an increased productivity [128]. In the same time, cell wash out problems, which generally occur in suspended continuous cell cultures, can be minimized [128]. Active immobilization of cells on a surface by a polymer matrix or covalent binding agents is often limited due to the toxicity on cell viability and activity and the instability of the polymer matrix [128]. However, passive immobilization through natural adsorption in the case of biofilm formation permits the growth of cells in a structural organized community [128]. The developed biofilm provides improved process stability since the adhered cells possess an enhanced stress resistance due to the self-produced, protective biofilm matrix [128, 139]. The improved process stability and resistance to stress make biofilm bioreactors potential candidates for the development of economically more interesting continuous fermentation processes [122, 138–140]. Moreover, the adhered biomass in the biofilm bioreactors permits a simplified product recovery and more efficient downstream process operations [122].

Yet, biofilm formation is linked to complex cellular regulatory mechanisms resulting in the development of pleiotropic cell phenotypes [49, 124]. The attachment of cells to surfaces followed by biofilm development is affected by surface, cellular and environmental factors [119]. This makes it difficult to control the biofilm growth and distribution inside the reactor. **Figure 15** resumes the different factors that have an impact on the biofilm formation in bioprocesses.

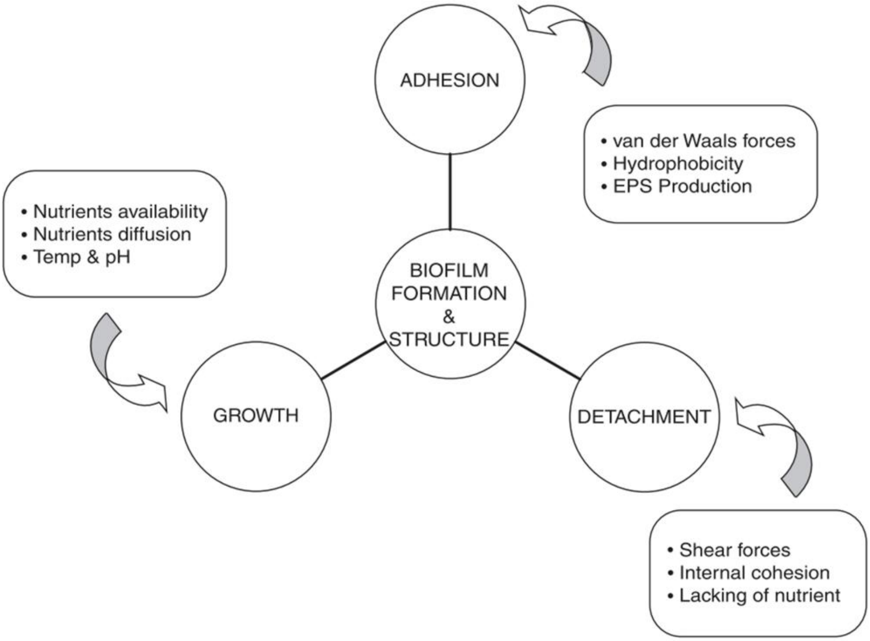
ADHESION
• van der Waals forces
• Hydrophobicity
• EPS Production
• Nutrients availability
• Nutrients diffusion
• Temp & pH
BIOFILM FORMATION & STRUCTURE
GROWTH
DETACHMENT
• Shear forces
• Internal cohesion
• Lacking of nutrient

Figure 15. Different factors that affect biofilm formation and structure in biofilm-based processes [122].

Mature biofilm are often linked to diffusion limitations of substrates and products resulting in concentration gradients of substrates and products which may affect the productivity and yield of the biofilm processes [138, 141]. However, it has also been shown that the architecturally complex structures developed within the biofilm by the microbial community facilitate the mass transport from and to the liquid medium [142]. It is of importance to improve the understanding of how biofilm development can be influenced through strain engineering, operating conditions and reactor design [143]. This knowledge can then be used as basis to generate targeted engineered biofilm structures for the development of more robust biofilm-based processes [143].

4.5 Trickle-bed biofilm reactor for enhanced lipopeptide production

In trickle-bed packed-bed biofilm reactors, the biofilm is developing on a static surface [141]. Compared to dumped packings, a structured packing reaches a higher gas-liquid contact area and thus provides better mass transfer characteristics and a higher catalyst effectiveness as well as avoids pockets of stagnant fluid [144, 145]. Durable stainless steel structured packings (**Figure 16**), as they are already used in the chemical industry for large scale distillation and surface catalysis, permit to achieve a very efficient gas-liquid mass transfer [141].

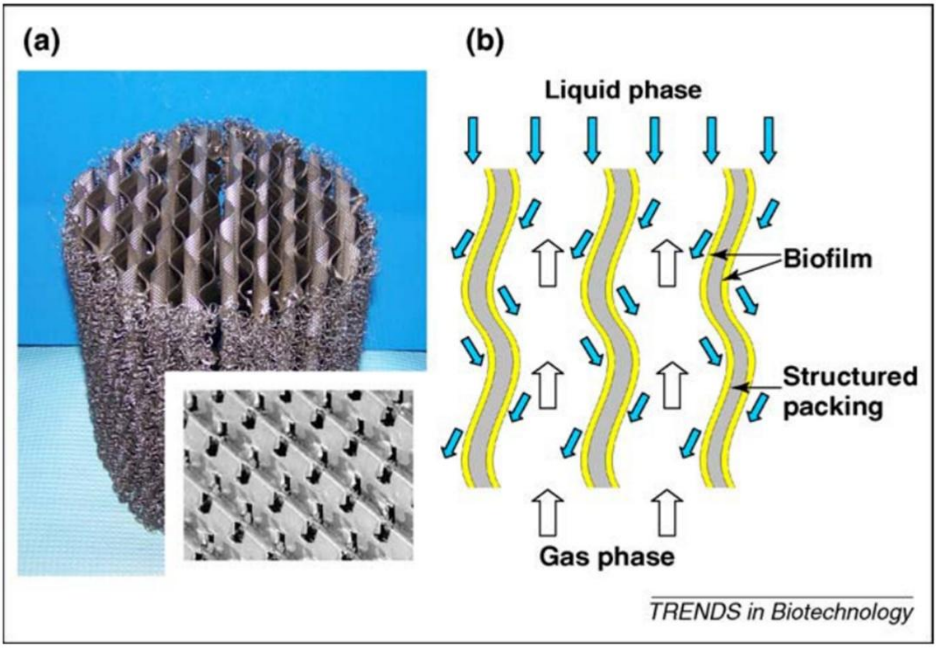

Figure 16. (a) Metal structured packing element for the trickle-bed biofilm reactor. The packing element is assembled with corrugated, structured, gauze stainless steel sheets. (b) Schematic representation of the enhanced gas-liquid mass transfer in the packing elements with developed biofilm on the packing surface [141].

The stainless steel structured packing elements possess a very high specific surface area of around 500 $m^2 m^{-3}$ to promote biofilm formation and provide optimal surface wetting capacities and an enhanced contact between liquid and gas phases [145]. They are especially suitable for biofilm bioprocesses that require an efficient aeration [141], as in the case of surfactin production.

Several microbial fermentation processes based on biofilm reactors containing a stainless steel structured packing element have been successfully implemented for the production of value-added products [92, 145–148]. Cultivations of *B. amyloliquefaciens* in a 20 L trickle-bed biofilm reactor (**Figure 17**) designed by Zune et al. [92] have shown to increase significantly the surfactin-to-biomass production yield in comparison to submerged cultures.

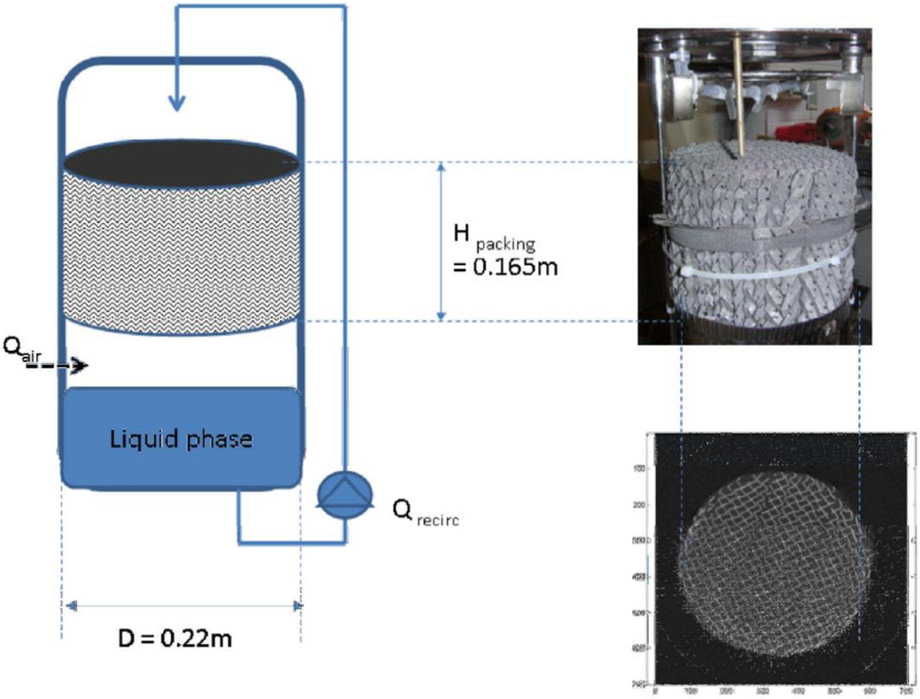

Figure 17. Experimental set-up of the 20 L trickle-bed biofilm reactor designed by Zune et al. [92]. The reactor vessel contains a structured metal packing element where the biofilm is developing. The nutrient delivery for the cells on the packing element is guaranteed through the continuous recirculating of the medium. Air is injected under the packing element to avoid foam formation.

In trickle-bed biofilm bioreactors no direct gas-liquid mixing takes place which avoids foam formation and makes this kind of reactor an interesting alternative for lipopeptide production [92]. Another advantage is also the scalability and possibility of process intensification since biofilm formation is mainly relying on the specific available surface area [92]. The well-defined geometrical properties of the packing element simplifies modeling approaches to optimize operating conditions [147, 149].

A drawback of the structured packing elements, also mentioned by Zhong et al. [145], is the difficulty to monitor the biofilm development during the reactor operation and to determine process-relevant biofilm characteristics such as the biofilm mass, structure, composition and metabolic activity. Zune et al. [92, 147] were able to visualize the biofilm distribution inside the metal structured packing element by X-ray tomography at the end of cultivation. They found that the liquid distribution affected strongly the biofilm distribution in the packing element [147]. A too high recirculation rate caused also cell detachment and resulted in an reduced biofilm development [147]. Biofilm formation occurred preferentially on wetted packing areas and an improved liquid dispersion resulted thus in an increased biofilm formation [147]. However, this approach did not provide any information of the biofilm development kinetics on the structured packing element during the cultivation process.

5. Metabolic or morphology engineering for the design of more efficient microbial cell factories?

5.1 Yield optimization through metabolic engineering

Microorganisms are used for the production of natural and chemical compounds [150]. However, microorganisms isolated from nature often show only low production efficiency of the target compound [150]. Strain modifications through metabolic engineering are necessary to transform the microorganisms in efficient microbial cell factories [150]. By means of metabolic engineering, metabolic fluxes are redirected towards the target product formation for an enhanced production yield [151]. For the metabolic flux optimization, several genetic engineering strategies are applied including enzyme engineering, balancing precursors availability, the overexpression or deletion of genes and co-factor engineering [151]. The development of high-throughput techniques combined with computational tools contributed to a great advance in deciphering genomes, transcriptomes, proteomes and metabolomes for targeted genetic engineering [150]. However, metabolic engineering approaches mostly neglect the microbial lifestyle and do not consider the morphology of cells and cell communities [152].

5.2 The approach of synthetic morphology

In nature, a multitude of micro- and macroshapes and structures were developed through evolution as a result of adaptation to different environments [152]. It is known that bacteria actively modulate their shapes in responses to internal metabolic and external environmental stimuli and thus morphology is an important trait to consider [152]. Yet, the morphology of prokaryotic cells has been so far rarely exploited to improve or facilitate metabolic tasks in cells [152]. Although many research has been performed on the processes involved in bacterial cell division and morphogenesis and despite significant advances that have been made in understanding the organization of bacterial communities like biofilms [152]. Volke and Nikel [152] are convinced that synthetic morphology of bacterial cells or more precisely redesigning the cell shape and spatial configuration of bacteria opens new ways to use bacteria in innovative fermentation processes.

5.3 Modulating the bacterial cell shape

The bacterial cell shape is mainly determined by the cell wall which has to be rigid and flexible in the same time and thus is subjected to regulatory processes at different levels [152, 153]. The bacterial cell wall is predominantly composed of cross-linked peptidoglycan polymers [153]. Rod-shaped bacteria like *B. subtilis* have two distinct modes affecting the cell shape: the axial cell elongation and the cell division [152, 153]. Cell elongation is modulated by the actin-like protein MreB and cell division through the tubulin-like protein FtsZ [153, 154]. The initiation of cell division takes place through the polymerization of FtsZ and the formation of a ring-like structure (Z ring) at the future division site [153]. The Z-ring placement is controlled by the Min system [155]. Subsequently, the Z ring serves as scaffold for the assembly of the division apparatus to complete the septum formation between two separating daughter cells [156]. The interactions of all these factors modulate the cell shape of bacteria [152].

Perturbations of the cell division machinery through the absence of involved proteins can yield in spherical [157, 158] or filamentous cells [159]. For example, the deletion of the septation protein SepF provoked severe perturbations during the division septum formation which resulted in less efficient cell division in *B. subtilis* [159]. SepF displays several activities including polymerization, FtsZ binding and membrane anchor for FtsZ that are required for the correct assembly of the FtsZ filaments during septum formation [160, 161]. Upon cell division, SepF forms a protein ring that bundles the FtsZ polymers for supporting the Z ring formation [155, 161] (**Figure 18A**). In the absence of SepF, the cell septa formation is defective and the cell separation is perturbed (**Figure 18B**). As a result, SepF knock-out *B. subtilis* mutants form elongated, filamentous cells [159, 161].

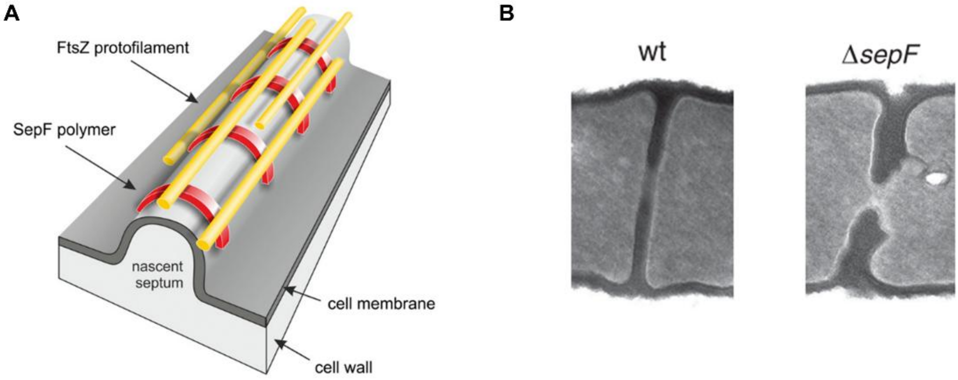

Figure 18. (A) Schematic representation of the septum formation in *B. subtilis* 168. The bundling of the FtsZ filaments (in yellow) is organized through protein rings formed by SepF (in red) that are anchored to the cell membrane [160]; (B) Septum formation in a unmodified *B. subtilis* 168 strain (left side) and in a *ΔsepF* mutant strain (right side), adapted from [161].

The cell division in *B. subtilis* is also influenced through the cell membrane composition [162]. The different membrane lipids possess defined physical properties that are responsible for the spatial organization, the localization of membrane proteins and the conducting of cell division [162, 163]. *B. subtilis* cells with alterations in membrane lipid composition exhibited aberrant cell morphologies [162]. After the inactivation of one or several genes involved in the biosynthesis of the different membrane lipids, highly filamentous cell growth and clumps of curled cells were observed (**Figure 19**) [162].

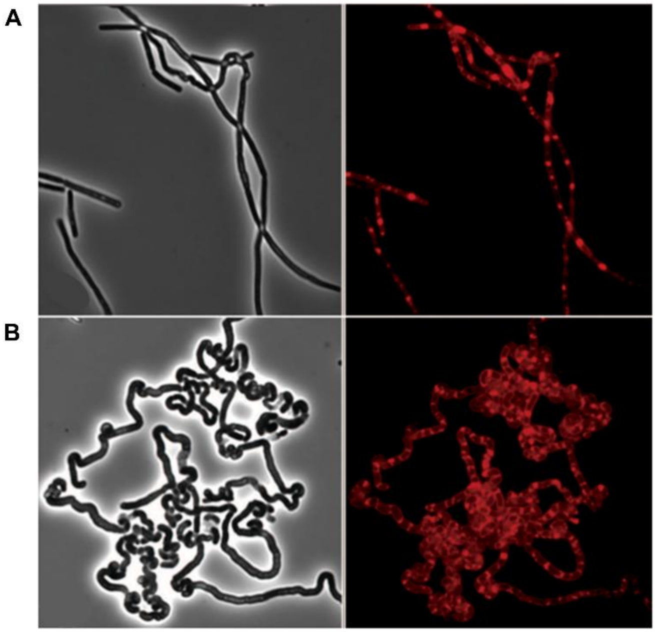

Figure 19. Atypical cell morphologies of *B. subtilis* CU1065 strains that have been observed after the alteration of the cytoplasmic membrane composition due to the deletion of several enzymes involved in the synthesis of membrane lipids (adapted from [162]). Cells from the exponential growth phase were strained with the fluorescent membrane dye FM 4-64. (A) Triple mutant (*ΔmprF*, *ΔpssA, ΔywnE*) exhibiting strongly filamentous cell growth. (B) Quadruple mutant (*ΔmprF, ΔpssA, ΔywnE, ΔugtP*) showing aggregates of curled cells.

5.4 Morphology engineering as new concept for process optimization

Up to now, the concept of morphology engineering for process optimization has been considered only by a few researchers. Primarily, these works are based on the idea to decrease the cost of biomass recovery and downstream processing for more economical processes.

In a recent study, Zhao et al. [164] have deleted several genes related to peptidoglycan hydrolases in a *B. subtilis* 168 strain. The gene deletions led to strong morphological changes in the bacterial cells due to the inhibition of cell division

[164]. Single gene deletions resulted in cell elongations and filamentous growth [164]. Multiple gene deletions introduced hyperfilamentous growth and the formation of fibres [164]. The generated mutant strains exhibited increased specific growth rates and improved enzyme production capacities [164]. However, after long cultivation, the cell lengths of the filamentous mutants were reduced to short rods similar to the control strain [164]. Probably, other, still active autolysins were activated to resume the task of cell shape modulation [164].

Vandermies et al. [165] introduced a mutation in the yeast *Yarrowia lipolytica* that provoked a filamentous cell morphology due to impaired cell division. They observed an increased self-immobilization of these cells on stainless steel structured packing elements. During cultivation, the majority of the cells remained attached on the packing element with a minimal cell release into the culture medium [165].

Jiang et al. [166] affected the cell shape of *E. coli* through the induced expression of the cell division inhibitor SulA and a weak constitutive expression of the actin-like protein MreB. The elongated cells could be maintained for more than 24h of culture [166]. The filamentous *E. coli* strains provided a larger cell volume for increased inclusion bodies accumulation of the biodegradable plastic polyhydroxyalkanoates (PHA) [166]. Moreover, the filamentous cells have shown to be beneficial for a simplified downstream processing due to a more convenient cell separation from the medium [157, 167, 168].

In another study, the morphology of cyanobacteria was modified through the tuning of different proteins from the Min cell division system in order to inhibit the cell division [169]. The highly elongated cells possessed better sedimentation and lysis properties and thus confirmed the potential of this novel approach to reduce operating costs associated with downstream process operations [169].

CHAPTER 2

Genetic engineering and screening of *B. subtilis* 168 strains with improved colonization capacities

1. Introduction

The Gram-positive bacterium *Bacillus subtilis* 168 is a potential producer of the very powerful biosurfactant called surfactin. Due to the exceptional foaming and emulsifying properties as well as various biological activities, surfactin represents an highly attractive compound for the phytosanitary, cosmetic, food or pharmaceutical industry [24]. Especially in the phytosanitary field, surfactin gains increasing interest since it is able to stimulate the systemic resistance in plants and thus could be used as biocontrol agent in sustainable agriculture [62].

However, further effort is needed to optimize the production process to reduce the cost price of surfactin for a more efficient industrial production. Sufficient aeration is necessary for the surfactin biosynthesis [77]. Yet, a high agitation rate provokes excessive foam formation making the production challenging [25]. Surfactin production using conventional stirred tank reactor with foam fractionation are linked to a high culture medium and cell loss as well as to complex downstream process operations [25, 76]. In previous works, promising production processes based on a trickle-bed biofilm reactor containing a structured packing [148] and a bubbleless bioreactor with an air/liquid membrane contactor [84] have been developed. In both processes the aeration is carried out without direct gas-liquid mixing in order to avoid foam formation [84, 147]. Cell immobilization and biofilm formation has shown to favor surfactin production in several works [75, 76, 78, 79, 84, 91, 93].

Although *B. subtilis* 168 is a good surfactin producer, the strain exhibits only poor biofilm formation capacities as a result of its domestication process [6]. Though, improved cell adhesion capacities are necessary in biofilm bioreactors for the development of a long-term stable continuous bioprocess. The objective of this work was to generate *B. subtilis* 168 mutants with enhanced adhesion and colonization capacities. Therefore, the natural immobilization step of the cells was intended to be increased through exopolysaccharide production and filamentous cell growth. Exopolysaccharide are known to be essential in biofilm formation to keep the cells together that are adhered to a surface. The change of cell shape has not been used so far to optimize bacterial biofilm formation for bioprocesses. However, natural filamentous microorganisms like fungi have shown to colonize very efficiently structured metal packing elements [146, 148]. Improved and long-lasting cell immobilization on a structured metal packing element has also been observed after the induction of filamentous growth in the yeast *Yarrowia lipolytica* [165].

In the first part of this work, filamentous *B. subtilis* mutants were generated with a markerless gene deletion strategy. For this purpose, single and multiple gene deletions provoking filamentous cell growth due to a less efficient cell division [159] and a change in membrane composition [162] were performed. Beside the additional impact of EPS restoration in *B. subtilis* 168 was studied. The generated mutants were characterized in terms of microcolony formation, surface colonization capacity, biofilm formation and surfactin production.

2. Materials and methods

2.1 Strains

The experiments were performed with *B. subtilis* 168 derivative strains. Competent *E. coli* JM 109 (Promega Corporation, Charbonnières-les-Bains, France) cells were used for plasmid construction and amplification. All *B. subtilis* mutants used in this work are summarized in **Table 2**. Generally, the *B. subtilis* 168 mutants can be divided into three groups:

(I) strains with restored biofilm formation (RL5260, RL5266 and RL5267)

(II) strains with less efficient cell division (TB92, BBG270) and additional biofilm matrix restoration (BBG512)

(III) strains with perturbed membrane composition (BBG403, BBG405, BBG406) and additional biofilm matrix restoration (BBG503, BBG505 and BBG506).

Table 2. Strains and plasmids used in this work with their corresponding genotype or plasmid composition.

Strains or plasmids	Genotype or plasmid composition	Source
Bacterial strains		
E. coli JM109	*end*A1, *rec*A1, *gyr*A96, *thi, hsd*R17 (r_k, m_k^+), *rel*A1, *sup*E44, Δ(*lac*-*pro*AB), [F´*tra*D36, *pro*AB, *laq*I^{q}ZΔM15]	Promega Corporation
***B. subtilis* 168**	*trpC2, epsC*^{0}, *sfp*^{0}	Lab stock
TF8A	*trpC2, epsC*^{0}, *sfp*^{0}*, ΔSPβ, ΔPBSX, Δskin element, Δupp::Pλ-neo; Neo*^{R}	Lab stock
Bcd-K7	*B. subtilis BSB1, Δbcd::K7(upp-Phleo-cI); Phleo* ^{R}	[170]
TB92	*trpC2, epsC*^{0}, *sfp*^{0}*, ΔsepF::spc; Spc*^{R} (derived from *B. subtilis* 168)	[159]
BBG111	*trpC2, amyE::sfp-cat, epsC*^{0}*; Cm*^{R} (derived from *B. subtilis* 168)	[86]
BBG270	*trpC2, ΔsepF::spc, amyE:: sfp-cat, epsC*^{0}*; Spc*^{R}, *Cm*^{R} (derived from TB92)	This study
Master strain BBG401	*trpC2, epsC*^{0}, *sfp*$^+$*; Δupp::Pλ-neo; Cm*^{R}, *Neo*^{R}, (derived from BBG111)	This study
BBG403	*trpC2, epsC*^{0}, *sfp*$^+$*; Δupp::Pλ-neo, ΔmprF; Cm*^{R}, *Neo*^{R} (derived from BBG401)	This study
BBG405	*trpC2, epsC*^{0}, *sfp*$^+$*; Δupp::Pλ-neo, ΔmprF, ΔpssA; Cm*^{R}, *Neo*^{R} (derived from BBG401)	This study
BBG406	*trpC2, epsC*^{0}, *sfp*$^+$*; Δupp::Pλ-neo, ΔmprF, ΔpssA, ΔywnE::phleo-upp-cI; Cm*^{R}, *Neo*^{R}, *Phleo*^{R} (derived from BBG401)	This study
RL5260	*trpC2, epsC*$^+$, *sfp*$^+$*; Erm*^{R}	[6]
RL5266	*trpC2, epsC*$^+$, *sfp*$^+$, *swrA*$^+$, *degQ*$^+$*; Spec*^{R}	[6]
RL5267	*trpC2, epsC*$^+$, *sfp*$^+$, *swrA*$^+$, *degQ*$^+$, *RapP*$^+$*; Cm*^{R}	[6]
Master strain BBG501	*trpC2, epsC*$^+$, *sfp*$^+$*; Δupp::Pλ-neo; Erm*^{R}, *Neo*^{R} (derived from RL5260)	This study
BBG503	*trpC2, epsC*$^+$, *sfp*$^+$*; Δupp::Pλ-neo, ΔmprF; Erm*^{R}, *Neo*^{R} (derived from BBG501)	This study
BBG505	*trpC2, epsC*$^+$, *sfp*$^+$*; Δupp::Pλ-neo, ΔmprF, ΔpssA; Erm*^{R}, *Neo*^{R} (derived from BBG501)	This study
BBG506	*trpC2, epsC*$^+$, *sfp*$^+$*; Δupp::Pλ-neo, ΔmprF, ΔpssA, ΔywnE::phleo-upp-cI; Erm*^{R}, *Neo*^{R}, *Phleo*^{R} (derived from BBG501)	This study
BBG512	*trpC2, epsC*$^+$, *sfp*$^+$*; Δupp::Pλ-neo; ΔsepF::phleo-upp-cI; Erm*^{R}, *Neo*^{R}, *Phleo*^{R} (derived from BBG501)	This study
Plasmids		
pGEM®-T Easy	Cloning vector	Promega Corporation
pBG129	*amyE-sfp-cat-amyE-spec* cloned into pGEM®-T Easy	[86]
pBG402	*upp*^{UP}*- λPr-neo-upp*^{DOWN} cloned into pGEM®-T Easy	This study

2.2 Media compositions

The *B. subtilis* strains were grown in lysogeny broth (LB) (10 g L^{-1} tryptone, 5 g L^{-1} yeast extract, 10 g L^{-1} NaCl) or Landy MOPS medium (20 g L^{-1} Glucose, 5 g L^{-1} glutamic acid, 1 g L^{-1} yeast extract, 0.5 g L^{-1} $MgSO_4$, 1 g L^{-1} K_2HPO_4, 0.5 g L^{-1} KCl, 1.6 mg L^{-1} $CuSO_4$, 1.2 mg L^{-1} $MnSO_4$, 0.4 mg L^{-1} $FeSO_4$, 21 g L^{-1} MOPS, 1.6 mg L^{-1} tryptophan). A detailed recipe of the Landy MOPS medium and the preparation procedure can be found in the Appendix II, **Table 19**, page 157. *E. coli* strains were grown in LB medium. For selective media preparation, various antibiotics were added to the culture medium: chloramphenicol (Cm) 5 µg mL^{-1}, neomycin (Neo) 5 µg mL^{-1}, erythromycin (Erm) 2 µg mL^{-1} or spectinomycin (Spc) 100 µg mL^{-1}.

2.3 Construction of the mutant strains

2.3.1 Plasmid, gDNA extraction and PCR fragment purification

Plasmid extractions have been performed according to the protocol with the GeneJET Plasmid Miniprep Kit (Thermo Fisher Scientific, Illkirch Cedex, France). For gDNA extraction the Wizard® Genomic DNA Purification Kit (Promega Corporation) has been used as indicated in the manual for Gram-positive bacteria. PCR fragments were purified with the GeneJET PCR purification Kit (Thermo Fisher Scientific) as described in the provided protocol.

2.3.2 Introduction of the *sfp* gene

A functional *sfp* gene has been inserted into the strain TB92 via the *amyE* locus through homologous recombination of the plasmid pBG129 (**Figure 20**).

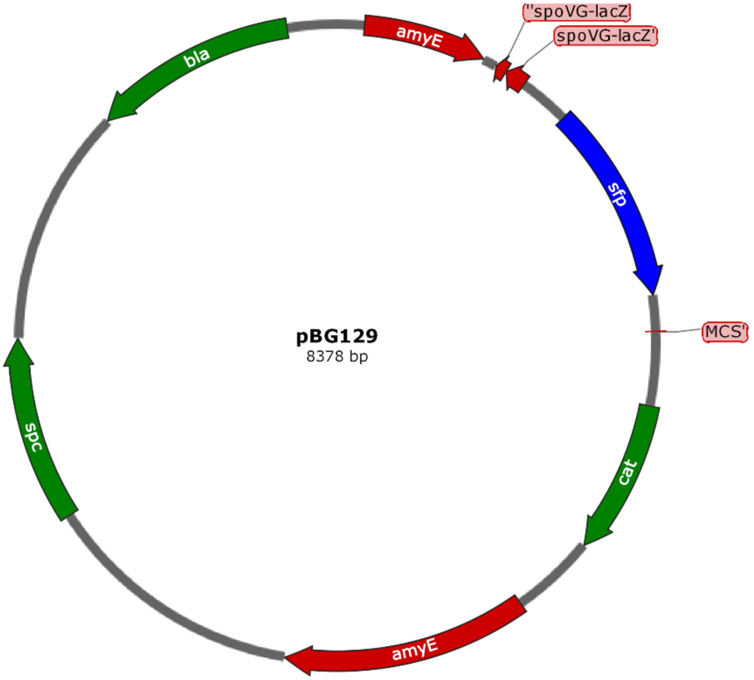

Figure 20. Genetic map of the plasmid pBG129 containing a functional *sfp* gene to restore the surfactin production in *B. subtilis* 168.

The pBG129 plasmid containing the sequence *AmyE (F) – pSfp – Cm*^{R} *– AmyE (R) – Spec*^{R} was previously constructed in the laboratory and transformed into competent JM109 *E. Coli* cells [86, 170]. For the transformation with the plasmid, natural competence medium (14 g L^{-1} $K_2HPO_4{\cdot}3H_2O$, 5.3 g L^{-1} KH_2PO_4, 20 g L^{-1} Glucose, 8.8 g L^{-1} Tri-Na Citrate, 0.22 g L^{-1} Ferric NH_4 citrate, 1 g casein hydrolysate, 2 g K glutamate, 1 M $MgSO_4$, 1.6 mg L^{-1} tryptophan) was inoculated with cells from an overnight plate culture and grown at 37°C and 160 rpm until the culture was turbid (~4-5 h). Subsequently, 200 µL of cell culture was mixed with ~500 ng of the plasmid and incubated for additional 1 h 30 min at 37°C and 160 rpm. The cell culture was then plated on selective antibiotic plates and incubated overnight at 37°C. Phenotypes with chloramphenicol-resistance and spectinomycin sensibility, resulting from a double homologous cross-over recombination, were selected by the replica plating method.

2.3.2.1 Evaluation of hemolytic activity

The *sfp* gene introduction was confirmed by a hemolytic activity test. Plates containing 25 mL of LB with 1,7 g/L agar and 5% of defibrinated horse blood were inoculated with liquid cultures of the transformed strains and incubated overnight at 37°C. The hemolytic activity through lipopeptide production was revealed by the development of a halo around the colony.

2.3.2.2 *Evaluation of amylase activity*

Besides, an amylase activity test has been performed. For this purpose, plates containing LB with 1.7 g/L and 1% of starch were inoculated with liquid cultures of the transformed strains and incubated overnight at 37°C. The amylase activity was revealed after staining with an iodine solution by the development of a halo around the colony.

2.3.3 Markerless gene deletion strategy “Pop in – pop out”

For the mutant construction a markerless gene deletion strategy was used, known as “Pop in – pop out” [171]. The principle of this method is demonstrated in **Figure 21**.

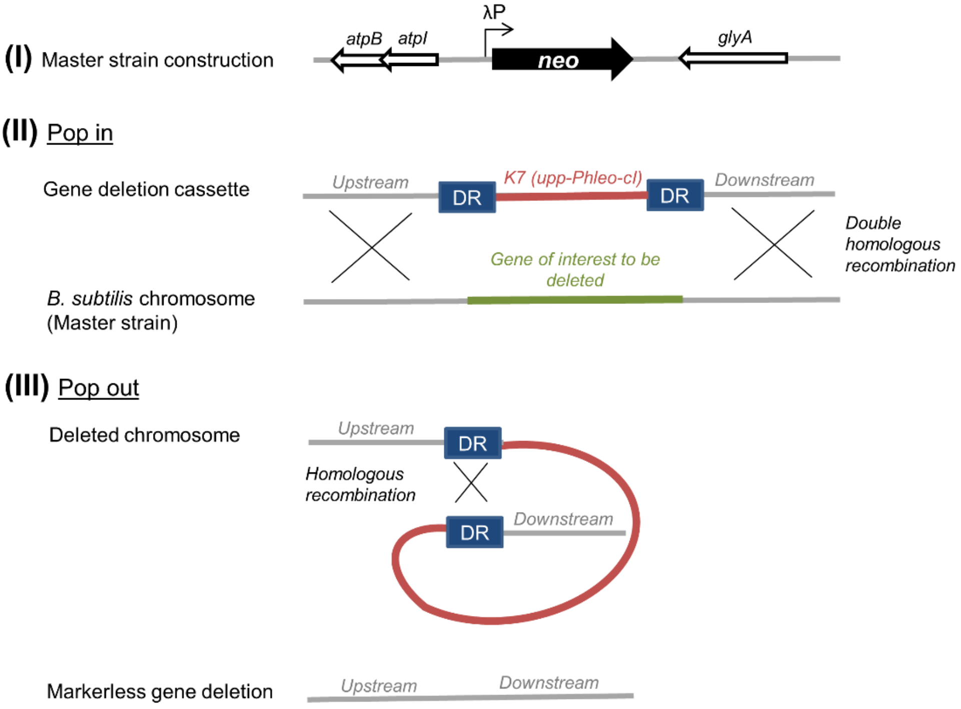
(I) Master strain construction
λP
atpB
atpI
neo
glyA
(II) Pop in
Gene deletion cassette
Upstream
DR
K7 (upp-Phleo-cI)
DR
Downstream
Double homologous recombination
Gene of interest to be deleted
B. subtilis chromosome (Master strain)
(III) Pop out
Deleted chromosome
Upstream
DR
Homologous recombination
DR
Downstream
Markerless gene deletion
Upstream
Downstream

Figure 21. Principle of the markerless gene deletion strategy “Pop in – pop out”. The technique consists of three principal steps: (I) Construction of the master strain, (II) replacement of the target gene by the gene deletion cassette and (III) the cassette excision through the direct repeat sequences.

First of all, a master strain is constructed where *upp* (uracil phosphoribosyltransferase) is replaced by a neomycin resistance gene under the control of a Lambda promoter (*λP-neo*). In the following, the gene deletions are introduced in the master strain by homologous replacement of the targeted gene sequence with the gene deletion cassette (“pop in”). The gene deletion cassette for the “pop in” is synthesized by means of PCR through the assemblage of different components: the up and down stream element of the gene to be deleted, the K7 element containing *upp* (for possible counter selection), a phleomycin resistance gene, the gene *cI* (a repressor of the Lambda promoter used for counterselection), and two direct repeats (DR) necessary for cassette eviction. The phleomycin resistance gene is used for the positive selection of cassette insertion. Furthermore, a second selection criterion can be used since the insertion of the *cI* repressor makes the strain sensible for neomycin. The cassette eviction (“pop out”) occurs due to the homologous recombination of the inserted direct repeats. Hence, the strain can be counter-selected due to the elimination of the phleomycin resistance and the restoration of the neomycin resistance since the *cI* repressor is turned off.

2.3.3.1 Master strain construction

First, the plasmid pBG402 containing the *λP-neo* sequence with the *upp* upstream and downstream sequence has been constructed (**Figure 22**).

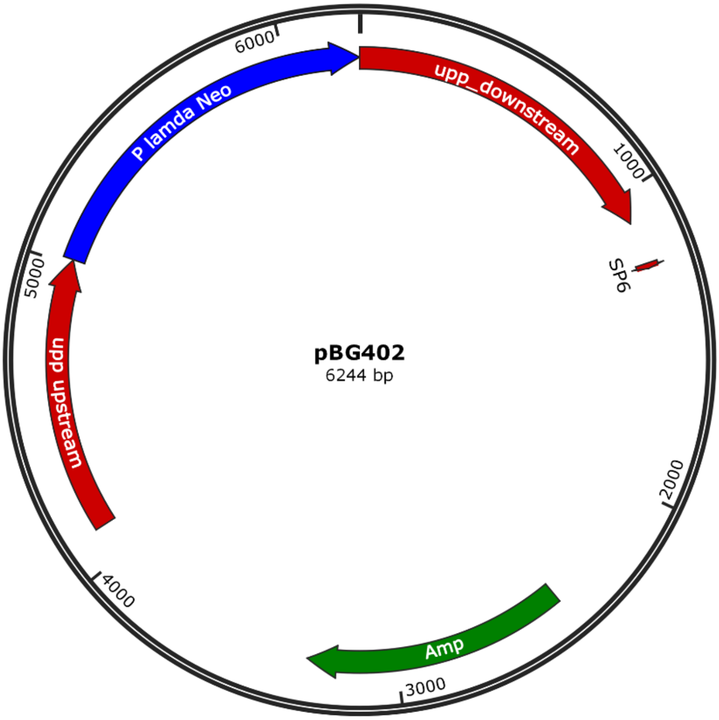

Figure 22. Genetic map of the plasmid pBG402 used to construct the master strain.

The DNA fragment has been extracted from the strain TF8A (*λP-neo*::*Δupp*). For the DNA fragment extraction, gDNA of TFA8 has been extracted from an overnight grown liquid culture. Then, a PCR has been performed using the extracted gDNA as template and the primer pair *upp_Fw_HB*, *upp_Rv_HB* (see Appendix I, **Table 18**, page 155 for a list of all primers used in this work) to amplify the desired *upp_*uppstream-*λP-neo-upp_*downstream DNA fragment.

For the polymerase chain reaction (PCR), a DreamTaq PCR Master Mix (2x) (Thermo Fisher Scientific) was used. The PCR mixture was prepared by mixing 10 µL DreamTaq Master Mix (2x) with 0.5 µM forward and reverse primer and gDNA (~200 ng) and filling up with pure water to 20 µL. The PCR reaction was performed using the following thermal cycling conditions: 5 min at 94°C (for initial denaturation); 30 s at 94°C for denaturation, 30 s at (55-60)°C for annealing and the necessary extension time at 72°C for 25 cycles; and 10 min at 72°C (final extension). The time for the extension after the primer annealing was chosen in function of the target sequence length to amplify. Generally, the Taq polymerase has an amplification rate of 1 min/kb. The amplified DNA fragment has been purified, the size has been verified with an agarose gel (0.8%) and the corresponding DNA concentration has been measured using a NanoDrop Lite Spectrophotometer (Thermo Fisher Scientific).

The DNA fragment has then been ligated into pGEM-T-easy vector (Promega Corporation). For the ligation a 1:2 vector:insert molar ratio has been used. The following ligation mix has been prepared: 5µL ligation buffer (2X) pGEM-T-easy vector 1 µL, PCR product 1.5 µL, T4 ligase filled up with pure water to 10 µL. The ligation mix has been incubated at 4°C overnight. A sample has been analyzed with a 0.8% agarose gel to confirm the correct size of the ligated vector. After a successful ligation, the vector has been transformed into *E. coli* JM109 cells according to the protocol delivered by Promega Corporation. The insertion of the DNA fragment has been verified by sequencing. The vector was then used to transform *B. subtilis* 168 strains to generate the master strain for further gene deletions. Phenotypes with neomycin resistance were selected. The introduction of the *λP-neo* sequence was verified by PCR and sequencing.

2.3.3.2 Construction of the gene deletion cassette

The gene deletion cassette was synthesized by PCR in several steps. For the PCR reactions a PCR mix containing 10 µL Q5 reaction buffer (5X), 1 µL dNTP’s (20 mM), 0.5 µL Q5 Hot Start High-fidelity DNA polymerase (all from NEW ENGLAND BioLabs, Ipswich, MA, USA), 0.5 µM of the corresponding primer pair, gDNA (~500 ng), filled up with pure water to 50 µL, was prepared. First of all, the up- and downstream element of the gene to be deleted were amplified by PCR using the corresponding primer pairs Fw – DRv and Rv – DFw, respectively. Though, the primers were designed by adding a direct repeat sequence and an overhanging sequence of the K7 element to the up and down stream element to reach a final length of at least 1 kb for the up and downstream DNA fragment (cf. **Figure 23**).

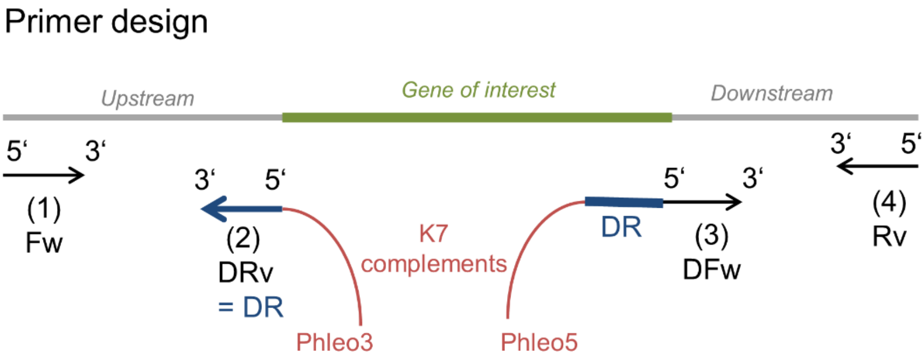

Figure 23. Primer design to extract the up- and downstream element of the gene of interest to be deleted for the gene deletion cassette synthesis.

The primers were designed with Primer3Plus[1] using the *B. subtilis* 168 reference sequence (NC_000964.3) available on the web page of the National Center for Biotechnology Information (NCBI)[2]. A complete list of the designed primers can be found in the Appendix I, **Table 18**, page 155.

The K7 DNA fragment containing the sequence of *upp-Phleo-cI* has been extracted from the strain Bcd-K7 constructed previously by [170]. Therefore, the gDNA of Bcd-K7 has been extracted from an overnight grown liquid culture. A PCR has been performed using the extracted gDNA as template and the primer pair Phleo3 and Phleo5 to amplify the desired K7 DNA fragment. The synthesized PCR fragments were purified and the correct size (~2.5 kbp) was verified by agarose gel (0.8%) electrophoresis.

In the following, the up and downstream elements were ligated to the K7 element by joining PCR. The PCR reaction was performed using the following thermal cycling conditions: 30 s at 98°C (for initial denaturation); 10s at 98°C for denaturation, 30 s at 57°C for annealing and 2:30 min at 72°C for extension for 35 cycles; and 2 min at 72°C (final extension). The composite DNA fragments were purified and the correct size was checked by agarose gel (0.8%) electrophoresis.

2.3.3.3 Pop in and pop out

For the "pop in", the gene deletions were introduced in the previous constructed master strain by homologous replacement of the targeted gene sequence by the corresponding gene deletion cassette. The transformation was done by means of natural competence as previously described in section 2.3.2. The cell culture was plated on phleomycin-LB agar plates and incubated overnight at 37°C. For a fast screening and confirmation of the cassette insertion, a colony PCR has been performed on the developed colonies.

---

[1] http://www.bioinformatics.nl/cgi-bin/primer3plus/primer3plus.cgi

[2] https://www.ncbi.nlm.nih.gov

Therefore, the colonies were picked with a sterile toothpick and suspended in pure water. A PCR mix containing 10 µL Phire Reaction Buffer, 0.4 µL Phire Hot Start II DNA Polymerase (both from Thermo Fisher Scientific), the Fw and Rv primer of the inserted cassette and 0.5 mL of the diluted colony, filled up to 20 mL with pure water. For the PCR reaction the following thermal cycling conditions were used: 30 s at 98°C (for initial denaturation); 10 s at 98°C for denaturation, 30 s at 57°C for annealing and 1:30 min at 72°C for extension for 25 cycles; and 2 min at 72°C (final extension). The size of the amplified DNA fragment was determined using agarose gel (0.8%) electrophoresis. The colonies of positive transformants were streaked on neomycin-LB and phleomycin-LB agar plates by the replica plate method. Strains that were resistant to phleomycin and did not grow on neomycin-LB agar plates were selected as positive clones. The cassette insertion was again confirmed through PCR using the extracted gDNA as template.

For the “pop out”, single colonies form the “pop in” strains were taken to inoculated 1 mL LB liquid medium. The cultures were grown for 6 to 7 h at 37°C at 160 rpm and spread on neomycin-LB agar plates (100 µL of culture per plate). The plates were incubated overnight at 37°C. The developed colonies were further streaked on neomycin-LB and phleomycin-LB agar plates by the replica plate method and incubated at 37°C for 24 h. Colonies that were grown on the neomycin-LB plates and did not grow on phleomycin-LB plates were selected as positive clones. The excision of the gene deletion cassette of each mutant was verified by a PCR. Furthermore, the gene deletion region of the “pop in/pop out” strains was sequenced in order to confirm the absence of the gene.

2.4 Analysis of microcolony formation on agarose pads

The cell morphology and growth behavior at single cell level was analyzed using an inverted phase-contrast time lapse microscope system (Eclipse Ti2, Nikon Instruments Europe BV, Amsterdam, Netherlands). The *B. subtilis* pre-cultures and agar pads were exactly prepared as described in the article of [172]. The pre-cultures were diluted to an $OD_{600\ nm}$ of 0.03 and the cells of the mutants were deposited on the solid agar surface. The microscope slide with the agar pad and the loaded cells was incubated at 37°C during 1 h prior to the microscope analysis. The prepared microscope slide was then placed on the pre-heated (37°C) microscope table and 100x oil immersion objective. The cell development of selected single cells was then followed in real-time during 8 h. Images were taken each 12 minutes.

2.5 LB agar plates colonization assay

The colonization capacity of the mutant strains was analyzed on 0.7% agar LB plates containing each 25 mL of solid medium. The agar LB plates were inoculated with 2.5 µL of diluted pre-cultures (OD_{600nm} = 1). When the plates were completely dried, they were incubated at 30°C for several days. The diameter of the developing colonies was measured each day.

2.6 Analysis of the biofilm formation capacity

The biofilm formation capacity of the strains was analyzed using a drip flow reactor (DFR) with six parallel flow chambers (**Figure 24**) (six-chamber Drip Flow Biofilm Reactor®, 224 x 127 x 37 mm, Biosurface Technologies Corporation, Montana, USA). Each chamber contained a silicone coupon (25 x 75 x 5 mm) with a rough surface where the cells can adhere and form a biofilm under low shear stress conditions.

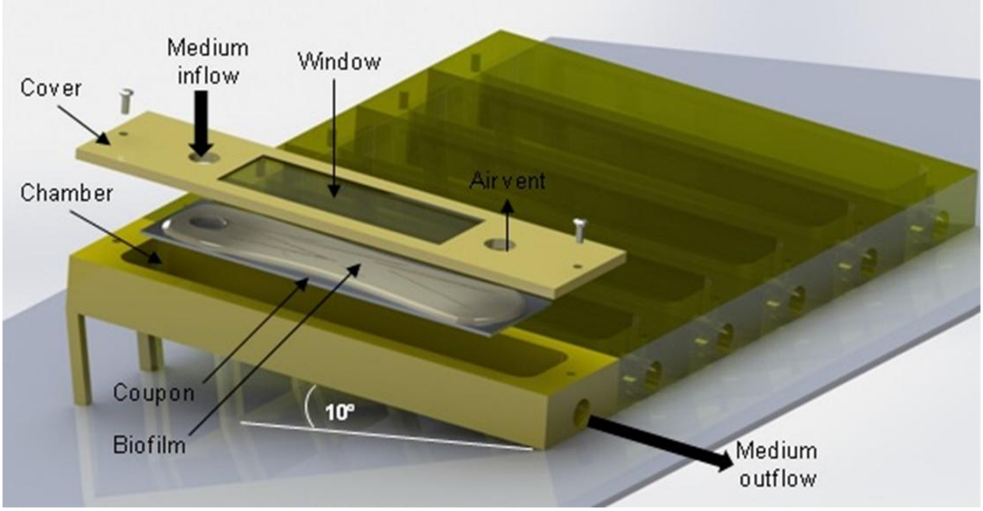

Figure 24. Set-up of the drip flow reactor device composed of six parallel flow chambers containing each a silicone coupon for biofilm development.

The strains were cultivated in Landy MOPS medium (see section 2.2, page 44) at 37°C. For the inoculation preparation, overnight cultures of the *B. subtilis* strains grown at 37° and an agitation rate of 160 rpm were diluted to an OD_{600nm} of 1. Then, 20 mL of the diluted culture was injected per chamber with a syringe while the reactor was kept horizontally. After the inoculation, a 6 h batch phase was started to let settle down the cells on the support. Then, the reactor was inclined and the continuous phase was launched with a flow rate of ~13 mL h^{-1} per chamber during 42 h.

2.7 Bacterial growth analysis in a micro-bioreactor fermentation system

The surfactin production of the engineered *B.* subtilis strains in planktonic cell cultures was analyzed by means of a high-through put BioLector® micro-biorector fermentation system (m2p-labs GmbH, Baesweiler, Germany). The strains were cultivated in 1 mL Landy MOPS medium (for the medium composition see section 2.2, page 44) in micro-bioreactors on a BioLector® 48-well flower plate at 37°C with a shaking frequency of 1100 rpm (which corresponds to a theoretical OTR of 50 mmol L^{-1} h^{-1}) during 48 h. For the inoculation, pre-cultures in tubes containing 2 mL LB with antibiotics were prepared by inoculating with a colony. The tubes were incubated for ~6 h at 37°C and 160 rpm. 500 µL of the pre-culture was then used to inoculate the main pre-culture in Landy MOPS medium. The main pre-culture was grown overnight at 37°C and 160 rpm and then diluted with Landy MOPS medium to an OD_{600nm} of 0.2 to inoculate the BioLector® 48-well flower plate. The BioLector® system measured automatically the biomass development by scattered light after each 15 min. In order to correlate the scattered light readings with the cell dry weight, calibration curves of the different mutant strains have been generated. Though, cultures in serial dilutions have been prepared with known dry cell weight and the corresponding scattered light values of the dilution series have been measured in the BioLector®. The cultivation of each strain was performed in triplicate. For surfactin analysis, the cultures were harvested after 48 h, centrifuged and the supernatant was collected. In the following, the lipopeptide concentrations were determined as described below.

2.8 Lipopeptide analysis

The cell culture or biofilm samples were centrifuged (10 min at 2400 x g) to separate the supernatant from the cell pellet. Subsequently, the supernatant was taken and filtered (0.2 µm) prior to the lipopeptide analysis.

The surfactin concentration in the cell culture samples from the Biolector® cultivations were analyzed by reversed-phase high-performance liquid chromatography (HPLC) (Agilent 1100 Series HPLC Value System, Agilent Technologies, Diegem, Belgium) with an Eclipse XDB C-18 column (3.5 µm, 2.1 x 150 mm) (Agilent Technologies, Diegem, Belgium). The analysis method was based on an isocratic elution profile with a flow rate of 0.4 mL min^{-1} using a mobile phase composition of 80% acetonitrile and 20% water containing 0.1% trifluoroacetic acid (TFA). The analysis time was 22 min per sample and the surfactin molecules were detected by UV at 214 nm. Purified surfactin samples (> 98%) (Lipofabrik, Villeneuve d'Ascq, France) were used for the identification of the retention time of the surfactin molecules and to determine a calibration curve.

Besides, cell culture samples from the Biolector® cultivations as well as cell culture and biofilm samples from the drip-flow reactor were analyzed by reversed-phase UPLC-MS (AQUITY UPLC H-Class, Waters, Zellik, Belgium) in order to be able to detect also low amounts of surfactin and fengycin. For the analysis an AQUITY UPLC BEH C-18 1.7 µm, 2.1 x 50 mm, column (Waters, Zellik, Belgium) coupled to a single quadrupole MS (AQUITY SQ Detector, Waters, Zellik, Belgium) was used. The source temperature was set at 130°C for the sample ionization with a desolvation temperature of 400°C, a nitrogen flow of 1000 L h^{-1} and a cone voltage of 120 V. The UPLC analysis method was based on an acetonitrile/water gradient containing 0.1% formic acid using a flow rate of 0.6 mL min^{-1} with an analysis time of 7 min per sample. The elution of the lipopeptides started at 30% of acetonitrile. After 2.43 min, acetonitrile was brought up to 95% and then at 5.1 min reduced to 30% until the end. Lipopeptides were detected by UV at 214 nm. Purified surfactin (> 98%) and fengycin (> 90%) samples (Lipofabrik, Villeneuve d'Ascq, France) were used to determine the retention time of the lipopeptides and a calibration curve.

2.9 Cell dry weight analysis of cells adhered to the DFR coupon

The colonized coupons of the DFR were taken after 48 h of incubation and put into a 50 mL Falcon tube containing 10 mL of phosphate buffered saline (PBS). The biofilm was suspended into the liquid by vigorous vortexing of the falcon tube. Subsequently, the coupon was taken out and the suspended biofilm has been gently sonicated (1 to 3 times for 40 s with 30% of amplitude). The sonication permitted to extract the surfactin molecules trapped in the biofilm matrix and dissolve the exopolysaccharides attached to the cells. The cells were separated by centrifugation from the supernatant. The cell pellets were washed once with distilled water and then resuspended in water and filtered (0.2 µm). The retained cells on the filter were then dried in the oven at 105°C and weighted for cell dry weight determination.

2.10 Biofilm composition analysis

The biofilm composition was analyzed for EPS$^+$ strains. Therefore, the wet weight of the developed biofilm on the DFR coupon was measured and then the biofilm was divided exactly into two parts. The first half was dried to determine the entire dry weight of the biofilm. The second half was dissolved in PBS and gently sonicated (1 to 3 times for 40 s with 30% of amplitude) to separate the cells from the produced exopolysaccharides. After centrifugation, the supernatant was taken for surfactin analysis and the dry weight of the cell pellet was determined as described in the previous section. The corresponding EPS dry weight was determined by subtracting the cell dry weight from the measured biofilm dry weight

3. Results and discussion

3.1 Robust biofilm formation in B. subtilis 168 strains modifies the lipopeptide biosynthesis

The basic laboratory *B. subtilis* 168 strain is impaired in robust biofilm formation due to several mutations that have accumulated during the domestication of this laboratory strain [6]. McLoon et al. [6] were able to repair these mutations in *B. subtilis* 168 and generated the strains able to form complex biofilm structures. The above-mentioned research group which works under the direction of Prof. Richard Losick (Harvard University, Cambrige, MA, USA) kindly provided us with three strains. The strains were all *sfp*$^+$ but contained different restored genetic modification levels involved in robust biofilm formation (cf. **Table 2**, page 43). These strains were tested in terms of growth, biofilm formation capacity and lipopeptide production.

The growth curves of suspended cultures that were recorded with a Biolector® system are shown in **Figure 25A**. The corresponding surfactin and fengycin concentration that were measured at the end of the cultivation are presented in **Figure 25B** and **C**.

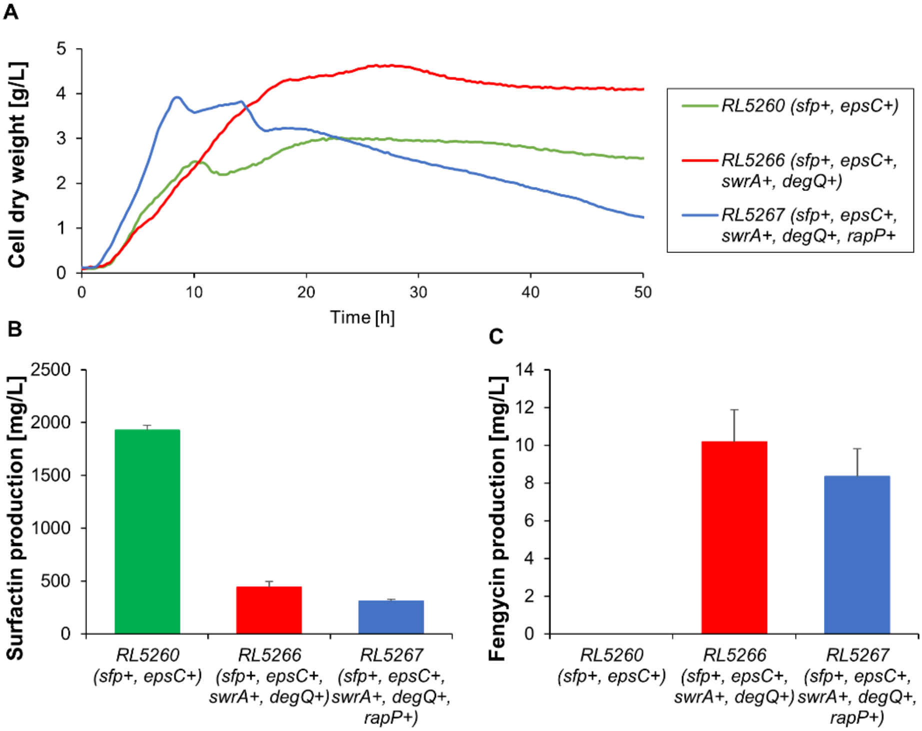

Figure 25. (A) Growth curves of the three *B. subtilis* 168 mutants with robust biofilm forming capacities recorded with a Biolector® micro-biorector fermentation system. (B) Surfactin concentration measured in the Biolector® cultures after 48 h. (C) Fengycin concentration present in the Biolector® cultures after 48 h.

Each strain showed a distinct growth curve. RL5260 and RL5266 presented a slightly extended lag phase at the beginning of the culture compared to RL5267. A diauxic growth profile was observed for RL5260. Probably, the cells changed from their primary energy source (glucose) to another energy source like glutamic acid or produced primary metabolites. During the stationery and death phase, the curves decreased stronger for RL5267 than for RL5260 and RL5260. This could be a result of different sporulation capacities. RL5260, RL5266 and RL5267 reached maximum specific growth rates of 0.61 ± 0.01 h^{-1}, 0.63 ± 0.01 h^{-1} and 0.62 ± 0.01 h^{-1}, respectively. The maximum specific growth rates of the strains were thus similar. A significant difference was observed for the surfactin production capacities. RL5260 produced four to six times more surfactin than RL5266 and RL5267. But, in the same time the fengycin production was upregulated for RL5266 and RL5267, whereas RL5260 did not produce any fengycin. The total amount of produced biomass was reduced for RL5260 compared to RL5266 and RL5267. Probably, RL5260 consumed more energy for surfactin production than for cellular growth compared to the other two strains.

In RL5266 and RL5267 *degQ* has been restored. This gene is negatively involved in the surfactin production regulation and thus explains the strong decrease of surfactin production. Recently, Miras and Dubnau [173] have shown that *srfA* expression in 3610 is repressed due to the phosphorylated DegU whose phosphorylation is stimulated through DegQ. In the presence of DegQ, the amount of ComK decreases which has a detrimental effect of surfactin expression [173]. Moreover, the restoration of RapP in RL5267 contributes to the inhibition of surfactin production since RapP controls negatively the major regulator of surfactin expression ComA~P [174]. It has also been shown that the introduction of the pleiotropic regulator DegQ in BS168 resulted in 10 times increased fengycin production [24, 175]. Through the insertion of a functional *degQ* gene in RL5266 and RL5267, the fengycin biosynthesis was stimulated and a higher production could be observed.

Figure 26A shows the colonized silicone coupons of the different mutant strains. The measured amount of adhered cells is presented in **Figure 26B** and the surfactin production of the strains at 48 h of culture in **Figure 26C**.

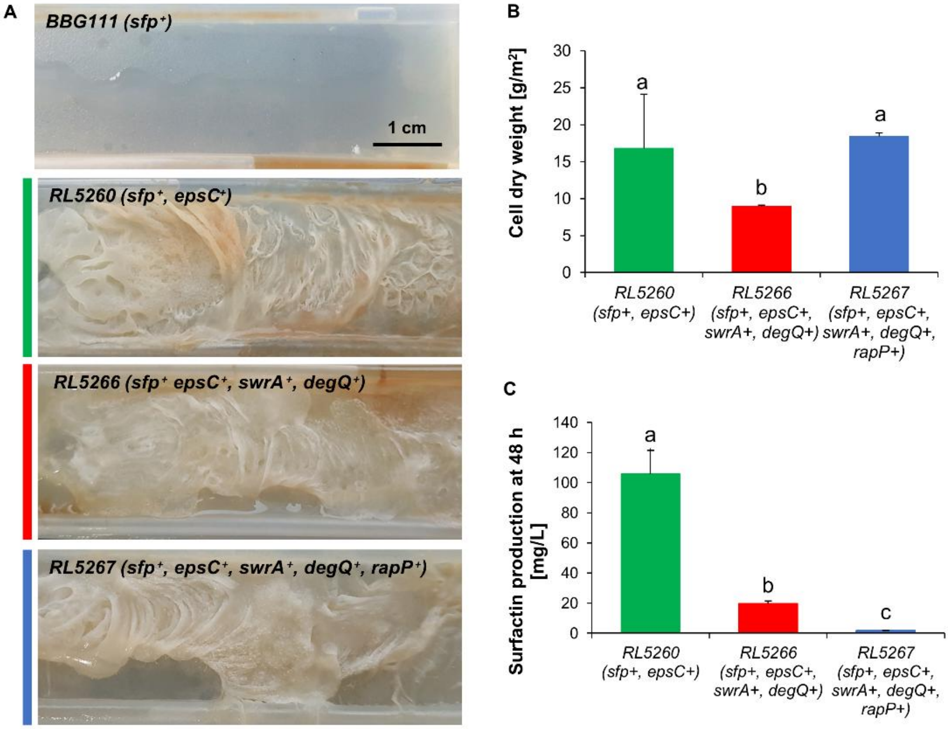

Figure 26. (A) DFR silicone coupons colonized by the control strain BBG111 and the *B. subtilis* mutants with restored biofilm formation after 48 h of incubation. (B) Measured cell dry weight of the adhered cells on the silicone coupons. (C) Measured surfactin concentration in mg L^{-1} of the *B. subtilis* mutants at the end of incubation (48 h) in the DFR.

When McLoon et al. [6] were able to restore the mutations in *B. subtilis* 168 linked to robust biofilm formation only the architecturally complex colony biofilm structure of the mutant strain RL5267 (five repaired mutations) was comparable with the colony structure of the wild-type strain NCIB6310 (cf. **Figure 3**, page 10). In this work, the biofilm formation capacities of the predecessor strains with two and four mutations reparation were also tested in the DFR. As **Figure 26A** shows, the restoration of the EPS production (*epsC*$^{+}$ mutant) was already sufficient to obtain a strong colonization of the reactor support including architecturally complex biofilm structures when compared to the control strain BBG111. Indeed, the adhered biomass on the coupon was similar for RL5260 and RL5267. RL5266 had a slightly decreased adherence capacity. Again, the surfactin production of RL5260 was significantly increased compared to the other strains. In the DFR, RL5260 produced nearly 60 times more surfactin than RL5267 and five times more than RL5266.

In this work, the main focus was relied on the surfactin production. In the following, RL5260 has been selected to improve further the cell adhesion capacities by genetic engineering in order to develop a continuous biofilm-based surfactin production process. Besides the produced EPS, which are known to be sticky sugar components and to contribute substantially to the cell attachment to surfaces, a second strategy based on morphology engineering was developed. Morphology engineering is a recent technique that has until now rarely been used to improve biotechnological processes.

3.2 Cell filamentation showed a strong impact on microcolony formation

The growth behavior of single cells has been analyzed by means of a time lapse microscopy. The mutants were placed on solid agarose pads and their cell development has been followed over time. Microscope images taken at different time points from the microcolony development are presented in **Figure 27** and **Figure 28**. The corresponding videos showing the microcolony development of the different strains can be found online via the links listed in **Table 20** in the Appendix III, page 158.

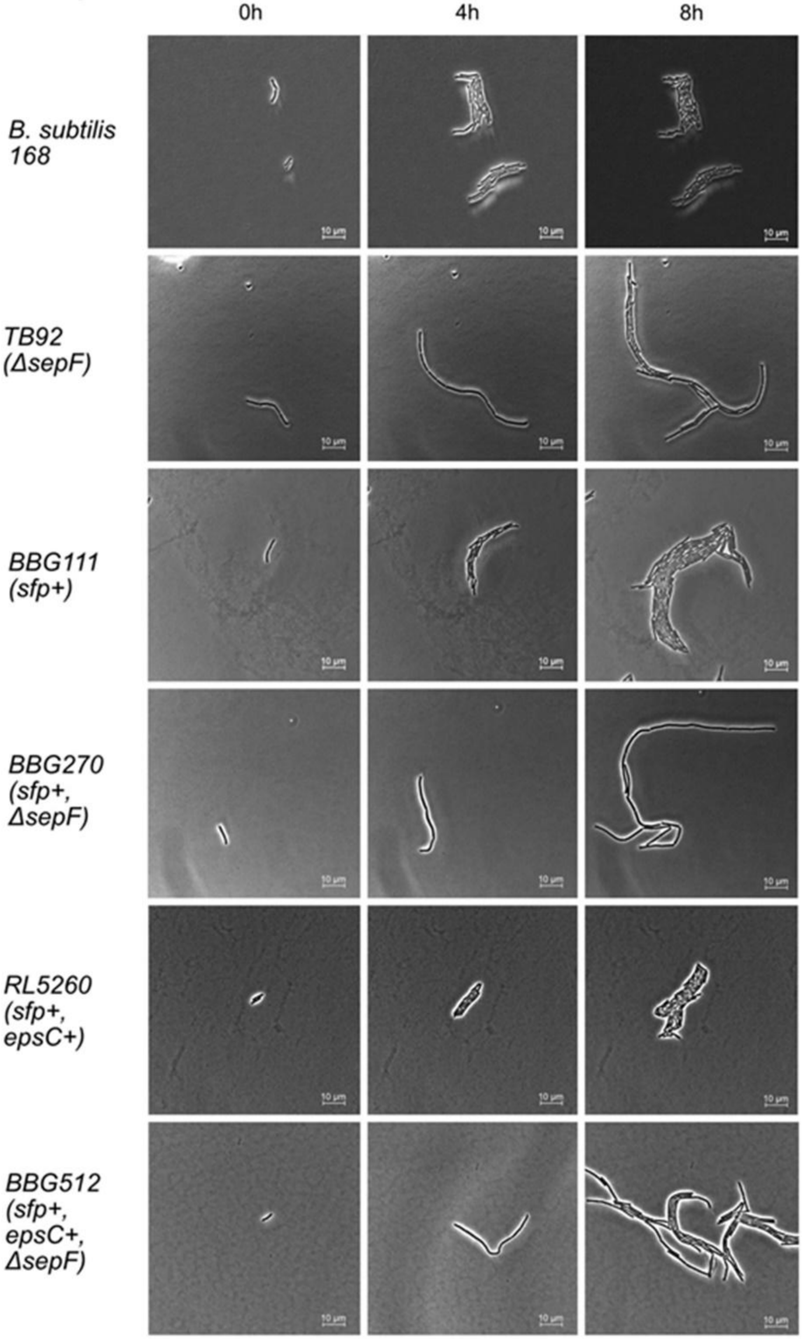
0h
4h
8h
B. subtilis 168
TB92 (ΔsepF)
BBG111 (sfp+)
BBG270 (sfp+, ΔsepF)
RL5260 (sfp+, epsC+)
BBG512 (sfp+, epsC+, ΔsepF)
10 µm

Figure 27. Single cell growth behavior of the genetically modified *B. subtilis* strains with less efficient cell division. Cultivations have been made on agarose pads and pictures have been taken after 0, 4 and 8 hours.

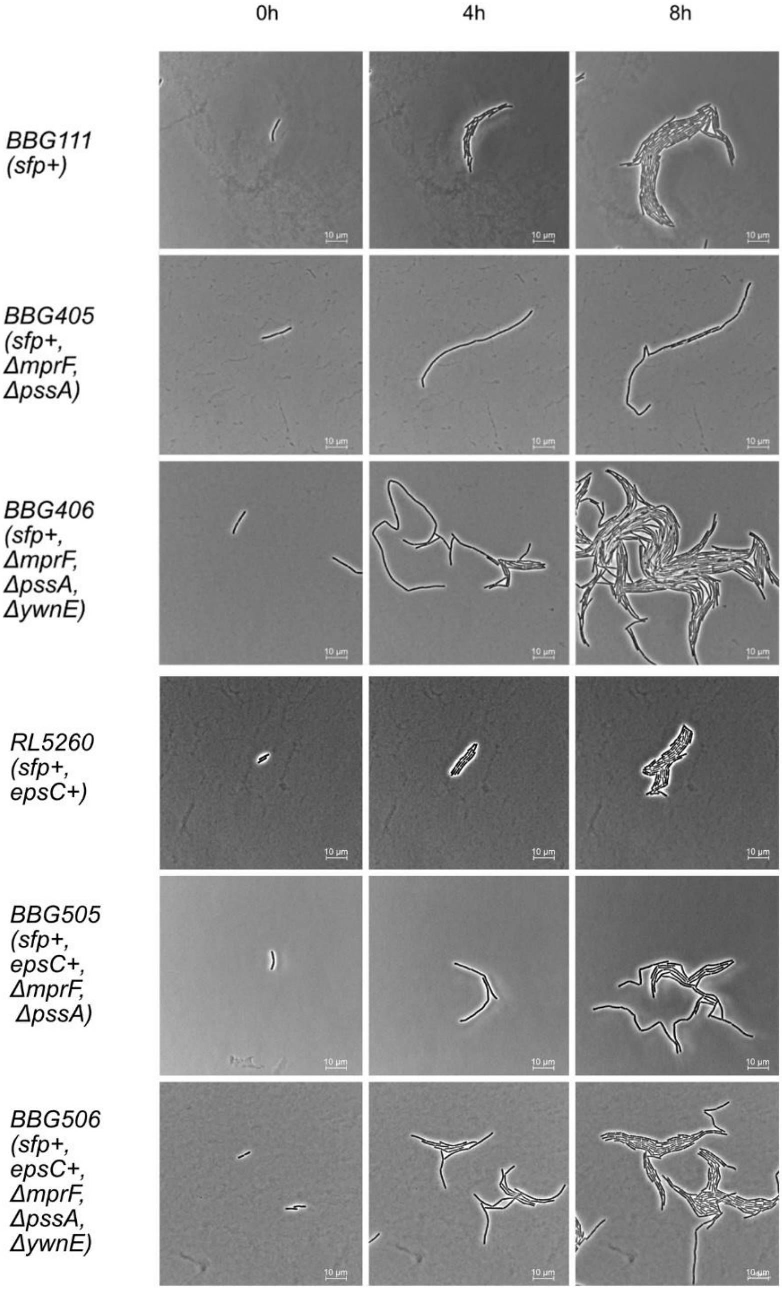
0h
4h
8h
BBG111 (sfp+)
BBG405 (sfp+, ΔmprF, ΔpssA)
BBG406 (sfp+, ΔmprF, ΔpssA, ΔywnE)
RL5260 (sfp+, epsC+)
BBG505 (sfp+, epsC+, ΔmprF, ΔpssA)
BBG506 (sfp+, epsC+, ΔmprF, ΔpssA, ΔywnE)
10 µm

Figure 28. Single cell growth behavior of the genetically modified B. subtilis strains with changed membrane composition. Cultivations have been made on agarose pads and pictures have been taken after 0, 4 and 8 hours.

The filamentous and/or EPS producing mutant strains exhibited distinct microcolony development patterns. For the mutants with induced morphological changes (less efficient cell division or changed membrane composition) the growth of elongated cells (> 5 µm) up to highly filamentous (> 20 µm) cells was observed. Due to the induced perturbation of the cell division machinery through the deletion of SepF and change in membrane composition, the cells did not divide properly anymore [159, 162]. The cell lengths of the mutants without change of cell shape were around 5 µm. Generally, the cell lengths of *B. subtilis* lie between 2 to 5 µm [154, 176]. Through cell elongation, the cells did not grow in a closed colony form and were able to spread over a greater distance than the non-filamentous cells. This resulted in a colony formation that covered a larger area but cell-free spaced within the colony were included. The EPS producing strain RL5260 formed much more dense colonies than non-producing strains. Obviously, the produced EPS kept the cells stuck together. In EPS producing filamentous cells, the cells seemed to accumulate closer together but open spaces without cells in the colony were still observed. The results show that change in cell shape affects strongly the microcolony formation behavior. The expansion of the microcolonies is significantly larger and thus the colonization capacities are increased. This is an interesting feature that could be exploited for the generation of mutant stains that colonize more homogenously and larger areas of the support material in biofilm bioreactors.

3.3 EPS production and cell filamentation improved the spreading and colonization capacity

In order to evaluate the spreading and colonization capacity which is important for enhanced and consistent bioreactor support colonization, the mutant strains were grown on 0.7% agar LB plates. The colony diameter was measured during 8 days. The results for the strain with less efficient cell division are presented in **Figure 29A** and for the strains with changed membrane composition in **Figure 29B**.

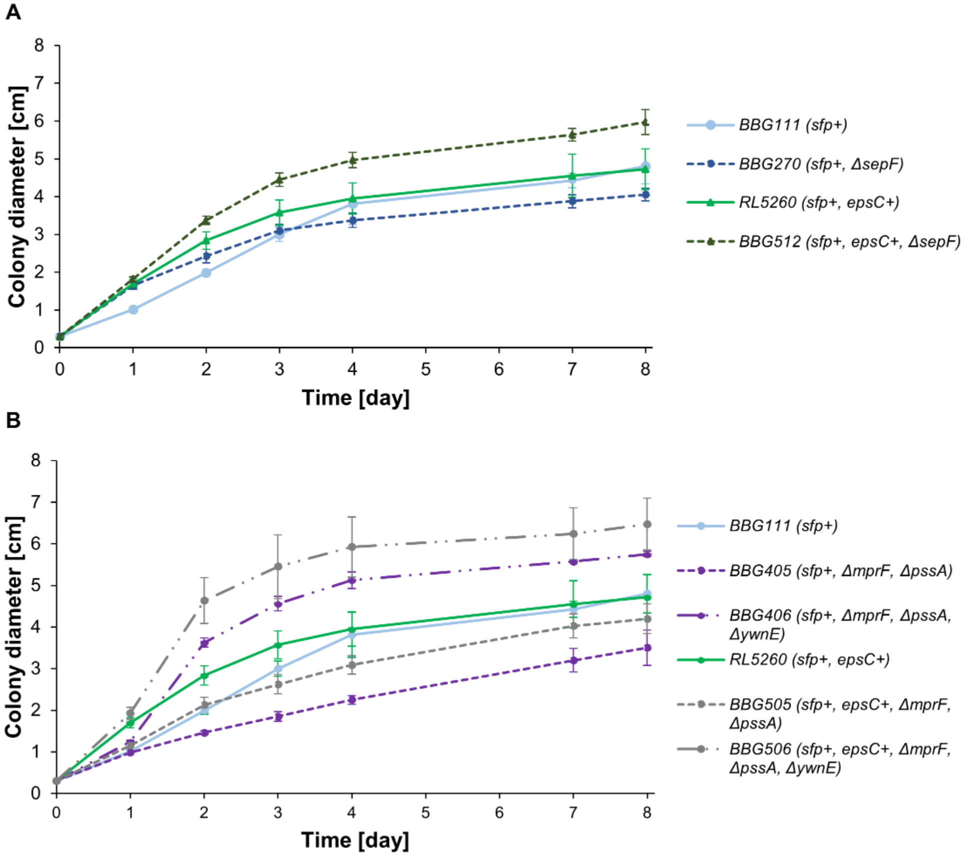

Figure 29. Spreading capacity of the *B. subtilis* 168 mutants with (A) less efficient cell division and (B) perturbed membrane composition on 0.7% agar LB plates. The colony development has been followed during 8 days by measuring the colony diameter. The standard deviation is indicated by error bars.

Regarding **Figure 29A**, the diameter of the developed colony was significantly increased up to day three for the filamentous strains (BBG270 and BBG512) compared to the non-filamentous strains BBG111 and RL5260, respectively. At the same time, the colony diameter was enhanced for the EPS^{+} mutants (RL5260 and BBG512) in comparison with the EPS^{-} strains BBG111 and BBG270. The EPS production seemed to be favorable for the agar plate colonization. The filamentous and EPS producing strains BBG512 developed the largest colony after 8 days. BBG111 showed the slowest colony development in the beginning of the experiment. However, after three days, this strain was overtaking BBG270 probably due to an increased growth rate and developed the same colony size than the EPS producing strain RL5260 after 8 days.

For the filamentous mutant strains with changed membrane composition, similar results were observed (**Figure 29B**). Especially, the triple knock-out mutants

BBG406 and BBG506 showed a strongly improved colonization capacity in comparison with the control strains BBG111 and RL5260, respectively. However, the colonization capacities of the strains with double knock-outs were reduced. EPS production additionally increased the colonization capacity in BBG506 and BBG505. Both strains developed a larger colony diameter than their EPS non producing counterparts.

The results confirmed that filamentous cell growth improves the colonization capacity as already pointed out by the time-lapse microscope experiments regarding the microcolony formation on agarose pads. The spreading test demonstrated also that the colonization can be additionally enhanced through the production of EPS. Seminara et al. [130] and Van Gestel et al. [129] made similar observation when they compared the colony spreading capacity of EPS producing and EPS deficient *B. subtilis* strains. EPS production improved significantly the spreading capacity of the strain resulting in an increased colony diameter.

3.4 The specific maximum cell growth rates were not strongly affected by the genetic modifications

All strains were grown in a Biolector® micro-bioreactor fermentation system to study their growth behavior in suspended cultures. **Figure 30** shows the recorded growth curves.

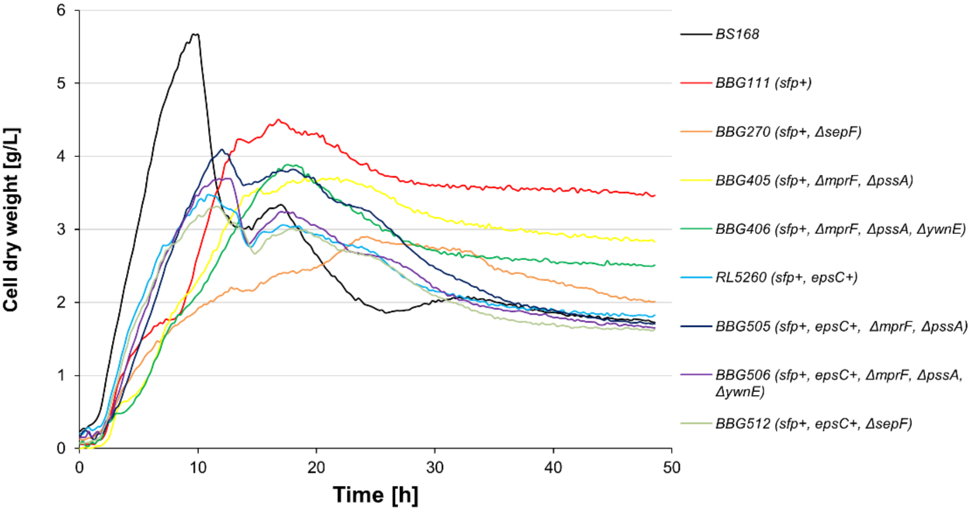

Figure 30. Growth curves of the different strains recorded with a Biolector® micro-bioreactor fermentation system.

Each strain exhibited a distinct grow curve. In general, the typical bacterial growth phases could be observed. The growth started with a short lag phase followed by an exponential growth phase between 2 and ~6 h, a linear or exponential growth phase between 6 and 10 h and a stationary growth phase between 10 and ~24 h followed by the final death phase. Some strains have shown diauxic growth, probably due to the change of carbon source during growth from glucose to glutamic acid or other primary metabolites produced. Interestingly, all EPS$^+$ and *B. subtilis* 168 have shown a similar death growth phase pattern after 35 h of cultivation. The growth curves decreased stronger than for the other EPS$^-$ strains. This could be linked to a different sporulation behavior. The determined maximum growth rates during the exponential growth phase are presented in **Table 3**.

Table 3. Maximum specific growth rates of the *B. subtilis* 168 mutants in the Biolector® cultures (determined between 2 to 6 h) with the corresponding standard deviation.

	BS168	***BBG111 (sfp+)***	***BBG270 (sfp+, ΔsepF)***	***BBG405 (sfp+, ΔmprF, ΔpssA)***	***BBG406 (sfp+, ΔmprF, ΔpssA, ΔywnE)***	***RL5260 (sfp+, epsC+)***	***BBG505 (sfp+, epsC+, ΔmprF, ΔpssA)***	***BBG506 (sfp+, epsC+, ΔmprF, ΔpssA, ΔywnE)***	***BBG512 (sfp+, epsC+, ΔsepF)***
μ_{max} [h^{-1}]	0.63 ± 0.02	0.69 ± 0.04	0.64 ± 0.02	0.64 ± 0.04	0.63 ± 0.03	0.61 ± 0.01	0.66 ± 0.02	0.72 ± 0.01	0.65 ± 0.02

The growth rates of the EPS$^+$ and filamentous strains were not strongly affected in suspended cultures, although EPS production reduces the fitness of individual cells through the increased energy consumption [129]. Probably, the strains are adapting to their environment and they exhibit a minimal or no EPS production in suspended cultures as it is less advantageous in this case. When Seminara et al. [130] compared suspended cultures of wild-type *B. subtilis* strains able to produce or not EPS, the growth curves were also similar.

3.5 Neither EPS production nor cell filamentation affected negatively the surfactin production in suspended cultures

At the end of the cultivation in the Biolector® micro-bioreactor fermentation system, cell culture samples were taken and the surfactin concentration was determined. The results are presented in **Figure 31**.

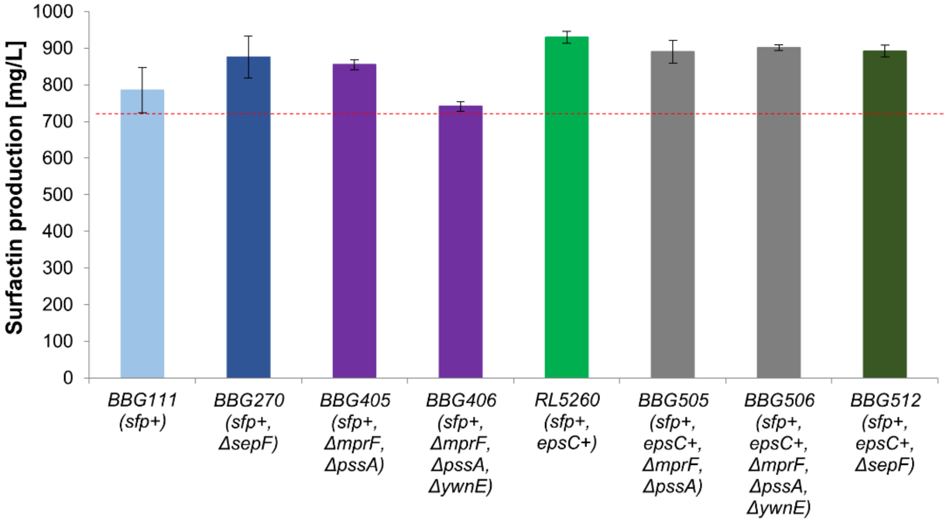

Figure 31. Surfactin concentration measured in suspended cell cultures of the engineered strains after 48h of incubation in a Biolector® system.

No decrease in surfactin production was observed after 48h of incubation in suspended cultures. The engineered strains produced similar amounts of surfactin than the control strain BBG111. Thus, the genetic modification did not negatively affect the surfactin production.

As mentioned in the previous section, most likely, the EPS production is limited in suspended cultures and thus did not influence the surfactin production. The change of cell shape had no negative effect on surfactin production. Hence, the introduced modification seemed to not alter the surfactin secretion or to diminish the cell resistance to surfactin.

3.6 *Biofilm formation capacities on DFR coupons under low shear stress*

3.6.1 EPS$^+$ mutants exhibited strong colonization capacities

The biofilm formation capacities of the mutants were analyzed by means of a drip flow biofilm reactor. This device permitted to study the biofilm development on a surface under low shear stress conditions with a continuous feeding rate. The colonized coupons are presented in **Figure 32** and the determined corresponding adhered cell dry weight in **Figure 33**.

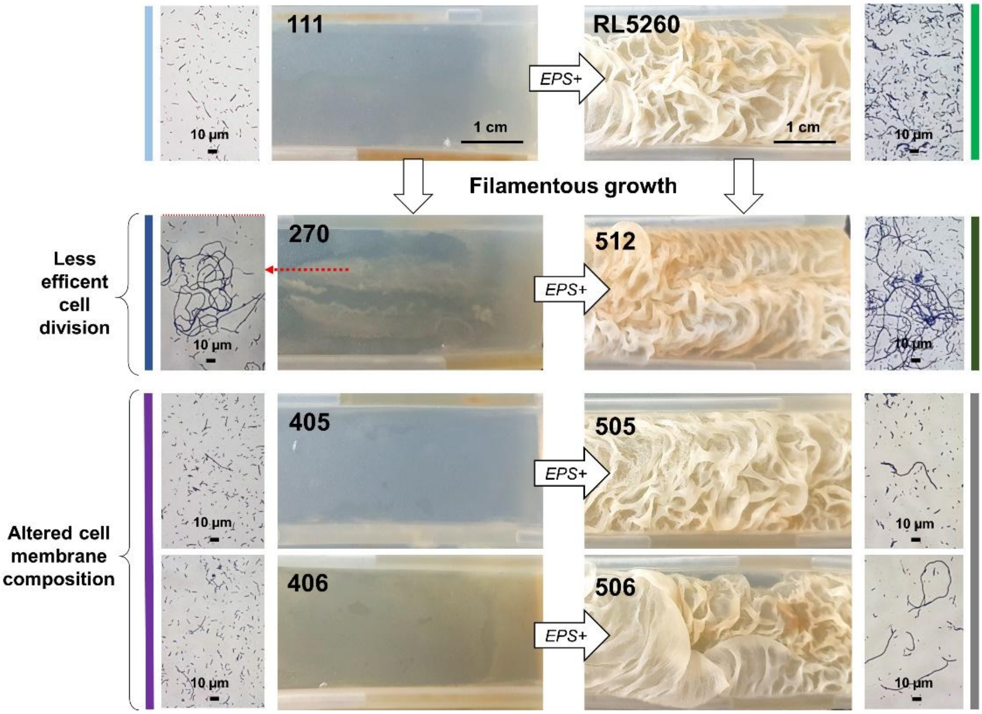
111
10 µm
1 cm
EPS+
RL5260
1 cm
10 µm
Filamentous growth
Less efficent cell division
10 µm
270
512
EPS+
10 µm
405
505
EPS+
10 µm
10 µm
Altered cell membrane composition
406
506
EPS+
10 µm
10 µm

Figure 32. DFR coupons colonized by the different *B. subtilis* mutant strains. Microscope images of Gram stained biofilm samples taken from the coupons are presented on the left or right side of the corresponding strain.

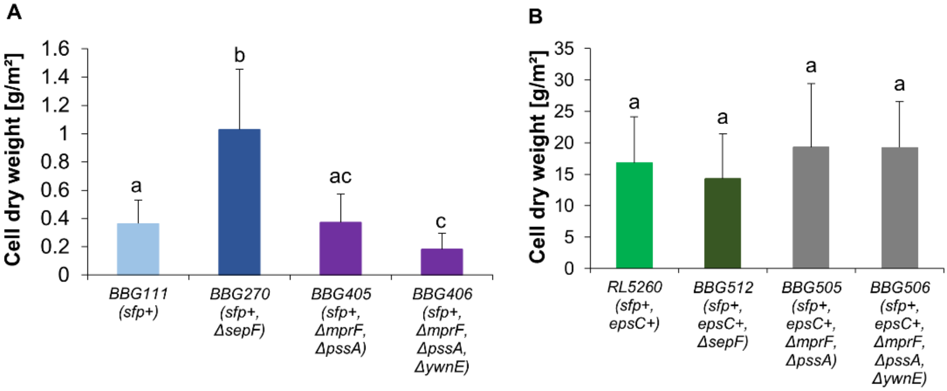

Figure 33. Determined cell dry weight of the cells adhered to the DFR coupons. (A) EPS$^-$ and (B) EPS$^+$ *B. subtilis* strains.

The adhesion capacity and the development of architecturally complex biofilm structures were clearly limited with EPS$^-$ strains. Generally, the EPS$^-$ strains developed only faint biofilm structures on the coupon. Only BBG270 showed some more pronounced structures compared to the other EPS$^-$ strains and seemed to colonize a large area of the coupon. In the case of BBG270, filamentous growth improved the cell attachment three times compared to the control strain BBG111 (**Figure 33A**). The spreading capacity was likewise increased since BBG270 covered a larger surface area than BBG111. Microscope images of samples taken from the biofilm revealed the presence of highly filamentous cells for BBG270. However, the EPS non producing mutants with altered membrane composition (BBG405 and BBG406), which have shown a filamentous growth character during microcolony development on agarose pads, did not show any improvement in terms of cell adhesion capacity compared to BBG111. The microscope images from biofilm samples did not show the development of highly filamentous cells, as observed for BBG270 or during the microcolony formation on agarose pads. Only some elongated cells were present. The improved colonization capacity observed for BBG406 on LB agar plates was not observed for the colonization of the silicone coupons in the DFR. The continuous flow in the DFR introduced a selective pressure and thus an additional obstacle to overcome for the colonization of the support. Apparently, BBG406 did not manage to resist against this supplementary stress. Since in this strain different membrane lipid types have been deleted, the membrane charge may have changed with a negative impact on cell adhesion on the used hydrophobic material (silicone).

The attachment capacity of the strains with restored robust EPS production increased up to 50-fold compared to the strains with reduced or no EPS production (**Figure 33B**). Here, the observed improved colonization capacities of LB agar plates were reflected. However, the magnitude was multiple times increased in the DFR. The strains with EPS production dealt much better with the shear stress and induced selective pressure of the continuous flow than the strains without EPS production. Furthermore, the biofilm developed architecturally complex wrinkled structures as well as a hydrophobic layer on the top of the biofilm (cf. section 3.7). In EPS$^+$ mutants, cell filamentation did not increase the cell adhesion capacity after 48 h of incubation. In the presence of EPS, cell filamentation seemed to play rather a minor role regarding cell adhesion and resistance to induced stress.

In general, the *B. subtilis* biofilm formation has been examined analyzing biofilm colony formation on agar plates or as pellicle at the liquid-air interface in static liquid cultures [9, 124]. Under more real conditions, biofilm formation has also often been studied on plant roots [124]. For the study of submerged biofilm, flow cells connected to confocal scanning laser microscopy are mostly used [121]. The methods complement each other and the combination of several systems for the biofilm analysis help to understand better the mechanisms involved in biofilm formation [126]. Yet, variations among the phenotypes can be observed in the different systems, since they have diverging advantages and limitations [126, 177]. This is also the case in this work since different capacities concerning the LB agar plate or the DFR coupon colonization have been observed for the strains as the growth conditions varied in the two systems.

The DFR used in this work has shown to be very suitable for the analysis of biofilm development of *B. subtilis* strains. This is certainly linked to the fact that *B. subtilis* forms preferentially biofilms at the air/liquid interface [178, 179], a condition fulfilled in the DFR [180]. In the DFR, the biofilm is developing on the coupon completely exposed to the surrounding air. The coupon is not submerged in the system since the alimentation is conducted only drop by drop on the upside of the coupon. The droplets are then flowing down on the coupon and deliver nutrients to the adhered cells. A biofilm development model on the DFR coupon has been developed in the following chapter. The DFR permitted to observe clearly the strong effect of EPS production in EPS$^+$ mutants in terms of biofilm development. The effect was much less pronounced in colony biofilms, as examined by McLoon et al. [6].

3.6.2 Strains with improved adhesion capacities produced higher amounts of surfactin

After the cultivation in the DFR, the amount of produced surfactin was measured in the whole liquid that passed the reactor, and in the biofilm developed on the coupon. The results are presented for the EPS$^-$ and EPS$^+$ strains in **Figure 34A** and **B**.

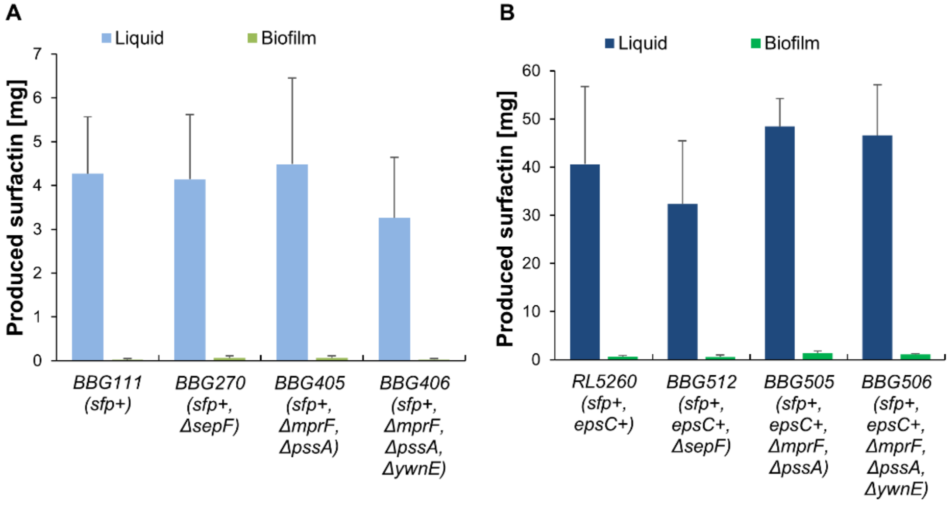

Figure 34. Amount of produced surfactin present in the total volume of liquid culture medium that passed the reactor and in the biofilm after 48 h of incubation in the DFR. (A) EPS$^-$ and (B) EPS$^+$ *B. subtilis* strains.

The overall surfactin production was up to ten times higher for EPS$^+$ strains than for EPS$^-$ strains. EPS production favored cell adhesion to the DFR coupon and provided a more favorable environment with improved biofilm stability. The resistance of the cells to the induced stress by the system was enhanced because of the biofilm matrix. This resulted in an increased surfactin production in EPS$^+$ strains. The biofilm contained only very little amounts of surfactin (< 2.8% of the total surfactin production). This pointed out that the surfactin molecules do not stay trapped in the biofilm after the secretion by the cells but are washed out with the medium which is very advantageously for a simplified downstream processing.

3.7 The task of exopolysaccharides in B. subtilis biofilms

As the previously presented results have shown, EPS are beneficial for enhanced cell adhesion to a support as well as contribute to the development of complex structures. The formation of complex wrinkled biofilm structures and the development of a hydrophobic protection layer, as **Figure 35** demonstrates, was only observed in the EPS^+ strains. The hydrophobicity has been revealed by the colored water droplets loaded on the top of the biofilm in **Figure 35**.

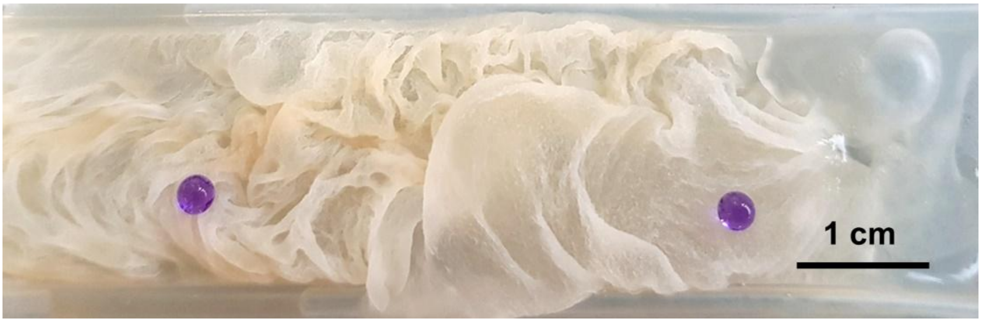

Figure 35. RL5260 biofilm developed on a DFR coupon with colored water droplets deposited on the biofilm surface to demonstrate the hydrophobicity.

Hence, the results confirmed that a functional *epsC* gene is required in *B. subtilis* 168 for the cell differentiation into matrix producing cells as well as the induction of BslA by DegU-P [49]. BslA is a hydrophobin that develops a protective layer on the surface of *B. subtilis* biofilms [135].

Regarding the wrinkled biofilm structures, it was interesting to know how much of the total biofilm weight can be assigned to the biofilm matrix and the number of present cells. Generally, the biofilm matrix is mainly composed of water and only 10 to 50% of the total biofilm volume is occupied by cells [119]. A high cell biovolume generally improves the reactor productivity since more cells are available per unit of biofilm for the metabolite production. Thus, the relative number of cells and amount of EPS in the biofilm were determined by separating the two components with mild sonication. The results are presented in **Table 4**.

Table 4. Biofilm dry weight and the relative amounts of EPS and cells present in the biofilm formed by EPS producing strains in the DFR.

Strain	Biofilm dry weight [%]	Relative amount of EPS [%]	Relative number of cells [%]
RL5260 ***(sfp$^+$, epsC$^+$)***	6.5 ± 1.0	80.9 ± 7.9	19.0 ± 7.9
BBG512 ***(sfp$^+$, epsC$^+$, ΔsepF)***	6.4 ± 1.6	80.9 ± 5.0	19.1 ± 5.0
BBG505 ***(sfp$^+$, epsC$^+$, ΔmprF, ΔpssA)***	8.2 ± 1.7	72.2 ± 8.4	27.8 ± 8.4
BBG506 ***(sfp$^+$, epsC$^+$, ΔmprF, ΔpssA, ΔywnE)***	7.6 ± 1.5	70.7 ± 9.5	29.3 ± 9.5

The biofilm dry weight of the EPS$^+$ strains was between 6.4 and 8.2% with a relative amount of 70 to 80% of EPS and 20 to 30% of cells, respectively. The cell fraction represents thus only a small part of the biofilm. The genetic modifications seemed to have no significant impact on the biovolume.

Dogsa et al. [181] measured a similar EPS and cell composition in *B. subtilis* NCIB3610 pellicles. They found that the formed biofilm pellicle was composed of around 70% of EPS and 30% of cells. In a cultivation system with higher shear forces, i.e. a trickle-bed biofilm bioreactor, Zune et al. [92] have determined an average cell composition of about 42% in *B. amyloliquefaciens* biofilms grown on a metal structured packing element. The biofilm dry matter content was comparable with 8.4%. It is generally supposed, that the mechanical and chemical properties of biofilms are attributed to the secretion of exopolymeric substances [182], as observed in this work. A recent work has shown that in *B. subtilis*, wrinkled biofilm structures are generated in combination with the presence of exopolymeric substances through a localized cell death pattern which spatially affects mechanical forces and initiates wrinkle formation [183].

Beside the protective aspect of the biofilm matrix, the structural development has a strong influence on the biofilm activity [140]. The presence of channels and voids in biofilms has shown to facilitate nutrient delivery and product removal [140, 142]. Yet, biofilm modeling studies have also revealed that pronounced three-dimensional biofilm structures are exposed to diffusion limits [140, 184]. Hence, the activity and substrate conversion rate could be higher in flat biofilms than in highly structured biofilms [140]. However, the importance of the presence of EPS should not be underestimated since EPS are structural and stabilizing components in biofilms and possibly serve as a nutritional reserve [181]. Accordingly, it is difficult to forecast if flat biofilms (EPS$^-$) or highly structured biofilms (EPS$^+$) will be more efficient and suitable for the development of biofilm-based processes. In this study, the DFR results have shown that EPS production seemed to provide a strong advantage for cell adhesion and the dealing with stress. However, the coupon surface is limited. It is not known how the EPS$^-$ and EPS$^+$ mutants will react when a high specific surface area is available for colonization and in the presence of higher shear forces as it is the case in the trickle-bed biofilm bioreactor used in the following chapters.

4. Conclusions

The restoration of *epsC* in *B. subtilis* 168 and the induction of filamentous growth did not have a negative impact on cell growth or surfactin production in suspended cultures. Filamentous growth affected strongly the microcolony formation which resulted in an enhanced surface spreading and the colonization of greater areas. The colonization capacities of LB agar plates were significantly improved in EPS$^+$ and/or filamentous mutants.

The DFR has shown to be a suitable tool for studying the biofilm development of *B. subtilis* strains on coupons under low shear stress. Characteristics of *B. subtilis* biofilms like the development of complex wrinkled structure and a hydrophobic protection layer could be observed. EPS production contributed significantly to enhanced cell adhesion and increased resistance to stress, whereas cell filamentation played a minor role. Yet, the attachment of strains deficient in EPS production could be significantly increased through genetically-induced filamentous growth in BBG270 (*sfp*$^+$*, ΔsepF*). Enhanced cell adhesion and biofilm development in EPS$^+$ strains were linked to an improved surfactin production. The most interesting strains seemed to be the strains with *sepF* deletions. The next chapter focuses on these strains regarding the adaptation of *B. subtilis* 168 to biofilm cultivation. The impact of surfactin production on the colonization capacity of the DFR coupons is studied as well as a colonization model of the DFR coupons is developed.

CHAPTER 3

Molecular strategies for adapting *B. subtilis* 168 biosurfactant production to biofilm cultivation mode

This chapter is related to the article H. L. Brück, F. Delvigne, P. Dhulster, P. Jacques, and F. Coutte, “Molecular strategies for adapting *Bacillus subtilis* 168 biosurfactant production to biofilm cultivation mode,” published in *Bioresource Technology*, vol. 293, no. 122090, pp. 1–8, 2019.

Abstract

Biofilm bioreactors have already been proven to be efficient systems for microbial lipopeptide production since they avoid foam formation. However, the cell adhesion capacities of the laboratory strain *B. subtilis* 168 to the biofilm bioreactor support are limited. In this work, we present a novel approach for increasing cell adhesion through the generation of filamentous and/or exopolysaccharide producing *B. subtilis* 168 mutants by genetic engineering. The single cell growth behavior was analyzed using time-lapse microscopy and the colonization capacities were investigated under continuous flow conditions in a drip-flow reactor. Cell adhesion could be increased three times through filamentous growth in lipopeptide producing *B. subtilis* 168 derivatives strains. Further restored exopolysaccharide production increased up to 50 times the cell adhesion capacities. Enhanced cell immobilization resulted in 10 times increased surfactin production. These findings will be of particular interest regarding the design of more efficient microbial cell factories for biofilm cultivation.

Keywords: *Bacillus subtilis*, biofilm bioreactor, filamentation, cell adhesion, surfactin

1. *Introduction*

The gram-positive soil bacterium *Bacillus subtilis* produces naturally different classes of lipopeptides as secondary metabolites [24]. These lipopeptides combine remarkable physicochemical properties and biological activities and thus have a wide range of applications in various fields [24]. Since lipopeptides are very powerful biosurfactants, the bioreactor design and operating conditions have to be chosen properly in order to control or to avoid foam formation [25].

Innovative lipopeptide production processes avoiding foam formation based on an air/liquid membrane contactor [74, 84] and on a trickle-bed biofilm reactor [92, 147] have been developed in previous works. Both systems have shown to promote biofilm formation. In the first system, a thin surfactin producing biofilm has been developed by *B. subtilis* 168 derivative strains on the air/liquid membrane contactor [84]. In the second system, the reactor contains a metal structured packing that provides a high specific surface area for the cell adhesion and biofilm development [92]. In this trickle-bed biofilm reactor, natural filamentous microorganism such as the fungi *Aspergillus oryzae* and *Tricoderma reesei* have shown to have much better cell adhesion capacities than the natural non-filamentous and lipopeptide producing bacterial strain *Bacillus amyloliquefaciens* [92, 146, 148]. Other interesting biofilm-based processes consisting of a rotating disc reactor [93] or an inverse fluidized bed bioreactor [78] have shown that the lipopeptide productivity could be increased through cell immobilization.

Biofilm bioreactors provide increased productivity and process stability through the generation of a highly active attached biomass with a high resistance to external influences and toxic compounds [128]. Especially for surfactin production, biofilm bioreactors can be conducive since surfactin is linked to the biofilm regulation mechanism as a trigger molecule for the expression of matrix genes [49].

The *B. subtilis* wild-type strain NCIB3610 forms robust and highly structured biofilms on solid surfaces and air/liquid interfaces [125], whereas the widely used laboratory strain *B. subtilis* 168 forms only thin and relatively undifferentiated biofilms [127]. McLoon et al. [6] have shown that several genetic mutations in *B. subtilis* 168, which have accumulated during the domestication process, contribute to impaired biofilm formation. Especially, a deficiency in exopolysaccharide (EPS) production, due to a point mutation in the *epsC* gene, is responsible for a strongly reduced matrix production [6]. Another known alteration is the defective *sfp* gene [6]. The gene *sfp* codes for a phosphopantetheine-transferase which is essential for the non-ribosomal peptide synthesis of lipopeptides such as surfactin [6, 86]. The defective biofilm formation is a limiting factor for a robust colonization of the biofilm bioreactor support by *B. subtilis* 168 derivatives strains. For a good bioreactor performance, enhanced support colonization capacities are necessary. In wild-type strains of *B. subtilis,* architecturally complex biofilm structures are associated with the growth in chains of cells that are bound together in bundles via exopolysaccharides [125]. Focusing on the spatial organization of the cells in the biofilm, it might be possible to improve the support colonization through the engineering of cell shapes.

Numerous metabolic engineering strategies have been already developed to design more efficient cell factories [152]. The manipulation of cell shapes has been rarely exploited to optimize bioprocesses [152]. Gene deletions affecting the cell division induce morphological changes in cells. In *B. subtilis*, the cell septation protein SepF has shown to be involved in the septum formation and is required for a later step in cell division but does not represent an essential gene [159]. The deletion of SepF perturbates the division septum assembly in the cells and thus provokes filamentous growth due to a deficiency in cell division [159]. Recently, Zhao et al. [185] have deleted several genes related to peptidoglycan hydrolases in a *B. subtilis* strain leading to elongated bacterial cells with increased specific growth rates and improved enzyme production capacities.

In this work, we investigate different possibilities of engineering *B. subtilis* 168 strains to improve the cell adhesion capacities through the change of cell shape and enhanced biofilm matrix production. The goal is to be able to produce surfactin in a continuous bioprocess with immobilized cells on a reactor support through the formation of a structural organized biofilm.

In the first step, the engineered strains are characterized at single cell level with a time lapse microscope to evaluate their growth dynamic. Then, the colonization and adhesion capacities of the engineered strains are tested under more real conditions in a drip-flow reactor (DFR) with continuous flow. Images with a live camera are taken to establish a cell colonization and biofilm formation model. Moreover, the surfactin production capacity of the adhered cells is analyzed. Based on the results, we discuss the impact of filamentous growth, surfactin production and biofilm formation on the performance of biofilm-based bioprocesses.

2. Materials and methods

2.1 Strains and strain construction

All genetically engineered strains that were used in this study are derived from the laboratory strain *B. subtilis* 168 (*trpC2*, sfp^0, $epsC^0$). The strains have been selected and/or modified focusing on three genetic modifications: the introduction or respectively the restoration of the genes *sfp* and *epsC* as well as the deletion of *sepF*. For a complete list of the strains and their corresponding genotype as well as the plasmid used in this work see **Table 5**.

Table 5. Bacterial strains and plasmids used in this study.

Strains or plasmids	Genotype or plasmid composition	Source
Bacterial strains		
Echerichia coli JM109	*end*A1, *rec*A1, *gyr*A96, *thi*, *hsd*R17 (r_k, m_k^+), *rel*A1, *sup*E44, Δ(*lac*-*pro*AB), [F´*tra*D36, *pro*AB, *laq*I^{q}ZΔM15]	Promega Corporation
***Bacillus subtilis* 168**	*trpC2, sfp*^{0}*, epsC*^{0}	Lab stock
TB92	*trpC2, sfp*^{0}*, epsC*^{0}*, ΔsepF::spc*; Spc^R *(derived from 168)*	[159]
BBG111	*trpC2, amyE::sfp-cat, epsC*^{0}; Cm^R *(derived from 168)*	[86]
BBG270	*trpC2, ΔsepF::spc, amyE:: sfp-cat, epsC*^{0}; Spc^R, Cm^R *(derived from TB92)*	This study
RL5260	*trpC2, epsC*$^+$*, sfp*$^+$*;* Erm^R	[6]
Master strain BBG501	*trpC2, epsC*$^+$*, sfp*$^+$*, Δupp:: λPr-neo*; Erm^R, Neo^R *(derived from RL5260)*	This study
BBG512	*trpC2, epsC*$^+$*, sfp*$^+$*, Δupp:: λPr*-neo, *ΔsepF::phleo-upp-cI*; Erm^R, Neo^R, Phleo^R *(derived from BBG501)*	This study
Plasmids		
pGEM®-T Easy	Cloning vector	Promega Corporation
pBG129	*amyE- sfp-cat-amyE-speccloned into pGEM®-T Easy*	[86]
pBG402	*upp*^{UP}*- Pλ-neo-upp*^{DOWN} *cloned into pGEM®-T Easy*	This study

For the transformation, *B. subtilis* strains have been grown in natural competence medium (14 g L^{-1} $K_2HPO_4 \cdot 3H_2O$, 5.3 g L^{-1} KH_2PO_4, 20 g L^{-1} Glucose, 8.8 g L^{-1} Tri-Na Citrate, 0.22 g L^{-1} Ferric-NH_4-citrate, 1g casein hydrolysate, 2 g K glutamate, 1 M $MgSO_4$, 1.6 mg L^{-1} tryptophan) at 37°C and 160 rpm to favor the DNA uptake and integration. Selective media were prepared by adding various antibiotics to lysogeny broth (LB) (10 g L^{-1} tryptone, 5 g L^{-1} yeast extract, 10 g L^{-1} NaCl) or LB containing 1.7% agar: chloramphenicol (Cm) 5 µg mL^{-1}, neomycin (Neo) 5 µg mL^{-1}, erythromycin (Erm) 1 µg mL^{-1}, spectinomycin (Spc) 100 µg mL^{-1}.

In *sfp*$^+$ *B. subtilis* 168 mutants, a functional *sfp* gene has been inserted into the *amyE* locus through homologous recombination of the plasmid pBG129, as previously described [86]. Positive clones, showing a chloramphenicol-resistance and spectinomycin sensibility due to a double cross-over homologous recombination of pBG129, were selected. A correct *sfp* gene transformation was further confirmed by a positive hemolytic test due to the presence of surfactin and negative amylase activity test as a result of the successful insertion of *sfp* into the *amyE* locus. Moreover, surfactin production of the *sfp*$^+$ strains was verified in planktonic cultures using reversed-phase UPLC-MS analysis (see section 2.7, page 81).

The gene deletion of *sepF* was performed by using the gene deletion strategy “Pop in – pop out”, previously described by Tanaka et al. [171]. Based on this technique, a master strain was constructed by replacing the *upp* gene with a neomycin resistance gene under the control of the Lambda Pr promoter (*λPr-neo*) through homologous recombination of the plasmid pBG402. Positive clones with a neomycin-resistance were selected. In the following, the gene deletions were introduced in the master strain through homologous recombination of the targeted gene sequence *sepF* with the gene deletion cassette. The gene deletion cassette was synthesized by polymerase chain reaction (PCR) through the assemblage of different components: the up and down stream element of the gene to be deleted (*sepF*) and the element containing a phleomycin resistance gene, the repressor gene of the Lambda promoter *cI* which is necessary for counterselection. Positive clones, showing a phleomycin resistance and neomycin sensitivity as a result of the cassette insertion, were selected. All genetic manipulations have been verified by PCR-based assays and the sequencing of the manipulated gene segment. **Figure 36** summarizes the different genetic modification strategies and their corresponding outcome for adapting *B. subtilis* 168 surfactin production to biofilm cultivation mode.

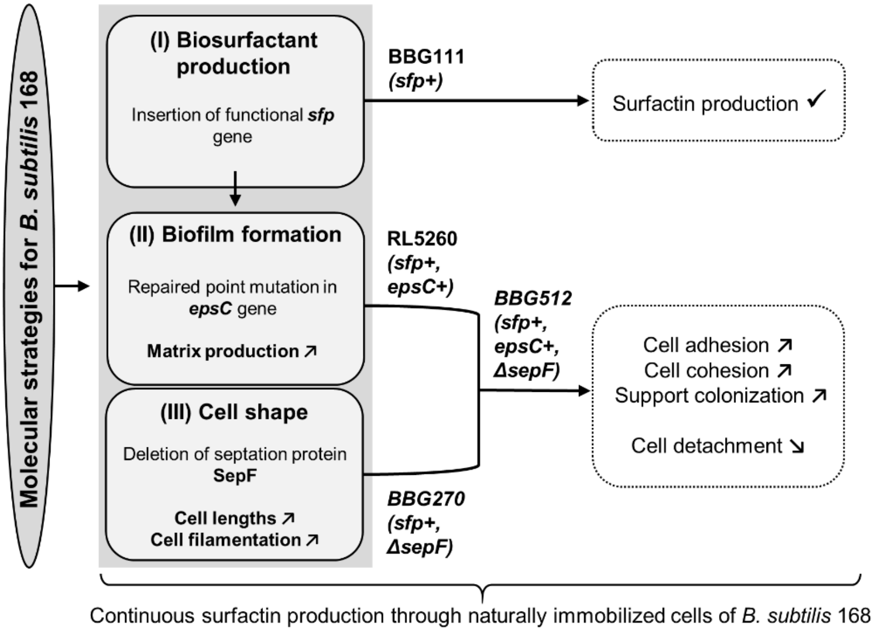
Molecular strategies for B. subtilis 168
(I) Biosurfactant production
Insertion of functional sfp gene
(II) Biofilm formation
Repaired point mutation in epsC gene
Matrix production ↗
(III) Cell shape
Deletion of septation protein SepF
Cell lengths ↗
Cell filamentation ↗
BBG111 (sfp+)
Surfactin production ✓
RL5260 (sfp+, epsC+)
BBG512 (sfp+, epsC+, ΔsepF)
BBG270 (sfp+, ΔsepF)
Cell adhesion ↗
Cell cohesion ↗
Support colonization ↗
Cell detachment ↘
Continuous surfactin production through naturally immobilized cells of B. subtilis 168

Figure 36. Molecular strategies to obtain a lipopeptide producing *B. subtilis* 168 strain adapted to biofilm cultivation mode: (I) insertion of a functional *sfp* gene [86], (II) restoration of the *epsC* gene [6], (III) provoking of filamentous growth through the gene deletion of *sepF* [159].

2.2 Time-lapse microscopy analysis of single *B. subtilis* cells

The cell morphology and growth behavior at single cell level was analyzed as previously described in chapter 2, section 2.4, page 50.

2.3 Drip-flow reactor composition and growth conditions

For the cell adhesion capacity analysis, biofilms were grown on silicone coupons in six parallel flow chambers per DFR (six-chamber Drip Flow Biofilm Reactor®, 224 x 127 x 37 mm, Biosurface Technologies Corporation, Montana, USA). The DFR facilitates the observation of biofilm initiation and spreading on a solid surface (called coupon) under low shear stress conditions. In our case, we used silicone coupons with a rough surface to increase the specific surface area that will be available for the initial cell adhesion and biofilm formation. The surface structure image of the silicone coupon was recorded with a 3D high resolution digital microscope VHX-6000 (KEYENCE International Belgium NV/SA, Mechelen, Belgium).

The strains were cultivated in Landy MOPS medium at pH 7.0 (20 g L^{-1} glucose, 5 g L^{-1} glutamic acid, 1 g L^{-1} yeast extract, 0.5 g L^{-1} $MgSO_4$, 1 g L^{-1} K_2HPO_4, 0.5 g L^{-1} KCl, 1.6 mg L^{-1} $CuSO_4$, 1.2 mg L^{-1} $MnSO_4$, 0.4 mg L^{-1} $FeSO_4$, 21 g L^{-1} MOPS, 1.6 mg L^{-1} tryptophan). The DFR was placed in a cell culture room kept at 37°C. For the inoculation, overnight cultures of the engineered strains grown in Landy MOPS medium at 37° and 160 rpm were diluted with Landy MOPS medium to an $OD_{600\ nm}$ of 1. The reactor was kept horizontally and 20 mL of the diluted culture was injected per chamber with a syringe. The inoculation has been followed by a 6 h batch phase permitting the cells to settle down and adhere on the support. After the batch phase, the reactor was inclined and the continuous phase with the delivery of fresh medium was launched with a flow rate of ~13 mL h^{-1} per chamber during 42 h, resulting in a total incubation time of 48 h. For each mutant the cell adhesion capacity has been analyzed with 1 to 3 technical replicates per experiment that has been repeated at least 3 times (biological replicates).

2.4 Cell counting after initial adhesion on the drip-flow reactor support

To determine the initial adhesion capacities of the mutants, the strains were cultivated and inoculated in the DFR as previously described (cf. section 2.3, page 80). After 6 h of batch phase, a continuous flow (˜13 mL h^{-1}) was launched during 1 h to flush gently non-attached cells from the coupons. Then, the coupons were taken out of the chambers and put into a 50 mL Falcon tube containing 10 mL of phosphate-buffered saline (PBS). After vigorous vortexing, ten-fold dilution series from 10^0 to 10^{-6} were performed with the cell suspensions. From each dilution, 100 µL of the cell suspension was dropped and plated on LB agar Petri dishes. The Petri dishes were incubated overnight at 37°C. The developed colony were counted to estimate the number of viable adhered cells on the coupon surface. The cell counting of each mutant was performed in triplicates.

2.5 Cell dry weight analysis of the adhered cells after 48 h

After 48 h, the silicone coupons with the developed biofilm on the surface have been taken out of the DFR and put into a 50 mL Falcon tube containing 10 mL of PBS. The biofilm was suspended into the liquid through vigorous vortexing. Then, the suspended biofilm has been gently sonicated (1 to 3 times for 40 sec with 30% of amplitude) to extract the surfactin molecules trapped in the biofilm matrix and dissolve the exopolysaccharides attached to the cells. After the sonication, the samples have been centrifuged. The supernatant was collected and the surfactin concentration was determined as described below (cf. section 2.7, page 81). The cell pellets were washed by resuspending them in distilled water followed by centrifugation in order to eliminate the dissolved exopolysaccharides. The supernatant was discarded and the remaining cell pellet was re-suspended in water and filtered (0.2 µm). The filter with the retained cells has been dried in the oven at 105°C and weighted to determine the corresponding cell dry weight.

2.6 Real-time observation of biofilm formation dynamics in the drip-flow reactor

For a better understanding of the support colonization by the mutants, the biofilm development in the DFR has been visualized by a real-time camera. For this purpose, the plastic cover of the chamber was replaced by a purpose-made cover composed of an integrated fully transparent glass window for growth observation. Images were taken with a live camera every 15 min for the whole incubation time of 48h. The image sequence has been used to build a general colonization model.

2.7 Surfactin production analysis

Cell culture samples were taken after a total incubation time of 48 h from the whole liquid phase that has passed and has been collected at each DFR chamber exit (~575 mL per chamber). Besides, the surfactin concentration has been determined in the sonicated biofilm samples (cf. section 2.5, page 81). The culture samples were centrifuged and the supernatant was filtered (0.2 µm) prior to the surfactin analysis by reversed-phase UPLC-MS (AQUITY UPLC H-Class, Waters, Zellik, Belgium) with an AQUITY UPLC BEH C-18 1.7 µm, 2.1 x 50 mm, column (Waters, Zellik, Belgium) coupled to a single quadrupole MS (AQUITY SQ Detector, Waters, Zellik, Belgium). For sample ionization, the source temperature was set at 130°C with a desolvation temperature of 400°C, a nitrogen flow of 1000 L h^{-1} and a cone voltage of 120 V. The UPLC analysis method was based on an acetonitrile/water gradient containing 0.1% formic acid with a flow rate of 0.6 $mLmin^{-1}$ and an analysis time of 7 min per sample. The elution was started at 30% of acetonitrile.

After 2.43 min acetonitrile was brought up to 95% and then again reduced to 30% at 5.1 min until the end.

Purified surfactin samples (> 98%) (Lipofabrik, Villeneuve d'Ascq, France) were used to determine the retention time of the surfactin molecules and a calibration curve. Surfactin isomers were further identified through the recorded mass spectra. Specific m/z peaks were observed at 994, 1008, 1022, 1036, 1050 $[M+H]^+$ and 1016, 1030, 1044, 1058, 1072 $[M+Na]^+$ representing the surfactin isomers C-12 to C-16 respectively (**Figure 37**). The overall surfactin concentration was calculated on the basis of the calibration curve.

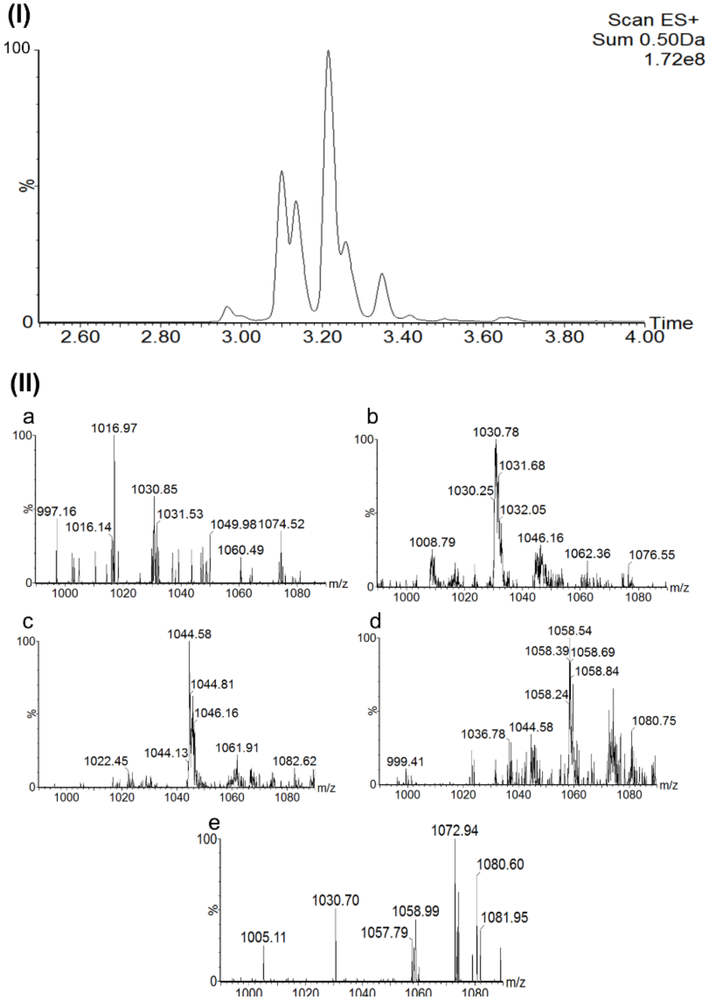

Figure 37. UPLC-MS analysis of a culture sample of *B. subtilis* RL5260. (I) Elution profile of the surfactin isomers. Small letters (a-e) indicate the corresponding recorded mass spectrum presented in (II); (II) Mass spectrum showing the $[M+H]^+$ and $[M+Na]^+$ m/z peaks of the surfactin isomers C-12 to C-16, respectively.

2.8 Statistical analysis

Comparison of the cell dry weight and colony forming unit results between groups of *B. subtilis* mutants were performed using a pairwise two-tailed Student’s t test. The differences between groups were considered as significant when $p < 0.05$.

3. Results and discussion

3.1 Single cell phenotypic characterization of filamentous B. subtilis strains

In the first part of this work, we looked at the dynamics of cell growth and spatial organization of the genetically engineered *B. subtilis* strains on agarose pads by time-lapse microscopy. Three main genetic targets have been selected, i.e. the introduction of a functional *sfp* gene necessary for lipopeptide synthesis, the restoration of the *epsC* gene required for the extracellular biofilm matrix production, and the deletion of the *sepF* gene involved in cell septation. The latter mutation is known to impair cell septation leading to cell filamentation [159, 161]. The growth of isolated *B. subtilis* cells on agarose pads and the resulting microcolonies (single layer) have been tracked with a time-lapse microscope until the stationary growth phase was reached. As expected and already described by Hamoen et al. [159], the deletion of *sepF* led to filamentous growth due to less efficient cell division. However, this deletion also had a considerable impact on the colony formation and colonization behavior. Cells with functional *sepF* (i.e. *B. subtilis* 168, BBG111 and RL5260) exhibited normal cell division dynamics which led to more packed colonies containing small cells that were easily distinguishable from each other with mean cell lengths comprised between 3 to 6 µm. For the filamentous strains containing the *sepF* deletion (i.e. *B. subtilis* TB92, BBG270 and BBG512), a less efficient cell division could be clearly observed in the exponential growth phase (~4 h), leading to elongated cells that developed in length. After the exponential growth phase, the filamentous cells also tended to separate. In the stationary phase at ~8 h, maximum cell lengths of up to 26 µm were observed with mean cell lengths comprised between 8 and 12 µm. The strains with *sepF* deletion (TB92, BBG270 and BBG512) developed rather loosely packed micro-colonies with large spaces that were devoid of cells due to the filamentous cell growth. Consequently, they explored a larger area on the agarose surface by comparison with the *sepF*$^{+}$ strains. The increased colonization capacity was also observed for the filamentous surfactin producing strains BBG270 and BBG512 during macroscopic colony development on 0.7% agar LB plates, as **Figure 38** shows.

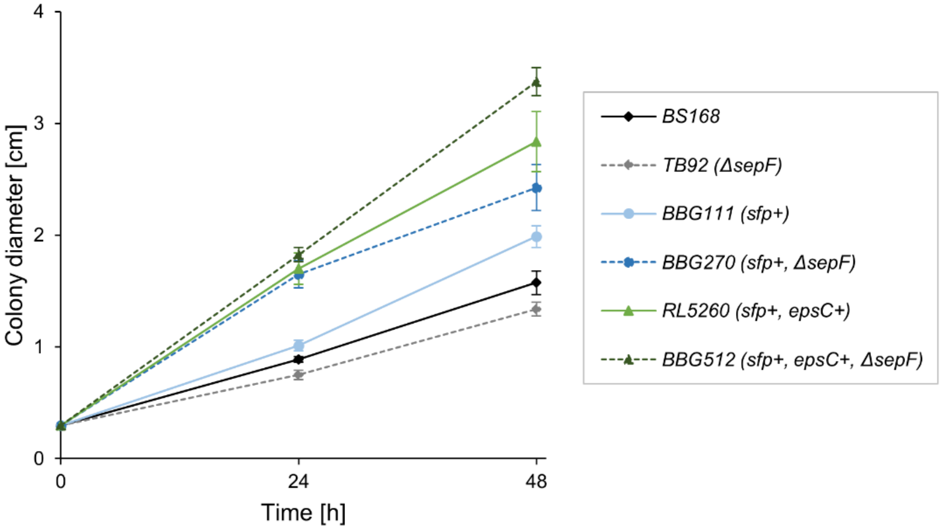

Figure 38. Colony development of the *B. subtilis* mutants on 0.7% agar LB plates. The agar LB plates were inoculated with 2.5 µL of diluted pre-cultures (OD = 1), allowed to dry and incubated at 30°C for 48h. Four replicates were performed per strain.

Hence, filamentous growth might be advantageous for a broader colonization of the bioreactor support material.

3.2 Evaluation of colonization and biofilm formation capacity in a continuous drip-flow reactor

As a second characterization step, the engineered *B. subtilis* strains have been cultivated in a drip-flow reactor (DFR) in order to investigate the biofilm formation capacity on a solid inert support and under continuous nutrient supply.

3.2.1 Initial cell adhesion capacity

Firstly, it was checked to what extend filamentous growth and EPS production is beneficial for the initial cell adhesion of surfactin producing *B. subtilis* strains on the DFR support. For this purpose, the bacterial cells present on the DFR support after 6 h of batch phase followed by 1 h of continuous flow have been counted. Therefore, the adhered cells have been detached and quantified by plate counting (**Figure 39**).

The initial cell adhesion capacities of the surfactin producing EPS$^+$ strains (i.e. RL5260 (*sfp*$^+$, *epsC*$^+$) and BBG512 (*sfp*$^+$, *epsC*$^+$, *ΔsepF*)) were up to ten-fold increased by comparison with the surfactin producing EPS deficient strains (i.e. BBG111 (*sfp*$^+$) and BBG270 (*sfp*$^+$, *ΔsepF*)).

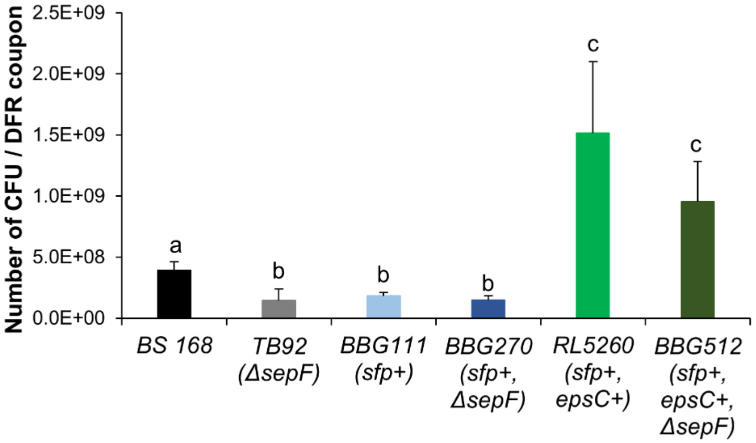

Figure 39. Initial cell adhesion capacity of the *B. subtilis* strains on the DFR coupons. Samples were taken after an incubation time of 6 h (batch phase) followed by 1 h of continuous flow (~13 mL h^{-1}) to flush gently away non-adhering cells in the DFR. The counted numbers of colony forming units are presented with the corresponding standard deviation. Significant differences ($p < 0.05$) between groups are indicated by small letters (a, b or c).

EPS are natural polymers composed of sticky sugar substances that help the cells to adhere to a surface and to each other in the case of biofilm formation [120, 186]. However, no significant differences have been observed inside the groups (i.e., neither EPS^+ nor EPS^- strains), suggesting that cell filamentation upon deletion of *sepF* has no significant impact on the cell's initial adhesion in the surfactin producing strains.

Regarding the non surfactin producing strains BS168 and TB92 (*ΔsepF*), the initial cell adhesion of the non-filamentous strain BS168 was slightly increased compared to the filamentous strain TB92. This negative impact of cell filamentation is probably linked to the less efficient cell division of TB92 which lead to coherent, not properly separated cells. Consequently, it is difficult to spread and plate single cells on the agar plate for a correct counting of the single colony forming units.

3.2.2 Biofilm formation capacity

In the next step, the engineered *B. subtilis* strains were incubated for 48 h, including a 6 h batch phase and 42 h phase with continuous nutrient supply, until the development of a biofilm on the DFR coupon was observed. A schematic view of the used device is presented in **Figure 40A**. **Figure 40B** shows the coupons colonized by the different *B. subtilis* strains after 48 h in the DFR. The corresponding amounts of cell dry weight that were measured in g per m^2 of coupon area are presented in **Figure 40C**. The surface structure of the silicone coupons used as support for the biofilm development in the DFR is presented in **Figure 40D**.

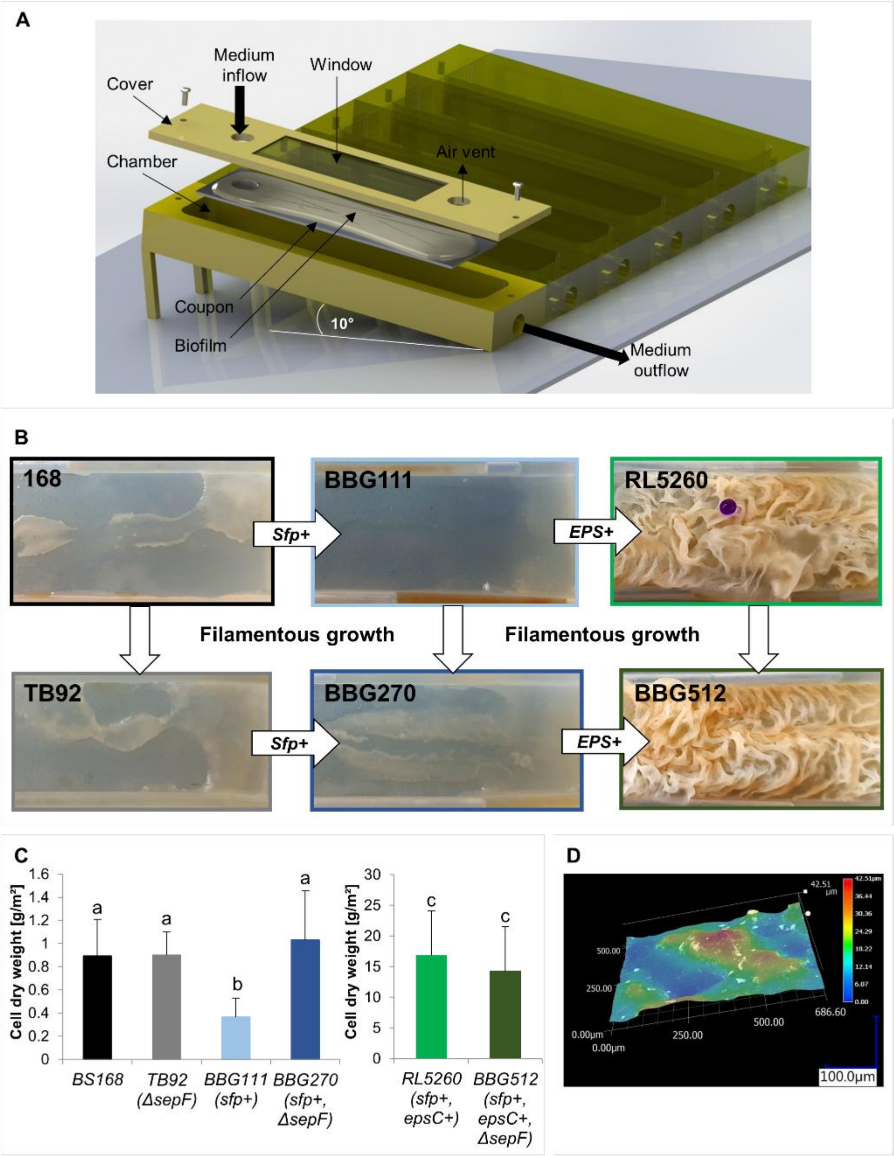

Figure 40. (A) Schematic view of the drip-flow cultivation device with six parallel growth chambers. Each chamber contains a coupon for evaluating biofilm development; An integrated glass window allows real-time analysis of the biofilm development. (B) Cell adhesion and biofilm formation capacities of the engineered *B. subtilis* strains on a silicone coupon in the DFR. A colored water droplet was placed on the top of the biofilm formed by RL5260 as an indicator for hydrophobicity. (C) Measured amount of cell dry weight in g per m^2 of coupon area. The values are represented with the corresponding standard deviation. Significant differences ($p < 0.05$) between groups are indicated by small letters (a, b or c). (D) Structure of the uncolonized silicone coupon surface recorded with a 3D high resolution digital microscope.

The induction of filamentous growth in the surfactin negative strain TB92 (*ΔsepF*) resulted in no significant increase in cell adhesion on the support compared to *B. subtilis* 168 (control), the cell adhesion capacities were similar. Since the silicone coupons possess a hydrophobic surface and these strains do not produce surfactin to decrease the surface tension, it is more difficult for the cells to spread. In this case, filamentous growth seemed to be neither advantageous nor unfavorable for the support colonization. Leclère et al. [178] have already demonstrated that it is necessary to reduce the surface friction to increase the surface colonization capacity of *B. subtilis* 168. Surfactin is a surface-active agent that reduces the surface tension and thus permits the cells to spread more easily, as already shown by several authors [16, 86, 178, 187–189].

The presence of surfactin showed a clear impact on the cell distribution on the coupon surfaces. The biofilm of the surfactin negative strains 168 and TB92 (*ΔsepF*) showed a clear front line on the coupon surface, whereas the border regions of the surfactin producing strains BBG111 (*sfp*$^+$) and BBG270 (*sfp*$^+$, *ΔsepF*) were smooth, an indicator for swarming motility due to the presence of surfactin [16]. The increased spreading capacity of BBG111 and BBG270 due to the presence of surfactin led to the colonization of larger zones with a lesser cell density. Hence, the surfactin producing strains BBG111 (*sfp*$^+$) and BBG270 (*sfp*$^+$, *ΔsepF*) were able to cover more homogenously the coupon surface by developing more smooth and better dispersed biofilms than the non surfactin producing strain BS168 or respectively TB92 (*ΔsepF*).

However, the cell adhesion capacity of BBG111 (*sfp*$^+$) decreased two to three times compared to BS168. This occurred probably due to cell detachment and the washing out of cells through the presence of surfactin. But the cell adhesion capacity was recovered upon induction of filamentous growth (strain BBG270 (*sfp*$^+$, *ΔsepF*)). The cell adhesion capacities of BBG270 were up to three times higher than the ones of the strain BBG111 (*sfp*$^+$) and thus similar to the cell adhesion capacities of *B. subtilis* 168.

Regarding the initial cell adhesion after the batch phase (6h), the number of cells present on the coupons were similar for the filamentous strain BBG270 (*sfp*$^+$, *ΔsepF*) and non-filamentous strain BBG111 (*sfp*$^+$). Though, after 48h of incubation, the results have shown that provoked filamentous growth in the surfactin producing strain BBG270 permitted to increase up to three times the cell adhesion capacity resulting in a higher biomass adhered to the support material. Möller et al. [190] have already demonstrated that the colonization of heterogeneous surfaces under physiological flow conditions is accelerated in filamentous *E. coli* cells. The bacterial cell shape adaption resulted in an improved ability of bridging non-adhesive distances [190]. As the coupon surface analysis with the digital microscope has revealed, the silicone coupons consist of a rough surface with height differences of up to 42.5 µm (cf. **Figure 40D**) that have an impact on the cell distribution and colonization. Probably, filamentous cells overcome more easily structural irregularities than small cells and consequently possess better colonization capacities. Furthermore, the formed cell aggregates of the filamentous cells seemed to have a better cohesion than the ones formed by small cells making the detaching and washing out of single cells more difficult, especially in the presence of surfactin. The advantages of the increased cohesion of filamentous cells is an interesting feature for biosurfactant production in biofilm reactors with *B. subtilis* strains to obtain a more efficient and stable colonization of the support materials and to reduce cell detachment from the biofilm.

The adhesion capacities of the strains with restored EPS production (RL5260 (*sfp*$^+$*, epsC*$^+$*)* and BBG512 (*sfp*$^+$, *epsC*$^+$, *ΔsepF*)) increased 10 to 50 times compared to the strains displaying reduced EPS production (168, TB92, BBG111, BBG270). Moreover, the EPS$^+$ mutants (RL5260 and BBG512) developed exceptional wrinkled biofilm structures on the DFR coupons. The provoked cell filamentation in BBG512 (*sfp*$^+$, *epsC*$^+$, *ΔsepF*) showed no significant improvement in initial cell adhesion and biofilm formation after 48h of incubation compared to RL5260 (*sfp*$^+$, *epsC*$^+$).

As expected, the presence of EPS was a key factor for initial cell adhesion and biofilm formation on the drip-flow biofilm reactor support. These natural sticky compounds that are produced by the cells are involved in surface-cell and cell-to-cell interactions [120, 131, 186]. Hence, the presence of EPS was found to increase the cell adhesion to a surprisingly high extent of up to 50-fold. No additional increase in cell adhesion was observed in EPS$^+$ mutants with induced filamentous growth (BBG512), neither at the initial cell adhesion after 6h of incubation nor after 48h of incubation. However, it has to be considered that the cell adhesion was analyzed using a simple coupon surface. Biofilm bioreactors such as the previously mentioned trickle-bed biofilm reactor [92] contain a highly structured packing with a very high specific surface area. In this case, probably, the cell adhesion capacities can be boosted much more through filamentous growth, even in EPS$^+$ mutants. Obviously, the presence of EPS outcompeted the advantage of filamentous cells to colonize the silicone coupons due to an improved adhesion. Seminara et al. [130] investigated the role of EPS in *B. subtilis* biofilm expansion. They found out that matrix production indeed contributes to biofilm spreading due to osmotic forces, probably to increase nutrient uptake. In this case, cell filamentation seemed to have a minor effect on biofilm formation than the EPS production.

In the EPS$^+$ mutants (RL5260 and BBG512), the biofilm developed very complex wrinkled structures, characteristic of mature *B. subtilis* biofilms [120]. Moreover, a hydrophobic layer on the top of the biofilm was observed. The surface hydrophobicity of this protection layer is demonstrated by the colored water droplet staying at the top of the biofilm of RL5260 in **Figure 40B**. This hydrophobic layer is composed of the protein BslA, a hydrophobin that is synthesized in the last stages of biofilm maturation, as already described by several researchers [49, 135, 191].

3.2.3 Cell colonization and biofilm development mode in the drip-flow reactor

As reported in the previous section (cf. 3.2.2, page 85) the EPS$^+$ *B. subtilis* mutants (RL5260, BBG512) were able to develop remarkable wrinkled biofilm structures within 48 h. Moreover, they were able to colonize the whole DFR coupon surface, whereas the EPS deficient strains colonized only a part of the DFR coupons after 48h. Since the cell colonization and structural biofilm development on the DFR support seemed to be rather a heterogeneous phenomenon, the dynamics of biofilm formation has been studied. For this purpose, the biofilm formation has been tracked in real time with a camera placed in front of a window integrated in the chamber cover (cf. **Figure 40A**). A schematic representation of the biofilm development is presented in **Figure 41**.

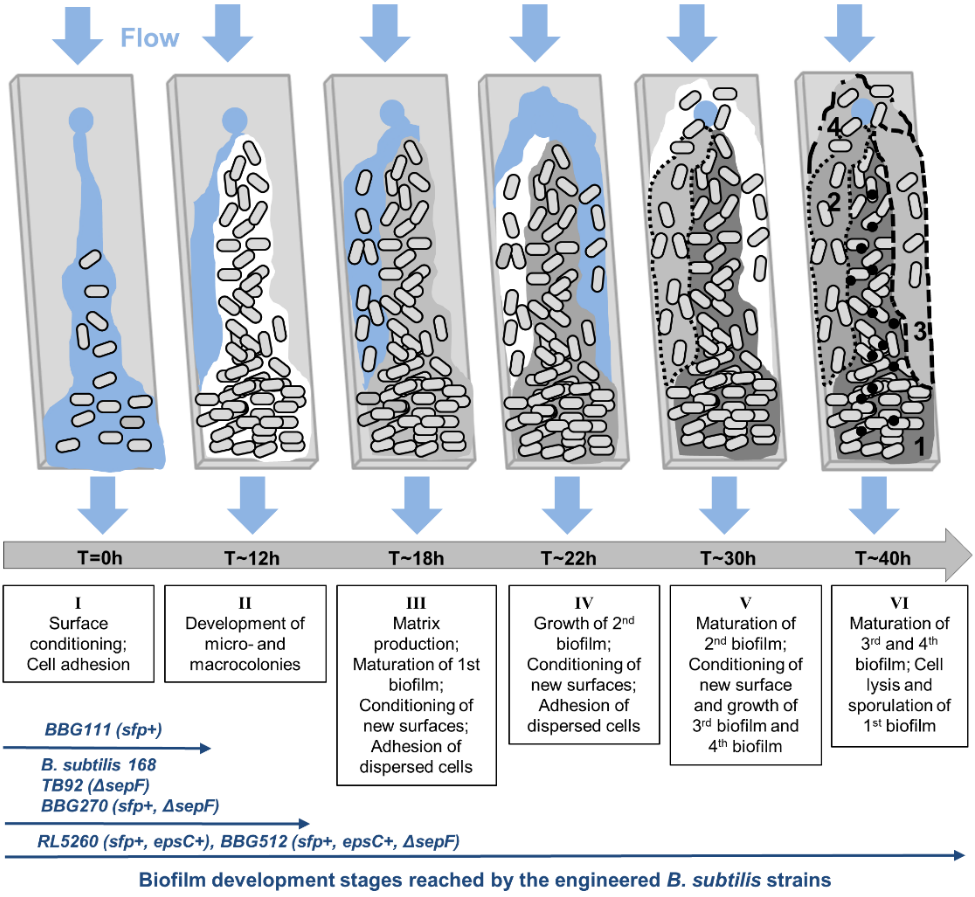
Flow
4
2
3
1
T=0h
T~12h
T~18h
T~22h
T~30h
T~40h
I Surface conditioning; Cell adhesion
II Development of micro- and macrocolonies
III Matrix production; Maturation of 1st biofilm; Conditioning of new surfaces; Adhesion of dispersed cells
IV Growth of 2nd biofilm; Conditioning of new surfaces; Adhesion of dispersed cells
V Maturation of 2nd biofilm; Conditioning of new surface and growth of 3rd biofilm and 4th biofilm
VI Maturation of 3rd and 4th biofilm; Cell lysis and sporulation of 1st biofilm
BBG111 (sfp+)
B. subtilis 168
TB92 (ΔsepF)
BBG270 (sfp+, ΔsepF)
RL5260 (sfp+, epsC+), BBG512 (sfp+, epsC+, ΔsepF)
Biofilm development stages reached by the engineered B. subtilis strains

Figure 41. Scheme displaying cell colonization and biofilm development over time on the silicone coupons in the DFR. The arrows in dark blue indicate which biofilm development stage was reached by the different engineered *B. subtilis* strains. A video showing the biofilm

growth dynamics of RL5260 can be found online (https://pod.univ-lille.fr/video/9995-biofilm-formation-dynamics-in-a-drip-flow-reactor/) with the password “DFR”.

Several biofilm development stages on the DFR coupon (I-VI) have been identified for the EPS$^+$ mutants. Biofilm formation displayed by mutants with no EPS production stopped during the second development phase since there is neither a structural complex biofilm development nor a maturation phase. Mutants with restored EPS production reached the last phase showing a structurally complex and mature biofilm covering the whole coupon. The biofilm formation took place according to the generally recognized biofilm developing steps: attachment – growth of micro- and macro-colonies – biofilm maturation – cell detachment and dispersion [120]. However, in the beginning, the surface conditioning and nutrient delivery was crucial for cell development. The cells only started to develop where the bulk medium was passing on the coupon. Since the medium had a quite low flow rate of ~13 mL h^{-1}, it entered only dropwise into the cultivation chamber and then flowed down randomly on the coupon surface. This means that not the complete coupon surface was continuously delivered by fresh medium. Consequently, the coupon became only partly colonized by a biofilm. The development of this first biofilm until its complete maturation required 18-20 h of incubation in the continuous mode preceding 6 h of batch phase. Due to the maturation, a hydrophobic protein layer covered the biofilm. This special feature of *B. subtilis* biofilms has already been mentioned previously in the upper part and demonstrated through the colored water droplet staying on the biofilm surface in **Figure 40B**, page 86. Since the hydrophobic surface became impervious to the bulk medium, the latter one bypassed to uncolonized surfaces on the coupon. This gave the starting point for a new biofilm development of dispersed cells until the whole coupon was colonized by multiple biofilms. Actually, the mature biofilm at the end of the cultivation (~ 40 h) was composed of several associated biofilms with different ages and maturations stages.

In EPS$^+$ mutants, a mature biofilm with complex wrinkled structures could be observed after 20 h of continuous nutrient supply in the DFR, a complete colonization of the DFR coupon was achieved after around 40 h, whereas EPS deficient mutants were neither able to develop an architecturally complex biofilm structure nor to colonize completely the DFR coupon. Besides, it has been demonstrated that EPS gave structural integrity to the biofilm and triggered its maturation through the formation of a hydrophobic protection layer. Although the biofilm matrix provides advantages in biofilm-based processes like increased adhesion capacities and protection from external forces such as shear forces or pH changes, there are also some drawbacks. The hydrophobic protection layer which is formed by *B. subtilis* at the final maturation stage through the secretion of the hydrophobin BslA represents an effective barrier that prevents the penetration of gas and liquids [135]. This may provoke undesirable nutrient limitations during fermentations in biofilm bioreactors with *B. subtilis*.

3.2.4 Enhanced biofilm formation leads to higher surfactin production

After characterizing the cell adhesion and colonization of the support, the resulting surfactin production has been analyzed using UPLC-MS as described in section 2.7, page 81. Hence, after 48 h of incubation, the surfactin concentration was measured in the biofilm as well as in the supernatant of the liquid passing the reactor chamber with a total volume of ~575 mL. The measured amounts of surfactin are presented in Table 6.

Table 6. Surfactin production and productivity of the engineered strains grown in continuous DFR biofilm cultures after 48h of cultivation with the corresponding standard deviation.

	BBG111 (sfp$^+$)	***BBG270 (sfp$^+$, ΔsepF)***	***RL5260 (sfp$^+$, epsC$^+$)***	***BBG512 (sfp$^+$, epsC$^+$, ΔsepF)***
Surfactin production in the liquid phase after 48h [mg/L]	7.42 ± 2.26	7.20 ± 2.56	70.64 ± 28.05	56.23 ± 22.80
Amount of surfactin present in the biofilm after 48h [mg]	0.02 ± 0.02	0.06 ± 0.04	0.66 ± 0.20	0.60 ± 0.38
Surfactin productivity per DFR chamber [mg/h]	0.09 ± 0.03	0.09 ± 0.03	0.85 ± 0.34	0.67 ± 0.27

Surfactin was mainly present in the liquid phase and only in small amounts in the biofilm. Apparently, the surfactin molecules released by the cells were effectively flushed out by the passing medium, only a low amount stayed trapped in the biofilm.

BBG111 (*sfp*$^+$) and BBG270 (*sfp*$^+$, *ΔsepF*) produced comparable amounts of surfactin, as well as RL5260 (*sfp*$^+$, *epsC*$^+$) and BBG512 (*sfp*$^+$, *epsC*$^+$, *ΔsepF*), suggesting that the deletion of *sepF* has no detrimental impact on surfactin production. Globally, the surfactin production in the EPS$^+$ strains was 8 to 10 times higher than in the EPS deficient strains as the number of adhered cells was also increased (10 to 50 times) compared to the EPS deficient strains.

4. *Conclusions*

In this work, genetic engineering strategies to improve support colonization in biofilm cultivations with *B. subtilis* 168 are presented. The support colonization capacity was three times increased in surfactin producing mutants through the induction of cell filamentation. The presence of EPS improved up to 50 times the support colonization whereby cell filamentation had a minor impact. EPS were essential for the initial cell adhesion and for giving structural integrity to the cells in the biofilm. The *B. subtilis* mutants are potential candidates for the future use in biofilm bioreactors to achieve an enhanced support colonization for an increased lipopeptide productivity.

Acknowledgement

This research received funding from the European INTERREG Va SmartBioControl / BioProd project and the ALIBIOTECH program funding administered by the Hauts-de-France Region. Met steun van het europees fonds voor regionale ontwikkeling. Avec le soutien du fonds européen de développement régional.

HB is supported by an international PhD grant co-funded by the Université de Liège and the Hauts-de-France Region. The authors are grateful to Prof. Leendert Hamoen from the University of Amsterdam for donation of the B. subtilis TB92 strain and Prof. Richard Losick from Harvard University for donation of the B. subtilis RL5260 strain. Furthermore, we would like to thank Jean-François Willaert (Gembloux Agro-Bio Tech – Université de Liège) for his technical assistance for the purpose-made DFR covers used for the biofilm growth observation as well as Andrew Zicler (Gembloux Agro-Bio Tech – Université de Liège) for his help with some of the figures.

CHAPTER 4

Growth dynamics of bacterial populations in a two-compartment biofilm bioreactor designed for continuous surfactin biosynthesis

This chapter is related to the article H. L. Brück, F. Coutte, P. Dhulster, S. Gofflot, P. Jacques, and F. Delvigne, “Growth Dynamics of Bacterial Populations in a Two-Compartment Biofilm Bioreactor Designed for Continuous Surfactin Biosynthesis,” published in *Microorganisms*, vol. 8, no. 679, pp. 1–19, 2020.

Abstract:

Biofilm bioreactors are promising systems for continuous biosurfactant production since they provide process stability through cell immobilization and avoid foam formation. In this work, a two-compartment biofilm bioreactor was designed consisting of a stirred tank reactor and a trickle-bed reactor containing a structured metal packing for biofilm formation. A strong and poor biofilm forming *B. subtilis* 168 strain due to restored exopolysaccharides (EPS) production or not were cultivated in the system to study the growth behavior of the planktonic and biofilm population for the establishment of a growth model. A high dilution rate was used in order to promote biofilm formation on the packing and wash out unwanted planktonic cells. Biofilm development kinetics on the packing were assessed through a total organic carbon mass balance. The EPS^+ strain showed a significantly improved performance in terms of adhesion capacity and surfactin production. The mean surfactin productivity of the EPS^+ strain was about 37% higher during the continuous cultivation compared to the EPS^- strain. The substrate consumption together with the planktonic cell and biofilm development were properly predicted by the model ($\alpha = 0.05$). The results show the efficiency of the biofilm bioreactor for continuous surfactin production using an EPS producing strain.

Keywords: biofilm reactor; continuous bioprocessing; biosurfactants; *B. subtilis*; exopolysaccharides

1. *Introduction*

Most of the biotechnological processes are based on planktonic cells in suspension in the cultivation medium [141]. Bioreactor operations are often limited to batch and fed-batch processes, although continuous processing would be more cost-efficient due to reduced downtime for the reactor cleaning, preparation and cell growth [141]. Cell retention and a long-term cell viability represent the main challenges in a continuous reactor [141].

Natural cell immobilization through biofilm formation presents an interesting alternative technique to design new continuous bioprocesses. In nature, biofilms are the predominant lifestyle of bacteria. A biofilm is a multicellular community of one or several bacterial species that is protected through a self-produced polymer matrix. Thereby, biofilms possess an enhanced tolerance to toxic substrates or products compared to the cells in planktonic state and thus, remain viable under unfavorable conditions as well as are able to regenerate themselves [139, 140]. Due to the high biomass density in biofilms and their stability, biofilm reactors have a high potential for long-term fermentation processes [122, 138]. However, the biofilm community is highly heterogeneous due to cell differentiation as a result of adaption to nutrients and oxygen gradients inside the biofilm. This heterogeneity makes it challenging to control the growth of the biofilm in the bioreactor.

Many microorganisms are able to grow naturally on diverse surfaces [140, 141]. In the medical sector, harmful biofilms are a heavy burden since they provoke severe infections and have detrimental effects on human health [138]. In industrial installation, biofilms can be responsible for biofouling and contaminations and thus present high hygienic risks [186, 192]. Yet, many industrial applications exist that are taking advantage of biofilms by using them as workhorses. These beneficial biofilms are for example used in the waste-water treatment, bioremediation or the production of bioenergy [123, 136, 193].

Bacillus spp. are well known for their ability to produce different families of biosurfactant lipopeptides with high application potential such as surfactins, fengycins and iturins [24]. Previous works have shown that cell immobilization in biofilm bioreactors is particularly favorable for the production of the above-mentioned compounds and allows the design of bioprocesses avoiding excessive foam formation ([78, 80, 84, 93, 147]), although biofilm development is a highly dynamic process with instabilities depending on the environmental conditions, such as the release of cells back into the liquid phase upon biofilm disruption. Biofilm development is difficult to assess during the cultivation due to restricted access to the support where the biofilm is growing. It is thus important to develop new measurement and control strategies for monitoring biofilm development and for designing robust processes.

In environmental biotechnology, mathematical modelling of biofilms is used to plan, design, optimize and evaluate processes in wastewater treatment plants [194]. The implementation of biofilm models permits to calculate the development over time of microbial species and substrates [195] and to get insights into relevant parameters that control the performance of the biofilm process [196]. It is important to select only the most relevant parameter to describe the physiological state of the organism and the behavior of the system to reduce the complexity of the model [197]. These models are developed through the set-up of mass balance equations for the relevant components involved in the bioprocess and the description of the corresponding kinetics expressions [197]. The components can generally be divided into two categories: the microorganisms and the consumed or produced materials of the microorganisms [196]. However, the mathematical modeling of biofilm reactors is not always straight forward due to the complexity of biological reactions involved in substrate conversion and the lack of accurate kinetic parameters for the biofilm development [198]. The approach of inverse modeling has been shown to be an attractive method for the numerical evaluation of kinetic parameters in biofilm processes. Through the validation of the biofilm model with the measured data, the parameters are determined in the way that the observed process behavior is approximately represented through the model [198].

In this work, a lab-scale two-compartment microbial system composed of a trickle-bed biofilm bioreactor and a stirred tank reactor was designed for the production of surfactin. Through a continuous operation mode, a strong selective pressure was induced on the cell populations. In the actual bioreactor design, biofilm development is promoted to achieve a high cell density on the packing element to increase the production yield. The planktonic cells, in contrast, are not favored and eliminated through a high dilution rate in order to simplify the downstream process of the secreted product. Experimental data are collected with a strong- and poor-biofilm-forming strain derived from *B. subtilis* 168 for establishing a growth model in order to get a deeper insight into the populations' behavior. The model is especially useful for predicting the kinetics of the biofilm development on the packing elements, a parameter difficult to assess during cultivation. Moreover, additional information on the system behavior can be obtained through the processing of the model. This provides important information for further process improvement through strain engineering.

2. Materials and methods

2.1 Strains

The two *B. subtilis* strains used in this study and their corresponding genotype are listed in **Table 7**. Both strains were derived from the laboratory strain *B. subtilis* 168 (*trpC2*, sfp^0, $epsC^0$).

Table 7. Strains used in this study.

B. subtilis **strains**	**Genotype**	**Source**
BBG111	*trpC2, sfp*$^+$*, epsC*^{0}*; Cm*^{R}	[22]
RL5260	*trpC2, sfp*$^+$*, epsC*$^+$*; Erm*^{R}	[23]

2.2 Biofilm growth visualization on drip-flow reactor coupons

The two *B. subtilis* strains were cultivated in a drip-flow reactor device during 48 h on silicone coupons, exactly as described in [199] or see chapter 3, section 2.3, page 80. The biofilm is developing on the surface of the coupons which permits to observe easily different biofilm phenotypes. The biofilm images were taken with a Samsung Dual Pixel 12 MP camera at the end of cultivation.

2.3 Design of the lab-scale trickle-bed biofilm reactor and culture conditions

A lab-scale (2 L) trickle-bed biofilm bioreactor has been designed on the basis of previous works carried out on a 20 L bioreactor containing a structured stainless steel packing element ([92, 147]). The experimental set-up of the designed reactor is presented in **Figure 42**.

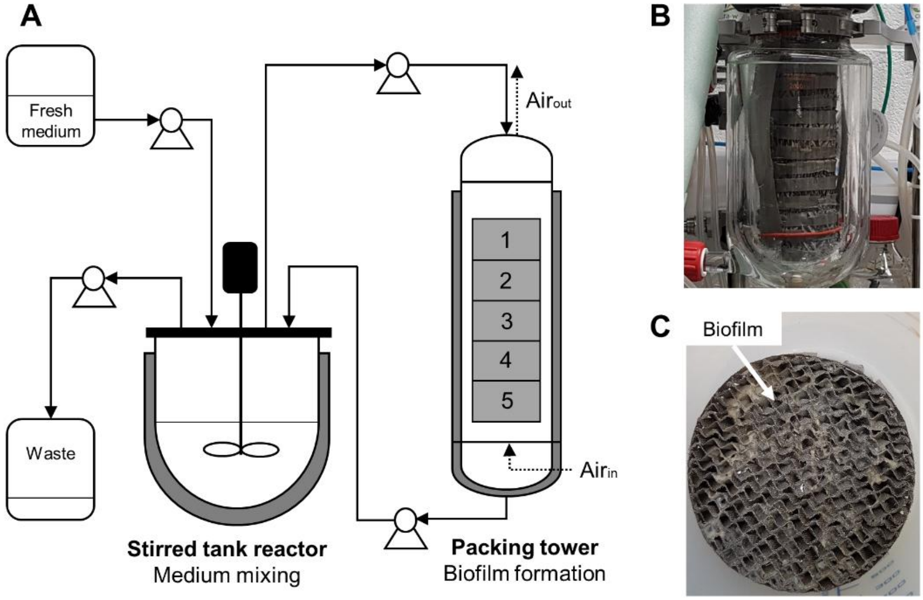

Figure 42. (A) Experimental set-up of the lab-scale trickle-bed biofilm reactor. (B) Packing tower (side view). (C) Top view image of one stainless steel structured packing element colonized by a biofilm.

For the lab-scale trickle-bed biofilm bioreactor, the system was separated into two main reactors: one for medium mixing and another that contained a tower of five structured metal packing elements for biofilm formation. The packing elements are composed of assembled corrugated gauze stainless steel sheets, a hydrophilic material with good wettability capacities (Laboratory packings, 83 × 55 mm, Sulzer Chemtech, Winterthur, Switzerland). Moreover, the metal structured packing provides an increased gas/liquid mass transfer.

The medium was recirculated continuously between these two devices with a flow rate of 85 mL min^{-1}. The medium was mixed at 300 rpm in the reactor. The mixing reactor was a conventional 2 L bioreactor (BIOSTAT B Plus, Sartorius Stedim, Schaerbeek, Belgium), whereas the reactor containing the packing elements was composed of a previous 2 L chemical reactor with a double jacket for temperature regulation (Reactor-Ready, Radleys, Shire Hill, Saffron Walden (Essex), UK). Since this type of reactor does not possess a condenser which is crucial to avoid filter clogging and pressure problems due to medium evaporation, the gas outlet was refrigerated by an additional cooling system to reduce evaporation in the packing reactor. The temperature of both reactors was regulated to 37°C. For security, the gas outlet was connected to a reservoir bottle with filters in case of too strong evaporation to collect the condensate. During the cultivation, there is no aeration in the mixing reactor. Air (1 L min^{-1}) is injected only on the downside of the packing reactor to prevent foam formation. The medium is injected on the upper side of the packing reactor and then flows down by gravity on the packing elements. Oxygen mass transfer is promoted through the counter-current flow of the injected air and the liquid. For the continuous process mode, an entry to and exit from the mixing reactor was added. Samples were taken from the mixing reactor by means of a sterile syringe.

For the reactor inoculation, a series of pre-cultures was prepared. First, 2 mL of lysogeny broth (LB) medium (10 g L^{-1} tryptone, 5 g L^{-1} yeast extract, 10 g L^{-1} NaCl) was inoculated with a colony. The first pre-culture was incubated for about 6 h at 37°C and 160 rpm. Then, a second pre-culture was prepared by a 10 times dilution of pre-culture I in LB medium. The second pre-culture was incubated overnight at 37°C and 160 rpm and then 10 times diluted with Landy MOPS medium (20 g L^{-1} glucose, 5 g L^{-1} glutamic acid, 1 g L^{-1} yeast extract, 0.5 g L^{-1} MgSO4, 1 g L^{-1} K2HPO4, 0.5 g L^{-1} KCl, 1.6 mg L^{-1} CuSO4, 1.2 mg L^{-1} MnSO4, 0.4 mg L^{-1} FeSO4, 21 g L^{-1} MOPS, 1.6 mg L^{-1} tryptophan) to prepare the main pre-culture. The main pre-culture was grown to an $OD_{600\ nm}$ between 2 and 3 and then used to inoculate the reactor (1 L working volume) with an $OD_{600\ nm}$ of 0.2 (corresponds to ~0.08 g L^{-1} cell dry weight). Before inoculation, the cells were washed once in a 0.9% NaCl solution to synchronize the cells and eliminate the produced primary and secondary metabolites. For this purpose, the cell culture was centrifuged (10 min at 2700× g) and the supernatant was discarded. The remaining cell pellet was resuspended in a 0.9% NaCl solution and then used to inoculate the reactor. The reactor contained Landy medium without MOPS buffer. The reactor pH regulation was executed using 1 M H_3PO_4 as acid and 3 M NaOH as base. The pH in the reactor was set at 7.0. To the reactor medium 50 µL L^{-1} of a silicone-free organic antifoaming agent (TEGO® Antifoam KS911, Evonik, Essen, Germany) was added. The culture was started with a batch fermentation during 16 h to increase the cell number in the reactor and to promote cell adhesion and biofilm development on the support. Then, the continuous phase was launched during ~28 h with a dilution rate of D = 0.5 h^{-1} which corresponds to a feeding rate of 500 mL h^{-1}. Two replicates of the biofilm cultivation experiments were performed per strain.

2.4 Determination of the mean residence time in the packing tower

For the mean residence time determination in the packing tower, tracer particles (1 µm) were injected on the top of the packing tower with a flow rate of 85 mL min^{-1} and collected at the packing tower exit at time intervals of 5 s. The collected particles were counted by flow cytometry (BF AccuriTM C6, BD Biosciences, Erembodegem-Dorp, Belgium). The mean residence time was then calculated with the measured tracer concentration over the time by equation (1):

$$\bar{t} = \frac{\int_0^\infty t*c(t)dt}{\int_0^\infty c(t)dt} \quad (1)$$

where c represents the measured tracer concentration at time point t.

2.5 Biomass dry weight determination

The cell culture samples were centrifuged (10 min at 2400× g) and the supernatant was collected to determine the surfactin concentration as described in section 2.7, page 103. The remaining cell pellets were washed by resuspending them in distilled water followed by centrifugation. After the centrifugation, the supernatant was discarded, and the remaining cell pellet was re-dissolved in water and filled into a pre weighted aluminum cup. The biomass sample in the aluminum cup has been dried in the oven at 105°C and weighted after 48 h to determine the corresponding cell dry weight.

After the cultivation, the packing elements were left for two hours in the reactor to let drain the residual liquid before they were weighted with the wet biofilm. It was not possible to dry the packing elements because the biomass is extremely difficult to remove once dried and this operation would spoil the packing elements for the next use. Therefore, a conversion factor from wet to dry biomass has been determined using cell cultures in flasks containing a small packing element of the same material. The flasks were incubated at 37°C with a low rotation rate (100 rpm) allowing the formation of a biofilm on the packing element. After 72 h, the packing element was weighted to get the wet biofilm weight and then dried in the oven at 105°C during 48 h to measure subsequently the dry biofilm weight. The cultures were performed in triplicates. A biofilm dry weight percentage of 7.9 ± 0.6 % for

RL5260 and 7.5 ± 0.7 % for BBG111 could be determined. The corresponding biofilm dry weight on the packing element was then calculated using the previously determined biofilm dry weight percentage.

2.6 Glucose Analysis

Glucose concentration was analyzed in the supernatant using high-performance liquid chromatography (HPLC) based on ion-moderated partitioning. A Waters Acquity UPLC® H-Class System (Waters, Zellik, Belgium) with an Aminex HPX-87H column 7.8 × 300 mm (Bio-Rad Laboratories N.V., Temse, Belgium) heated up to 50°C was used for analysis. A metabolite analysis was carried out with an isocratic flow rate of 0.6 mL min^{-1} for 25 min. The mobile phase was composed of water containing 5 mM H_2SO_4. Elution profiles were monitored through a Waters Acquity® Refractive Index Detector (RID) (Waters, Zellik, Belgium). A glucose standard solution (Sigma-Aldrich, Overijse, Belgium) was used to determine the retention time and to establish a calibration curve.

2.7 Surfactin analysis

The supernatants from the centrifuged cell culture samples were filtered (0.2 µm) and the surfactin concentration was determined by reversed-phase HPLC (Agilent 1100 Series HPLC Value System, Agilent Technologies, Diegem, Belgium) with an Eclipse XDB C−18 column (3.5 µm, 2.1 × 150 mm) (Agilent Technologies, Diegem, Belgium). The HPLC analysis method was based on an isocratic elution profile with a mobile phase composition of 80% acetonitrile and 20% water containing 0.1% trifluoroacetic acid (TFA). The flow rate was set at 0.4 mL min^{-1} with an analysis time of 22 min per sample. The surfactin molecules were detected by UV at 214 nm. Purified surfactin samples (> 98%) (Lipofabrik, Villeneuve d'Ascq, France) were injected to identify the retention time of the surfactin molecules and to determine a calibration curve.

2.8 Total organic carbon analysis and establishment of the mass balance

Total organic carbon (TOC) measurements of the culture medium were performed in order to estimate the TOC consumption of the cells. The planktonic cells were separated from the bulk medium by centrifugation. Subsequently, the TOC content of the culture medium was measured using a Lotix Combustion TOC Analyzer (TELEDYNE TEKMAR, Mason, Ohio, United States). The diluted culture medium samples were injected into the combustion tube where the samples were completely oxidized to CO_2 through catalytic combustion at 720°C. Subsequently, the produced CO_2 was detected by flow-through non-dispersive infrared spectroscopy. The instrument was calibrated with a standard solution of potassium hydrogen phthalate for a calibration range of 0 to 20 ppm.

A TOC mass balance for the batch and continuous cultivation phase has been established to estimate the TOC consumed by the cells present in the system. The TOC consumption in the batch phase was determined by equation (2):

$$TOC_{consumed,\ t1}=TOC_{medium,\ t0}-TOC_{medium,\ t1} \qquad (2)$$

and for the continuous phase, with equation (3):

$$TOC_{consumed,t1}=(TOC_{in\ medium,\ t0}-TOC_{medium,\ t1})*D*\Delta t \qquad (3)$$

where TOC represents the amount of total organic carbon in g at a certain time point t in h, D is the dilution rate in h^{-1} and Δt the difference between time point t_0 and t_1 in h. For the mass balance of the continuous phase, it was assumed that the TOC consumption rate remains constant during the measured time interval.

2.9 Biofilm reactor compartment model

The trickle-bed bioreactor system can be simplified into two main compartments representing the main places of residence in the system for sessile and planktonic cells. The first compartment comprises the sessile cells which form a biofilm on the packing tower where cells have unlimited access to dissolved oxygen. In the second compartment, the planktonic cells are growing under limited dissolved oxygen conditions. The overall growth conditions for the cells are better in the packing tower since there is more dissolved oxygen available as well as enough nutrients since the medium is continuously recirculated. In the present system, the contact between the injected gas and the adhered bacteria on the packing elements is strongly enhanced which favors additionally an interfacial oxygen transfer through a direct bacteria-air contact contributing to an increased total oxygen transfer [200].

The objective of this process is to increase the adhered biomass on the packing tower and reduce or eliminate the presence of planktonic cells in the stirred tank reactor through a high dilution rate ($D > \mu$). Increased cell density on the packing elements means increased production yield. The elimination of planktonic cells would strongly facilitate the downstream process since the secreted product in the bulk medium could be easily recovered. This means that the aim for this system is not to reach a steady state as in a normal chemostat reactor ($\mu = D$), but a steady state with a planktonic cells number close to zero and a continuously and stable growing biofilm.

In this work, the development of the two populations (sessile and planktonic cells) was investigated in order to acquire more information about their behavior for further process optimization. By means of experimental data, a simple ordinary differential equations (ODEs) model was established on the basis of bacterial growth equations. A schematic description of the model is presented in **Figure 43**.

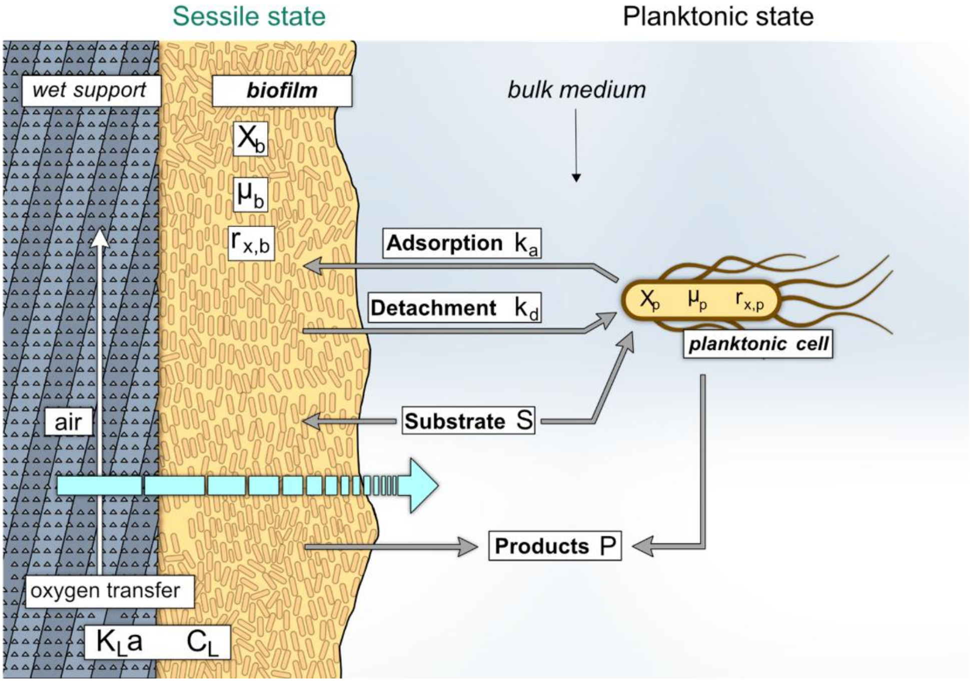
Sessile state
Planktonic state
wet support
biofilm
bulk medium
X_b
μ_b
$r_{x,b}$
Adsorption k_a
Detachment k_d
X_p μ_p $r_{x,p}$
planktonic cell
air
Substrate S
Products P
oxygen transfer
K_La C_L

Figure 43. Schematic description of the growth model developed for the two-compartment trickle-bed biofilm reactor. The transition of the cells between the two compartments from the sessile (1) and planktonic (2) state and vice versa takes place in the packing tower (see **Figure 42**, page 100, for a scheme of the cultivation set-up). The scheme shows an enlarged view of a support element inserted in the packing tower and describes the parameters that were used to build the growth model (see **Table 8**, page 106, for a detailed description).

2.10 Determination of the volumetric oxygen mass-transfer coefficient K_La in the stirred tank reactor by dynamic gassing-in/gassing-out method

The oxygen transfer rate from a gas to a liquid phase is given by equation (4):

$$OTR = K_L a\,(C_{sat} - C_L) \tag{4}$$

where K_La is the volumetric oxygen mass-transfer coefficient, C_{sat} the oxygen concentration at saturation in the liquid medium in equilibrium to the gas phase and C_L the dissolved oxygen concentration in the liquid medium [201]. In a stirred tank reactor where the liquid phase is well mixed, the accumulation of oxygen in the liquid phase can be described through equation (5):

$$\frac{dC_L}{dt} = OTR - OUR \tag{5}$$

where OTR is the oxygen transfer rate from the gas to the liquid and the OUR represents the oxygen uptake rate by the biomass [201]. Since the volumetric oxygen mass-transfer coefficient K_La has been measured in the absence of biomass, OUR = 0, equation (5) can be simplified to equation (6):

$$\frac{dC_L}{dt} = K_La\,(C_{sat} - C_L)\,. \tag{6}$$

And thus can be transformed into equation (7):

$$\ln\left(\frac{C_{sat} - C_{L2}}{C_{sat} - C_{L1}}\right) = K_La\,(t_2 - t_1)\,. \tag{7}$$

The dynamical absorption method [201] was applied in order to determine the K_La value. This method consists of the elimination of oxygen in the liquid phase to obtain an oxygen concentration close to zero through the injection of nitrogen. This permits to simplify further equation (7) with $t_1 = 0$ and $C_{L1} = 0\%$. Then, the liquid is again put into contact with air and the increase of the dissolved oxygen concentration is measured over the time. The K_La can then be deviated through the slope of the $\ln(\frac{C_{sat}-C_{L2}}{C_{sat}})$ vs. time plot. Measurements were performed in triplicates.

2.11 Mathematical development of a growth model to describe the microbial population dynamics

The following assumptions are made for the model construction: (i) no oxygen limitation in the biofilm compartment with the packing tower, (ii) the oxygen concentration in the planktonic cell compartment is limited, (iii) the dilution rate is affecting directly the planktonic cell compartment but not the biofilm compartment. The used model parameters are listed in **Table 8**.

Table 8. List of parameters used for the model construction.

Parameter	Description	Unit
μ_{max}	Maximum growth rate of cells	h^{-1}
C_L	Dissolved oxygen concentration	$g\ L^{-1}$
C_{sat}	Dissolved oxygen concentration at saturation	$g\ L^{-1}$
k_a	Switching rate liquid to biofilm (adsorption)	h^{-1}
k_d	Switching rate biofilm to liquid phase (detachment)	h^{-1}
K_La	Volumetric oxygen mass-transfer coefficient	h^{-1}
K_o	Oxygen affinity constant	$g\ L^{-1}$
K_s	Substrate affinity constant	$g\ L^{-1}$
$r_{x,b}$	Growth speed sessile cells	$g\ L^{-1}\ h^{-1}$
$r_{x,p}$	Growth speed planktonic cells	$g\ L^{-1}\ h^{-1}$
S	Substrate concentration in the reactor	$g\ L^{-1}$
S_{in}	Substrate concentration at the reactor entry	$g\ L^{-1}$
X_b	Biofilm biomass concentration	$g\ L^{-1}$
X_p	Planktonic biomass concentration	$g\ L^{-1}$
$Y_{X/O}$	Oxygen-biomass conversion coefficient	$g\ g^{-1}$
$Y_{X/S}$	Substrate-biomass conversion coefficient	$g\ g^{-1}$

2.11.1 Batch fermentation

The growth rate of bacteria can be described through the well-known Monod equation of growth represented by equation (8):

$$\mu = \frac{r_x}{X} = \frac{\mu_{max} S}{K_s + S}. \qquad (8)$$

The total biomass development in the trickle-bed biofilm reactor can be divided into the growth of sessile and planktonic cells. For the planktonic cells, two limiting factors have to be taken into account: the substrate and dissolved oxygen concentration. If oxygen is a limiting factor, the specific growth rate varies with the dissolved oxygen concentration according to the Monod equation like for any other substrate limitation. In our case, oxygen and substrate are complementary substrates and thus, the product rule is applied [202]. The growth speed for the planktonic cells is thus given through equation (9):

$$r_{x,p} = \mu_{max} \left(\frac{S}{K_s + S}\right) \left(\frac{C_L}{K_o + C_L}\right) X_p . \qquad (9)$$

However, for the simulations with the model, equation (9) was adapted as shown in equation (10) according to the approach used by Roels [203]:

$$r_{x,p} = \mu_{max} * \min \left[\frac{S}{K_s+S}, \frac{C_L}{K_o+C_L}\right] X_p . \qquad (10)$$

Hence, for the model the growth speed of the planktonic cells is assumed to be influenced by the more pronounced limiting factor which means the minimum value of the term representing either the substrate limitation or the limited dissolved oxygen availability.

The biomass development for the planktonic cells can be described by the differential equation (11):

$$\frac{dX_p}{dt} = r_{x,p} - k_a X_p + k_d X_b \qquad (11)$$

where k_a represents the switching rate from the planktonic state to the sessile state of the cells (adsorption) and k_d the releasing rate of the sessile cells to the planktonic state (detachment). Thus, the term $k_a X_p$ correspond to the number of planktonic cells that adhere to the support, whereas $k_d X_b$ describes the sessile cells detaching from the support.

The growth speed for the sessile cells can be described through equation (12) by taking into account the substrate limitation due to the randomly distributed medium on the packing elements:

$$r_{x,b} = \mu_{max} \left(\frac{S}{K_s + S}\right) X_b . \qquad (12)$$

In this case, dissolved oxygen limitations are not considered for the sessile cells in the model. It can be assumed that the aeration is very efficient in the packing tower and the biofilm thickness is sufficiently low to neglect oxygen gradients.

The development of the biofilm on the packing elements can be described by equation (13):

$$\frac{dX_b}{dt} = r_{x,b} + k_a X_p - k_d X_b \,. \tag{13}$$

The terms $k_a X_p$ and $k_d X_b$ represent the corresponding biomass that is adhering or detaching as described above.

The substrate consumption of the sessile and planktonic cells is given by equation (14):

$$\frac{dS}{dt} = - \frac{r_{x,b}}{Y_{X/S}} - \frac{r_{x,p}}{Y_{X/S}} \,. \tag{14}$$

The availability of dissolved oxygen can be described by equation (15):

$$\frac{dC_L}{dt} = k_L a\,(C_{sat} - C_L) - \frac{r_{x,b}}{Y_{X/O}} - \frac{r_{x,p}}{Y_{X/O}} \tag{15}$$

where the terms $\frac{r_{x,b}}{Y_{X/O}}$ and $\frac{r_{x,p}}{Y_{X/O}}$ represent the oxygen uptake rate of the biofilm and planktonic cells, respectively. For the model, it was assumed that the dissolved oxygen concentrations were equivalent for both compartments due to the continuous recirculation of the medium between the stirred tank reactor and the packing tower.

2.11.2 Continuous fermentation

For the continuous fermentation, the dilution rate affects only the planktonic phase. The supply and removal of dissolved oxygen through the alimentation and elimination is neglected. This means that equation (11) describing the development of the planktonic biomass is extended with the term in bold in equation (16):

$$\frac{dX_p}{dt} = r_{x,p} - k_a X_p + k_d X_b \mathbf{- DX_p} \,. \tag{16}$$

And equation (14) describing the substrate consumption is extended as shown by equation (17):

$$\frac{dS}{dt} = - \frac{r_{x,b}}{Y_{X/S}} - \frac{r_{x,p}}{Y_{X/S}} + \mathbf{D(S_{in} - S)} \,. \tag{17}$$

The ODEs were coded and solved with Python 3.7 via the Anaconda–Spyder interface using the odeint function (see Appendix IV, page 159 for the code).

3. Results

3.1 Design of a two-compartment biofilm reactor to promote the biofilm proliferation

In a previously designed trickle-bed biofilm reactor ([92, 147]), the co-existence of a planktonic and biofilm population was recurrently observed during the cultivation of *B. amyloliquefaciens* GA1 which hindered data interpretation and probably decreased the production yield. The actual set-up (**Figure 42**, page 100) is split into two compartments: (i) a stirred bioreactor containing exclusively planktonic cells and (ii) a packing column where the biofilm is attached and on which liquid medium recirculated from the stirred bioreactor is fed. Three constraints have been considered for promoting the proliferation of the biofilm population and to reduce the planktonic one, i.e., a short residence time in the packing column (only the most performant strains will attach) coupled with a high dilution rate through the two-compartment set-up (washing out of planktonic cells) and a strong oxygen limitation in the liquid phase (unfavorable growth conditions in the stirred tank reactor).

A mean residence time of ~37 s was determined in the packing tower with tracer particles. This is quite short compared to the residence time of ~10 min of the cells in the stirred tank reactor (corresponds to the recirculation time of one reactor volume). Since in the present case study, the objective was to promote the biofilm formation and decrease the number of planktonic cells, a dilution rate higher than the maximum growth rate of the cells (i.e. $D = 0.5\ h^{-1}$) was considered.

In order to avoid foam formation and to limit the growth of planktonic cells in the stirred tank reactor, air was only injected into the compartment containing the packing elements. The oxygen mass transfer to the bulk medium and the planktonic cells occurs only when the liquid phase flows down on the packing tower during recirculation. Whereas the oxygen availability in the stirred tank reactor is strongly limited, the adhered biomass on the structured metal packing benefits from a good gas/liquid mass transfer.

The volumetric oxygen mass-transfer coefficient K_La of the system was determined using a dissolved oxygen probe placed in the stirred tank reactor. The oxygen uptake of the medium occurs only in the packing tower where the air is injected. The structured metal packing elements exhibit a high specific surface area (~500 m^2m^{-3} [92, 145]) and were designed for improving contact between air and liquid phases. The K_La measurement was performed without the presence of cells via the dynamical absorption method as described in the material and methods section 2.10, page 105. The K_La reached a value of $3.0 \pm 0.1\ h^{-1}$.

3.2 The EPS⁺ strain exhibited enhanced performance in the biofilm reactor

Biofilm cultivations with a strong (RL5260) and poor (BBG111) biofilm producing *B. subtilis* 168 strain were performed in the previously described trickle-bed biofilm reactor (cf. materials and methods section 2.3, page 100). RL5260 is able to produce exopolysaccharides (EPS), a crucial element for the biofilm matrix formation, whereas BBG111 is deficient in EPS production and thus cell aggregates are formed only in thin layers. **Figure 44** demonstrates clearly the different biofilm phenotypes of RL5260 and BBG111 when they were cultivated on silicone coupons in a drip-flow reactor, as described in a previous work ([199] or see chapter 3, section 2.3, page 80).

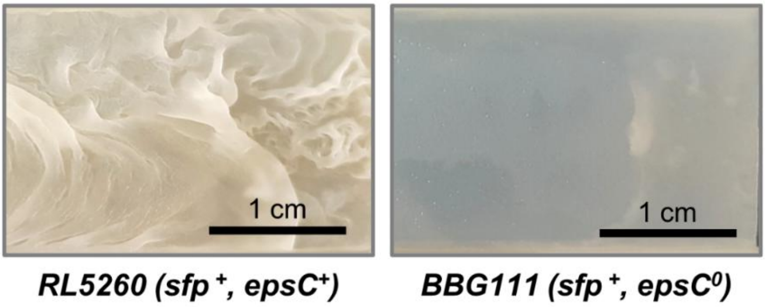

Figure 44. Demonstration of the biofilm development of a strain producing exopolysaccharides (RL5260, left side) or not (BBG111, right side). The images show sections of colonized silicone coupons incubated under identical growth conditions in a drip-flow reactor for 48 h.

3.2.1 Planktonic cell growth and biofilm development

The growth of the planktonic cells in the trickle-bed biofilm reactor was followed overtime and the weight of the attached biomass on the reactor support has been measured at the end of the cultivation. The results are presented in **Figure 45A** and **B**.

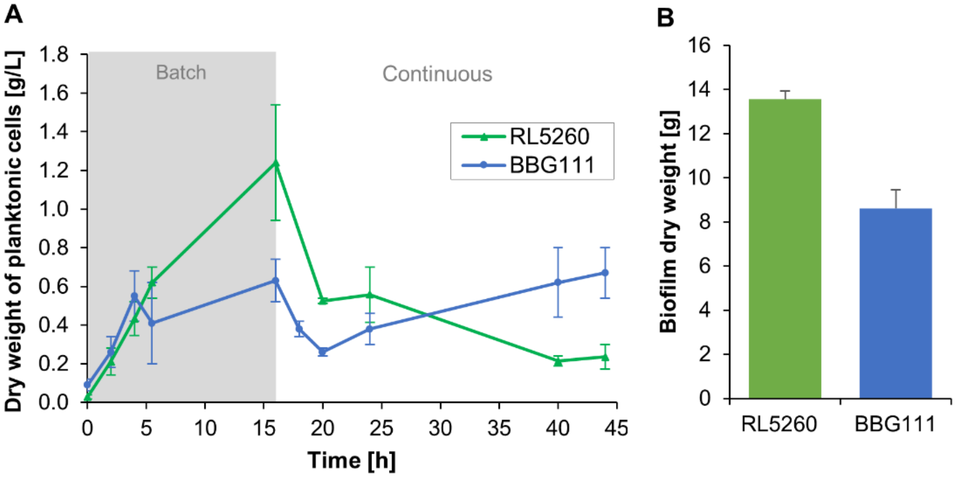

Figure 45. A) Growth curves of planktonic cells and (B) amount of adhered dry biomass on the packing tower at the end of the continuous culture measured for each strain in the trickle-bed biofilm reactor. The standard deviation is indicated by error bars.

During the batch culture (0–16 h), both strains started growing rapidly in the liquid medium which is continuously recirculated between the stirred tank reactor and the packing tower. BBG111 and RL5260 reached a similar maximum specific growth rate of 0.39 ± 0.07 h^{-1} and 0.38 ± 0.04 h^{-1}, respectively. After 4 h, the growth of BBG111 remained stagnant and then restarted to increase slightly. After starting the continuous culture, the number of cells in the liquid medium dropped strongly (16–20 h) due to the washing out of cells since the dilution rate (0.5 h^{-1}) has been chosen higher than the specific growth rate of the cells in order to eliminate non-adherent cells. During the continuous cultivation phase, the number of planktonic cells decreased for RL5260, whereas for BBG111, the number of planktonic cells increased with the time. Increased standard deviations are probably due to not completely synchronized cultures between the performed repetitions. For the whole cultivation, BBG111 produced 7.8 ± 1.5 g of planktonic cells (dry weight) and RL5260 6.6 ± 1.1 g. BBG111 and RL5260 reached respectively a total amount of 8.6 ± 0.8 and 13.5 ± 0.4 g attached dry biofilm on the packing tower. Hence, RL5260 produced about 1.6 times more adhered biomass than BBG111. This resulted in a biomass ratio of biofilm vs. planktonic cells of 1.2 ± 0.3 for BBG111 and 2.1 ± 0.4 for RL5260. The biomass ratio of RL5260 was 1.8 higher compared to BBG111.

3.2.2 Both strains displayed similar glucose consumption profiles

Figure 46 describes the glucose consumption of the strains during the cultivation process. Interestingly, the consumption rates of BBG111 and RL5260 were similar.

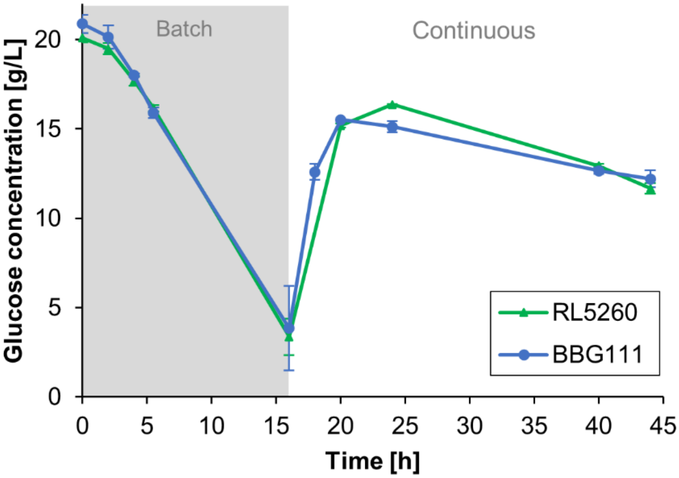

Figure 46. Glucose concentrations present in the bulk medium for the two *B. subtilis* 168 strains during the cultivation. The standard deviation of the measurements is indicated by error bars.

For the present system, the substrate-to-biomass conversion yield was 0.16 ± 0.02 g g^{-1} for BBG111 and 0.20 ± 0.01 g g^{-1} for RL5260 calculated for the total biomass produced (planktonic cells and biofilm) per total amount of consumed glucose. For comparison, a substrate-to-biomass conversion yield $Y_{X/S}$ of 0.22 ± 0.02 g g^{-1} for

BBG111 and 0.26 ± 0.03 g g^{-1} for RL5260 was determined from shake flasks experiments during the exponential growth phase by measuring the glucose consumption and the corresponding cell dry weight.

3.2.3 Increased biofilm development enhanced the surfactin productivity

The mean surfactin productivities determined for both stains are summarized in **Table 9**. The mean surfactin productivity was comparable for both strains during the initial batch cultivation step. Yet, the mean surfactin productivity of the strong biofilm former RL5260 was about 37% higher during the continuous phase compared to the mean productivity of BBG111.

Table 9. Surfactin productivity of the two *B. subtilis* 168 strains measured in the bulk medium during batch and continuous cultivation.

Cultivation phase		***BBG111* (*sfp*$^+$, *epsC*^{0})**	***RL5260* (*sfp*$^+$, *epsC*$^+$)**
Batch	Mean surfactin productivity (mg L^{-1} h^{-1})	107.4 ± 5.6	130.4 ± 25.3
Continuous	Mean surfactin productivity (mg L^{-1} h^{-1})	168.1 ± 22.0	231.0 ± 14.2

3.2.4 Carbon utilization pointed out a totally different biofilm formation rate between the two *B. subtilis* strains

The overall glucose consumption in the system did not show any difference between the two *B. subtilis* strains although the biofilm development and surfactin production was significantly increased for RL5260. In order to examine the carbon consumption by the cells, a TOC mass balance was performed for elucidating the behavior of the different strains. **Figure 47** shows the results of the TOC analysis for both strains.

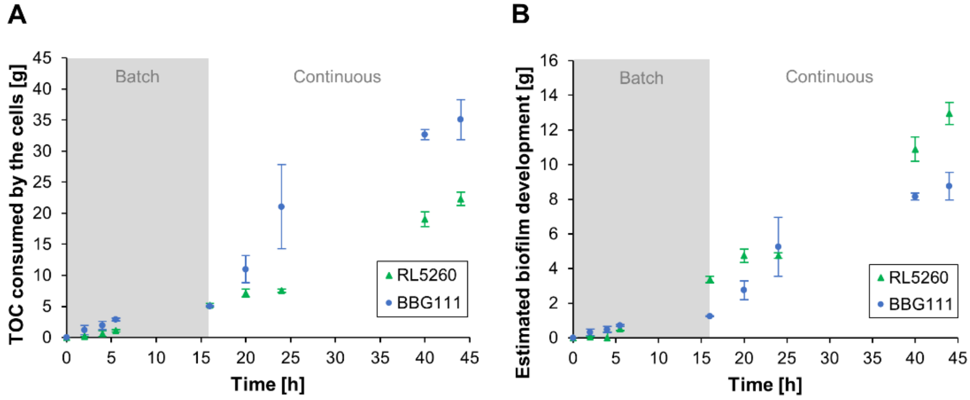

Figure 47. (A) Cumulative total organic carbon (TOC) consumption by the cells during the cultivation of the two *B. subtilis* 168 strains. (B) Cumulative biofilm development on the

packing elements estimated via the TOC mass balance and obtained biomass-TOC conversion yields. Error bars indicate the standard deviation of the measurements.

The estimated TOC consumption of the cells was similar for both stains during the batch cultivation phase. Surprisingly, BBG111 showed a significant increased TOC consumption during the continuous cultivation compared to RL5260, although BBG111 produced a significant lesser amount of adhered biomass than RL5260. During the continuous cultivation phase, the TOC consumption can be mainly attributed to the biofilm. The TOC consumption of the planktonic cells can be neglected since they are largely washed out due to the high dilution rate or mainly derived from the biofilm as a consequence of detachment. Thus, the results demonstrate different metabolic behaviors between RL5260 and BBG111 during biofilm formation.

As a result, the yield of the produced biofilm per consumed TOC ($Y_{biofilm/TOC}$) was found to be more than two times higher for RL5260 (0.61 ± 0.05 $g\ g^{-1}$) than for BBG111 (0.25 ± 0.05 $g\ g^{-1}$). Based on these conversion yields, we were able to plot a biofilm development curve during the cultivation, as presented in **Figure 6B**. At the end of the batch phase (at 16 h), RL5260 developed a significantly higher amount of adhered biomass. After the start of the continuous phase, the biofilm development of RL5260 seemed to be reduced and even to be stagnant around 20 h according to the TOC measurements. Probably, RL5260 took some time to adapt to the high dilution rate. After the adaptation, the growth of RL5260 restarted strongly until the end of the cultivation. BBG111 appeared to develop an increased adhered biomass upon starting the continuous phase but then the growth slowed down, probably as a result of cell detachment due to limited adhesion capacities. In order to verify the estimated biofilm development via the TOC measurements, a bacterial growth model was developed to predict the biofilm development kinetics in the two-compartment system as presented in the following section.

3.3 Modeling of microbial population dynamics

Two subpopulations of cells are co-existing in the biofilm bioreactor, i.e., the planktonic cells mainly present in the stirred tank reactor and the sessile cells adhered to the packing tower. The growth dynamics of the planktonic cells could be measured during the cultivation experiment. However, it was challenging to get more information about the growth dynamic of the biofilm on the packing tower. An established TOC mass balance (see section 3.2.4, page 112) led to more information about the biofilm development on the packing elements for both strains. However, the reliability of the biomass-TOC conversion yield was not certainly approved. Hence, we developed a microbial growth model based on ODEs for predicting the growth behavior of the biofilm in the system to get a deeper insight into the populations' behavior. The model was fed with some parameters measured in this work and with appropriate parameters described in literature that are listed in **Table**

10. The outcome of the model was then compared to the measured values for verification and validation.

The substrate affinity constant K_s was set to 0.015 g L^{-1} as used by Guez et al. [72] in a previous work in our laboratory for modelling fed-batch cultures of *B. subtilis* in Landy medium. For the dissolved oxygen saturation concentration, C_{sat} = 6.73 mg L^{-1} was used. The value corresponds to the oxygen concentration at saturation in water at 37°C and has been extracted from the online data base DOTABLES[3]. For the oxygen-biomass conversion coefficient $Y_{X/O}$, a value of 1 g g^{-1} was given as used by Lin et al. [204] and Xu et al. [205]. The oxygen affinity constant K_o was set to 0.005 g L^{-1}, a slightly higher value of the affinity constants found by Guisasola et al. [206]. Through the introduction of a higher K_O value, the oxygen affinity of the planktonic cells is reduced which comes along with the exposure to very low oxygen concentrations in the non-aerated stirred tank reactor and the possible switch to anaerobic growth [207, 208].

For the oxygen mass transfer, an estimated correction factor for the determined K_La value was introduced given that the oxygen mass transfer was only determined with the medium in the absence of biomass. The presence of microorganism affects significantly the oxygen mass transfer rate as a result of cell respiration [209]. The phenomenon that the oxygen uptake rate (OUR) increases with the cell concentration coupled to an increase in K_La is called biologically enhanced oxygen transfer [210] and can be characterized by an enhancement factor E [201]. In the literature, enhancement factors up to 5 are described in the presence of high cell concentrations [210]. In the present system, an additional high interfacial oxygen transfer occurs through the direct contact of adhered cells with the injected air resulting in an increased total oxygen transfer [200]. Surfactin production in *B. subtilis* depends strongly on the oxygenation. For an appropriate surfactin production a K_La value over 10.8 h^{-1} is necessary, as shown by Fahim et al. [77]. Comparable surfactin production rates to this work were achieved by Yeh et al. [76] in a foaming bioreactor with solid carriers with a K_La value of 30.96 h^{-1} using *B. subtilis* ATC 21332 and Coutte et al. [84] in a bubbleless membrane bioreactor with a K_La value of 40 h^{-1} by using a *B. subtilis* 168 derivative strain. K_La values between 10 h^{-1} and 40 h^{-1} were tested on the model, the most appropriate values were between 35 h^{-1} and 40 h^{-1} resulting in enhancement factors of around 12 to 13.

Table 10. General model parameters and their corresponding values used for *B. subtilis* BBG111 (*sfp*$^+$, *epsC*^{0}) and RL5260 (*sfp*$^+$, *epsC*$^+$).

Parameter	Description	Unit	BBG111	RL5260
μ_{max}	Max. growth rate of cells	h^{-1}	0.39	0.38
C_{sat}	Dissolved oxygen concentration at saturation	g L^{-1}	0.00673	0.00673
K_La	Volumetric oxygen mass-transfer with enhancement factor	h^{-1}	35	40

---

[3] https://water.usgs.gov/software/DOTABLES/

K_o	Oxygen affinity constant	$g\ L^{-1}$	0.005	0.005
K_s	Substrate affinity constant	$g\ L^{-1}$	0.015	0.015
S_{in}	Substrate concentration at the reactor entry	$g\ L^{-1}$	20.00	20.00
$Y_{X/O}$	Oxygen-biomass conversion coefficient	$g\ g^{-1}$	1.00	1.00
$Y_{X/S}$	Substrate-biomass conversion coefficient	$g\ g^{-1}$	0.16	0.20

Two hypotheses were verified with the established model:

(i) The significant difference in biofilm development of RL5260 and BBG111 was due to unequal adhesion capacities as a result of the presence or not of EPS.

(ii) The high dilution rate during the continuous fermentation exerted a strong washing out of the planktonic cells. No additional cell adhesion occurred on the packing elements, only cell detachment took place.

For testing the first hypothesis, the different adhesion capacities of BBG111 and RL5260 were modelized through different k_a and k_d values and thus, a different k_a/k_d ratio during the batch cultivation phase. Though, the values were orientated on the previously mentioned biofilm vs. planktonic cells ratio for both strains (section 3.2.1, page 110). For the second hypothesis ka was set to zero in the model for the continuous cultivation phase. **Table 11** summarizes the introduced parameters. The model results and the corresponding experimental results are presented in **Figure 48A** for BBG111 and in **Figure 48B** for RL5260.

Table 11. Parameters related to cell adhesion and detachment that were introduced into the model.

Parameter	Description	Unit	BBG111	RL5260
k_a	Switching rate to biofilm (adsorption) (batch/continuous)	h^{-1}	(1.2/0)	(2.1/0)
k_d	Releasing rate to planktonic state (detachment) (batch/continuous)	h^{-1}	(1/0.345)	(1/0.332)
k_a/k_d	Ratio switching / releasing rate (batch/continuous)	-	(1.2/-)	(2.1/-)

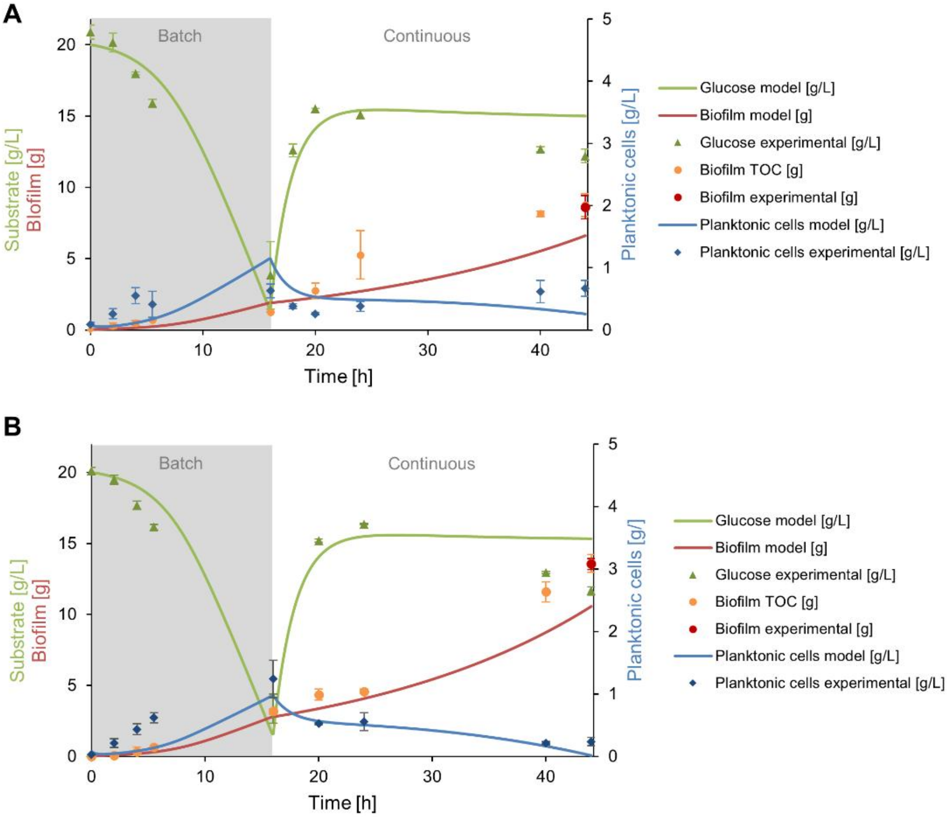

Figure 48. Glucose consumption, planktonic cells and biofilm development predicted by the model for the two-compartment system for BBG111 (A) and RL5260 (B). The model results are drawn with a continuous line and the experimental results are added as point references for comparison.

The simulations show that the established growth model is able to describe the development of the biofilm and planktonic population in the two-compartment reactor. For the biofilm development of BBG111 (**Figure 48A**), the model represented well the experimental values at the beginning of the batch phase and during the continuous phase. The values at the end of the continuous phase were slightly underestimated. The model predicted less accurate the development of the planktonic cells when compared to the experimental values. The glucose consumption was quite correctly predicted during the batch cultivation and for the continuous cultivation until 24 h. After that time point, the prediction and experimental values are diverging which resulted in a light underestimation of the consumed glucose.

For RL5260 (**Figure 48B**), the model predicted quite correctly the development of the planktonic cells during the continuous cultivation and underestimated slightly the number of planktonic cells during the batch cultivation regarding the experimental values. The biofilm development seemed to fit with the measured biofilm development via the TOC analysis. However, the final biofilm dry weight value measured on the packing elements was slightly underestimated. The glucose consumption was correctly predicted compared to the experimental values, except for the time points t = 40 h and 44 h where the model predicted slightly higher values than measured in the system.

The overall model predictions were close to the experimental values. A Chi-square goodness of fit test confirmed that there were no significant differences between the observed and predicted values for both strains with a significance level of $\alpha = 0.05$. All calculated p-values were extremely high, which resulted in the acceptance of the null hypothesis that no significant differences exist between the observed and predicted values (for the test results see Appendix V, pages 164/165, **Table 21** for BBG111 and **Table 22** for RL5260)

4. Discussion

The objective of this work was to develop a model able to describe the growth dynamics of the biofilm and planktonic population present in the designed trickle-bed biofilm reactor in order to understand better the behavior of the system for further process intensification. In particular, biofilm development on the packing elements gives important information about the process, but is difficult to monitor during cultivation. The growth model was used in order to confirm the two hypotheses that the significant difference in biofilm development of BBG111 and RL5260 is linked to the production or not of EPS, and that the high dilution rate washes out the non-adherent or detaching cells in the designed system.

The experimental data are in good accordance with those obtained with the developed growth model by using a combination of the first hypothesis (different k_a/k_d ratio during batch cultivation) and the second one ($k_a = 0$) during continuous cultivation) for both strains. This was confirmed by a Chi-square goodness to fit test with a confidence level of $\alpha = 0.05$. The two hypotheses made initially for the present system have thus been validated. The model also confirmed the biofilm development dynamics determined via experimental TOC measurements and the established TOC mass balance.

The increased k_a/k_d ratio for RL5260 during the batch cultivation was linked to the capacity of EPS secretion which has shown to improve the colonization capacity and reduce cell detachment. The presence of EPS permitted RL5260 to build up a functional biofilm structure and to protect the adhered cells from external influences. Once adhered, the cells produced EPS and proliferated on the packing elements to construct their own environment. Several works on *B. subtilis* biofilm formation have shown that EPS production facilitates cell spreading and promotes the colonization of a solid support ([129, 130, 199]). Since BBG111 is a poor biofilm former and does not produce EPS, the biofilm formation capacities were reduced (lower k_a/k_d ratio) and cell detachment occurred more frequently after the cell adhesion step than in the case of RL5260. Moreover, the additional high dilution rate carried out a strong selective pressure on the planktonic cells and limited the re-adherence during the continuous cultivation due to the washing out of the planktonic cells ($k_a = 0$).

Globally, BBG111 and RL2560 produced comparable amounts of planktonic cells. RL5260 produced more planktonic cells during the batch phase. However, when the continuous cultivation phase was launched, the planktonic cells were mostly washed out for RL5260, whereas the number of planktonic cells of BBG111 increased during the continuous phase. This was probably a result of the limited adhesion capacities of this strain due to the absence of EPS. The maximum specific growth rates of 0.39 h^{-1} and 0.38 h^{-1} for BBG111 and RL5260 were comparable in the two-compartment system. They were close to the values of 0.35 h^{-1} and 0.38 h^{-1} determined by Guez et al. [72] and Martínez et al. [211] as growth rates for *B. subtilis* in glucose-limited fed-batch cultures. However, the EPS^+ strain RL5260 produced about 1.6 more adhered biomass than BBG111 (EPS^-) which resulted in an important difference regarding the biofilm versus planktonic cell ratio. This ratio was nearly two times higher for RL5260.

Although EPS production is advantageous for cell adhesion and leads to enhanced biofilm formation, it is metabolically expensive [212]. Thus, EPS production may reduce the cell growth and affects negatively the surfactin production. Nevertheless, the results have shown that the mean surfactin productivity of the strain RL5260 with increased biofilm formation capacity through EPS production was about 37% improved during the continuous phase compared to BBG111. This indicates clearly the improved performance of the EPS^+ strain in this system compared to the EPS-strain.

Surprisingly, both strains showed a similar glucose consumption profile when the concentration was measured in the bulk medium. For the same amount of consumed glucose, RL5260 produced significantly more adhered biomass as well as higher amounts of surfactin than BBG111. This indicated that both strains had a completely different cell physiology in the system due to the differences in EPS production.

Regarding the performed TOC measurements, the TOC consumption profile for BBG111 was significantly increased compared to RL5260 during the continuous phase. This was most likely linked to the different biofilm development capacities due to the production of EPS or not of RL5260 and BBG111. Hence, RL5260 and BBG111 used the available carbon source in the medium in a different way. Given that BBG111 is not able to synthesize a biofilm matrix, the adhered biomass consisted mainly of cells, whereas the adhered biomass of RL5260 contained a mixture of cells and biofilm matrix. Biofilm composition measurements of RL5260 that were performed in our laboratory using biofilms developed on drip-flow reactor coupons revealed a relative EPS amount of 81% and a cell content of 19%. Both strains show comparable glucose-to-biomass conversion yields for the cellular production in suspended cell cultures ($Y_{X/S,cells}$ of 0.22 g g^{-1} for BBG111 and $Y_{X/S,cells}$ = 0.26 g g^{-1} for RL5260). The yields were similar or close to the yield of 0.22 g g^{-1} previously reported by Guez et al. [72] for *B. subtilis* ATCC6633 grown in Landy medium in shaking flasks. Assuming a substrate-to-EPS conversion yield that is significantly higher than the conversion yield for cellular production, e.g., $Y_{x/s,EPS}$ ~ 0.57 g g^{-1} as obtained by Huang et al. for the production of poly-γ-glutamic acid (PGA), a major extracellular compound of *B. subtilis* CGMCC1250 [213], RL5260 used in total lesser amounts of carbon sources than BBG111 for the biofilm development. This assumption is further confirmed through the determined yield of the produced biofilm per consumed TOC $Y_{biofilm/TOC}$ for both strains. RL5260 reached a yield of $Y_{biofilm/TOC}$ = 0.61 g g^{-1}, whereas BBG111 reached only 0.25 g g^{-1}. This shows the lower energy consumption of RL5260 for the biomass production due to the increased biosynthesis of EPS instead of cells.

The reduced energy consumption of RL5260 for the biofilm development resulted in a more efficient surfactin production. It can be considered that surfactin was mainly produced by the cells present in the biofilm since a sufficient aeration is necessary for the production which was not guaranteed for the planktonic cells in the stirred tank reactor. Consequently, the specific surfactin production was significantly increased for RL5260. Hence, RL5260 reached a mean specific surfactin production of 90 mg L^{-1} h^{-1} per g of adhered cell dry weight, whereas BBG111 produced only 20 mg L^{-1} h^{-1} per g of adhered cell dry weight.

In conclusion, the two-compartment biofilm reactor designed in this study has shown to be suitable for continuous surfactin production. The EPS^+ strain exhibited significantly improved performances in terms of cell adhesion and surfactin production in this system by comparison with the EPS^- strain. The surfactin yield and population stability inside the reactor could be further improved by engineering the biofilm formation capacity of the cells. For a good process performance, a trade-off between enhanced cell adhesion and increased productivity has to be chosen. EPS production could be modulated in favor of surfactin production by guaranteeing a sufficient cell adhesion through a controlled EPS production while increasing the numbers of potential cell factories. Moreover, cell morphology engineering could improve cell adhesion and further reduce cell detachment.

Author Contributions: Conceptualization, H.L.B. and F.D.; methodology, H.L.B., S.G. and F.D.; software, H.L.B. and F.D.; validation, H.L.B., S.G. and F.D.; formal analysis, H.L.B.; investigation, H.L.B.; resources, S.G., P.J. and F.D.; data curation, H.L.B.; writing—original draft preparation, H.L.B.; writing—review and editing, F.C., P.D., S.G., P.J. and F.D.; visualization, H.L.B.; supervision, F.C., P.D., P.J. and F.D.; project administration, H.L.B.; funding acquisition, F.C, P.D., P.J. and F.D. All authors have read and agreed to the published version of the manuscript.

Funding: This research received funding from the European INTERREG Va SmartBioControl / BioProd project and the ALIBIOTECH program funding administered by the Hauts-de-France Region. Met steun van het europees fonds voor regionale ontwikkeling. Avec le soutien du fonds européen de développement régional. HB is supported by an international PhD grant co-funded by the Université de Liège and the Hauts-de-France Region.

Acknowledgments: The authors would like to thank Prof. Richard Losick from Harvard University for donation of the B. subtilis RL5260 strain. We are grateful to Catherine Helmus, Andrew Zicler and Samuel Telek (all from MiPI, Gembloux Agro-Bio Tech – Université de Liège) for their technical assistance for the reactor assembling. Furthermore, we wish to thank Neil Moustier (CRA-W, Gembloux) for the glucose analysis and Virginie Byttebier (BEAGx, Gembloux Agro-Bio Tech – Université de Liège) for the performed TOC analysis as well as Andrew Zicler for his help with Figure 2.

CHAPTER 5

Impact of filamentous *B. subtilis* 168 mutants on the process performance and stability of a continuous trickle-bed biofilm reactor

1. Introduction

As described previously in this document, the production of microbial biosurfactants in a continuous process with biofilm bioreactors presents many advantages. Cell immobilization avoids cell loss as well as the installation of cell recycle systems and has also shown to be favorable for biosurfactant production with *B. subtilis* [75–77, 79, 91, 93]. Moreover, biofilm bioreactors provide further downstream process simplification since the biomass remains attached to the support as well as they permit the design of bioprocesses avoiding foam formation [92]. However, the cell adhesion capacity of the widely used and potentially strong surfactin producing *B. subtilis* 168 strain is limited due to a deficiency in biofilm formation. Consequently, this strain is not well adapted to biofilm-based processes.

The objective of this work was to improve the natural immobilization of *B. subtilis* 168 on the packing elements through biofilm formation and to achieve a highly active biomass that produces surfactin in a stable continuous process while avoiding cell detachment. For this purpose, different surfactin producing *B. subtilis* 168 mutants possessing improved adhesion capacities due to provoked cell filamentation and restored exopolysaccharide production have been generated and investigated for the cultivation in biofilm bioreactors. In the previous chapters (2 and 3), cell filamentation induction through the deletion of *sepF* and EPS production has revealed an improved performance in terms of cell adhesion and support colonization in the DFR. In this device, the cells were exposed only to low shear stress. In the newly designed trickle-bed biofilm bioreactor (chapter 4) for continuous surfactin production, the shear forces are significantly higher and have an impact on the biofilm formation and distribution [147]. In chapter 4, the behavior of an EPS^- (BBG111) and EPS^+ (RL5260) *B. subtilis* 168 strain has been studied in the reactor to develop a growth model. The EPS^+ strain exhibited an enhanced performance in terms of surfactin production and biofilm formation capacity.

In the last part of this work, the filamentous EPS^- and EPS^+ mutants (BBG270 and BBG512) were cultivated in the trickle-bed biofilm reactor to study if cell filamentation can additionally to EPS contribute to an improved cell adhesion on the highly structured metal packing as well as reduce cell detachment to limit the presence of planktonic cells in the reactor for further process intensification. Moreover, the impact of nutrient depletion on the populations’ behavior and biofilm stability has been studied and the possibility to simulate these conditions via the previous developed model. This is especially interesting for the development of a future feeding strategy through simulations with the model.

2. Materials and methods

2.1 Strains

The experiments were performed with the previously designed and described *B. subtilis* 168 derivative strains. All used strains are listed in **Table 12**.

Table 12. *B. subtilis* 168 derivative strains used in this study.

Strains	Genotype	Source
BBG111	*trpC2, amyE::sfp-cat, epsC*^{0}*; Cm*^{R}	[86]
BBG270	*trpC2, ΔsepF::spc, amyE::sfp-cat, epsC*^{0}*; Spc*^{R}*, Cm*^{R}	[199]
RL5260	*trpC2, epsC*$^+$*, sfp*$^+$*; Erm*^{R}	[6]
BBG512	*trpC2, epsC*$^+$*, sfp*$^+$*, Erm*^{R}*, Δupp::Pλ-neo, ΔsepF::phleo-upp-cI; Erm*^{R}*, Phleo*^{R}*, Neo*^{R}	[199]

2.2 Set-up of the lab-scale trickle biofilm reactor and culture conditions

The experimental set-up with the corresponding culture conditions have been used as described in chapter 4, section, 2.3, page 100.

2.3 Cell morphology analysis by microscopy

Biofilm samples were taken directly form the packing elements, resuspended into PBS and spread on a microscope slide. Microscope images were taken with an inverted phase-contrast microscope system (Eclipse Ti2, Nikon Instruments Europe BV, Amsterdam, Netherlands) using an 100x magnification oil immersion objective.

2.4 Biomass dry weight determination

The biomass dry weight determination was conducted as previously described in chapter 4, section 2.5, page 102.

2.5 Metabolite analysis

Glucose, acetic acid and lactic acid have been analyzed in the supernatant by high-performance liquid chromatography (HPLC) based on ion-moderated partitioning using a Waters Acquity UPLC® H-Class System (Waters, Zellik, Belgium) with an Aminex HPX-87H column 7.8 x 300 mm (Bio-Rad Laboratories N.V., Temse, Belgium) heated up to 50°C. The metabolite analysis was carried out with an isocratic flow rate of 0.6 mL/min for 25 min using a mobile phase of water containing 5mM H_2SO_4. Elution profiles were monitored through a refractive index detector (RID). Pure metabolites samples of glucose, acetic acid and lactate de silicium (Sigma-Aldrich, Overijse, Belgium) were used to determine the retention time of the corresponding metabolite and to establish a calibration curve.

2.6 Surfactin analysis

The surfactin concentration in the cell culture samples were analyzed as previously described in chapter 4, section 2.7, page 103.

3. Results and discussion

3.1 Impact of filamentous growth and/or EPS production on the process performance

In previous works, a 20 L trickle-bed biofilm reactor containing a highly structured metal packing for promoting biofilm formation has been developed [92, 146, 147]. This device has shown to be advantageous for the use in a non-foaming lipopeptide production process since it provides a high surface area for cell immobilization and a high air/liquid mass transfer. To develop further this process and to test different lipopeptide producing strains more easily, this reactor has been downscaled to a typical lab-scale reactor volume of 2 L (working volume = 1 L). However, the configuration of the lab-scale reactor was changed. The mixing unit and packing elements were separated into two devices. The reactor has been characterized as well as a growth model for the planktonic and biofilm population has been developed in the previous chapter using BBG111 (EPS^-) and RL5260 (EPS^+). Here, the filamentous EPS^- and EPS^+ counterparts (BBG270 and BBG512) have been cultivated to study the impact of filamentous growth on the cell adhesion capacity and cell detachment in the trickle-bed reactor as well as on the stability of the process.

3.1.1 Cell adhesion and detachment

The growth of the planktonic cells was followed overtime. The results are presented in **Figure 49**.

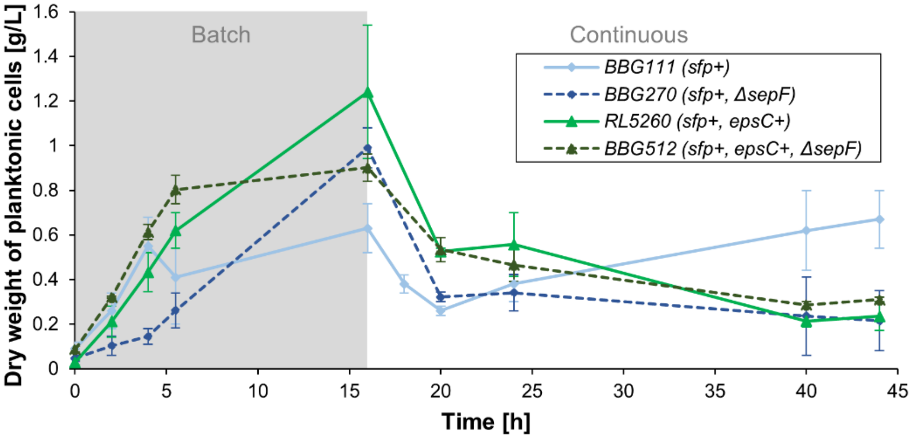

Figure 49. Development of the planktonic cells in the medium for the different mutant strains. The non-filamentous strains are presented with a continuous line and their filamentous counterparts with a dashed line in the same color.

During the first hours (0 – 4h) all mutants (except BBG270) grew very efficiently in the liquid medium (cf. **Figure 49**). BBG270 needed more time to adapt to the reactor environment which resulted in an extended lag phase compared to the other strains. The maximum specific growth rates of RL5260, BBG512 and BBG111 were comparable ($0.38 \pm 0.07\ h^{-1}$, $0.35 \pm 0.04\ h^{-1}$ and $0.39 \pm 0.04\ h^{-1}$, respectively), whereas BBG270 reached a strong reduced maximum specific growth rate of $0.08 \pm 0.03\ h^{-1}$. The growth of BBG111 remained stagnant after 4 h. After launching the continuous cultivation phase, the number of cells in the liquid medium dropped down strongly during the first four hours. This was linked to the high dilution rate ($0.5\ h^{-1}$) that has been set in order to wash out non-adherent cells. After 20 h the number of planktonic cells decreased slower for all strains, except for BBG111. For this latter strain, the number of cells was increasing until the end of the cultivation. At the end of the cultivation, comparable low numbers of cells were present in the liquid phase for RL5260, BBG512 and BBG270. In total, BBG111 produced 7.8 ± 1.5 g, BBG270 5.2 ± 1.8 g, RL5260 6.6 ± 1.1 g and BBG512 6.1 ± 0.0 g of planktonic cells (dry weight).

The results pointed out that filamentous growth affected positively the cell adherence of BBBG270 and reduced the cell detachment after launching the continuous phase. In this case filamentous growth seemed to have the same affect than EPS production permitting a better cohesion between the cells as well as an improved adhesion to the support. Cell filamentation and EPS production together did not show any synergistic or sum of the individual effects in terms of cell detachment. This indicates, that cell filamentation in the presence of EPS had a minor effect under this process conditions as already observed in the DFR cultivation studies.

3.1.2 Biofilm distribution on the packing elements

The weight of the attached biomass on the reactor support has been measured at the end of the cultivation on the different packing elements of the tower. The results are presented in **Figure 50**.

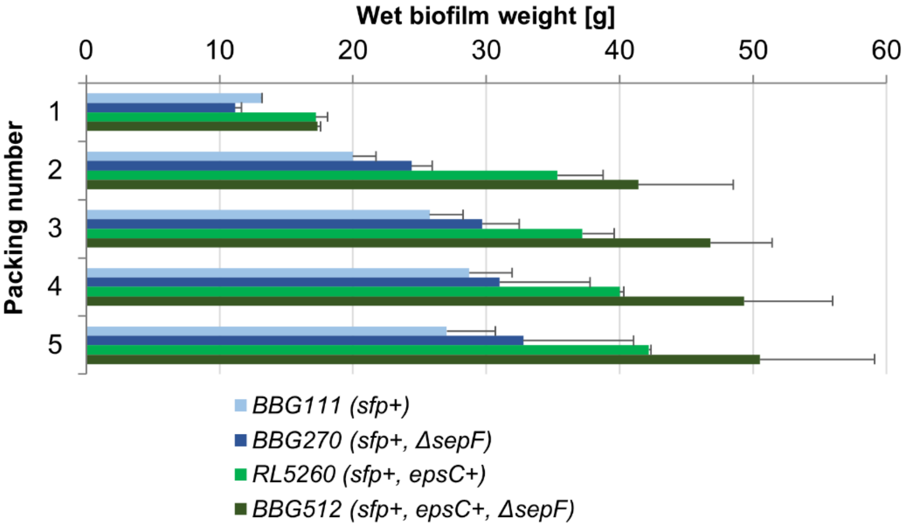

Figure 50. Biofilm distribution on the different packing elements; number 1 to 5 correspond to the packing order from the top to the bottom of the packing tower.

RL5260, BBG512, BBG270 and BBG111 reached a total amount of 172 ± 5 g (13.5 ± 0.4 g), 205 ± 27 g (16.2 ± 2.1 g), 129 ± 20 g (9.7 ± 1.5 g) and 115 ± 11g (8.6 ± 0.8 g) attached wet biomass (or dry biomass weight) on the reactor packing, respectively. The adhesion capacity of the EPS deficient strains was significantly reduced. However, the difference between the EPS deficient and EPS$^+$ strains was not as distinctive as observed in the drip flow reactor (DFR). This is probably linked to the increased shear stress present in the trickle-bed biofilm reactor compared to the DFR. Moreover, the high specific surface area promoted certainly the cell adhesion. The metal structured packing reacts like a microstrainer. The continuous recirculation of the planktonic cells increased the chances of cells to adhere during the batch cultivation. In the DFR, no recirculation of the culture medium has been performed.

Figure 50 shows the biofilm distribution on the five packing elements from the upside (1) to the downside (5). For all strains similar colonization profiles were observed. More precisely, with increasing packing number, the biofilm development was enhanced for all strains. Packing 1 on the top of the packing tower showed the lowest biofilm development. Since the liquid is injected on the top, the first packing element serves as liquid distribution element. Obviously, the cells have lesser time for adhering to the first packing element and a worse liquid distribution and nutrition delivery compared to the packing elements in lower positions in the packing tower. Zune et al. [147] observed similar colonization profiles in the 20 L trickle-bed biofilm bioreactor with *B. amyloliquefaciens,* when the cell colonization was analyzed via X-ray tomography.

The determined biomass ratios (g biofilm dry weight per g planktonic cells dry weight) are listed for each strain in **Table 13**.

Table 13. Biomass ratio (g biofilm dry weight / g planktonic cell dry weight) determined for each strain.

	BBG111 (sfp$^+$)	***BBG270 (sfp$^+$, ΔsepF)***	***RL5260 (sfp$^+$, epsC$^+$)***	***BBG512 (sfp$^+$, ΔsepF, epsC$^+$)***
Biomass ratio [g biofilm dry weight per g planktonic cell dry weight]	1.2 ± 0.3	2.2 ± 1.04	2.1 ± 0.4	2.7 ± 0.3

BBG512 reached the highest biomass ratio which was more than two times higher than for BBG111. The mean biomass ratios for RL5260 and BBG270 were comparable and also considerable higher than for BBG111. Yet, a great variability between the replicates were observed for BB270 resulting in a high standard deviation.

3.1.3 Filamentous growth resulted in stronger cell cohesion and aggregate formation in the developed biofilm

Microscope images were recorded from biofilm samples taken from the structured metal packing. The images are presented in **Figure 51**.

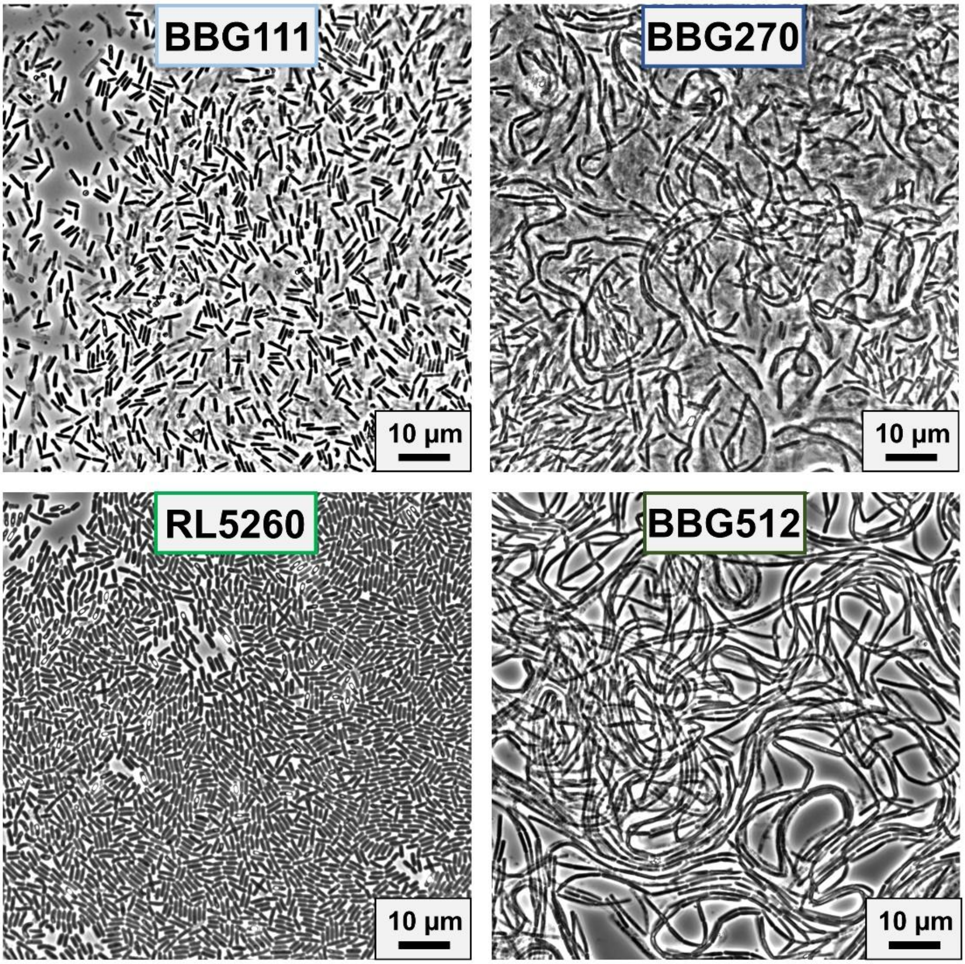

Figure 51. Microscope images of biofilm samples taken from the packing elements.

Strongly different cell morphologies were observed for the non-filamentous (BBG111, RL5260) and filamentous (BBG270 and BBG512) strains. For the non-filamentous strains, short, correctly separated cells were arranged close to each other. The biofilm of the filamentous cells was organized in multiple cell aggregates composed of long cell filaments. The observed cell morphology could explain the reduced cell detachment of BBG270 as a result of filamentous growth. The image of BBG270 illustrates the increased cohesion in the biofilm du to filamentous growth in the absence of EPS explaining the reduced cell detachment observed previously.

3.1.4 Main carbon source consumption

The measured glucose concentration in the culture medium is presented in **Figure 52** and the calculated glucose-to-biofilm conversion yields $Y_{Biofilm/S}$ are presented in **Table 14** for each strain.

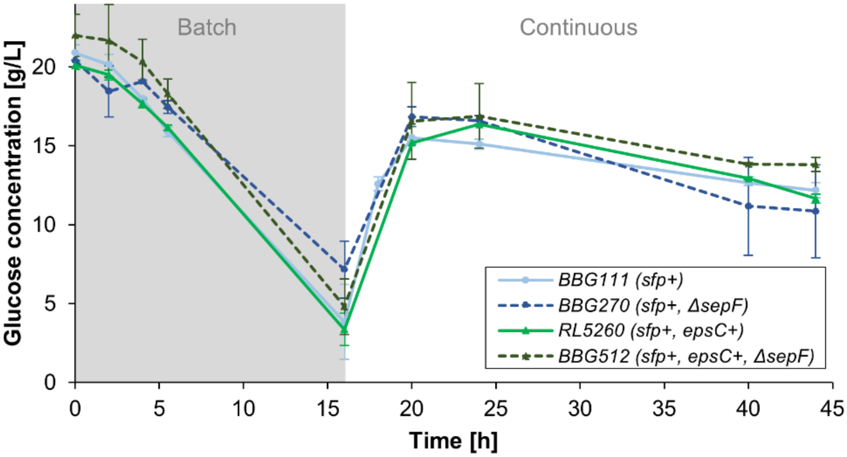

Figure 52. Glucose concentration measured in the culture medium for each strain during the batch and continuous (D = 0.5 h^{-1}) cultivation phase.

The glucose consumption profiles were similar for all strains during the batch cultivation and the continuous cultivation. Yet, the biofilm yield was strongly decreased for BBB111 and BBG270 in comparison with RL5260 and BBG512 (**Table 14**).

Table 14. Determined glucose-to-biofilm conversion yields $Y_{Biofilm/S}$ for the different strains.

	BBG111 (sfp$^+$)	***BBG270 (sfp$^+$, ΔsepF)***	***RL5260 (sfp$^+$, epsC+)***	***BBG512 (sfp$^+$, ΔsepF, epsC$^+$)***
Biofilm yield $Y_{Biofilm/S}$ [g dry biofilm per g glucose]	0.08 ± 0.01	0.10 ± 0.01	0.14 ± 0.00	0.18 ± 0.04

3.1.5 Surfactin productivity

The measured mean surfactin productivities and surfactin production yields of the different strains are presented in **Table 15**.

Table 15. Surfactin mean productivities and production yields during the cultivation.

	BBG111 (sfp$^+$)	***BBG270 (sfp$^+$, ΔsepF)***	***RL5260 (sfp$^+$, epsC$^+$)***	***BBG512 (sfp$^+$, ΔsepF, epsC$^+$)***
Mean surfactin productivity [mg L^{-1} h^{-1}]				
Batch	107.4 ± 5.6	42.8 ± 18.0	130.4 ± 25.3	157.5 ± 22.1
Continuous	168.1 ± 22.0	64.9 ± 31.5	231.0 ± 14.2	208.5 ± 40.1
Total amount of produced surfactin [g]				
- Liquid phase	6.4 ± 0.5	2.5 ± 1.2	8.6 ± 0.1	8.5 ± 1.3
- Biofilm	0.3 ± 0.05	0.3 ± 0.1	0.5 ± 0.1	0.3 ± 0.1
Surfactin yield $Y_{P/S}$ [mg surfactin per g glucose]	63.1 ± 4.7	27.5 ± 3.4	90.0 ± 2.7	97.6 ± 6.6
Surfactin yield $Y_{P/X}$ [mg surfactin per g total dry biomass]	408.8 ± 12.4	190.2 ± 74.9	448.8 ± 7.0	398.3 ± 97.1
Surfactin yield $Y_{P/biofilm}$ [mg surfactin per g dry biofilm]	792.4 ± 132.0	280.0 ± 66.7	666.6 ± 33.5	567.6 ± 165.7
Specific mean surfactin productivity (continuous phase) $Y_{P/X}$ [mg L^{-1} h^{-1} per g total dry biomass]	10.2 ± 0.9	4.4 ± 2.2	11.5 ± 0.3	9.3 ±2.5
Specific mean surfactin productivity (continuous phase) $Y_{P/cells}$ [mg L^{-1} h^{-1} per g adhered cells]	21.6 ± 2.8	5.8 ± 2.8	87.3 ± 5.4	78.1 ± 15.0

The mean surfactin productivities of RL5260 and BBG512 were comparable during the batch cultivation phase, whereas as the mean productivity of BBG111 was slightly reduced and the one of BBG270 was more than two times reduced. During the continuous cultivation phase, the EPS$^+$ strains RL5260 and BBG512 exhibited similar mean surfactin productivities. RL5260 reached a mean specific surfactin productivity of up to 231 mg L^{-1} h^{-1}. BBG111 and BBG270 had a significant lower surfactin productivity. Concerns about the diffusion limits of the product into the bulk medium, as mentioned by [141], are not justified since only a minor amount of surfactin stays trapped in the biofilm (between 3 and 11% of the total produced amount of surfactin) as already observed with the DFR in chapter 2 and 3.

The glucose-to-surfactin conversion yields $Y_{P/S}$ were likewise significantly increased for the EPS$^+$ strains in comparison to the EPS$^-$ strains. This is certainly linked to the different biofilm composition as explained in the previous chapter.

Regarding the surfactin yield per g of total dry biomass $Y_{P/X}$ (biofilm and planktonic cells), RL5260 reached the highest value with around 450 mgg^{-1}. The $Y_{P/X}$ values of BBG111 and BBG512 were slightly reduced and the one of BBG270 more than two times lower in comparison with RL5260.

Interestingly, the strains RL5260, BBG512 and BBG111 have shown similar specific mean surfactin productivities per g of total produced biomass (between 9.3 and 11.5 mg L^{-1} h^{-1} g^{-1}). Probably, the measured numbers of planktonic cells in the bulk medium also contributed to the surfactin production before they were detaching from the packing elements. Once the cells detached, it is rather unlikely that they produce significant amounts of surfactin since the cells are prone to be washed-out rapidly due to the high dilution rate. Besides, the dissolved oxygen concentration in the stirred tank reactor, the main place of residence, is limited.

BBG111 reached the highest surfactin yield per g dry biofilm $Y_{P/Biofilm}$. However, we can assume that the biofilm of BBG111 and BBG270 is mainly composed of cells and the one of RL5260 and BBG512 of around 19% of cells and 81% of EPS as shown in chapter 2, section 3.7, page 68. If the biofilm composition is taken into account for the strains, the specific mean surfactin productivity during the continuous cultivation was up to four times higher for RL5260 and BBG512 compared to BGG111 and up to 15 times higher when compared to BBG270. The filamentous growth did not have an impact on the surfactin production in the case of the EPS^{+} strains. However, the filamentous EPS^{-} strains BBG270 showed a strongly decreased surfactin production capacity. In planktonic cultures, no reduction in surfactin production has been observed for BBG270 compared to BBG111 (cf. chapter 2, section 3.5, page 63). Although the surfactin-biofilm production yield $Y_{P/biofilm}$ for BBG111 was quite high, this value will certainly decrease during a long-term cultivation process. Given that BBG111 has reduced adhesion capacities, cell detachment will occur continuously and thus decrease the overall cellular productivity since the detached cells will be washed out.

In a previously demonstrated continuous surfactin production processes based on an air/liquid membrane contactor, Coutte et al [84] achieved a surfactin productivity of 110 mg L^{-1} h^{-1} using a dilution rate of 0.2 h^{-1}. The mean surfactin productivity in the here presented system was two times higher which confirms the efficiency of the molecular strategies carried out to enhance the surfactin production in the biofilm bioreactor. In the future, it would be interesting to cultivate a modified surfactin overproducing strain with improved adhesion capacities to further increase the surfactin production yield.

3.1.6 Primary metabolite production

The surfactin production of BBG270 was surprisingly low. *B. subtilis* is known to produce several primary metabolites such as acetic acid and lactic acid as by-products in the presence of sufficient amounts of carbon source due to overflow metabolism which can reduce the production of the target molecule. In order to test to what extent *B. subtilis* is producing such by-products in the present system, the concentration of lactic acid and acetic acid was measured in the culture medium (**Figure 53A** and **B**).

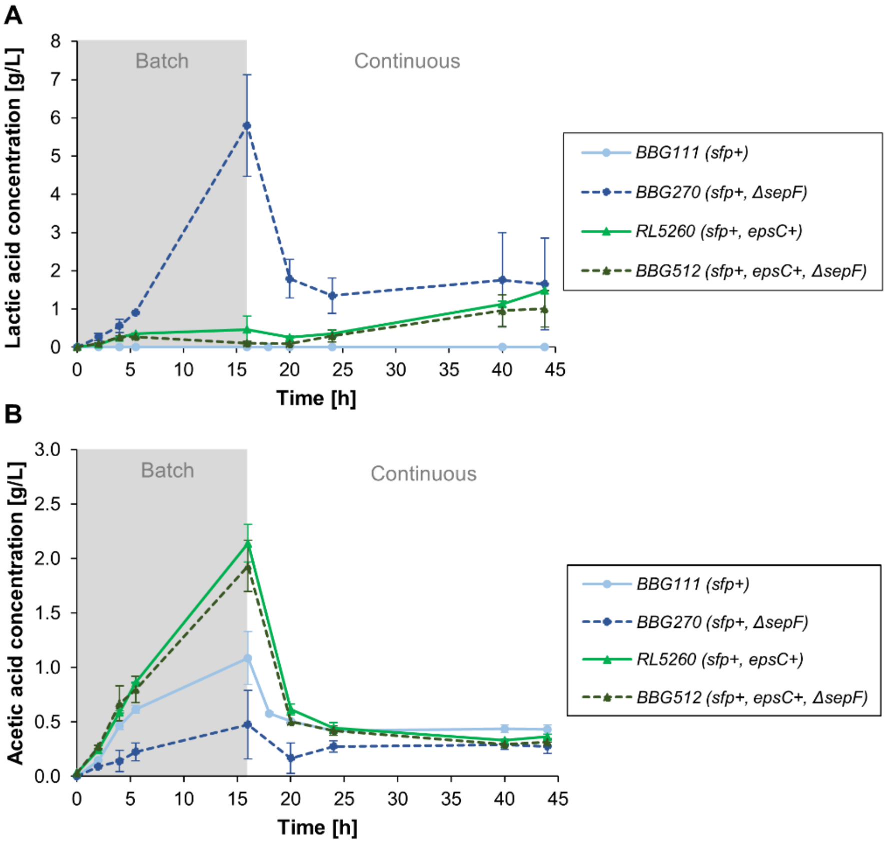

Figure 53. (A) Lactic acid and (B) acetic acid concentration measured in the culture medium for all strains cultivated in the trickle-bed biofilm bioreactor.

Among the strains, a great variability of primary metabolite production was observed. This is certainly linked to the biofilm heterogeneity as a result of nutrient gradients present in the biofilm. BBG111 did not produce any measurable amounts of lactic acid but produced similar amounts of acetic acid than RL5260 and BBG512 during the continuous phase. Unexpectedly, BBG270 produced high amounts of lactic acid during batch cultivation and continued to produce during the continuous cultivation. Thus, BBG270 showed a significant different behavior than the other EPS$^-$ strain BBG111. The production of acetic acid was significantly lower during the batch cultivation phase compared to the other strains (**Figure 53B**). The increased lactic acid production may explain the reduced surfactin yield previously determined for BBG270. An explanation for the increased lactic acid production could be given through the increased presence of stress in the cell aggregates formed by BBG270. As the microscope images have shown (**Figure 51**, page 131), filamentous growth results in the formation of dense cell aggregates. Probably, the cell aggregates of the filamentous EPS$^-$ strain are more tightly arranged than in the presence of EPS. Consequently, inner cells are more exposed to stress due to reduced nutrient and oxygen availability which could have triggered the lactic acid production in BBG270. RL5260 and BBG512 produced similar amounts of lactic and acetic acid. The production of acetic acid remained constant during the continuous production process, whereas the production of lactic acid increased until the end of the cultivation. This may be linked to an increased biofilm thickness and occurring oxygen gradients in the biofilm.

Coutte et al. [84] observed as well the production of considerable amounts of acetic acid and lactic acid during the continuous surfactin production in the air/liquid membrane contactor with a *B. subtilis* 168 derivative strain. As already mentioned by Coutte et al [84], high glucose concentration and limited oxygen conditions may not be fully suitable for lipopeptide production due to important production of primary metabolites although high surfactin production yields can be achieved. The production of these by-products is linked to a not negligible loss of energy. In order to avoid the production of these by-products, metabolic engineering of the synthesis pathways could also be envisaged.

3.2 Impact of nutritional stress on the behavior of the bacterial populations

3.2.1 The filamentous EPS$^+$ strain BBG512 exhibited increased adhesion capacities under limited nutritional growth conditions

The biomass development of BBG512 under unlimited glucose conditions on the packing elements was only slightly increased compared to RL5260 after 44 h of cultivation. Hence, the filamentous growth had a minor impact on the support colonization than the EPS production. However, it was interesting to see what will happen if the cells in the biofilm are exposed to an additional stress factor like nutrient depletion of their main carbon source. Will cell detachment from the biofilm increase since the cells are constrained to search for new nutrients? Does the production of undesired by-products like lactic acid and acetic acid decrease?

Figure 54 shows the result of the measured glucose concentration and number of planktonic cells in the medium as well as the developed amount of biofilm for BBG512 and RL5260 when they were cultivated under glucose limited conditions (1 g L^{-1} h^{-1}) during the continuous culture phase after a 16 h batch phase. As **Figure 54A** shows, glucose limitation occurred in the culture from 20 h until the end for both strains.

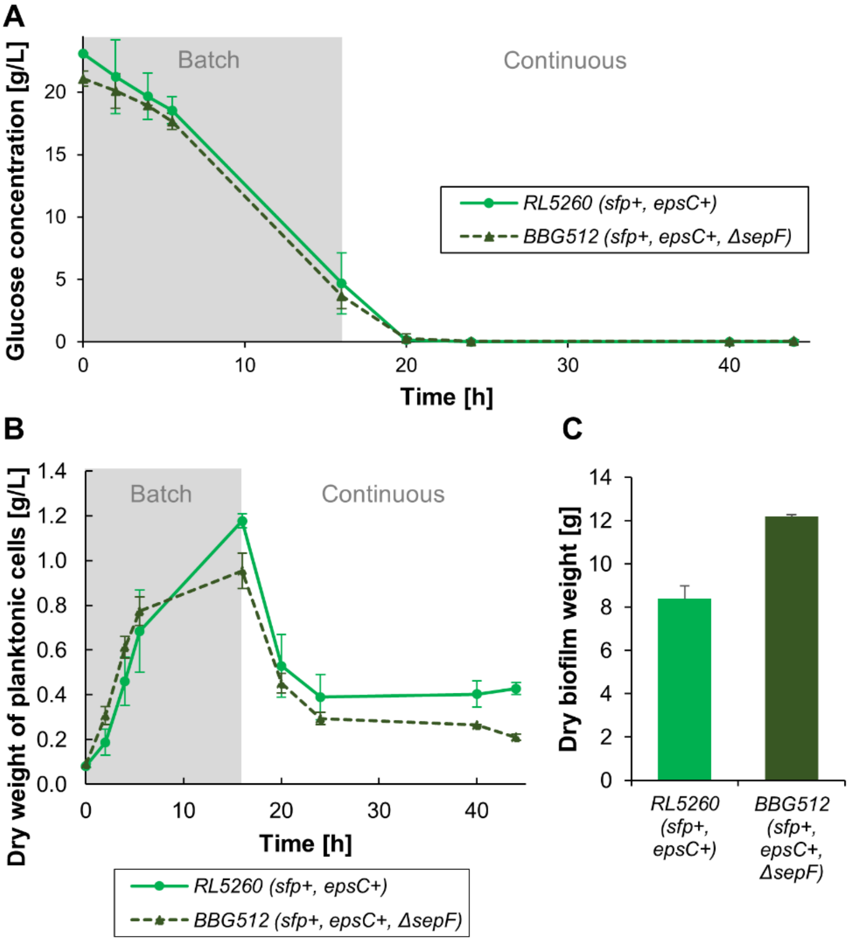

Figure 54. (A) Measured glucose concentration in the medium; (B) development of the planktonic cells in the medium and (C) final amount of adhered biofilm for RL5260 and BBG512 cultivated under limited glucose conditions during the continuous cultivation phase (feeding rate 1 g L^{-1} h^{-1}) in the trickle-bed biofilm reactor.

The planktonic cells started to grow in a similar same way for both strains at the beginning of the batch cultivation (**Figure 54B**). At the end of the continuous cultivation, slightly less planktonic cells were present for BBG512 than for RL5260. The total number of produced planktonic cells was 7.7 ± 0.8 g for RL5260 and 5.6 ± 0.12 g for BBG512. In chapter 4, the model confirmed that the planktonic cells present in the medium during the continuous cultivation consist mainly of cells that are detaching from the biofilm. Hence, BBG512 produced slightly lesser amounts of planktonic cells due to a reduced cell detachment as a result of better cell cohesion and adhesion capacities in case of nutritional stress. In total, RL5260 produced 8.4 ±

0.6 and BBG512 12.2 ± 0.1 g of biofilm dry weight on the packing element (**Figure 54C**). This corresponds to 106.4 ± 7.7 g and 154.6 ± 1.8 g wet biofilm weight, respectively. Indeed, BBG512 has produced significantly more adhered biomass than RL5260 after 44h of cultivation. Probably, the biofilm development was significantly reduced for RL5260 due to higher detachment rates of the cells. The biofilm of the filamentous EPS$^+$ seemed to have a higher stability under nutritional stress than the non-filamentous strain since filamentous cells have a stronger cohesion (cf. **Figure 51**, page 131) which limits cell detachment.

3.2.2 Reduced glucose availability increased the biofilm yield

Table 16 presents different calculated parameters to compare the behavior of the EPS$^+$ mutant strains with and without filamentous growth.

Table 16. Strain comparison of RL5260 and BBG512 under limited glucose feeding conditions.

Glucose limited conditions	***RL5260 (sfp$^+$, epsC$^+$)***	***BBG512 (sfp$^+$, ΔsepF, epsC$^+$)***
Total dry biofilm [g]	8.4 ± 0.6	12.2 ± 0.1
Biofilm yield [g dry biofilm per g glucose]	0.19 ± 0.01	0.27 ± 0.02
Mean surfactin productivity during continuous phase [mg L^{-1} h^{-1}]	110.6 ± 14.5	122.7 ± 16.1
Total produced amount of surfactin [g]	5.6 ± 0.6	6.0 ± 0.2
Surfactin yield $Y_{P/S}$ [mg surfactin per g glucose]	113.8 ± 10.4	130.5 ± 1.8
Surfactin yield $Y_{P/X}$ [mg surfactin per g biofilm]	48.1 ± 2.4	37.8 ± 2.7
Mean primary metabolite production during continuous phase [g L^{-1} h^{-1}]		
Lactic acid	0.14 ± 0.05	0.06 ± 0.02
Acetic acid	0.29 ± 0.02	0.28 ± 0.04

For the continuous culture with glucose limitation, the biofilm yield was increased of up to 29% for RL5260 and 50% for BBG512. This is probably linked to the enhanced cohesion of the filamentous cells which prevents cell detachment from the packing elements. For the continuous culture without glucose limitation, the biofilm yield (g biofilm per g glucose) was only slightly increased for BBG512 in comparison with RL5260, as shown previously. Yet, the increased yield of biomass resulted obviously in a decreased surfactin production. Since glucose is the main energy source, the limitation decreased strongly the surfactin production and the cells rather produced biomass. This is a behavior that is generally observed for microorganisms under nutrient limitations of the carbon source [214].

The production of lactic and acetic acid was not considerable reduced under glucose limited conditions. Probably, nutrient gradients exist in the biofilm that stimulate cell differentiation and the production of these overflow metabolites. Christiano-Fajardo et al. [215] made similar observation when they cultivated *B. amyloliquefaciens* 83 in continuous cultures. The biomass yield increased under nutritional limitations and the presence of low glucose concentrations since the strains preferentially produced biomass [215]. Whereas at high glucose concentrations, the production of primary and secondary metabolites was favored due to over-flow metabolism [215]. However, the *Bacillus* strain was also able to produce carbon overflow metabolites under glucose limitation [215]. Christiano-Fajardo et al. [215] proposed that this is linked to the fact that low glucose concentration also triggers the sporulation process in *Bacillus* strains followed by cellular differentiation resulting in the development of heterogeneous cell populations that are responsible for the production of the overflow metabolites.

3.3 Nutritional stress simulation

In the following, the limited glucose conditions have been simulated with the previous developed model (chapter 4) and compared to the experimental data. The introduced parameters are listed in **Table 17**.

Table 17. Introduced model parameters for the simulation of nutritional stress in the trickle-bed biofilm bioreactor.

Parameter	Description	Unit	RL5260	BBG512
μ_{max}	Max. growth rate of cells	h^{-1}	0.38	0.35
C_{sat}	Dissolved oxygen concentration at saturation	$g\ L^{-1}$	0.00673	0.00673
k_a	Switching rate to biofilm (adsorption) (batch/continuous)	h^{-1}	(2.1/0)	(2.7/0)
k_d	Releasing rate to planktonic state (detachment) (batch/continuous)	h^{-1}	(1/0.12)	(1/0.11)
K_La	Specific oxygen mass transfer coefficient	h^{-1}	40	40
K_o	Oxygen affinity constant	$g\ L^{-1}$	0.005	0.005
K_s	Substrate affinity constant	$g\ L^{-1}$	0.015	0.015
S_{in}	Substrate concentration at the reactor entry	$g\ L^{-1}$	2.00	2.00
$Y_{X/O}$	Oxygen-biomass conversion coefficient	$g\ g^{-1}$	1.00	1.00
$Y_{X/S}$	Substrate-biomass conversion coefficient (batch/continuous)	$g\ g^{-1}$	(0.20/0.40)	(0.25/0.45)

For the simulation, the previously mentioned maximum specific growth rates for RL5260 and BBG512 (see section 3.1.1, page 128) were used. For the batch cultivation phase, a higher k_a value was chosen for BBG512 than for RL5260 as well as a slightly lower k_d value during the continuous cultivation phase due to the increased adhesion capacities of BBG512. The introduced k_a and k_d values were oriented on the previously calculated biomass ratio in **Table 13**, page 130. For the yield $Y_{X/S}$ 0.20 g g^{-1} was used for RL5260 and 0.25 g g^{-1} for BBG512 (calculated for the total biomass produced (planktonic cells and biofilm) per total amount of consumed glucose). The yield $Y_{X/S}$ was increased after the batch phase since the biomass development was more important under limited glucose conditions. The K_La value was set at 40 h^{-1}. For C_{sat}, K_O, K_S and $Y_{X/O}$ the same values as previously reported in chapter 4 (see section 3.3, page 113) were introduced. The results of the simulation and the corresponding experimental values are presented in **Figure 55**.

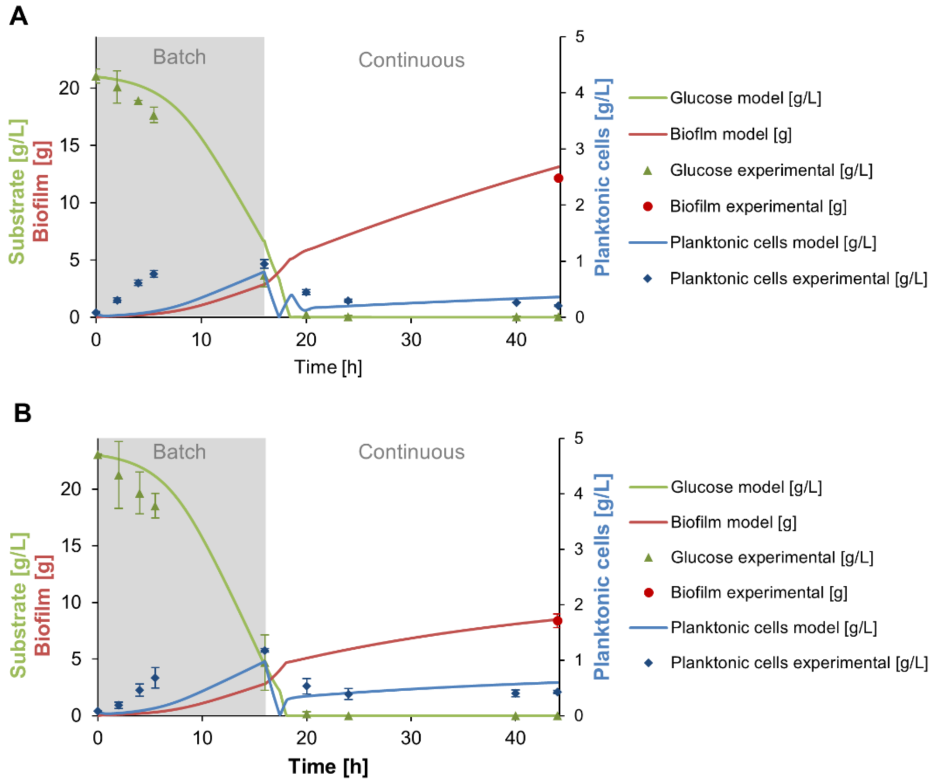

Figure 55. Glucose consumption, planktonic cells and biofilm development under glucose limited conditions predicted by the model for BBG512 (A) and RL5260 (B). Simulations results are drawn with a continuous line and the experimental results are shown as point references for comparison.

The glucose consumption profiles were quite correctly described for both strains by the model, as well as the biofilm development reached the final measured value quite close. The planktonic cell development was slightly underestimated during the first hours of the batch cultivation phase in both cases. In general, the nutrient stress simulation via the developed model predicted properly the measured experimental values which was further confirmed by a Chi-square of goodness test (for the test results see Appendix V, pages 165/166, **Table 23** for BBG512 **Table 24** for RL5260). The test results have shown no significant differences between the observed and predicted values for the glucose consumption and planktonic cell development for both strains with a significance level of $\alpha = 0.05$. Hence, the model is able to simulate stress conditions in the system. This could be exploited to develop a feeding strategy in order to adapt the feeding rate to the biomass development.

4. Conclusions

BBG111 even with lesser attachment capacity has shown to produce high amounts of surfactin in this system without foam formation. However, this strain is not well adapted to the system. Due to the restricted cell adhesion capacities of this strain, a long-term fermentation would result in a continuously decrease of surfactin productivity due to the continuous wash out of the detached cells from the packing.

The filamentous growth of BBG270 has shown to improve the cell adhesion as well as the cell cohesion resulting in lower cell detachment. This is preferential for an easy downstream process of the produced surfactin molecules since the necessary cell separation step can be simplified. However, although the adhesion capacity of this strain was increased compared to BBG111, the surfactin production of this strain was significantly reduced in comparison with BBG111.

RL5260 and BBG512 have increased adhesion capacities compared to BBG270 and BBG111 through the restored exopolysaccharide production. However, these sticky sugar substances are less desired since it means additional impurities in the bulk medium, that have to be removed for a pure product and they risk to clog filter elements often used for cell culture separation. Nonetheless, EPS favored cell attachment and thus increased the overall process performance. The surfactin productivity of the two EPS$^+$ strains BBG512 and RL5260 were comparable. Both strains showed similar adhesion capacities under unlimited glucose conditions where filamentous growth seemed to have a minor effect. However, filamentous cells have a better cohesion and thus cell detachment is reduced in case of additional stress like nutrient limitation.

The simulation results of the limited carbon conditions with the model were close to the experimental values. Simulations could be used to develop a feeding strategy using a nutrient gradient adapted to the biofilm development in order to minimize the waste of unused medium and to guarantee a sufficient nutrient supply during the continuous cultivation process.

To conclude, the presence of exopolysaccharide as well as the filamentous growth increased significantly the support colonization and reduced the presence of planktonic cells. Under nutrient depletion, cell filamentation resulted in decreased cell detachment in EPS^+ strains. The results of this work show that morphology engineering presents an attractive alternative strategy to metabolic engineering for optimizing biofilm-based processes through the development of custom-made biofilm patterns. Nevertheless, the presence of EPS has shown to be crucial for a good process performance in the designed system. The modulation of EPS expression could also be interesting to further increase the biofilm stability.

CHAPTER 6

General conclusions and perspectives

1. General conclusions

The objective of this work was to develop a continuous biofilm-based surfactin production process by using a widely used *B. subtilis* 168 strain with strongly limited biofilm formation capacities.

Two main strategies have been pursued to increase the colonization and biofilm formation capacities of *B. subtilis* 168 based on the restoration of EPS production and the change of cell shape through the induction of filamentous cell growth. The contribution of both, EPS production and cell filamentation, has been examined at microscopic scale through the observation of the micro-colony development by time-lapse microscopy, as well as at macroscopic scale through agar plate colonization assays. Both modifications have shown to positively affect the cell colonization capacities on agarose pads or LB agar plates. Moreover, it has been verified that the introduced genetic modifications did not have a negative impact on the surfactin production in suspended cultures.

In the next step, in order to get better insights into the biofilm growth dynamics, the mutant strains were cultivated under low shear stress with continuous feeding in a DFR. Several factors, including liquid distribution, lipopeptide and exopolysaccharide production, biofilm maturation state and filamentous growth, have shown to have a significant impact on the process that can be positive as well as negative.

The liquid distribution had a considerable impact on the coupon colonization. The biofilm started to develop preferentially were the bulk medium passes. The presence of lipopeptides increased the colonized surface through enhanced spreading. This resulted in a better and homogenous cell dispersion. However, lipopeptides provoked as well the wash out of cells and thus reduced the number of adhered cells. Exopolysaccharides production has shown to be a key element for support colonization and biofilm formation. Cell adhesion and cohesion were significantly improved (up to 50 times compared to EPS$^-$ strains) which promoted the formation of a structured and wrinkled biofilm. Through the production of exopolysaccharides, the maturation of the *B. subtilis* biofilm was triggered which resulted in the development of a hydrophobic protection layer. Although this hydrophobic layer protects the cells in the biofilm from external influences, it represents also a barrier for nutrient delivery and thus may provoke increased cell death. Moreover, the production is energetically expensive and thus may have negative consequences on surfactin production. Nevertheless, the improved cell adhesion and increased biofilm development in EPS$^+$ strains resulted in an enhanced surfactin production. Filamentous growth favored the coupon colonization and reduced cell detachment. The support colonization capacity on DFR coupons was up to three times increased in surfactin producing *ΔsepF* mutants without EPS production. In EPS$^+$ strains, filamentous growth had a minor impact on the coupon colonization capacity.

Subsequently, several strains with *ΔsepF* mutation and/or EPS restoration that have shown a good performance in the DFR have been selected for the cultivation in a trickle-bed biofilm bioreactor. A 2 L lab-scale trickle-bed biofilm bioreactor has been designed on the basis of previous works using a 20 L bioreactor and showing promising results for non-foaming biosurfactant production.

The process parameters have been adapted in order to promote biofilm formation and to reduce the number of planktonic cells for a more simplified downstream processing. For the first 16 h, the system was operated in batch mode to increase the cell numbers for the biofilm formation initiation. Then, a continuous fermentation with a dilution rate higher than the maximum specific growth rate has been conducted. Thereby, non-adherent cells were washed out. When cultivations were performed in the newly designed lab-scale trickle-bed biofilm bioreactor, the planktonic cell development could be easily followed through simple cell density measurements. Yet, the biofilm development kinetics could not be directly assessed during cultivation due to the restricted access to the packing elements. However, to evaluate the process performance, this is an essential parameter to know. Therefore, the biofilm development was indirectly estimated via a TOC mass balance. For confirmation and to get additional information, a bacterial growth model based on simple ODEs has been developed that is describing the development of the planktonic cells and the biofilm in the system. The experimental values were in accordance with the results of the model simulations. Through simulations with the model, two hypotheses could be confirmed. First, the significant different biofilm formation capacities result from different adhesion capacities due to the presence or not of EPS. And secondly, the high dilution rate that has been applied during the continuous fermentation leads to a strong washing out of the undesired planktonic cells. The model was also able to simulate the development of the bacterial populations under limited glucose conditions.

In the trickle-bed biofilm bioreactor, a slight increase in biofilm formation of the filamentous EPS$^+$ strains BBG512 was observed compared to the non-filamentous EPS$^+$ strain RL5260. Generally, the biofilm development of the EPS$^+$ strains (RL5260 and BBG512) was up to two times increased compared to the EPS$^-$ strains (BBG111 and BBG270) since the presence of EPS improved the cell adherence and colonization capacity in the system. However, the improvement factor was considerably lower as observed for the cultivations in the DFR. Probably, the high specific surface area of the packing elements and the continuous recirculation of the culture medium containing the planktonic cells promoted better the cell adhesion of the EPS$^-$ strains than the conditions in the DFR. The filamentous EPS$^-$ strain (BBG270) exhibited slightly increased biofilm formation capacities in comparison with its non-filamentous counterpart (BBG111), as cell filamentation resulted in a better cell cohesion. EPS production and cell filamentation contributed both to a more stable process due to lower cell detachment. This resulted in a three times reduced presence of planktonic cells at the end of the continuous cultivation in comparison with the control strain BBG111.

The surfactin productivity of the filamentous EPS$^-$ strain BBG270 (64.9 mg L^{-1} h^{-1}) decreased strongly compared to the non-filamentous EPS$^-$ strain BBG111 (168.1 mg L^{-1} h^{-1}). This was not observed for suspended cell cultures where the surfactin production of BBG270 and BBG111 was similar. An explanation could be that the tight cell aggregates formed by the filamentous cells of BBG270 provoked an increased stress response due to nutrient and oxygen gradients. This affected the surfactin production adversely in the trickle-bed biofilm bioreactor and triggered rather the lactic acid production. The filamentous EPS$^+$ strain BBG512 produced comparable amounts of surfactin in comparison with its non-filamentous counterpart RL5260. Beside the EPS production, the strains reached quite high mean surfactin productivities of up to 231 mg L^{-1} h^{-1}. The mean surfactin productivity was more than two times higher in comparison with values described in literature for the cultivation of a *B. subtilis* 168 derivative strain in a continuous surfactin production process based on an air/liquid membrane contactor [84]. In comparison to the EPS$^-$ strains, the EPS$^+$ strains produced between 1.4 to 4 more surfactin during the continuous cultivation phase. Regarding the specific mean surfactin productivity, the EPS$^+$ strains reached 4 to 15 times higher production rates than the EPS$^-$ strains.

In summary, the filamentous and non-filamentous EPS$^+$ strains were definitely better adapted to the trickle-bed biofilm bioreactor than the EPS$^-$ strains. The EPS$^+$ strain showed a significantly increased performance regarding the biofilm formation and surfactin production capacities in the designed system. Hence, the goal to obtain *B. subtilis* 168 strains with increased adhesion capacities and a high surfactin productivity allowing a simplified downstream processing was reached in this work.

2. Perspectives

EPS has shown to be a crucial element in the biofilm development of *B. subtilis* 168 and his adaptation to biofilm cultivations. Modulation of the EPS expression could be used to further optimize the process in order to increase the biofilm stability. Moreover, other gene deletions like *ΔcodY* [82] could be introduced in the filamentous EPS$^+$ strain to generate surfactin over-producing strains to further enhance the productivity in the trickle-bed biofilm bioreactor. The co-culture of matrix producing and surfactin over-producing strains could also be a possibility to enhance the process performance.

The analysis of other *B. subtilis* 168 mutant strains in the DFR revealed a surprising biofilm formation behaviour of the strain TF8A containing the deletion of three prophages (*ΔSPß*, *Δskin* and *ΔPBSX*) when the strain was cultivated in Landy MOPS medium (for the results see Appendix VI, page 167). A strong biofilm formation with wrinkled structures, comparable to the structure of RL5260, has been observed for the strain TF8A although no EPS production has been restored in this strain. In the future, it would be interesting to investigate more into detail the impact of prophage elements on the biofilm formation of *B. subtilis* 168 and the possible exploitation in biofilm-based processes.

An important point is to investigate more into detail the aeration conditions and oxygen transfer rate in the trickle-bed biofilm bioreactor in the presence of the biofilm since oxygen availability is a key element for good surfactin productivity. It could be checked if the aeration model that has been developed for the air/liquid membrane contactor in Lille by Berth et al. [216] could be used for the trickle-bed biofilm bioreactor.

Although filamentous growth has shown to have a lower impact on the overall colonization capacity than EPS, it contributed to a more stable biofilm with lesser cell detachment. A feature that could be exploited in other biofilm-based processes to simplify the downstream processing. Improved cell adhesion capacities facilitate the recovery of the secreted products and limit cell wash out problems and thus the necessity to install cell recycle systems. This new concept, often named as “morphology engineering”, provides additional valuable solutions to metabolic engineering for process optimization. Yet, the development and consideration of this novel approach is still in the start-up phase. To further assess the impact of bacterial morphology on the population behavior in biofilm structures, other genes involved in the cell shape modulation could be targeted.

The here designed trickle-bed biofilm bioreactor process could be used to reduce process costs for lipopeptides production or other molecules that are produced by biofilm forming microorganisms via long-term continuous fermentations. Simulations of the developed growth model could be used to develop a feeding strategy adapted to the biomass development during the continuous culture in order to limit the presence of too high substrate concentrations and the waste of unused medium, as well as to prevent nutrient limitations. It could be tested if the growth model is also applicable on other biofilm-based processes such as the continuous surfactin production process developed in Lille based on an air/liquid membrane contactor [84].

A process up-scale could be performed by increasing the packing size and the packing number to provide a higher surface for biofilm formation. Therefore, the recirculation and aeration rate should be adapted. A liquid and air distributor plate on the top and bottom side of the packing tower could help for a sufficient nutrient delivery and aeration of the biofilm on the enlarged packing elements.

The here developed biofilm-based process may also find application for the production of rhamnolipids which are mainly produced by *Pseudomonas* species. Rhamnolipids induce as surfactin severe foam formation during fermentation which represents a major drawback for industrial process scale-up. Rhamnolipid production processes have been mostly developed on the basis of foaming bioreactors with integrated foam fractionation and cell recycle systems [55, 113]. Many *Pseudomonas* strains are naturally able to form biofilms and thus could maybe be used for rhamnolipid production in the trickle-bed biofilm bioreactor.

APPENDIX

I. Primers

Table 18. List of primers that were used to construct the master strain and the gene deletion cassette. The name, sequence and number of nucleotides (Nt) is mentioned in the list.

Name	**Sequence**	**Nt**
upp_Fw_HB	AAAACAATCACACTCGCCACAG	22
upp_Rv_HB	ACAAGCAAACATGGCAGTGTAC	22
Phleo3	AGCTTGCATGCCTGCAGGTCG	21
Phleo5	CGACGGCCAGTGAATTCGAGC	21
sepF_fw	AACAAATCGGACGCATCATGACG	23
sepF_rv	AATGTGAAGAGCGGAAAGCTCG	22
sepF_Dfwd	GCTCGAATTCACTGGCCGTCGCGAATACATTGAAACGGAGCAGGATATGATCAGGCGAAAAGAATCGTCG	70
sepF_Drev	CGACCTGCAGGCATGCAAGCTATCCTGCTCCGTTTCAATGTATTCG	46
mprF_Fw_HB	CGAACAGGCAAACCTCAATGAG	22
mprF_Rv_HB	GGGATTGACACTCTTAACACTGC	23
mprF_Dfw_HB	GCTCGAATTCACTGGCCGTCGCAAACGTACGCTCATGGTCATCTCCTCGTTACACGTCTGATTGG	65
mprF_Drv_HB	CGACCTGCAGGCATGCAAGCTGATGACCATGAGCGTACGTTTG	43
pssA_Fw_HB	CCTTTCTTTGTGGCCGATTGAG	22
pssA_Rv_HB	GTTGATTTACCGGGTATGAGCG	23
pssA_Dfw_HB	GCTCGAATTCACTGGCCGTCGGATTGCTGGCGATTCATTCCTTTGGAGTCTGGGAGATGGAATTAG	66
pssA_Drv_HB	CGACCTGCAGGCATGCAAGCTAAGGAATGAATCGCCAGCAATC	43
ugtP_Fw_HB	TTTAATCCCAAGCACACACACG	22
ugtP_Rv_HB	TCTAGCATCCTCAATGGCTTGG	22
ugtP_Dfw_HB	GCTCGAATTCACTGGCCGTCGGAAATGGACATGTGCAGGTAGCTCAGAAATGATGACCGCCAAAC	65
ugtP_Drv_HB	CGACCTGCAGGCATGCAAGCTGCTACCTGCACATGTCCATTTC	43
ywnE_Fw_HB	TAATGATGAGACAGGACAGGGC	22
ywnE_Rv_HB	GCCTGTAGCTTTTCCCCATTTC	22
ywnE_Dfw_HB	GCTCGAATTCACTGGCCGTCGCGTGGCTGCTTGTTCTTTTCTTATTCACCTATGAGGAGTATCTGC	66
ywnE_Drv_HB	CGACCTGCAGGCATGCAAGCTAAGAAAAGAACAAGCAGCCACG	43
Plamda-	AAAGCTCAGCTGGCAATTGAATGGGAGGCT	30

neo_Fw_HB		
Plamda-neo_Rv_HB	CCGGCATGCGAGTTAACAATTATTAGAGGTCATCGTTCA	39
Neo_Fw_HB	TGGCAATTGAATGGGAGGCT	20
Neo_Rv_HB	TTAACAATTATTAGAGGTCATCGTTCA	27
HB_Seq_K7_1	CTTCTAAGTGACGGCTGCATAC	22
HB_Seq_K7_2	TCCAATAAATGCGACACCAACC	22
HB_Seq_K7_3	TAATATCCCCGACTGGCAATGC	22
Seq_Fw1_pssA	CTGCGCTTTTACCAGGCATATG	22
Seq_Rv1_pssA	TTTTCGACAGCACATCTTTCCC	22
Seq_Fw2_pssA	CCATCAGCAAATGGCCTTTGAG	22
Seq_Rv2_pssA	TTCTTTTAAGCCGACCCACTTG	22
Seq_Fw1_mprF	TCAGCCGCGATATCAGAAAGAG	22
Seq_Rv1_mprF	TGCCTTTTTGCAGATCATGATC	22
Seq_Fw2_mprF	TTCAGCAATGTCGCTCACTTTC	22
Seq_Rv2_mprF	TTAGACCAGCTTGGCTTCAAAC	22
Seq_Fw1_ugtP	TCAGATTGCTTGGAAATTCGCC	22
Seq_Rv1_ugtP	ATTCAGGATCATCGAGAGCTGC	22
Seq_Fw2_ugtP	CCAAGAAACTCCTTATGAATGGGAC	25
Seq_Rv2_ugtP	GTCTCCGCCTTCAACTTCAATG	22
Seq_Fw1_ywnE	GCATTGCTGCTTTTGAGAACAC	22
Seq_Rv1_ywnE	AATAATTTGCAGTACGCCTGGC	22
Seq_Fw2_ywnE	TTTCTGTTTTGATGAACCCCGG	22
Seq_Rv2_ywnE	TCGATTTACAGACGAATTGCGG	22
Seq_Fw1_ftsH	CGTTCCATCATCCTTTTCAGCC	22
Seq_Rv1_ftsH	CTTCTCCTTTGGCATTGGCATC	22
Seq_Fw2_ftsH	GCACTTCCTTTTATGGCGGATC	22
Seq_Rv2_ftsH	CTGGACCAACAATTTGAGGCTC	22
Seq_Fw1_sepF	TGATCCGGTTAAGTCGCTTGTC	22
Seq_Rv1_sepF	GCCAAAACCTCTGATAGACAGC	22
Seq_Fw2_sepF	GGTACTGTACGATGCTTTGTGC	22
Seq_Rv2_sepF	CTATGTAAAGAGGCTTGGCTGC	22
Seq_upp_Fw1	TTGCGGACGAAATCAACAATCC	22
Seq_upp_Rv1	GAGCATGTAAACGTTCAGCCTC	22
Seq_upp_Fw2	ACGCTGTTAAACCATAACCCAG	22
Seq_upp_Rv2	TTCGGTGAAGTATTGCAGGACG	22

II. Landy MOPS medium recipe

Table 19. Components of the Landy MOPS medium.

Components	Stock solution	Volume of stock solution added for final solution (1L)	Final concentration
Solution A (20x):			
Yeast extract	20 g/L	50 mL	1 g/L
$MgSO_4$	10 g/L		0.5 g/L
Solution B (20x):			
K_2HPO_4	20 g/L	50 mL	1 g/L
KCl	10 g/L		0.5 g/L
Solution C (20x):			
- $CuSO_4$	32 mg/L	50 mL	1.6 mg/L
- $MnSO_4$	24 mg/L		1.2 mg/L
- $FeSO_4$	8 mg/L		0.4 mg/L
Glucose (10x)	200 g/L	100 mL	20 g/L
Glutamic acid (5x)	25 g/L	200 mL	5 g/L
MOPS (20x)	420 g/L	50 mL	21 g/L
L-Tryptophan (100x)	1.6 g/L	10 mL (filter sterilize)	16 mg/L
Water		500	

For the Landy MOPS medium preparation, the components were mixed the following order:

1) dH_2O
2) Sol. A
3) Sol. B
4) Glucose
5) MOPS
6) L-Tryptophan
7) Glutamic acid
8) Sol. C.

Then, the medium was adjusted to pH 7 with a sterile 3M KOH solution. For this purpose, 25 mL of prepared Landy MOPS medium was taken and adjusted to pH7 with 3M KOH. With the known added quantity of 3M KOH, the necessary volume for the medium bottle and was calculated and the corresponding volume of sterile 3M KOH was added to the medium.

III. *Videos of microcolony formation*

Table 20. List of the direct links to the video files showing the microcolony development of the different strains and the corresponding password to get access.

Strain	Link	Password
***B. subtilis* 168**	http://pod.univ-lille.fr/video/10008-microcolony-formation-bs168/	BS168
TB92 **(*ΔsepF*)**	http://pod.univ-lille.fr/video/10006-microcolony-formation-tb92/	TB92
BBG111 **(*sfp*$^+$)**	http://pod.univ-lille.fr/video/9998-microcolony-formation-bbg111/	BBG111
BBG270 **(*sfp*$^+$, *ΔsepF*)**	http://pod.univ-lille.fr/video/9999-microcolony-formation-bbg270/	BBG270
RL5260 **(*epsC*$^+$, *sfp*$^+$)**	http://pod.univ-lille.fr/video/10005-microcolony-formation-rl5260/	RL5260
BBG512 **(*epsC*$^+$, *sfp*$^+$, *ΔsepF*)**	http://pod.univ-lille.fr/video/10004-microcolony-formation-bbg512/	BBG512
BBG405 **(*sfp*$^+$, *ΔmprF*, *ΔpssA*)**	http://pod.univ-lille.fr/video/10000-microcolony-formation-bbg405/	BBG405
BBG406 **(*sfp*$^+$, *ΔmprF*, *ΔpssA*, *ΔywnE*)**	http://pod.univ-lille.fr/video/10001-microcolony-formation-bbg406/	BBG406
BBG505 **(*epsC*$^+$, *sfp*$^+$, *ΔmprF*, *ΔpssA*)**	http://pod.univ-lille.fr/video/10002-microcolony-formation-bbg505/	BBG505
BBG506 **(*epsC*$^+$, *sfp*$^+$, *ΔmprF*, *ΔpssA*, *ΔywnE*)**	http://pod.univ-lille.fr/video/10003-microcolony-formation-bbg506/	BBG506

IV. *Python 3.7 code of the growth model*

```
# -*- coding: utf-8 -*-

import numpy as np
from matplotlib import pyplot as plt
from scipy.integrate import odeint
import pandas as pd
import xlsxwriter

#Create the function for the batch phase and define the variables
def batch(state,t):
  X_p = state[0]
  X_b = state[1]
  S = state[2]
  C_L = state[3]
  mu = 0.38 # growth rate (h-1)
  Ks =  0.015 #substrate affinity constant (g/L)
  Yxs = 0.2 #conversion coefficient (g/g)
  Yxo = 1 #conversion coefficient (g/g)
  Kla = 24 #oxygen transfer rate (h-1)
  Ko = 0.001 #affinity constant (g/L)
  ka = 2.1 #switching rate to biofilm (h-1)
  C_sat = 0.00673 # saturation for dissolved oxygen (g/L)
  kd = 1 #releasing rate to the planktonic phase (h-1)

  rx_p = mu * min (S/(Ks+S) , C_L/(Ko+C_L))*X_p #Roels approach
  rx_b = mu*(S/(Ks+S))*X_b
  dX_pdt = rx_p - ka*X_p + kd*X_b
  dX_bdt = rx_b + ka*X_p - kd*X_b
  dSdt = -rx_p/Yxs -rx_b/Yxs
  dC_Ldt = Kla*(C_sat-C_L)-(rx_p/Yxo)-(rx_b/Yxo)

  return [dX_pdt,dX_bdt,dSdt,dC_Ldt]

#Define initial conditions and call odeint to generate solution
```

```
 t = np.arange(0,16,0.1)
 state0 = [0.08,0,20,0.00673]
 state = odeint(batch,state0,t)

 Pfinal= state[159,0]
 Bfinal = state[159,1]
 Sfinal = state[159,2]
 C_Lfinal = state [159,3]

 #Create and plot figure
 plt.figure(1)
 plt.plot(t,state[:,0], 'g')
 plt.plot(t,state[:,1], 'b')
 plt.plot(t,state[:,2], 'k')



 #Create a data frame
 data1=(state[:,0])
 data2=(state[:,1])
 data3=( state[:,2])
 dataframe=pd.DataFrame(
         {'Time': t,
          'Planktonic cells':data1,
          'Biofilm': data2,
          'Substrate': data3})
 writer_object   =   pd.ExcelWriter('RL5260_Cultivation_Batch.xlsx',
engine='xlsxwriter')
 dataframe.to_excel(writer_object, sheet_name='Batch',
                   startrow=1)

 #Create xlsxwriter workbook object
 workbook_object = writer_object.book

 #Create xlsxwriter worksheet object
 worksheet_object = writer_object.sheets['Batch']

 #Close the Pandas Excel writer
```

```
  #Object and output the Excel file.
  writer_object.save()

  #Create the function for the continuous phase and define the variables
  def continuous(state,t):
    X_p = state[0]
    X_b = state[1]
    S = state[2]
    C_L = state[3]
    mu = 0.38 # growth rate (h-1)
    Ks =  0.015 #substrate affinity constant (g/L)
    Yxs = 0.2 #conversion coefficient (g/g)
    Yxo = 1 #conversion coefficient (g/g)
    Kla = 24 #oxygen transfer rate (h-1)
    Ko = 0.001 #affinity constant (g/L)
    ka = 0 #switching rate to biofilm (h-1)
    C_sat = 0.00673 # saturation for dissolved oxygen (g/L)
    kd = 0.315 #releasing rate to the planktonic phase (h-1)
    D = 0.5 # dilution rate (h-1)
    Sin = 20 #glucose (g/L)

    rx_p = mu * min (S/(Ks+S) , C_L/(Ko+C_L))*X_p-D*X_p
    rx_b = mu*(S/(Ks+S))*X_b
    dX_pdt = rx_p - ka*X_p + kd*X_b - D*X_p
    dX_bdt = rx_b + ka*X_p - kd*X_b
    dSdt = -rx_p/Yxs -rx_b/Yxs+D*(Sin-S)
    dC_Ldt = Kla*(C_sat-C_L)-rx_p/Yxo-rx_b/Yxo

    return [dX_pdt,dX_bdt,dSdt,dC_Ldt]

  t = np.arange(16,44.1,0.1)

  #Define initial conditions and odeint to generate the solution
  state0 = [Pfinal,Bfinal,Sfinal, C_Lfinal]
  state = odeint(continuous,state0,t)
  #Add data to figure (1)
  plt.figure(1)
  plt.plot(t,state[:,0], 'g', label='Planktonic cells')
  plt.plot(t,state[:,1], 'b', label='Biofilm')
  plt.plot(t,state[:,2], 'k', label='Substrate')

  plt.ylim([0,20])
  plt.xlabel('Time (h)')
  plt.ylabel('Glucose (g/L), planktonic cells (g/L), biofilm (g)')
  plt.legend(bbox_to_anchor=(1.05,1), loc=2, borderaxespad=0.)
  plt.title('Cultivation')

  Pfinal_con= state[280,0]
  Bfinal_con = state[280,1]
  Sfinal_con = state[280,2]
  C_Lfinal_con = state [280,3]



  #Create a data frame
  data1=(state[:,0])
  data2=(state[:,1])
  data3=( state[:,2])
  dataframe=pd.DataFrame(
          {'Time': t,
           'Planktonic cells':data1,
           'Biofilm': data2,
           'Substrate': data3})
  writer_object                                                    =
pd.ExcelWriter('RL5260_Cultivation_Continuous.xlsx',
engine='xlsxwriter')
  dataframe.to_excel(writer_object, sheet_name='Continuous',
                     startrow=1)

  #Create xlsxwriter workbook object
  workbook_object = writer_object.book

  #Create xlsxwriter worksheet object
```

```
worksheet_object = writer_object.sheets['Continuous']

#Close the Pandas Excel writer
#Object and output the Excel file
writer_object.save()
```

V. Statistical analysis: Chi-square goodness of fit test

The following null hypothesis H0 has been defined: no significant differences exist between the observed and predicted values with a significance level of $\alpha = 0.05$. The results of the Chi-square goodness of fit test are presented in **Table 21** for BBG111 and in **Table 22** for RL5260 for chapter 4. The results of the Chi-square goodness of fit test from simulation under limited glucose feeding for chapter 5 are presented in **Table 23** for BBG512 and in **Table 24** for RL5260.

Table 21. Results of the Chi-square goodness of fit test for the model and experimental data obtained with BBG111 (chapter 4).

	BBG111										
	Glucose [g/L]				**Planktonic cells [g/L]**				**Biofilm dry weight [g]**		
#	**Observed (mean value)**	**Estimated**	**Chi-sq**	**#**	**Observed (mean calue)**	**Estimated**	**Chi-sq**	**#**	**Observed (mean value)**	**Estimated**	**Chi-sq**
1	20.89	20.00	0.0396	1	0.09	0.08	0.0012	1	0.00	0.00	0.0000
2	20.15	19.61	0.0147	2	0.26	0.06	0.6175	2	0.30	0.08	0.6270
3	17.99	18.86	0.0400	3	0.55	0.11	1.6777	3	0.48	0.15	0.7461
4	15.89	17.94	0.2358	4	0.41	0.18	0.3117	4	0.71	0.23	0.9900
5	3.84	1.47	3.7870	5	0.63	1.14	0.2316	5	1.25	1.90	0.2231
6	15.52	14.11	0.1404	6	0.26	0.53	0.1389	6	2.74	2.27	0.1000
7	15.12	15.39	0.0049	7	0.38	0.49	0.0228	7	5.26	2.71	2.3905
8	12.66	15.07	0.3865	8	0.62	0.33	0.2427	8	8.15	5.53	1.2364
9	12.19	15.00	0.5271	9	0.67	0.26	0.6589	9	8.76	6.61	0.6930

DF	**Sum Chi-Sq**	**p-value**		**DF**	**Sum Chi-Sq**	**p-value**		**DF**	**Sum Chi-Sq**	**p-value**
8	5.1759	0.7386		8	3.9029	0.8658		7	7.0061	0.4282

Table 22. Results of the Chi-square goodness of fit test for the model and experimental data obtained with RL5260 (chapter 4).

	RL5260										
	Glucose [g/L]				**Planktonic cells [g/L]**				**Biofilm dry weight [g]**		
#	**Observed (mean value)**	**Estimated**	**Chi-Sq**	**#**	**Observed (mean value)**	**Estimated**	**Chi-Sq**	**#**	**Observed (mean value)**	**Estimated**	**Chi-Sq**
1	20.10	20.00	0.0005	1	0.03	0.08	0.0324	1	0.00	0.00	0.0000
2	19.49	19.66	0.0015	2	0.21	0.05	0.5941	2	0.08	0.10	0.0049
3	17.68	19.00	0.0904	3	0.43	0.09	1.3773	3	0.33	0.19	0.0957
4	16.15	18.15	0.2207	4	0.62	0.14	1.6771	4	0.66	0.31	0.3832
5	3.35	1.59	1.9340	5	1.24	0.97	0.0741	5	3.17	2.79	0.0521
6	15.19	14.04	0.0936	6	0.53	0.57	0.0028	6	4.35	3.37	0.2830
7	16.36	15.49	0.0485	7	0.56	0.50	0.0061	7	4.58	4.08	0.0621
8	12.94	15.38	0.3862	8	0.21	0.16	0.0146	8	11.59	8.73	0.9361
9	11.66	15.33	0.8788	9	0.24	0.015	3.3521	9	13.59	10.57	0.8668

DF	**Sum Chi-Sq**	**p-value**
8	3.6542	0.8869

DF	**Sum Chi-Sq**	**p-value**
8	7.1306	0.5226

DF	**Sum Chi-Sq**	**p-value**
7	2.6840	0.9126

Table 23. Results of the Chi-square goodness of fit test for the model and experimental data obtained with BBG512 under limited glucose feeding conditions (chapter 5).

	BBG512						
	Glucose [g/L]				**Planktonic cells [g/L]**		
#	**Observed (mean value)**	**Estimated**	**Chi-Sq**	**#**	**Observed (mean value)**	**Estimated**	**Chi-Sq**
1	21.08	21.00	0.0003	1	0.09	0.08	0.0011
2	20.10	20.75	0.0199	2	0.31	0.04	1.9373
3	18.94	20.26	0.0869	3	0.61	0.07	4.2815
4	17.66	19.66	0.2026	4	0.77	0.11	4.1120
5	3.68	6.70	1.3641	5	0.95	0.81	0.0268
6	0.26	0.01	4.5437	6	0.45	0.13	0.8160
7	0.06	0.01	0.1907	7	0.29	0.20	0.0409
8	0.04	0.01	0.1166	8	0.26	0.33	0.0147
9	0.07	0.01	0.4614	9	0.21	0.36	0.0647

DF	**Sum Chi-Sq**	**p-value**
8	6.9862	0.5381

DF	**Sum Chi-Sq**	**p-value**
8	11.2949	0.1855

Table 24. Results of the Chi-square goodness of fit test for the model and experimental data obtained with RL5260 under limited glucose feeding conditions (chapter 5).

	RL5260						
	Glucose [g/L]				**Planktonic cells [g/L]**		
#	**Observed (mean value)**	**Estimated**	**Chi-Sq**	**#**	**Observed (mean value)**	**Estimated**	**Chi-Sq**
1	23.07	23.00	0.0002	1	0.08	0.08	0.0000
2	21.25	22.66	0.0883	2	0.19	0.05	0.4375
3	19.66	21.99	0.2469	3	0.46	0.09	1.6104
4	18.55	21.15	0.3203	4	0.68	0.14	2.1546
5	4.69	4.59	0.0022	5	1.18	0.97	0.0438
6	0.15	0.01	1.7215	6	0.53	0.35	0.0897
7	0.01	0.01	0.0000	7	0.39	0.41	0.0009
8	0.01	0.01	0.0000	8	0.40	0.57	0.0486
9	0.01	0.01	0.0000	9	0.43	0.60	0.0486

DF	**Sum Chi-Sq**	**p-value**		**DF**	**Sum Chi-Sq**	**p-value**
8	2.3795	0.9671		8	4.4342	0.8160

The null hypothesis is not rejected, all p-values are much higher than 0.05. This means no significant differences exist between the observed and predicted values for all strains.

VI. *Impact of prophage elements on the biofilm formation of B. subtilis 168*

The *B. subtilis* 168 strain TF8A with three prophage deletions (*ΔSPß*, *Δskin* and *ΔPBSX*) developped an unexpected strong and wrinkled biofilm structure on the DFR reactor coupons. **Figure 56A** shows the biofilm development of TF8A in comparison to *B. subtilis* 168 and RL5260.

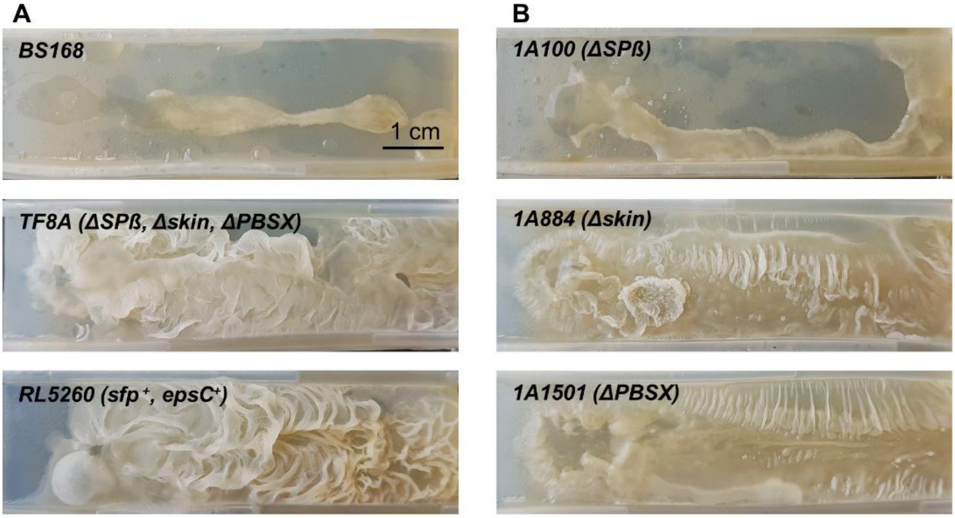

Figure 56. Biofilm development of the strain TF8A lacking three prophages (*ΔSPß*, *Δskin* and *ΔPBSX*) on the DFR coupons in comparison to *B. subtilis* 168 and RL5260 (*sfp*$^{+}$, *epsC*$^{+}$) (A) and mutant strains lacking one of the prophages (B) after 48 h of incubation in the DFR with Landy medium.

Although the EPS production has not been restored in TF8A, the strain was able to develop a architectually complex and structured biofilm similar to the one of RL5260 which is capable to produce EPS. After the analysis of mutants strains lacking each of the prophage (**Figure 56B**), it seems that the deletion of the skin element and the prophage PBSX have a strong impact on the biofilm formation of *B. subtilis* 168. In both cases a structured and wrinkled biofilm was observed.

Based on these observations, the hypothesis arises that the prophage deletion may trigger the production and accumulation of exopolymeric matrix components. The genes of prophage are often composed of several degradative enzymes involved in host cell lysis. It could be possible that through the deletion of the prophage these degradative enzymes are removed and thus can not contribute anymore to the degradation of exopolymeric substances and dead cells or cell debris that are usually present during the biofilm development of *B. subtilis* 168. Since the skin element is involved in the spore formation in *B. subtilis*, a changed sporulation behavior could also affect the biofilm formation. It would be interesting to investigate more into detail the biofilm matrix composition in the different strains to indentify the origin of this biofilm structure.

References

[1] F. Kunst, N. Ogasawara, I. Moszer, a M. Albertini, *et al.*, “The complete genome sequence of the gram-positive bacterium *Bacillus subtilis*,” *Nature*, vol. 390, no. 6657, pp. 249–256, 1997.

[2] M. M. Nakano and P. Zuber, “Anaerobic growth of a "strict aerobe” (*Bacillus subtilis*),” *Annu. Rev. Microbiol.*, vol. 52, pp. 165–190, 1998.

[3] S. Mukherjee and D. B. Kearns, “The Structure and Regulation of Flagella in *Bacillus subtilis*,” *Annu. Rev. Genet.*, vol. 48, no. 1, pp. 319–340, 2014.

[4] D. R. Zeigler, Z. Prágai, S. Rodriguez, B. Chevreux, *et al.*, “The origins of 168, W23, and other *Bacillus subtilis* legacy strains,” *J. Bacteriol.*, vol. 190, no. 21, pp. 6983–6995, 2008.

[5] H. J. Conn, “The Identity of *Bacillus* subtilis,” *J. Infect. Dis.*, vol. 46, no. 4, pp. 341–350, 1930.

[6] A. L. McLoon, S. B. Guttenplan, D. B. Kearns, R. Kolter, *et al.*, “Tracing the domestication of a biofilm-forming bacterium,” *J. Bacteriol.*, vol. 193, no. 8, pp. 2027–2034, 2011.

[7] P. R. Burkholder and N. H. Giles, “Induced biochemical mutations in *Bacillus subtilis*,” *Am. J. Bot.*, vol. 34, no. 6, pp. 345–348, 1947.

[8] J. Spizizen, “Transformation of biochemically deficient strains of *Bacillus subtilis* by deoxyribonucleate,” *Pathol. Microbiol.*, vol. 44, pp. 1072–1078, 1958.

[9] R. Gallegos-Monterrosa, E. Mhatre, and A. T. Kovacs, “Specific *Bacillus subtilis* 168 variants do form biofilms on nutrient rich medium,” *Microbiology*, pp. 1–11, 2016.

[10] L. Westers, H. Westers, and W. J. Quax, “*Bacillus subtilis* as cell factory for pharmaceutical proteins: A biotechnological approach to optimize the host organism,” *Biochim. Biophys. Acta - Mol. Cell Res.*, vol. 1694, no. 1-3 SPEC.ISS., pp. 299–310, 2004.

[11] A. M. Earl, R. Losick, and R. Kolter, “Ecology and genomics of *Bacillus subtilis*,” *Trends Microbiol.*, vol. 16, no. 6, pp. 269–275, 2008.

[12] V. Barbe, S. Cruveiller, F. Kunst, P. Lenoble, *et al.*, “From a consortium sequence to a unified sequence : the *Bacillus subtilis* 168 reference genome a decade later,” *Microbiology*, vol. 155, pp. 1758–1775, 2009.

[13] M. A. Marahiel, “Working outside the protein-synthesis rules: Insights into non-ribosomal peptide synthesis,” *J. Pept. Sci.*, vol. 15, no. 12, pp. 799–807, 2009.

[14] R. Finking and M. A. Marahiel, “Biosynthesis of Nonribosomal Peptides,” *Annu. Rev. Microbiol.*, vol. 58, no. 1, pp. 453–488, 2004.

[15] S. S. Branda, J. E. González-Pastor, S. Ben-Yehuda, R. Losick, *et al.*,

“Fruiting body formation by *Bacillus subtilis*,” *Proc. Natl. Acad. Sci. U. S. A.*, vol. 98, no. 20, pp. 11621–6, 2001.

[16] D. B. Kearns and R. Losick, “Swarming motility in undomesticated *Bacillus subtilis*,” *Mol. Microbiol.*, vol. 49, no. 3, pp. 581–590, 2003.

[17] J. E. Patrick and D. B. Kearns, “Laboratory strains of *Bacillus subtilis* do not exhibit swarming motility,” *J. Bacteriol.*, vol. 191, no. 22, pp. 7129–7133, 2009.

[18] D. B. Kearns, F. Chu, R. Rudner, and R. Losick, “Genes governing swarming in *Bacillus subtilis* and evidence for a phase variation mechanism controlling surface motility,” *Mol. Microbiol.*, vol. 52, no. 2, pp. 357–369, 2004.

[19] M. M. Nakano, N. Corbell, J. Besson, and P. Zuber, “Isolation and characterization of *sfp*: a gene that functions in the production of the lipopeptide biosurfactant, surfactin, in *Bacillus subtilis*,” *MGG Mol. Gen. Genet.*, vol. 232, no. 2, pp. 313–321, 1992.

[20] L. E. N. Quadri, P. H. Weinreb, M. Lei, M. M. Nakano, *et al.*, “Characterization of Sfp, a *Bacillus subtilis* phosphopantetheinyl transferase for peptidyl carder protein domains in peptide synthetases,” *Biochemistry*, vol. 37, no. 6, pp. 1585–1595, 1998.

[21] D. Lopez, H. Vlamakis, and R. Kolter, “Generation of multiple cell types in *Bacillus subtilis*,” *FEMS Microbiol. Rev.*, vol. 33, no. 1, pp. 152–163, 2009.

[22] M. Schallmey, A. Singh, and O. P. Ward, “Developments in the use of *Bacillus* species for industrial production,” *Can. J. Microbiol.*, vol. 50, pp. 1–17, 2004.

[23] J. M. van Dijl and M. Hecker, “*Bacillus subtilis*: From soil bacterium to super-secreting cell factory,” *Microb. Cell Fact.*, vol. 12, no. 1, pp. 1–6, 2013.

[24] P. Jacques, “Surfactin and Other Lipopeptides from *Bacillus spp.*,” in *Biosurfactants, Microbiology Monographs*, G. Soberón-Chávez, Ed. Berlin Heidelberg: Springer Verlag Berlin Heidelberg, 2011, pp. 57–91.

[25] F. Coutte, D. Lecouturier, K. Dimitrov, J. Guez, *et al.*, “Microbial lipopeptide production and purification bioprocesses, current progress and future challenges,” *Biotechnol. J.*, vol. 12, no. 1600566, pp. 1–10, 2017.

[26] Y. Hathout, Y. P. Ho, V. Ryzhov, P. Demirev, *et al.*, “Kurstakins: A new class of lipopeptides isolated from *Bacillus thuringiensis*,” *J. Nat. Prod.*, vol. 63, no. 11, pp. 1492–1496, 2000.

[27] C. Luo, X. Liu, X. Zhou, J. Guo, *et al.*, “Unusual biosynthesis and structure of locillomycins from *Bacillus subtilis* 916,” *Appl. Environ. Microbiol.*, vol. 81, no. 19, pp. 6601–6609, 2015.

[28] A. Koumoutsi, X.-H. Chen, A. Henne, H. Liesegang, *et al.*, “Structural and Functional Characterization of Gene Clusters Directing Nonribosomal

Synthesis of Bioactive Cyclic Lipopeptides in *Bacillus amyloliquefaciens* Strain FZB42," *J. Bacteriol.*, vol. 186, no. 4, pp. 1084–1096, 2004.

[29] A. Kakinuma, H. Sugino, M. Isono, G. Tamura, *et al.*, "Determination of fatty acid in surfactin and elucidation of the total structure of surfactin," *Agric. Biol. Chem.*, vol. 33, no. 6, pp. 973–976, 1969.

[30] F. Peypoux, J. M. Bonmatin, and J. Wallach, "Recent trends in the biochemistry of surfactin," *Appl. Microbiol. Biotechnol.*, vol. 51, no. 5, pp. 553–563, 1999.

[31] S. A. Cochrane and J. C. Vederas, "Lipopeptides from *Bacillus* and *Paenibacillus* spp.: A Gold Mine of Antibiotic Candidates," *Med. Res. Rev.*, vol. 36, no. 1, pp. 4–31, 2009.

[32] M. Geissler, K. M. Heravi, M. Henkel, and R. Hausmann, "Lipopeptide Biosurfactants From *Bacillus* Species," in *Biobased Surfactants*, Second Edi., Elsevier Inc., 2019, pp. 205–240.

[33] M. Kowall, J. Vater, B. Kluge, T. Stein, *et al.*, "Separation and characterization of surfactin isoforms produced by *Bacillus subtilis* OKB 105," *J. Colloid Interface Sci.*, vol. 204, no. 1, pp. 1–8, 1998.

[34] A. Bartal, A. Vigneshwari, B. Bóka, M. Vörös, *et al.*, "Effects of Different Cultivation Parameters on the Production of Surfactin Variants by a *Bacillus subtilis* strain," *Molecules*, vol. 23, no. 10, 2018.

[35] M. Deleu, M. Paquot, and T. Nylander, "Effect of Fengycin, a Lipopeptide Produced by *Bacillus subtilis*, on Model Biomembranes," *Biophys. J.*, vol. 94, no. April, pp. 2667–2679, 2008.

[36] J. Schneider, K. Taraz, H. Budzikiewicz, D. Magali, *et al.*, "The Structure of Two Fengycins from *Bacillus subtilis* S499," *Verlag der Zeitschrift für Naturforsch. C. A J. Biosci.*, vol. 54, no. 11, pp. 859–866, 1999.

[37] N. Vanittanakom, "Fengycin - A novel antifungal lipopeptide antibiotic produced by *Bacillus subtilis* F-29-3," *J. Antibiot. (Tokyo).*, vol. XXXIX, no. 7, pp. 888–901, 1986.

[38] A. A. Kaki, N. Smargiasso, M. Ongena, M. Kara, *et al.*, "Characterization of New Fengycin Cyclic Lipopeptide Variants Produced by *Bacillus amyloliquefaciens* (ET) Originating from a Salt Lake of Eastern Algeria," *Curr. Microbiol.*, vol. 77, no. 3, pp. 443–451, 2020.

[39] J.-M. Bonmatin, O. Laprevote, and F. Peypoux, "Diversity Among Microbial Cyclic Lipopeptides: Iturins and Surfactins. Activity-Structure Relationships to Design New Bioactive Agents," *Comb. Chem. High Throughput Screen.*, vol. 6, no. 6, pp. 541–556, 2003.

[40] M. Ongena, E. Jourdan, A. Adam, M. Paquot, *et al.*, "Surfactin and fengycin lipopeptides of *Bacillus subtilis* as elicitors of induced systemic resistance in plants," *Environ. Microbiol.*, vol. 9, no. 4, pp. 1084–1090, 2007.

[41] A. Koglin, F. Löhr, F. Bernhard, V. V. Rogov, *et al.*, "Structural basis for the selectivity of the external thioesterase of the surfactin synthetase," *Nature*, vol. 454, no. 7206, pp. 907–911, 2008.

[42] S. A. Sieber and M. A. Marahiel, "Molecular mechanisms underlying nonribosomal peptide synthesis: Approaches to new antibiotics," *Chem. Rev.*, vol. 105, no. 2, pp. 715–738, 2005.

[43] F. I. Kraas, V. Helmetag, M. Wittmann, M. Strieker, *et al.*, "Functional dissection of surfactin synthetase initiation module reveals insights into the mechanism of lipoinitiation," *Chem. Biol.*, vol. 17, no. 8, pp. 872–880, 2010.

[44] P. Serror and A. L. Sonenshein, "CodY is required for nutritional repression of *Bacillus subtilis* genetic competence," *J. Bacteriol.*, vol. 178, no. 20, pp. 5910–5915, 1996.

[45] L. W. Hamoen, G. Venema, and O. P. Kuipers, "Controlling competence in *Bacillus subtilis*: Shared use of regulators," *Microbiology*, vol. 149, no. 1, pp. 9–17, 2003.

[46] O. Chumsakul, H. Takahashi, T. Oshima, T. Hishimoto, *et al.*, "Genome-wide binding profiles of the *Bacillus subtilis* transition state regulator AbrB and its homolog Abh reveals their interactive role in transcriptional regulation," *Nucleic Acids Res.*, vol. 39, no. 2, pp. 414–428, 2011.

[47] F. Chu, D. B. Kearns, A. McLoon, Y. Chai, *et al.*, "A novel regulatory protein governing biofilm formation in *Bacillus subtilis*," *Mol. Microbiol.*, vol. 68, no. 5, pp. 1117–1127, 2008.

[48] E. J. Murray, T. B. Kiley, and N. R. Stanley-Wall, "A pivotal role for the response regulator DegU in controlling multicellular behaviour," *Microbiology*, vol. 155, no. 1, pp. 1–8, 2009.

[49] B. Mielich-Süss and D. Lopez, "Molecular mechanisms involved in *Bacillus subtilis* biofilm formation," *Environ. Microbiol.*, vol. 17, no. 3, pp. 555–565, 2015.

[50] A. L. Sonenshein, "CodY, a global regulator of stationary phase and virulence in Gram-positive bacteria," *Curr. Opin. Microbiol.*, vol. 8, no. 2, pp. 203–207, 2005.

[51] R. Jahan, A. M. Bodratti, M. Tsianou, and P. Alexandridis, "Biosurfactants , natural alternatives to synthetic surfactants : Physicochemical properties and applications," *Adv. Colloid Interface Sci.*, vol. 275, p. 102061, 2020.

[52] A. A. Jimoh and J. Lin, "Biosurfactant : A new frontier for greener technology and environmental sustainability," *Ecotoxicol. Environ. Saf.*, vol. 184, no. June, p. 109607, 2019.

[53] N. S. Shaligram and R. S. Singhal, "Surfactin - A review on biosynthesis, fermentation, purification and applications," *Food Technol. Biotechnol.*, vol. 48, no. 2, pp. 119–134, 2010.

[54] D. Altmajer Vaz, E. Jurado Alameda, E. J. Gudina, J. A. Teixeira, *et al.*, “Performance of a biosurfactant produced by a *Bacillus subtilis* strain isolated from crude oil samples as compared to commercial chemical surfactants,” *Colloids Surfaces B Biointerfaces*, vol. 89, pp. 167–174, 2012.

[55] P. Singh, Y. Patil, and V. Rale, “Biosurfactant production: emerging trends and promising strategies,” *J. Appl. Microbiol.*, vol. 126, no. 1, pp. 2–13, 2018.

[56] Y. Zhang, C. Liu, B. Dong, X. Ma, *et al.*, “Anti-inflammatory Activity and Mechanism of Surfactin in Lipopolysaccharide-Activated Macrophages,” *Inflammation*, vol. 38, no. 2, pp. 756–764, 2015.

[57] M. Kracht, H. Rokos, M. Ozel, M. Kowall, *et al.*, “Antiviral and Hemolytic Activities of Surfactin Isoforms and Their Methyl Ester Derivatives,” *J. Antibiot. (Tokyo).*, vol. 52, no. 7, pp. 613–619, 1999.

[58] D. Vollenbroich, G. Pauli, O. Muhsin, J. Vater, *et al.*, “Antimycoplasma Properties and Application in Cell Culture of Surfactin, a Lipopeptide Antibiotic from *Bacillus subtilis*,” *Appl. Environ. Microbiol.*, vol. 63, no. 1, pp. 44–49, 1997.

[59] D. P. Sachdev and S. S. Cameotra, “Biosurfactants in agriculture,” *Appl. Microbiol. Biotechnol.*, vol. 97, pp. 1005–1016, 2013.

[60] E. Jourdan, G. Henry, F. Duby, J. Dommes, *et al.*, “Insights into the Defense-Related Events Occurring in Plant Cells Following Perception of Surfactin-Type Lipopeptide from *Bacillus subtilis*,” *Mol. Plant-Microbe Interact.*, vol. 22, no. 4, pp. 456–468, 2009.

[61] H. Cawoy, M. Mariutto, G. Henry, C. Fisher, *et al.*, “Plant Defense Stimulation by Natural Isolates of *Bacillus* Depends on Efficient Surfactin Production,” *Mol. Plant-Microbe Interact.*, vol. 27, no. 2, pp. 87–100, 2014.

[62] M. Ongena and P. Jacques, “*Bacillus* lipopeptides: versatile weapons for plant disease biocontrol.,” *Trends Microbiol.*, vol. 16, no. 3, pp. 115–25, 2008.

[63] D. K. F. Santos, R. D. Rufino, J. M. Luna, V. A. Santos, *et al.*, “Biosurfactants: Multifunctional biomolecules of the 21st century,” *Int. J. Mol. Sci.*, vol. 17, no. 3, pp. 1–31, 2016.

[64] J. Vater, “Lipopeptides, an attractive class of microbial surfactants,” *Prog. Colloid Polym. Sci.*, vol. 72, pp. 12–18, 1986.

[65] M. Landy, G. H. Warren, S. B. Rosenmanm, and L. G. Colio, “Bacillomycin: An Antibiotic from *Bacillus subtilis* Active against Pathogenic Fungi,” *Exp. Biol. Med.*, vol. 67, no. 4, pp. 539–541, 1948.

[66] D. G. Cooper, C. R. Macdonald, S. J. B. Duff, and N. Kosaric, “Enhanced Production of Surfactin from *Bacillus subtilis* by Continuous Product Removal and Metal Cation Additions,” vol. 42, no. 3, pp. 408–412, 1981.

[67] V. Rangarajan and K. G. Clarke, "Process development and intensification for enhanced production of *Bacillus* lipopeptides," *Biotechnol. Genet. Eng. Rev.*, vol. 31, no. 1–2, pp. 46–68, 2015.

[68] Y. H. Wei, C. C. Lai, and J. S. Chang, "Using Taguchi experimental design methods to optimize trace element composition for enhanced surfactin production by *Bacillus subtilis* ATCC 21332," *Process Biochem.*, vol. 42, no. 1, pp. 40–45, 2007.

[69] W. C. Chen, R. S. Juang, and Y. H. Wei, "Applications of a lipopeptide biosurfactant, surfactin, produced by microorganisms," *Biochem. Eng. J.*, vol. 103, pp. 158–169, 2015.

[70] S. Chenikher, J. S. Guez, F. Coutte, M. Pekpe, *et al.*, "Control of the specific growth rate of *Bacillus subtilis* for the production of biosurfactant lipopeptides in bioreactors with foam overflow," *Process Biochem.*, vol. 45, no. 11, pp. 1800–1807, 2010.

[71] C.-Y. Chen, S. C. Baker, and R. C. Darton, "Batch production of biosurfactant with foam fractionation," *J. Chem. Technol. Biotechnol.*, vol. 81, pp. 1923–1931, 2006.

[72] J. S. Guez, S. Chenikher, J. P. Cassar, and P. Jacques, "Setting up and modelling of overflowing fed-batch cultures of *Bacillus subtilis* for the production and continuous removal of lipopeptides," *J. Biotechnol.*, vol. 131, no. 1, pp. 67–75, 2007.

[73] D. A. Davis, H. C. Lynch, and J. Varley, "The application of foaming for the recovery of Surfactin from *B. subtilis* ATCC 21332 cultures," *Enzyme Microb. Technol.*, vol. 28, no. 4–5, pp. 346–354, 2001.

[74] F. Coutte, D. Lecouturier, S. A. Yahia, V. Leclère, *et al.*, "Production of surfactin and fengycin by *Bacillus subtilis* in a bubbleless membrane bioreactor," *Appl. Microbiol. Biotechnol.*, vol. 87, no. 2, pp. 499–507, 2010.

[75] M. S. Yeh, Y. H. Wei, and J. S. Chang, "Enhanced production of surfactin from *Bacillus subtilis* by addition of solid carriers," *Biotechnol. Prog.*, vol. 21, no. 4, pp. 1329–1334, 2005.

[76] M. S. Yeh, Y. H. Wei, and J. S. Chang, "Bioreactor design for enhanced carrier-assisted surfactin production with *Bacillus subtilis*," *Process Biochem.*, vol. 41, no. 8, pp. 1799–1805, 2006.

[77] S. Fahim, K. Dimitrov, F. Gancel, P. Vauchel, *et al.*, "Impact of energy supply and oxygen transfer on selective lipopeptide production by *Bacillus subtilis* BBG21," *Bioresour. Technol.*, vol. 126, pp. 1–6, 2012.

[78] S. Fahim, K. Dimitrov, P. Vauchel, F. Gancel, *et al.*, "Oxygen transfer in three phase inverse fluidized bed bioreactor during biosurfactant production by *Bacillus subtilis*," *Biochem. Eng. J.*, vol. 76, pp. 70–76, 2013.

[79] O. Chtioui, K. Dimitrov, F. Gancel, and I. Nikov, "Biosurfactants production by immobilized cells of *Bacillus subtilis* ATCC 21332 and their recovery by

pertraction," *Process Biochem.*, vol. 45, no. 11, pp. 1795–1799, 2010.

[80] O. Chtioui, K. Dimitrov, F. Gancel, P. Dhulster, *et al.*, "Selective fengycin production in a modified rotating discs bioreactor," *Bioprocess Biosyst. Eng.*, vol. 37, no. 2, pp. 107–114, 2013.

[81] C.-Y. Chen, S. C. Baker, and R. C. Darton, "Continuous production of biosurfactant with foam fractionation," *J. Chem. Technol. Biotechnol.*, vol. 81, pp. 1915–1922, 2006.

[82] D. Dhali, F. Coutte, A. A. Arias, S. Auger, *et al.*, "Genetic engineering of the branched fatty acid metabolic pathway of *Bacillus subtilis* for the overproduction of surfactin C14 isoform," *Biotechnol. J.*, vol. 12, no. 7, pp. 1–23, 2017.

[83] F. Coutte, J. Niehren, D. Dhali, M. John, *et al.*, "Modeling leucine's metabolic pathway and knockout prediction improving the production of surfactin, a biosurfactant from *Bacillus subtilis*," *Biotechnol. J.*, pp. 1216–1234, 2015.

[84] F. Coutte, D. Lecouturier, V. Leclère, M. Béchet, *et al.*, "New integrated bioprocess for the continuous production, extraction and purification of lipopeptides produced by *Bacillus subtilis* in membrane bioreactor," *Process Biochem.*, vol. 48, pp. 25–32, 2013.

[85] M. M. Nakano, Y. P. Dailly, P. Zuber, and D. Clark, "Characterization of anaerobic fermentative growth of *Bacillus subtilis*: Identification of fermentation end products and genes required for growth," *J. Bacteriol.*, vol. 179, no. 21, pp. 6749–6755, 1997.

[86] F. Coutte, V. Leclère, M. Béchet, J. S. Guez, *et al.*, "Effect of *pps* disruption and constitutive expression of *srfA* on surfactin productivity, spreading and antagonistic properties of *Bacillus subtilis* 168 derivatives," *J. Appl. Microbiol.*, vol. 109, no. 2, pp. 480–491, 2010.

[87] E. H. Duitman, D. Wyczawski, L. G. Boven, G. Venema, *et al.*, "Novel methods for genetic transformation of natural *Bacillus subtilis* isolates used to study the regulation of the mycosubtilin and surfactin synthetases," *Appl. Environ. Microbiol.*, vol. 73, no. 11, pp. 3490–3496, 2007.

[88] H. Razafindralambo, Y. Popineau, M. Deleu, C. Hbid, *et al.*, "Foaming Properties of Lipopeptides Produced by *Bacillus subtilis*: Effect of Lipid and Peptide Structural Attributes," *J. Agric. Food Chem.*, vol. 46, no. 3, pp. 911–916, 1998.

[89] F. Hu, Y. Liu, and S. Li, "Rational strain improvement for surfactin production: Enhancing the yield and generating novel structures," *Microb. Cell Fact.*, vol. 18, no. 1, pp. 1–13, 2019.

[90] G. Gong, Z. Zheng, H. Chen, C. Yuan, *et al.*, "Enhanced production of surfactin by *Bacillus subtilis* E8 mutant obtained by ion beam implantation," *Food Technol. Biotechnol.*, vol. 47, no. 1, pp. 27–31, 2009.

[91] F. Gancel, L. Montastruc, T. Liu, L. Zhao, *et al.*, “Lipopeptide overproduction by cell immobilization on iron-enriched light polymer particles,” *Process Biochem.*, vol. 44, no. 9, pp. 975–978, 2009.

[92] Q. Zune, D. Soyeurt, D. Toye, M. Ongena, *et al.*, “High-energy X-ray tomography analysis of a metal packing biofilm reactor for the production of lipopeptides by *Bacillus subtilis*,” *J. Chem. Technol. Biotechnol.*, vol. 89, no. 3, pp. 382–390, 2013.

[93] O. Chtioui, K. Dimitrov, F. Gancel, P. Dhulster, *et al.*, “Rotating discs bioreactor, a new tool for lipopeptides production,” *Process Biochem.*, vol. 47, no. 12, pp. 2020–2024, 2012.

[94] N. Krieger, D. C. Neto, and D. A. Mitchell, “Production of Microbial Biosurfactants by Solid-State Cultivation,” in *Biosurfactants*, R. Sen, Ed. Landes Bioscience and Springer Science + Business Media, 2010, pp. 203–210.

[95] A. Ohno, T. Ano, and M. Shoda, “Production of a Lipopeptide Antibiotic, Surfactin, by Recombinant *Bacillus subtilis* in Solid State Fermentation,” *Biotechnol. Bioeng.*, vol. 47, pp. 209–214, 1995.

[96] C. T. Slivinski, E. Mallmann, J. M. De Araújo, D. Alexander, *et al.*, “Production of surfactin by *Bacillus pumilus* UFPEDA 448 in solid-state fermentation using a medium based on okara with sugarcane bagasse as a bulking agent,” *Process Biochem.*, vol. 47, no. 12, pp. 1848–1855, 2012.

[97] A. Ohna, T. Ano, and M. Shoda, “Effect of Temperature on Production of Lipopeptide Antibiotics, Iturin A and Surfactin by a Dual Producer, *Bacillus subtilis* RB14, in Solid-State Fermentation,” *J. Ferment. Bioeng.*, vol. 80, no. 5, pp. 517–519, 1995.

[98] K. Brindle and T. Stephenson, “The Application of Membrane Biological Reactors for the Treatment of Wastewaters,” *Biotechnol. Bioeng.*, vol. 49, pp. 601–610, 1996.

[99] V. Rangarajan and K. G. Clarke, “Towards bacterial lipopeptide products for specific applications — a review of appropriate downstream processing schemes,” *Process Biochem.*, vol. 51, no. 12, pp. 2176–2185, 2016.

[100] M. Henkel, M. Geissler, F. Weggenmann, and R. Hausmann, “Production of microbial biosurfactants : Status quo of rhamnolipid and surfactin towards large-scale production,” *Biotechnol. J.*, vol. 12, no. 1600561, pp. 1–10, 2017.

[101] T. Yoneda, Y. Miyota, K. Furuya, and T. Tsuzuki, “Production Process of Surfactin,” US7011969B2, 2006.

[102] Independent Commodity Intelligence Services (ICIS news), “Japan’s Kaneka begins selling bio-sufactant,” *Press release*, Tokyo, p. 1, 31-Aug-2009.

[103] Lipofabrik, “A ground-breaking biomolecular production platform for safer, more efficient and sustainable pest control and crop health management,” *Fact Sheet European Project HORIZON2020*, 2019. [Online]. Available:

https://cordis.europa.eu/project/id/849713. [Accessed: 06-Aug-2020].

[104] R. Czinkóczky and Á. Németh, "Techno-economic assessment of Bacillus fermentation to produce surfactin and lichenysin," *Biochem. Eng. J.*, pp. 1–46, 2020.

[105] I. N. A. Van Bogaert, K. Saerens, C. De Muynck, D. Develter, *et al.*, "Microbial production and application of sophorolipids," *Appl. Microbiol. Biotechnol.*, vol. 76, pp. 23–34, 2007.

[106] I. N. A. Van Bogaert, J. Zhang, and W. Soetaert, "Microbial synthesis of sophorolipids," *Process Biochem.*, vol. 46, no. 4, pp. 821–833, 2011.

[107] K. K. S. Randhawa and P. K. S. M. Rahman, "Rhamnolipid biosurfactants — past, present, and future scenario of global market," *Front. Microbiol.*, vol. 5, no. 454, pp. 1–7, 2014.

[108] E. Kulakovskaya and T. Kulakovskaya, "Prospects of Practical Application of Sophorolipids, Cellobiose Lipids, and MELs," in *Extracellular Glycolipids of Yeasts*, 1st ed., E. Kulakovskaya and T. Kulakovskaya, Eds. Academic Press, 2014, pp. 75–83.

[109] S. Linneweber and J. Krauter, "Evonik commercializes biosurfactants," *Press release*, Essen, pp. 1–3, 21-Jun-2016.

[110] J. Jiang, Y. Zu, X. Li, Q. Meng, *et al.*, "Recent progress towards industrial rhamnolipids fermentation : Process optimization and foam control," *Bioresour. Technol.*, vol. 298, no. 122394, pp. 1–10, 2020.

[111] H.-J. Daniel, M. Reuss, and C. Syldatk, "Production of sophorolipids in high concentration from deproteinized whey and rapeseed oil in a two stage fed batch process using Candida bombicola ATCC 22214 and Cryptococcus curvatus ATCC 20509," *Biotechnol. Lett.*, vol. 20, no. 12, pp. 1153–1156, 1998.

[112] T. Tiso, S. Thies, M. Müller, L. Tsvetanova, *et al.*, "Rhamnolipids: Production, Performance, and Application," in *Consequences of Microbial Interactions awith Hydrocarbons, Oils, and Lipids: Production of Fuel and Chemicals, Handbook of Hydrocarbon and Lipid Microbiology*, D. Y. Lee, Ed. Springer International Publishing AG, 2017, pp. 1–37.

[113] H. Chong and Q. Li, "Microbial production of rhamnolipids: opportunities, challenges and strategies," *Microb. Cell Fact.*, vol. 16, no. 137, pp. 1–12, 2017.

[114] D. C. Neto, J. A. Meira, E. Tiburtius, P. P. Zamora, *et al.*, "Production of rhamnolipids in solid-state cultivation : Characterization , downstream processing and application in the cleaning of contaminated soils," *Biotechnol. J.*, vol. 4, pp. 748–755, 2009.

[115] Z. Gong, Q. He, C. Che, J. Liu, *et al.*, "Optimization and scale - up of the production of rhamnolipid by *Pseudomonas aeruginosa* in solid - state fermentation using high - density polyurethane foam as an inert support,"

Bioprocess Biosyst. Eng., no. 0123456789, 2019.

[116] G. Narendrakumar, N. M. D. Saikrishna, P. Prakash, and T. V Preethi, “Production, characterization, and optimization of rhamnolipids produced by,” *Int. J. Green Pharm.*, vol. 11, no. 2, pp. 92–97, 2017.

[117] J. Krauter, “Evonik and Unilever team up for large-scale production of world’s first ‘green’ biosurfactant,” *Press release*, Essen, pp. 1–4, 18-Dec-2019.

[118] R. M. Donlan, “Biofilms : Microbial Life on Surfaces,” vol. 8, no. 9, pp. 881–890, 2002.

[119] F. Costa, B. Silva, and T. Tavares, “Biofilm Bioprocesses,” in *Current Developments in Biotechnology and Bioengineering: Bioprocesses, Bioreactors and Controls*, Elsevier B.V., 2017, pp. 143–175.

[120] H. Vlamakis, Y. Chai, P. Beauregard, R. Losick, *et al.*, “Sticking together: building a biofilm the *Bacillus subtilis* way,” *Nat. Rev. Microbiol.*, vol. 11, no. 3, pp. 157–168, 2013.

[121] S. S. Branda, Å. Vik, L. Friedman, and R. Kolter, “Biofilms: The matrix revisited,” *Trends Microbiol.*, vol. 13, no. 1, pp. 20–26, 2005.

[122] A. Demirci, T. Pongtharangkul, and A. L. Pometto III, “APPLICATIONS OF BIOFILM REACTORS FOR PRODUCTION OF VALUE-ADDED PRODUCTS BY MICROBIAL FERMENTATION,” in *Biofilms in the Food Environment*, 1st ed., H. P. Blaschek, H. H. Wang, and M. E. Agle, Eds. Blackwell Publishing, 2007, pp. 167–189.

[123] R. Singh, D. Paul, and R. K. Jain, “Biofilms : implications in bioremediation,” *TRENDS Microbiol.*, vol. 14, no. 9, 2006.

[124] L. S. Cairns, L. Hobley, and N. R. Stanley-Wall, “Biofilm formation by *Bacillus subtilis* : new insights into regulatory strategies and assembly mechanisms,” *Mol. Microbiol.*, vol. 93, no. 4, pp. 587–598, 2014.

[125] D. B. Kearns, F. Chu, S. S. Branda, R. Kolter, *et al.*, “A master regulator for biofilm formation by *Bacillus subtilis*,” *Mol. Microbiol.*, vol. 55, no. 3, pp. 739–749, 2005.

[126] K. P. Lemon, A. M. Earl, H. C. Vlamakis, C. Aguilar, *et al.*, “Biofilm Development with an Emphasis on *Bacillus subtilis*,” *Curr. Top. Microbiol ogy Immunol.*, vol. 322, pp. 1–16, 2008.

[127] S. S. Branda, E. Gonza, E. Dervyn, S. D. Ehrlich, *et al.*, “Genes Involved in Formation of Structured Multicellular Communities by *Bacillus subtilis*,” *J. Bacteriol.*, vol. 186, no. 12, pp. 3970–3979, 2004.

[128] D. Ercan and A. Demirci, “Current and future trends for biofilm reactors for fermentation processes,” *Crit. Rev. Biotechnol.*, vol. 35, no. 1, pp. 1–14, 2015.

[129] J. Van Gestel, F. J. Weissing, O. P. Kuipers, and Á. T. Kovács, “Density of

founder cells affects spatial pattern formation and cooperation in *Bacillus subtilis* biofilms," *ISME J.*, vol. 8, no. 10, pp. 2069–2079, 2014.

[130] A. Seminara, T. E. Angelini, J. N. Wilking, H. Vlamakis, *et al.*, "Osmotic spreading of *Bacillus subtilis* biofilms driven by an extracellular matrix," *Proc. Natl. Acad. Sci.*, vol. 109, no. 4, pp. 1116–1121, 2012.

[131] M. Marvasi, P. T. Visscher, and L. Casillas Martinez, "Exopolymeric substances (EPS) from *Bacillus subtilis*: polymers and genes encoding their synthesis," *FEMS Microbiol. Lett.*, vol. 313, no. 1, pp. 1–9, 2010.

[132] S. Kesel, B. von Bronk, C. F. Garcia, A. Götz, *et al.*, "Matrix composition determines the dimensions of *Bacillus subtilis* NCIB 3610 biofilm colonies grown on LB agar," *RSC Adv.*, vol. 7, pp. 31886–31898, 2017.

[133] L. Chai, H. Vlamakis, and R. Kolter, "Extracellular signal regulation of cell differentiation in biofi lms," vol. 36, no. May, pp. 374–379, 2011.

[134] S. S. Branda, F. Chu, D. B. Kearns, R. Losick, *et al.*, "A major protein component of the *Bacillus subtilis* biofilm matrix," vol. 59, pp. 1229–1238, 2006.

[135] S. Arnaouteli, C. E. Macphee, and N. R. Stanley-wall, "Just in case it rains: building a hydrophobic biofilm the *Bacillus subtilis* way," *Curr. Opin. Microbiol.*, vol. 34, pp. 7–12, 2016.

[136] K. J. Martin and R. Nerenberg, "The membrane biofilm reactor (MBfR) for water and wastewater treatment: Principles, applications, and recent developments," *Bioresour. Technol.*, vol. 122, pp. 83–94, 2012.

[137] B. Halan, K. Buehler, and A. Schmid, "Biofilms as living catalysts in continuous chemical syntheses," *Trends Biotechnol.*, vol. 30, no. 9, pp. 453–465, 2012.

[138] K. C. Cheng, A. Demirci, and J. M. Catchmark, "Advances in biofilm reactors for production of value-added products," *Appl. Microbiol. Biotechnol.*, vol. 87, no. 2, pp. 445–456, 2010.

[139] X. Z. Li, J. S. Webb, S. Kjelleberg, and B. Rosche, "Enhanced Benzaldehyde Tolerance in *Zymomonas mobilis* Biofilms and the Potential of Biofilm Applications in Fine-Chemical Production," *Appl. Environ. Microbiol.*, vol. 72, no. 2, pp. 1639–1644, 2006.

[140] X. Z. Li, B. Hauer, and B. Rosche, "Single-species microbial biofilm screening for industrial applications," *Appl. Microbiol. Biotechnol.*, vol. 76, pp. 1255–1262, 2007.

[141] B. Rosche, X. Z. Li, B. Hauer, A. Schmid, *et al.*, "Microbial biofilms: a concept for industrial catalysis?," *Trends Biotechnol.*, vol. 27, no. 11, pp. 636–643, 2009.

[142] D. De Beer, P. Stoodley, F. Roe, and Z. Lewandowski, "Effects of biofilm structures on oxygen distribution and mass transport," *Biotechnol. Bioeng.*,

vol. 43, no. 11, pp. 1131–1138, 1994.

[143] E. Morgenroth and K. Milferstedt, "Biofilm engineering : linking biofilm development at different length and time scales," *Rev. Environ. Sci. Biotechnol.*, vol. 8, pp. 203–208, 2009.

[144] M. J. W. Frank, J. A. M. Kuipers, G. F. Versteeg, and W. P. M. V. A. N. Swaaij, "The performance of structured packings in trickle-bed reactors," *Trans IChemE*, vol. 77, no. October, pp. 567–582, 1999.

[145] X. Z. Li, B. Hauer, and B. Rosche, "Catalytic Biofilms on Structured Packing for the Production of Glycolic Acid," *J. Mcirobiolgy Biotechnolgy*, vol. 23, no. 2, pp. 195–204, 2013.

[146] M. Khalesi, Q. Zune, S. Telek, D. Riveros-Galan, *et al.*, "Fungal biofilm reactor improves the productivity of hydrophobin HFBII," *Biochem. Eng. J.*, vol. 88, pp. 171–178, 2014.

[147] Q. Zune, S. Telek, S. Calvo, T. Salmon, *et al.*, "Influence of liquid phase hydrodynamics on biofilm formation on structured packing: Optimization of surfactin production from *Bacillus amyloliquefaciens*," *Chem. Eng. Sci.*, vol. 170, pp. 628–638, 2017.

[148] Q. Zune, A. Delepierre, S. Gofflot, J. Bauwens, *et al.*, "A fungal biofilm reactor based on metal structured packing improves the quality of a Gla::GFP fusion protein produced by *Aspergillus oryzae*," *Appl. Microbiol. Biotechnol.*, vol. 99, no. 15, pp. 6241–6254, 2015.

[149] S. Aferka, A. Viva, E. Brunazzi, P. Marchot, *et al.*, "Tomographic measurement of liquid hold up and effective interfacial area distributions in a column packed with high performance structured packings," *Chem. Eng. Sci.*, vol. 66, no. 14, pp. 3413–3422, 2011.

[150] J. W. Lee, D. Na, J. M. Park, J. Lee, *et al.*, "Systems metabolic engineering of microorganisms for natural and non-natural chemicals," *Nat. Chem. Biol.*, vol. 8, no. 6, pp. 536–546, 2012.

[151] S. Y. Park, D. Yang, S. H. Ha, and S. Y. Lee, "Metabolic Engineering of Microorganisms for the Production of Natural Compounds," *Adv. Biosyst.*, vol. 1700190, pp. 1–41, 2018.

[152] D. C. Volke and P. I. Nikel, "Getting Bacteria in Shape: Synthetic Morphology Approaches for the Design of Efficient Microbial Cell Factories," *Adv. Biosyst.*, vol. 1800111, pp. 1–21, 2018.

[153] D. Claessen, R. Emmins, L. W. Hamoen, R. A. Daniel, *et al.*, "Control of the cell elongation – division cycle by shuttling of PBP1 protein in *Bacillus subtilis*," *Mol. Microbiol.*, vol. 68, no. 4, pp. 1029–1046, 2008.

[154] J. Errington and L. J. Wu, "Cell Cycle Machinery in *Bacillus subtilis*," in *Prokaryotic Cytoskeletons, Subcellular Biochemistry*, 84th ed., J. Löwe and L. A. Amos, Eds. Springer, Cham, 2017, pp. 67–101.

[155] E. Król, S. P. van Kessel, L. S. van Bezouwen, N. Kumar, *et al.*, "*Bacillus subtilis* SepF binds to the C-terminus of FtsZ," *PLoS One*, vol. 7, no. 8, 2012.

[156] L. G. Monahan, A. Robinson, and E. J. Harry, "Lateral FtsZ association and the assembly of the cytokinetic Z ring in bacteria," *Mol. Microbiol.*, vol. 74, no. 4, pp. 1004–1017, 2009.

[157] X. Jiang and G. Chen, "Morphology engineering of bacteria for bio-production," *Biotechnol. Adv.*, vol. 34, no. 4, pp. 435–440, 2016.

[158] T. Kruse, J. Bork-Jensen, and K. Gerdes, "The morphogenetic MreBCD proteins of Escherichia coli form an essential membrane-bound complex," *Mol. Microbiol.*, vol. 55, no. 1, pp. 78–89, 2005.

[159] L. W. Hamoen, J. C. Meile, W. De Jong, P. Noirot, *et al.*, "SepF, a novel FtsZ-interacting protein required for a late step in cell division," *Mol. Microbiol.*, vol. 59, no. 3, pp. 989–999, 2006.

[160] R. Duman, S. Ishikawa, I. Celik, H. Strahl, *et al.*, "Structural and genetic analyses reveal the protein SepF as a new membrane anchor for the Z ring.," *Proc. Natl. Acad. Sci. U. S. A.*, vol. 110, no. 48, pp. E4601-10, 2013.

[161] M. E. Gündoğdu, Y. Kawai, N. Pavlendova, N. Ogasawara, *et al.*, "Large ring polymers align FtsZ polymers for normal septum formation.," *EMBO J.*, vol. 30, no. 3, pp. 617–626, 2011.

[162] L. I. Salzberg and J. D. Helmann, "Phenotypic and Transcriptomic Characterization of *Bacillus subtilis* Mutants with Grossly Altered Membrane Composition," *J. Bacteriol.*, vol. 190, no. 23, pp. 7797–7807, 2008.

[163] V. Norris and I. Fishov, "Hypothesis : Membrane domains and hyperstructures control bacterial division," *Biochimie*, vol. 83, pp. 91–97, 2001.

[164] L. Zhao, J. Ye, J. Fu, and G. Q. Chen, "Engineering peptidoglycan degradation related genes of *Bacillus subtilis* for better fermentation processes," *Bioresour. Technol.*, vol. 248, pp. 238–247, 2018.

[165] M. Vandermies, T. Kar, F. Carly, J. Nicaud, *et al.*, "*Yarrowia lipolytica* morphological mutant enables lasting in situ immobilization in bioreactor," pp. 5473–5482, 2018.

[166] X. R. Jiang, H. Wang, R. Shen, and G. Q. Chen, "Engineering the bacterial shapes for enhanced inclusion bodies accumulation," *Metab. Eng.*, vol. 29, pp. 227–237, 2015.

[167] Y. Wang, H. Wu, X. Jiang, and G. Chen, "Engineering *Escherichia coli* for enhanced production of poly(3-hydroxybutyrate-co-4-hydroxybutyrate) in larger cellular space," *Metab. Eng.*, vol. 25, pp. 183–193, 2014.

[168] Y. Wang, C. Ling, Y. Chen, X. Jiang, *et al.*, "Microbial engineering for easy downstream processing," *Biotechnol. Adv.*, no. September 2018, pp. 0–1, 2019.

[169] A. Jordan, J. Chandler, J. S. MacCready, J. Huang, *et al.*, “Engineering cyanobacterial cell morphology for enhanced recovery and processing of biomass,” *Appl. Environ. Microbiol.*, vol. 83, no. 9, pp. 1–13, 2017.

[170] D. Dhali, “Correlation between lipopeptide biosynthesis and their precursor metabolism in *Bacillus subtilis*,” 2016.

[171] K. Tanaka, C. S. Henry, J. F. Zinner, E. Jolivet, *et al.*, “Building the repertoire of dispensable chromosome regions in *Bacillus subtilis* entails major refinement of cognate large-scale metabolic model,” *Nulceic Acids Res.*, vol. 41, no. 1, pp. 687–699, 2013.

[172] I. G. De Jong, K. Beilharz, O. P. Kuipers, and J.-W. Veening, “Live Cell Imaging of *Bacillus subtilis* and *Streptococcus pneumoniae* using Automated Time-lapse Microscopy,” *J. Vis. Exp.*, vol. 53, no. July, pp. 1–6, 2011.

[173] M. Miras and D. Dubnau, “A DegU-P and DegQ-Dependent regulatory pathway for the K-state in *Bacillus subtilis*,” *Front. Microbiol.*, vol. 7, no. NOV, pp. 1–14, 2016.

[174] S. Pollak, S. Omer Bendori, and A. Eldar, “A complex path for domestication of *B. subtilis* sociality,” *Curr. Genet.*, vol. 61, no. 4, pp. 493–496, 2015.

[175] K. Tsuge, T. Ano, Mi. Hirai, Y. Nakamura, *et al.*, “The Genes *degQ*, *pps*, and *lpa-8* (*sfp*) Are Responsible for Conversion of *Bacillus subtilis* 168 to Plipastatin Production,” *Antimicrob. Agents Chemother.*, vol. 43, no. 9, pp. 2183–2192, 1999.

[176] M. E. Sharpe, P. M. Hauser, and R. G. Sharpe, “*Bacillus subtilis* Cell Cycle as Studied by Fluorescence Microscopy : Constancy of Cell Length at Initiation of DNA Replication and Evidence for Active Nucleoid Partitioning,” *J. Bacteriol.*, vol. 180, no. 3, pp. 547–555, 1998.

[177] J. Azeredo, N. F. Azevedo, R. Briandet, N. Cerca, *et al.*, “Critical review on biofilm methods,” *Crit. Rev. Microbiol.*, vol. 43, no. 3, pp. 313–351, 2017.

[178] V. Leclère, R. Marti, M. Béchet, P. Fickers, *et al.*, “The lipopeptides mycosubtilin and surfactin enhance spreading of *Bacillus subtilis* strains by their surface-active properties,” *Arch. Microbiol.*, vol. 186, no. 6, pp. 475–483, 2006.

[179] M. Morikawa, “Beneficial biofilm formation by industrial bacteria *Bacillus subtilis* and related species.,” *J. Biosci. Bioeng.*, vol. 101, no. 1, pp. 1–8, 2006.

[180] D. M. Goeres, M. A. Hamilton, N. A. Beck, K. Buckingham-meyer, *et al.*, “A method for growing a biofilm under low shear at the air – liquid interface using the drip flow biofilm reactor A method for growing a biofilm under low shear at the air – liquid interface using the drip flow biofilm reactor,” *Nat. Protoc.*, vol. 4, no. 5, pp. 783–788, 2009.

[181] I. Dogsa, M. Brloznik, D. Stopar, and I. Mandic-Mulec, “Exopolymer Diversity and the Role of Levan in *Bacillus subtilis* Biofilms,” *PLoS One*,

vol. 8, no. 4, pp. 2–11, 2013.

[182] D. Schultz, N. Onuchic, and E. Ben-Jacob, “Turning death into creative force during biofilm engineering,” *PNAS*, vol. 109, no. 46, pp. 18633–18634, 2012.

[183] M. Asally, M. Kittisopikul, P. Rué, Y. Du, *et al.*, “Localized cell death focuses mechanical forces during 3D patterning in a biofilm,” *PNAS*, vol. 109, no. 46, pp. 18891–18896, 2012.

[184] C. Picioreanu, M. C. M. Van Loosdrecht, and J. J. Heijnen, “A Theoretical Study on the Effect of Surface Roughness on Mass Transport and Transformation in Biofilms,” *Biotechnol. Bioeng.*, vol. 68, no. 4, pp. 355–369, 2000.

[185] L. Zhao, J. Ye, J. Fu, and G. Q. Chen, “Engineering peptidoglycan degradation related genes of *Bacillus subtilis* for better fermentation processes,” *Bioresour. Technol.*, vol. 248, pp. 238–247, 2018.

[186] H.-C. Flemming, J. Wingender, U. Szewzyk, P. Steinberg, *et al.*, “Biofilms : an emergent form of bacterial life,” *Nat. Rev. Microbiol.*, vol. 14, no. 9, pp. 563–575, 2016.

[187] D. Julkowska, M. Obuchowski, I. B. Holland, and S. J. Séror, “Branched swarming patterns on a synthetic medium formed by wild-type *Bacillus subtilis* strain 3610 : detection of different cellular morphologies and constellations of cells as the complex architecture develops,” *Microbiology*, no. 150, pp. 1839–1849, 2004.

[188] D. Julkowska, M. Obuchowski, I. B. Holland, and S. J. Se, “Comparative Analysis of the Development of Swarming Communities of *Bacillus subtilis* 168 and a Natural Wild Type : Critical Effects of Surfactin and the Composition of the Medium,” *J. Bacteriol.*, vol. 187, no. 1, pp. 65–76, 2005.

[189] M. Deleu, H. Razafindralambo, Y. Popineau, P. Jacques, *et al.*, “Interfacial and emulsifying properties of lipopeptides from *Bacillus subtilis*,” *Colloids Surf. A Physicochem. Eng. Asp.*, vol. 152, pp. 3–10, 1999.

[190] J. Möller, P. Emge, I. A. Vizcarra, P. Kollmannsberger, *et al.*, “Bacterial filamentation accelerates colonization of adhesive spots embedded in biopassive surfaces,” *New J. Phys.*, vol. 15, no. 125016, pp. 1–19, 2013.

[191] K. Kobayashi and M. Iwano, “BslA(YuaB) forms a hydrophobic layer on the surface of *Bacillus subtilis* biofilms,” *Mol. Microbiol.*, vol. 85, no. May, pp. 51–66, 2012.

[192] T. R. Garrett, M. Bhakoo, and Z. Zhang, “Bacterial adhesion and biofilms on surfaces,” *Prog. Nat. Sci.*, vol. 18, pp. 1049–1056, 2008.

[193] A. F. Miranda, N. Ramkumar, C. Andriotis, T. Höltkemeier, *et al.*, “Applications of microalgal biofilms for wastewater treatment and bioenergy production,” *Biotechnol. Biofuels*, vol. 10, no. 120, pp. 1–23, 2017.

[194] J. P. Boltz, E. Morgenroth, and D. Sen, “Mathematical modelling of biofilms and biofilm reactors for engineering design,” *Water Sci. Technol.*, vol. 3, no. 1, pp. 1821–1836, 2010.

[195] O. Wanner and E. Morgenroth, “Biofilm modeling with AQUASIM,” *Water Sci. Technol.*, vol. 49, no. 11, pp. 137–144, 2004.

[196] B. E. Rittmann, J. P. Boltz, D. Brockmann, G. T. Daigger, *et al.*, “A framework for good biofilm reactor modeling practice (GBRMP),” *Water Sci. Technol.*, vol. 77, no. 5, pp. 1149–1164, 2018.

[197] A. Esener, T. Veerman, J. A. Roels, and N. W. F. Kossen, “Modeling of bacterial growth; Formulation and evaluation of a structured model,” *Biotechnol. Bioeng.*, vol. XXIV, no. August 1982, pp. 1749–1764, 1982.

[198] K. R. Rao, T. Srinivasan, and C. Venkateswarlu, “Mathematical and kinetic modeling of biofilm reactor based on ant colony optimization,” *Process Biochem.*, vol. 45, no. 6, pp. 961–972, 2010.

[199] H. L. Brück, F. Delvigne, P. Dhulster, P. Jacques, *et al.*, “Molecular strategies for adapting *Bacillus subtilis* 168 biosurfactant production to biofilm cultivation mode,” *Bioresour. Technol.*, vol. 293, no. 122090, pp. 1–8, 2019.

[200] S. Reiber and D. Stensel, “Biologically Enhanced Oxygen Transfer in a Fixed-Film System,” *Water Pollut. Control Fed.*, vol. 57, no. 2, pp. 135–142, 1985.

[201] F. Garcia-Ochoa and E. Gomez, “Bioreactor scale-up and oxygen transfer rate in microbial processes : An overview,” *Biotechnol. Adv.*, vol. 27, no. 2, pp. 153–176, 2009.

[202] S. Liu, “How Cells Grow,” in *Bioprocess Engineering: Kinetics, Sustainability, and Reactor Design*, 2nd ed., Elsevier B.V., 2017, pp. 629–697.

[203] J. A. Roels, “Application of Macroscopic Principles to Microbial Metabolism,” *Biotechnol. Bioeng.*, vol. 103, no. 1, pp. 2–59, 2009.

[204] H. Y. Lin, B. Mathiszik, B. Xu, S. Enfors, *et al.*, “Determination of the Maximum Specific Uptake Capacities for Glucose and Oxygen in Glucose-Limited Fed-Batch Cultivations of *Escherichia coli*,” *Biotechnol. Bioeng.*, vol. 73, no. 5, pp. 347–357, 2001.

[205] B. Xu, M. Jahic, and S.-O. Enfors, “Modeling of Overflow Metabolism in Batch and Fed-Batch Cultures of *Escherichia coli*,” *Biotechnol. Prog.*, vol. 15, pp. 81–90, 1999.

[206] A. Guisasola, I. Jubany, J. A. Baeza, J. Carrera, *et al.*, “Respirometric estimation of the oxygen affinity constants for biological ammonium and nitrite oxidation,” *J. Chem. Technol. Biotechnol.*, vol. 80, pp. 388–396, 2005.

[207] M. Marino, T. Hoffmann, R. Schmid, H. Möbitz, *et al.*, “Changes in protein

synthesis during the adaptation of *Bacillus subtilis* to anaerobic growth conditions," *Microbiology*, vol. 146, pp. 97–105, 2000.

[208] E. Härtig and D. Jahn, "Regulation of the Anaerobic Metabolism in *Bacillus subtilis*," in *Advances in Microbial Physiology*, vol. 61, Elsevier Ltd., 2012, pp. 195–216.

[209] F. Garcia-Ochoa and E. Gomez, "Prediction of Gas-Liquid Mass Transfer Coefficient in Sparged Stirred Tank Bioreactors," *Biotechnol. Bioeng.*, vol. 92, no. 6, pp. 762–772, 2005.

[210] L.-K. Ju and A. Sundararajan, "Model Analysis of Biological Oxygen Transfer Enhancement in Surface-Aerated Bioreactors," *Biotechnol. Bioeng.*, vol. 40, pp. 1343–1352, 1992.

[211] A. Martínez, O. T. Ramírez, and F. Valle, "Effect of growth rate on the production of β-galactosidase from *Escherichia coli* in *Bacillus subtilis* using glucose-limited exponentially fedbatch cultures," *Enzyme Microb. Technol.*, vol. 22, no. 6, pp. 520–526, 1998.

[212] P. G. Jayathilake, S. Jana, S. Rushton, D. Swailes, *et al.*, "Extracellular polymeric substance production and aggregated bacteria colonization influence the competition of microbes in biofilms," *Front. Microbiol.*, vol. 8, no. SEP, 2017.

[213] J. Huang, Y. Du, G. Xu, H. Zhang, *et al.*, "High yield and cost-effective production of poly(γ-glutamic acid) with *Bacillus subtilis*," *Eng. Life Sci.*, vol. 11, no. 3, pp. 291–297, 2011.

[214] M. Dauner, T. Storni, and U. Sauer, "*Bacillus subtilis* Metabolism and Energetics in Carbon-Limited and Excess-Carbon Chemostat Culture," *J. Bacteriol.*, vol. 183, no. 24, pp. 7308–7317, 2001.

[215] S. A. Cristiano-Fajardo, C. Flores, N. Flores, R. Tinoco-valencia, *et al.*, "Glucose limitation and glucose uptake rate determines metabolite production and sporulation in high cell density continuous cultures of *Bacillus amyloliquefaciens* 83," *J. Biotechnol.*, vol. 299, no. April, pp. 57–65, 2019.

[216] A. Berth, D. Lecouturier, K. Loubiere, P. Dhulster, *et al.*, "Modelling and optimisation of gas-liquid mass transfer in a microporous hollow fiber membrane aerated bioreactor used to produce surfactin," *Biochem. Eng. J.*, vol. 145, pp. 109–119, 2019.